Formation, Growth and Quantification of Ultrafine Particles in Selected Microenvironments of Megacity Delhi

By

SHAILENDRA KUMAR YADAV

Environmental Engineering Department

Submitted

In fulfilment of the requirements of the degree

of

DOCTOR OF PHILOSOPHY

to

DEPARTMENT OF ENVIRONMENTAL ENGINEERING

DELHI TECHNOLOGICAL UNIVERSITY

DELHI-110042, INDIA

AUGUST 2022

Formation, Growth and Quantification of Ultrafine Particles in Selected Microenvironments of Megacity Delhi

A Thesis

Submitted in fulfilment of the
requirements for the award of the degree
Of

DOCTOR OF PHILOSOPHY
In
Environmental Engineering

By
SHAILENDRA KUMAR YADAV
Roll No. 2K16/Ph.D./EN/01

ENVIRONMENTAL ENGINEERING DEPARTMENT

Under the guidance of
Dr. Rajeev Kumar Mishra
And
Prof. B. R. Gurjar
Department of Civil Engineering, IIT, Roorkee

DEPARTMENT OF ENVIRONMENTAL ENGINEERING
DELHI TECHNOLOGICAL UNIVERSITY
DELHI-110042, INDIA

AUGUST 2022

DELHI TECHNOLOGICAL UNIVERSITY

(Formerly Delhi College of Engineering, Since 1941)

Department of Environmental Engineering

Shahbad Daulatpur, Bawana road, Delhi- 110042

DECLARATION

I hereby declare that the research work presented in this thesis entitled "**Formation, Growth and Quantification of Ultrafine Particles in Selected Microenvironments of Megacity Delhi**" is original and carried out by me under the supervision of Dr. Rajeev Kumar Mishra, Assistant Professor, Department of Environmental Engineering, Delhi Technological University, Delhi, and co-supervision of Prof. B. R. Gurjar, Professor, Department of Civil Engineering, Indian Institute of Technology, Roorkee, Uttarakhand, being submitted for the award of Ph.D. degree to Delhi Technological University, Delhi, India. The content of this thesis has not been submitted either in part or whole to any other university or institute for the award of any degree or diploma.

Date: / /2022 (Shailendra Kumar Yadav)

Place: DTU, Delhi. En. No. – 2K16/Ph.D./EN/01

DELHI TECHNOLOGICAL UNIVERSITY

(Formerly Delhi College of Engineering, Since 1941)

Department of Environmental Engineering

Shahbad Daulatpur, Bawana road, Delhi- 110042

Date: - / /2022

CERTIFICATE

This is to certify that the Ph.D. thesis entitled "**Formation, Growth and Quantification of Ultrafine Particles in Selected Microenvironments of Megacity Delhi**", is being submitted by **Mr. Shailendra Kumar Yadav** for the fulfilment of the requirements for the award of the degree of Doctor of Philosophy in Environmental Engineering, to the Department of Environmental Engineering, Delhi Technological University, Delhi, India, is a bonafide record of original research work carried out by him under my supervision. The results embodied in this thesis have not been submitted to any other university or institution for the award of any degree or diploma.

Dr. Rajeev Kumar Mishra
Supervisor
Department of Environmental Engineering
Delhi Technological University

Prof. B. R. Gurjar
Co - Supervisor
Department of Civil Engineering
Indian Institute of Technology, Roorkee

Prof. S.K. Singh
DRC, Chairman
Department of Environmental Engineering
Delhi Technological University

Prof. A. K. Haritash
HOD
Department of Environmental Engineering
Delhi Technological University

Dedicated

To

My Parents

Late Sh. Shyam Chandra Yadav,

Late Mrs. Suraj Mukhi Yadav

And

My Wife 'Urmila' and Daughter 'Anaya'

ACKNOWLEDGEMENTS

I would like to express my appreciation to the people who have helped me most during my research work. First and foremost, I am deeply grateful to my research supervisor, Dr. Rajeev Kumar Mishra, and co- supervisor Prof. B. R. Gurjar for their nonstop guidance, enduring patience, and nurturing support throughout this research. It has been an honor to be associated with such a great supervisor and learn from his experience.

I accord my heartfelt thanks to Prof. S.K. Singh, DRC, Chairman and Prof. A. K. Haritash, Head, Department of Environmental Engineering, DTU and Dr. Sobhan Kumar Kompalli, Scientist - SF Space Physics Laboratory (SPL) Vikram Sarabhai Space Centre (VSSC) Indian Space Research Organization (ISRO) Thiruvananthapuram, who was a source of inspiration for me to take up this research work. I extend my thanks to Dr. Ajay Nagpure, Director, Air Quality, WRI India and Pramod Kumar (Sir Ji). It would not have been possible without the support of central instrumentation facilities laboratory technicians; I am thankful to them.

I am grateful to my colleagues, Dr. Amrit Kumar, Dr. Manvendra Verma, Mr. Abhinav Pandey, Mr. Amrit Krishnan, Mr. Kanagaraj R., Mr. Vignesh M., Ms. Monika Sharma and Mr. Ravi Pratap Singh Jadon for providing me with critical comments and suggestions and all those who interacted and exchanged ideas with me in completing the research.

I want to extend special thanks to my family's immense contribution, especially my wife, who not only encouraged and supported me but also stood by me like a pillar and gave me constant motivation. All my family members have shown enormous patience during this process and have cheerfully sacrificed the time that rightfully belonged to them. Finally, I extend a profound expression of respect to all elders in the family and especially my parents who have always showered me with their blessings and made me who I am today.

LIST OF PUBLICATIONS

Research Publication

Published research article

1- Shailendra Kumar Yadav, Rajeev Kumar Mishra, Bhola Ram Gurjar, 2022. Ultrafine Particle Number Concentration and its size distribution during Diwali festival in megacity Delhi, India: Are 'Green Crackers' Safe?", Journal of Environmental Management. 317, 115459. https://doi.org/10.1016/j.jenvman.2022.115459 (SCI journal with IF 8.9).

2- Shailendra Kumar Yadav, Rajeev Kumar Mishra, Bhola Ram Gurjar, 2022. Quasi-ultrafine particle (qUFP) number concentration and size-resolved elemental distribution induced by fireworks in a megacity, Delhi, India. Arab. J. Geosci. 15. https://doi.org/10.1007/s12517-021-09385-1 (SCI journal with IF 1.89).

3- Shailendra Kumar Yadav, Rajeev Kumar Mishra, Bhola Ram Gurjar, 2022. Assessment of the effect of the judicial prohibition on firecracker celebration at the Diwali festival on air quality in Delhi, India". Environmental Science Pollution Research (2022). https://doi.org/10.1007/s11356-021-17695-w (SCI journal with IF 5.7)

4- Shailendra Kumar Yadav, Sharma, R., Kumar, S., Agarwal, A., Mohan, V., Mishra, R.K., Shukla, A., 2021. Urban air pollution reduction: evidence from phase-wise analysis of COVID-19 pandemic lockdown. Arab. J. Geosci. 14. https://doi.org/10.1007/s12517-021-07777-x (SCI journal with IF 1.89).

5- Shailendra Kumar Yadav, Kompalli, S.K., Gurjar, B.R., Mishra, R.K., 2021. Aerosol number concentrations and new particle formation events over a polluted megacity during the COVID-19 lockdown. Atmos. Environ. 259, 118526. https://doi.org/10.1016/j.atmosenv.2021.118526 (SCI journal with IF 5.4).

6- Rajeev Kumar Mishra, Shailendra Kumar Yadav, Deepak Baghel, Mridul Arora, 2018. "Study on Indoor Air Quality Status of Fine Particulate Matter: A Case Study"

International Journal of Engineering Technology Science and Research, ISSN 2394 – 3386 Volume 5, Issue 4.

Book Chapter (published)

1- Shailendra Kumar Yadav, Rajeev Kumar Mishra, Bhola Ram Gurjar, “Ultrafine Particles in concern of Vehicular Exhaust: An overview” 2019. Book Chapter of Engine Exhaust Particulates, Energy, Environment, and Sustainability, edited by A. K. Agrawal, Springer Nature Singapore Pvt Ltd. P. 7- 38. https://doi.org/10.1007/978-981-13-3299-9_2

Communicated / about to communicate

1- Shailendra Kumar Yadav & Rajeev Kumar Mishra et al., 2021. Investigating the Impact of Odd-Even Policy on Particle Number Size Distribution of Coarse, Fine, Sub-fine and Quasi-UFP in Megacity Delhi", communicated with the journal of Sustainable cities and Society, SCI journal with IF 6.7.

2- Shailendra Kumar Yadav, Rajeev Kumar Mishra, Bhola Ram Gurjar, 2022 Nano-particle monitoring and evaluation near roadside microenvironment. (About to communicate)

3- Shailendra Kumar Yadav & Rajeev Kumar Mishra et al., 2022, Fate of UFP in road microenvironment in Asian cities- a critical review. (About to communicate)

ABSTRACT

The present study investigates the particle number concentrations and size distributions in the ultrafine and fine-sized regimes over a polluted megacity, New Delhi (28.75° N, 77.12° E), India. The field experiments were conducted from November 2019 to June 2021 including the strict social and travel restrictions (lockdown) imposed by the Government of India aiming to control the spread of Coronavirus Disease 19 (COVID-19) pandemic. The different phases of the COVID-19 lockdown witnessed restrictions of varying magnitudes with the significant cessation of anthropogenic sources, *viz.*, industrial, road, railways, and air traffic emissions. The impact of varying urban emissions on particle number size distributions and new particle formation events were examined during these restrictions. The mean total number concentrations were in the range of ~ (2 to 3.5) x 10^4 cm^{-3} and depicted a gradual increase (~26%) with progressive unlock of the anthropogenic activities. At the same time, accumulation particle concentrations were doubled. However, ultrafine particles (UFP) (diameter < 100 nm) dominated (50-88%) the total number concentrations during most of the days and several new particle formation (NPF) events resulted in elevated (2 - 5 fold) UFP concentrations. Subsequently, the particles grew to larger sizes with rates ~3.31- 8.37 nm hr^{-1}. The NPF events occurred during the daytime, and during the events, a clear enhancement in the concentrations of [H_2SO_4] proxy (2 to 3.5 x 10^7 molecules cm^{-3}; 2-3 orders higher than the non-event values), suggesting the role of strong gas-phase photochemistry. Also, some of the NPF events were associated with increased odd oxygen concentrations [Ox = O_3+NO_2], indicating the regional nature of the precursors and participation of VOC precursors in nucleation/growth. Interestingly, different classes of NPF events were seen during the strictest lockdown period, whereas more frequent and well-defined NPF events were witnessed when anthropogenic activities were opened up with conditional relaxations. These events demonstrated the competition between source strengths of precursor vapors from anthropogenic activities and primary particles acting as condensation sink restricting NPF. This study highlighted that urban pollution mitigation

policies must consider ultrafine particles emanating from the secondary aerosol formation process from traffic emissions.

Since the air pollution and noise generated from fireworks are related to air quality and human health, the regulatory bodies had implemented the eco-friendly "Green Crackers" in megacity Delhi, India, to celebrate Diwali 2019 with the permission of a specific time slot (8:00 PM to 10:00 PM). The present study was conducted on a residential, educational institute campus to evaluate the particle number size distribution (PNSD) of green cracker emissions. During the Diwali event period, the high peak of particle number concentration (PNC) reached 1.7 x 10^5 # cm^{-3} with a geometric mean diameter (GMD) of ~44 nm. The average PNC increment on Diwali day was 138 % and 97 % compared to pre (26^{th} October 2019) and post (28^{th} October 2019) Diwali period, respectively, including 468 %, 142 %, 65 %, 75 % on pre-Diwali and 485 %, 110 %, 32 %, 26 % on post-Diwali 2019 period in terms of Nucleation mode (10 nm < D_p < 20 nm), Small Aitken mode (20 nm < D_p < 50 nm), Large Aitken mode (50 nm < D_p < 100 nm), and Accumulation mode (100 nm < D_p < 1000 nm), respectively. Unlike traditional firework emissions, green crackers had a high UFP/N_{total} ratio of 0.72, including Nucleation mode-0.35, Aitken mode-0.30, and Accumulation mode 0.35, distinguishing it from other pre-and post-Diwali particle number size distribution-dN/dlogDp curves. These observations indicate that green crackers emit more particles with smaller diameters than traditional crackers. Recommendations for using green crackers for Diwali celebrations may be an option if lower size-diameter particle emission could be controlled by changing the material composition of the green cracker. More research studies need to be conducted to assess atmospheric emissions of green crackers and their health impacts to evaluate whether they are better or worse than traditional crackers.

Research studies have proved that smaller-sized particulate matter is more dangerous to human health when its particle number concentration is high. In the urban transport microenvironment, vehicular emission is a significant source of smaller size particulate matter. The Odd-Even scheme was implemented in Delhi in 2019 on vehicle movement to curb air pollution during the winter season. This study selected three locations, namely Najafgarh, Pitampura, and Panchkuian road, to evaluate the Odd-Even scheme 2019. This study revealed a reduction of 24 to 26 % in PM_1 particle number concentration along

with their particle number size distribution as QuasiUFP (24 to 25.4%), sub-fine (26 to 42.7%) and fine (16.5 to 24.1%) in particle number concentrations. This study also covers the coarse particle size, with the lowest reduction (7 to 10%) at all the selected locations. Car & taxi, on which Odd-Even scheme was effective, has shown a reduction of 12.6 to 26.4%.

TABLE OF CONTENTS

LIST OF FIGURES

LIST OF TABLES

LIST OF ABBREVIATION

ABL	Atmospheric Boundary Layer
ADMS	Advanced Dispersion Model Software
AERMIC	The American Meteorological Society/Environmental Protection Agency Regulatory Model Improvement Committee
AERMOD	American Meteorological Society/Environmental Protection Agency Regulatory Model
ANN	Artificial Neural Network
ANOVA	Analysis of Variance
APM	Particle Mass Analyzer
AQI	Air Quality Index
AT	Atmospheric Temperature
BAU	Business as Usual
BES	Best Estimate Scenario
BLPI	Berner Low Pressure Impactor
BRANN	Bayesian Regularized Artificial Neural Network
CCN	Cloud Condensation Nuclei
CERC	Cambridge Environmental Research Consultants
CFD	Computational Fluid Dynamics
CNAAQS	China National Ambient Air Quality Standards

CNG	Compressed Natural Gas
COVID	Coronavirus Disease
CPC	Condensation Particle Counter
CPCB	Centre Pollution Control Board
CPMA	Centrifugal Measurement of Particle Mass
CPSU	Central Public Sector Enterprises
CS	Condensation Sink
CSIR	Council of Scientific and Industrial Research
DELPI	Dekati Electrical Low-Pressure Impactor
DES	Discomfort Eye Syndrome
DLPI	Dekati Low Pressure Impactor
DMA	Differential Mobility Analyzer
DMPS	Differential Mobility Particle Sizers
DMS	Differential Mobility Spectrometer
DPF	Diesel Particulate Filter
DTC	Delhi Transport Corporation
EAA	Electrical Aerosol Analyzer
EC	Elementary Carbon
EDA	Exploratory Data Analysis
EDB	Electrical Diffusion Battery'
ELPI	Electrical Low-Pressure Impactor

EPA	Environmental Protection Agency
FIMS	Fast Integrated Mobility Spectrometer
FMPS	Fast Mobility Particle Sizer
FR	Formation Rate
GAM	Generalized Additive Model
GIS	Geographic Information System
GMD	Geometric Mean Diameter
GR	Growth Rate
HCV	Heavy Commercial Vehicle
HDV	Heavy-Duty Vehicles
HEI	Health Effects Institute
HOM	Highly Oxygenated Organic Molecules
ICP-MS	Inductively Coupled Plasma Mass Spectrometry
IGI	Indira Gandhi International Airport
IPCC	Intergovernmental Panel on Climate Change
KW-Test	Kruskal-Wallis Test
LCV	Light Commercial Vehicles
LDMA	Long Differential Mobility Analyzer
LDV	Light Duty Vehicles
LII	Laser Induced Incandescence
LPI	Low Pressure Impactor

LUR	Land Use Regression
MPPD	Multiple Path Particle Dosimeter
MSW	Municipal Sewage Treatment
NAAQS	National Ambient Air Quality Standards
NCR	National Capital Region
CSIR-NEERI	Council of Scientific and Industrial Research–National Environmental Engineering Research Institute
NJF	Najafgarh Road
NOAA	National Oceanic and Atmospheric Administration
NPF	New Particle Formation
OPC	Optical Particle Counter
OSPM	Operational Street Pollution Model
PAMS	Portable Aerosol Mobility Spectrometer
PANC	Panchkuian Road
PASS	Photoacoustic Soot Sensor
PITM	Pitampura Road
PMC	Particle Mass Concentration
PNC	Particle Number Concentration
PND	Particle Number Distribution
PNSD	Particle Number Size Distribution
PTEF	Polytetrafluoroethylene Membrane Filters

QCM-MOUDI Quartz Crystal Microbalance-Micro-Orifice Uniform Depositor Impactor

RDD	Respirable Depository Dose
RH	Relative Humidity
ROS	Reactive Oxygen Species
SAPE	Severe Air Pollution Episode
SD	Standard Deviation
SEM	Scanning Electron Microscope
SLPE	State-Level Public Enterprises
SMPS	Scanning Mobility Particle Sizer
SR	Solar Radiation
TCP-MS	Transmission Control Protocol Mass Spectrophotometry
TEM	Transmission Electron Microscopy
TEOM	Tapered Element Oscillating Microbalances
TVC	Total Vehicles Count
UFP	Ultra Fine Particulates
URMe	Urban Road Microenvironment
UT	Union Territory
VOC	Volatile Organic Compounds
VTDMA	Volatile Tandem Differential Mobility Analyzer
WARS	Wide Range Aerosol Spectrometer
WHO	World Health Organization

WRF	Weather Research Forecast
WS	Wind Speed
WSIC	Water- Soluble Inorganic Chemicals

CHAPTER-1

1 INTRODUCTION

1.1 Background

The term "particulate matter" in concern of air pollution and its quality is not a foreign word to most residents of megacities. Because significant unidirectional urbanisation, industrialization, and transportation in developing nation's megacity like Delhi, India have direct or indirect (short-term or long-term) health consequences on the populace (Chauhan et al., 2022; Goyal et al., 2020; Hakkim et al., 2022; Markandeya et al., 2021; Mishra et al., 2019). Particulate matter is primarily composed of liquid droplets (aerosol) and solid particles of varying sizes. Atmospheric particulate matter comes in various sizes, ranging from a few nanometers for molecular clusters to several tens of micrometres for windblown dust. Because of its irregular shape, diameter is frequently used for the size measurement of particulate matter (PM), referred to as 'Derived Diameter.' According to Dey et al. (2012), there are several distinct measures of particles size but generally two derived diameters are most used; aerodynamic and electrical mobility diameter. PMs became an immediate problem in the 1950s and early 1960s, raising concerns about PM in ambient air quality. Since the 1960s, there has been a rapid advancement in science, technology, and multidisciplinary engineering applications to reduce environmental pollution. PM in air pollution is becoming more visible to health workers, policymakers, legislators, and environmentalists due to its physicochemical properties and continuous improvement in measurement techniques, health risk assessment, and monitoring system (Franco et al., 2019). With the advancement of measuring technology, PM has a different size of characterization; $PM_{10} \leq$ 10µm (thoracic fraction), $PM_{2.5} \leq$ 2.5µm (respirable fraction), $PM_1 \leq$ 1µm (alveolar fraction), ultrafine particulate matter (UFP) ≤ 100nm, and nanoparticles ≤ 30nm. Most of researchers measure PM_{10}, $PM_{2.5}$, and PM_1 by mass concentration, but UFP and Nano particles are measured by particle number count (PNC) due to their negligible mass contribution. The Environmental Protection Agency (EPA) regularly determines the classification of PM and its standard by the National Ambient Air Quality Standard

(NAAQS). Although the EPA or any other agency has yet to adopt a standard for UFP, research communities are working trying to comprehend its origins, formation, and health impacts.

However, the air quality of Delhi over the last few years has reached a more critical level in the winter period and puts pressure on the policy of the concerned agencies (Balakrishnan et al., 2019; Dholakia et al., 2013; Gurjar et al., 2016; Mukerjee and Shukla, 2016). New Delhi, along with the National Capital Region (NCR), had an approximate population of 22.2 million in 2011 with a decennial increase of 7.96 % (Ministry of Home Affairs, 2011) and a projected vehicle population of 25.6 x 10^6 numbers with an annual rise of 5.83 % based on business as usual (BAU) estimates (Kumar et al., 2011), the second-largest urban area in the world. However, in addition to the unique geographical and landlock conditions in Delhi, the situation of winter and low dispersion worsens the ambient air quality (Chaudhari et al., 2016; Guttikunda et al., 2019; Kumar et al., 2017) and public health conditions (Health Effects Institute, 2019; Singh et al., 2019). For the reasons set out above, in November 2016, Kanawade et al. (2020) described as a Severe Air Pollution Episode (SAPE), the Air Quality Index (AQI) reached an abysmal level (Sati and Mohan, 2014) (Source -National Air Quality Index; https://app.cpcbccr.com/AQI_India/). Many experts have also named Delhi the "Gas Chamber" (Shukla and Anisha., 2016). The mean concentration of $PM_{2.5}$ in New Delhi before, during and after the SAPE were 142 µg/m^3, 563 µg/m^3 and 240 µg/m^3 respectively. The Government, central public sector enterprises and state-level public enterprises (CPSU and SLPE), and other concerned organizations have taken a variety of measures to reduce air pollution, such as a ban on old vehicles (Goyal and Gandhi, 2016; Kumar et al., 2017), potential construction activities, biomass burning, diesel generator, and Parali burning in and around Delhi (Srivastava and Jain, 2008). As vehicle emissions are one of the major sources of ambient air pollution in Delhi (Nagpure et al., 2013), the Government of Delhi introduced an odd-even scheme in which an odd and even number of vehicles are allowed on an alternative day basis. Many experts have documented the positive effects of this study and have suggested that it is not a permanent solution (Chandra et al., 2018; Kumar et al., 2017; Mishra et al., 2019; Mohan et al., 2017). A judiciary prohibition was also implemented on firecrackers for buying, selling and its bursting timing in and around the Delhi region in 2017 (TOI, 2016) Since; as mentioned

earlier, Diwali also comes in early winter from October to November. The burning of stubble in Haryana and Punjab is a significant precursor to the arrival of Delhi's airborne pollution in November (Jain et al., 2014). However, the magnitude of their contribution to Delhi air quality is still being monitored.

Regarding emission rates of PNC, whistling sparkles (during Diwali) show the highest PM emission rates (3.24×10^{10} particles per gram of burnt sparkler than 1.68×10^{10} particles per gram of sparkler burnt for low smoke sparklers) and also get quickly deposited in the respiratory system (Betha and Balasubramanian, 2013). To date, only a few studies have been conducted on particles of lower size (ultrafine and quasi-ultrafine particles), particle mass, and PNC (Apte et al., 2011; Arub et al., 2020; Gani et al., 2020, 2018; Saraswat et al., 2013a; Singh et al., 2019; Yadav et al., 2021, 2019a). For Delhi, Kumar et al. (2011) estimate the total PNC for vehicular emissions from 2010 to 2030 based on business as usual (BAU) and best estimate scenario (BES) as 1.37×10^{25} for 2010, which are expected to increase by four times in 2030-BAU but decrease by 18 times in 2030-BES due to fuel replacement for sustainability. Saraswat et al. (2013) calculated the PNC (10 nm to 1000 nm) 4×10^3 #/cm^3 with a geometric mean particle diameter of 43 nm in Delhi using a spatiotemporal land-use regression model for urban background PNC. However, PNC increased ~ 7 fold (280×10^3 #/cm^3) in the road microenvironment of Delhi (Apte et al., 2011). Apte et al. (2011) reported results from ~180 h of real-time ultrafine particle number concentration measurements inside a common vehicle, the auto-rickshaw, in New Delhi, India. Long-term PNC monitoring in Delhi and mass conversion with chemical characterization are covered in detail by Gani et al. (2019), Hagan et al. (2019), Arub et al. (2020b) and Bhandari et al. (2020). A study found a higher PNC (10 nm to 350 nm) concentration in 2018 than in 2017 during autumn (mid-September to November) in Delhi (Patel et al., 2021). More information on the formation, growth rate, and classification of ultrafine (few nanometres to several nanometres size range) particles in Delhi can be found in the study conducted by Gani et al. (2020), Kanawade et al. (2020) and Yadav et al. (2021). But still, there are few studies on the road microenvironment. Diwali celebration is also a significant source of short-term air pollution in Delhi, so there is a need to investigate the field of PNC of lower size particles, which have a higher potential for health effects (Schraufnagel, 2020). Quasi ultrafine Particle (qUFP) is 0.25µm > Dp < 0.50 µm range (Saffari et al., 2013). During

such events as Diwali (firecracker celebration), PNC has increased (Drewnick et al., 2006; Wehner et al., 2000). Betha and Balasubramanian (2013) found that fireworks emit 60 to 85 % ultrafine size range (below 100 nm) particles (Betha and Balasubramanian, 2013). During the spring festival season in China, the total PNC was found 42% and 57% with Aitken and accumulation mode, respectively, during firework emission (Yang et al., 2014). The average PNC of 2.5 x 10^4 cm^{-3} was reported during Spring festival fireworks. Wehner et al. (2000) detailed the PNC increase in the accumulation range (less than 10 µm) in the events of firework (Wehner et al., 2000).

Therefore, keeping this in mind, the monitoring and assessment of ultra-fine particulate matter in the road microenvironment and studies such as Diwali air pollution and Odd-Even scheme-II were carried out in this research study.

1.2 Objective of studies

This thesis entitled "Quantification, Formation and Growth Rate of Ultrafine Particles in Selected Microenvironment in Mega City, Delhi" has the following research objective.

- Quantification of UFPs classification based on selected microenvironment of Megacity Delhi.
- Investigating the fate and transformation of UFPs from roadway.
- Correlation of UFPs with NOx, and SOx under variable, meteorological condition.

1.3 Thesis organization

The thesis has been divided into five chapters. Each chapter has discussed different defined aspects of research objectives.

Chapter 1 is the thesis's introduction part, in which the air pollution and its specific episodes and causes are discussed, with some specific episodes such as Diwali air pollution and Odd-even scheme II. The introduction to the following section discusses the status of ultrafine particulate matter research in India, particularly in Delhi; this

establishes the writing platform for the subsequent literature review and results in thesis writing discussion.

Chapter 2 provides a comprehensive review of the available literature on the UFP in polluted urban areas. The review of literature is divided into subheadings such as UFP definition, size range, mode classification; UFPs in urban road microenvironment; UFP measurement and instrumentation at URMe; and UFP health impact. This chapter discusses the classification of UFPs in various modes based on particle size diameter, as well as the formation of new particles in the road microenvironment. It also discusses the effects of NPF and their roles under various conditions. The importance of instruments and their detection limits in determining particle number concentration cannot be overstated. As a result, this chapter also discusses the details of other available instruments for monitoring the road microenvironment. The health impact of UFP exposure in the road microenvironment has been addressed in the final section of this chapter, along with the expected route of penetration into the human body.

Chapter 3 represents the research methodology, that includes the location of the monitoring site and statistics on monitored data management. A new particle formation decision flow chart, as well as the equations and particle number size distribution model, have been presented.

Chapter 4 provides detailed results discussion of analysed data and figure with their interpretation. The first section covers the number concentration and new particle formation events near the road microenvironment in megacity Delhi, further subdivided into the temporal variation of particle number concentration and particle number size distribution which classify the NPF events (Figure 2 a and b). The subheading characteristic of nucleation events includes the discussion of the Growth Rate of particles (GR) and Condensation Sink (CS). The succeeding section covers the association between the particle concentrations, precursors, meteorological variables, and trace species (SOx, NOx) with the diurnal variation of particle number concentration in a different mode (Nucleation mode, Aitken mode, and Accumulation mode). The second section covers the investigation of the UFP and qUFP in detail at selected location during

a specific duration (pollution episodes- Diwali and Odd-Even scheme-II) in megacity Delhi.

Chapter 5 describes the detailed conclusions of the experimental investigations, and statistical analysis regarding PNC of UFP in the road microenvironment of Delhi, India. It also describes the effects of various parameters on the performance of the UFP's NPF. The fraction of ultrafine particles gradually decreased from ~0.70 ± 0.09 to 0.58 ± 0.16 during this period (Lockdown 2021), with the doubling of the accumulation mode particle concentrations (N_{accu}). This highlighted the effect of intensified anthropogenic activities on particle number concentrations.

CHAPTER-2

2 LITERATURE REVIEW

2.1 Introduction

In the recent year, there has been a growing consensus amongst health experts and researchers that, Particulate matters (PMs) are the principal pollutants and have a significant impact on human health (killing almost 9 million people per year worldwide (Loxham et al., 2020) and nearly 2.7% of global illness can be linked to respirable PM (Hetland et al., 2000; Junaid et al., 2018). The growing population, industrialization, and urbanization encourage people to live and work with and around the microenvironment of the road. Therefore PMs exposure study is essential because urban transport is an integral source of PMs (such as ultrafine particulate matter; UFP)(Ababio-Donkor et al., 2020; Agustian et al., 2020; CPCB, 2014; Health Effects Institute, 2019; IQAir, 2019; Iqbal et al., 2022; Kumar et al., 2010). The outdoor environment impacts indoor air quality, which increases the risk of small size PMs exposure, especially in developing countries like India (Beig et al., 2010) & China (Mazaheri et al., 2019). India has seven cities in the list of 10 most polluted cities globally (based on $PM_{2.5}$), as per the report published in 2019 (IQAir, 2019). Air pollution has become a persistent problem in Asian urban cities like Delhi. And Beijing having serious implications (directly as well as indirectly) on the health issues like arrhythmia, hypertension, reduced lung function, etc., (Delfino et al., 2005; Frampton et al., 2013; Schraufnagel, 2020). Small size particles have more penetration efficiency in human body but there's still, no universal standard for monitoring and regulation of fine or ultrafine particulate matter (Brugge and Fuller, 2021).

2.2 UFPs definition, size range and mode classification

PMs can be defined as a complex mixture of aerosols with extremely small particles suspended in air having complex chemical characteristics and showing a wide range of sizes from a few nanometres (molecular clusters) to several tens of micrometers (windblown dust) (Yadav et al., 2019b). It is mainly classified on the basis of the size of

their diameter (aerodynamic diameter, stroke's diameter, electrical mobility diameter (Kumar et al., 2010)) instead of chemical composition (due to the highly heterogeneous nature of their chemical composition). Recently, there has been unanimity of opinion amongst researchers all across the globe that the particulate matters in nano sizes (Dp < 1000 nm) and ultrafine range (Dp < 100nm) are having a significant vulnerable effect on the human health regarding carcinogenicity and cardiovascular diseases (Yadav et al., 2019b) as various studies have shown that particles in nano and ultrafine range can easily penetrate the respiratory system and transfer to the extra-pulmonary organs such as the central nervous system (Oberdörster, 2000; Oberdörster et al., 2005, 2004; Riesenfeld et al., 2000; Schraufnagel, 2020). Ultrafine particles (UFP; Dp < 100 nm) are ubiquitous in the urban environment (Kumar et al., 2014), contributing upto 70-80% of total particles number in the road microenvironment (Hussein et al., 2005) and owing to their adverse effects on human health (Araujo et al., 2008; Atkinson et al., 2010). UFPs are a sub-fraction of the currently regulated $PM_{2.5}$ (Although they have a negligible contribution to the total mass of $PM_{2.5}$, they contribute to up to 90% of the total PNC of $PM_{2.5}$ (Air Quality Expert Group, 2018; Hussein et al., 2005). Just like $PM_{2.5}$, UFPs also consist of a mixture of inorganic and organic solids and aerosol particles of various sizes, shapes, and compositions. In general respect, a UFP would have a diameter ~ 600 times smaller than a human hair (Ahmed, 2017). Although, their boundary conditions are not very well defined at the moment as there is no accord in the scientific community regarding the size range for UFP (Baldauf et al., 2016). Different studies have used different parameters for UFP size, for example, Sportisse (2007) defined as particles having size in between 10 - 510 nm, Chang et al., (2009) as size 10 -200 nm, Layale, (2014) as size < 300 nm, while Campagnolo et al., (2019) and Kumar et al., (2010a) as size < 100 nm. As negligible mass contribution of UFPs, it is measured based on 'Particle Number Count; (PNC)', It shows most of the UFPs almost 80 - 90 % fall below 100 nm (Kumar et al., 2010; Solomon, 2012). As per Air Quality Expert Group, (2018), UFP refer to PM that has at least one dimension less than 100 nm and this could be the reason why most of the researchers defined UFP as particles having an aerodynamic diameter of < 100 nm or 0.1μm and particles in the size range of 100 - 250 nm are as quasi-Ultra Fine particles (qUFP) (Saffari et al., 2013; Segalin et al., 2020). Thus they are classed by various researchers depending on their size mode (Yadav et al., 2019a). The modal classification

approach is predominantly used in aerosol research but has also been adopted in another research to classify anthropogenic UFP. The Particle Number Size Distribution (PNSD) of urban atmospheric UFP varies significantly depending on location, local weather conditions, and particle sources. The size distribution is typically composed of distinct particle modes formed by particles with similar formation and transformation processes or sources. Using this modal approach for UFPs aids in understanding their formation and interaction because particles of different modes (size) have distinct characteristics, formation mechanisms, sources, and interactions with other particles (Kumar et al., 2010). The UFP is classified into three modes, namely nucleation mode, Aitken mode, and accumulation mode. Nucleation mode includes particles with a size range of < 30 nm (Air Quality Expert Group, 2018); some studies have used different ranges for nucleation mode depending on the purpose of their studies and equipment use. Lingard, (2006) defined nucleation mode as particle size 3-20 nm (Lingard et al., 2006), while Charron et al. (2008) defined it as a particle having a size range 18-33 nm. Generally, natural NPF studies use a smaller size cut-off range (3 nm > dm < 30 nm) of nucleation mode to get more insight into its influencing components (Kanawade et al., 2020b). It is found that the nucleation mode particles dominate the PNC in the early stages of UFP formation; hence, their number concentration remains high near the source (Carpentieri et al., 2011; Kumar et al., 2021, 2018; Lingard et al., 2006). Also, as per (Kulmala et al., 2012; Yadav et al., 2019a), nucleation mode particles are further divided into small nucleation mode (<10 nm) and large nucleation mode (< 20 or 30 nm) (Joshi et. al., 2018). Aitken mode does not have a very defined boundary layer. It consists of a particle size having between nucleation mode and accumulation mode. Almost its higher size cut-off is 100 nm. Some studies have defined Aitken mode as a particle having a size of 20 nm-90 nm or as a particle having size 33 nm - 90 nm or 30 nm - 100 nm, (Air Quality Expert Group, 2018; Charron et al., 2008; Lingard et al., 2006). It acts as a transition mode between nucleation and accumulation mode. Due to this uncertainty, Aitken mode particles are generally not considered alone and termed with the accumulation mode as Aitken - accumulation mode particles. These particles are formed through nucleation and well as accumulation (Kumar et al., 2010). Traffic emission significantly affects the PNC of Aitken mode than particle growth in New Particle Formation (NPF) in URMe. UFP is a combination of nucleation mode and Aitken mode. Accumulation mode includes

particles having a size range of 90 -1000 nm (Kulmala et al., 2004; Lingard et al., 2006). Some studies have also defined accumulation particles as particle size 90-120 mm (Charron et al., 2008). Accumulation mode particles are formed when the nucleation mode particles and Aitken mode start accumulating over larger particles (mainly soot). As a result, accumulation mode is also referring as soot mode particles. Accumulation mode particles are also released directly into the air as the by-product of fuel burning in the internal combustion engine (Kumar et al., 2010). In a broader sense, we can say that nucleation and Aitken mode differ in concern of Urban pollution oriented to new particle formation (i.e., for nucleation mode, lower cut diameter varies from 5 to 10 nm (Pirjola et al., 2015) and upper cut diameter 25 to 30 nm (Lingard et al., 2006) for urban pollution). The largest mode, the coarse particle mode, contains typically relatively large mechanically generated particles (with a diameter typically larger than 1 μm). The accumulation mode of particle size distribution (100 nm > diameter > 1 μm) is linked especially with aged, long-range transported aerosol and soot particle emissions.

Since measuring "true" UFP often requires expensive instrumentation, many studies use total particle number concentration (PNC, e.g., as measured with a condensation particle counter) as an alternative metric. There is no established reference method for measuring PNC and there can be substantial differences between instruments using different operating principles. For example, differences in the lower cut point can lead to higher UFP concentrations when measuring total particle counts with a condensation particle counter (CPC, lower cut point <10 nm) than with differential or scanning mobility particle sizers (DMPS or SMPS, cut point generally 10–20 nm) (Morawska et al., 2008). On road microenvironment <10 nm has 3.4 higher to >10 nm of PNC of UFP. There is also insufficient epidemiological data to determine whether "true" UFP, PNC, $PM_{0.1}$, or other metrics are most connected to health.

2.3 UFPs in urban road microenvironment

The PNC of UFP in URMe near the roadway is a combination of ambient background concentration and vehicle emissions. UFP concentration near roadways depends not only on vehicle emission but also depends on nearby emission sources that produce distinct ambient background concentrations (Li et al., 2018). In urban areas, several combustion

sources (engines, biomass burning, power generation plants, industrial facilities) are directly emitting UFP into the atmosphere and, in addition, the gaseous emissions from the same sources can participate in atmospheric UFP formation (Giechaskiel et al., 2014; Kumar et al., 2018, 2015, 2014a, 2013b, 2010; Pacheco et al., 2017; Rönkkö et al., 2017). The number of road vehicles in Beijing (China) increased from about 1.5 million in 2000 to over 5 million in 2014 and in Delhi (India), it is expected to increase from 4.74 million in 2010 to 25.6 million by 2030 (Kumar et al., 2018, 2017). URMe's UFP can be formed either via nucleation in the URMe atmosphere known as secondary UFP or be directly emitted to the URMe atmosphere known as primary UFP (Charron and Harrison, 2003; Shi et al., 1999b). Particularly in traffic-influenced environments, the primary UFP concentrations can be high, reaching even concentrations higher than 10^5 cm^{-1} (Al-Dabbous and Kumar, 2015; Kittelson et al., 2004), but its number concentration in the tailpipe can be as high as 10^7–10^9 cm^{-1} (Kumar et al., 2012; Rönkkö and Timonen, 2019). Although natural NPF can reach to 10^3-10^4 cm^{-1} PNC with high Condensation Sink (CS) and Growth Rate (GR) values in the polluted urban environment (Kerminen et al., 2018; Kulmala et al., 2017; Nieminen et al., 2018; Yu et al., 2017; Zhang et al., 2021). UFP's number concentration in URMe varies from Asia > Europe > USA as 6.65 ± 2.88 x10^4 cm^{-3}, 4.81 ± 2.61 x 10^4 cm^{-3} and 3.78 ± 2.01 x 10^4 cm^{-3} respectively with overall number concentration of 5.29 ± 2.74 x10^4 cm^{-3} in URMe (Kumar et al., 2018). UFP contributes 80 to 90 % number concertation in the urban environment (Kumar et al., 2010) and people residing in Asian, European, and North American cities spend similar sums of time on travel 7-10 percent of the day. But in that case in Asian cities, it may increase due to urbanization and people who live in the densely populated area near and around the road. Kumar et al. (2018b) elucidate that the average exposure to outdoor UFPs in Asian cities is about four times larger than that in European cities but impacts on human health are largely unknown. Congested traffic, a common phenomenon in Asia's metro cities, can increase PNC on roads in surrounding areas (Berghmans et al., 2009; Colvile et al., 2001; Goel and Kumar, 2016; Patton et al., 2016) when vehicles are constantly accelerating and decelerating (Goel and Kumar, 2015), because immediate mobile origin pollutants do not spread widely, and open modes of road transport, along with closed modes, are the most popular ways of Asian URMe (Arphorn et al., 2018; Kumar et al., 2015, 2013a; Rivas et al., 2017; Zuurbier et al., 2010). There is a limited research paper

available on primary UFP in the Asian transport microenvironment as Apte et al., 2011; Both et al., 2013; Kaminsky et al., 2009; Rakowska et al., 2014; Tan et al., 2017; Tsang et al., 2008; Yang et al., 2015. On the other side Natural NPF (known as secondary formation or in-situ formation) occurring in traffic influenced polluted area are significantly influencing the PNC of UFP by combining with Primary UFP (Belkacem et al., 2020; Chu et al., 2019; Lv et al., 2020; Rönkkö and Timonen, 2019; Sharma et al., 2012). Pre-existing particles, precursor gases and local meteorological parameter have significant level effect on the number concentration and particle dynamics & its transformation of both natural NPF and vehicular emission of UFP (Brines et al., 2015; Yu et al., 2017; Zhang et al., 2021).

The key objective of this literature is to investigate the current knowledge of ultrafine particles present, especially in Asia, those emitted by on-road automobiles and by new particle formation (NPF) in the Urban Road Microenvironment (URMe). Asian URMe may become progressively exposed in the future, as the number of road-based vehicles powered by rising populations and economies grows. This article is majorly divided into three part; 1) UFP in URMe, 2) UFP measurement at URMe, 3) UFP and health effect.

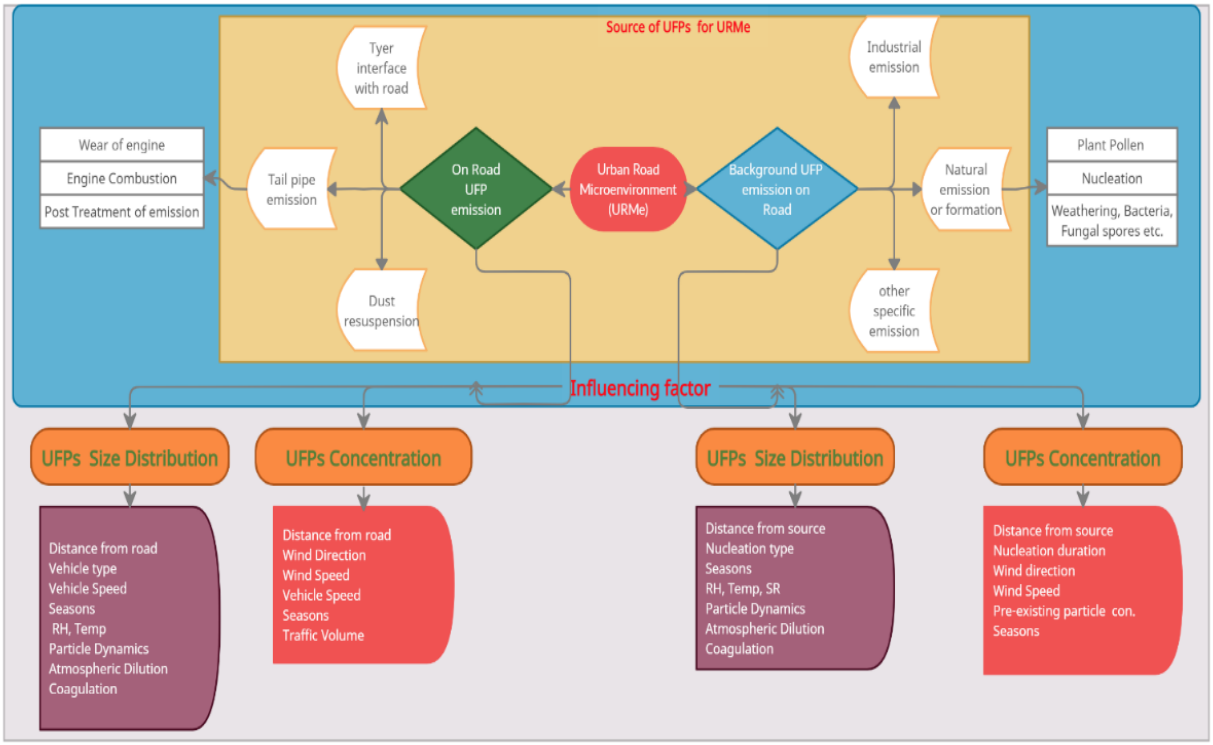

Figure 2.1: Overview of sources of UFPs in URMe

UFP in URMe denotes additional categories of vehicular emissions and the factors that influence them. This does not, however, cover the vehicle type, on-board tail pipe emissions, or the ambience PNC of the vehicle cabin and other categories in URMe, such as NPF or Natural UFP, with their influencing factors.

Based on Figure 2.1 UFP emission and its particle size distribution in urban transport microenvironment, URMe includes two broad categories: 1) on road UFP emission, 2) background UFP on the road. Tire interface with the road, Tail pipe emission, & dust resuspension are three major components of on-road UFP emission. Tire interface with the road depends on road conditions, materials, vehicle speed & tire compositions, while in dust resuspensions, except tire composition, include all characteristic mentioned above. Although more studies from both these sources have been done in Asia on the tailpipe emission, it is also one of the major sources. Therefore, to get insight into tail pipe emissions, it is subcategories into the following: 1) Wear of engine in which during wear and tear of running engine's component contribute UFP, 2) Engine combustion, it includes fuel & additive emission during combustion in the engine, 3) post-treatment of emission in which catalytic converter and its efficiency affect the concentration of UFP through tailpipe exhaust.

In the case of background UFP in urban road microenvironment, its sources vary from location to location, such as industry-specific emissions, demographic & geographic-specific emissions. Moreover, some emissions are found everywhere, like nucleation of new particle formation, which occurs throughout the photochemical reaction in ambient air with the balance between particle GR, CS of particles and the presence of the pre-existing particulate matter. This literature attempts to approach engine combustion and new particle formation clearer, highlighting the factors influencing the size distribution and concentration of ultra-fine particulate matter on Asian URMe.

2.3.1 URMe UFP in natural environment

As shown in Figure 2.1, the variation in the source of the background UFPs depends on anthropogenic activities, effects of geographical location and the relationship of the origin of incoming air masses with meteorological are also considered around the URMe (Bousiotis et al., 2019; Deng et al., 2020; Kanawade et al., 2020a; Zhang et al., 2021).

New particle formation (NPF) start from molecular clustering, which occurs globally natural almost everywhere and all the time in the atmosphere (Kulmala et al., 2017) except in some pristine forest environment (Lee et al., 2016; Neitola et al., 2011), are one of the significant sources among those background sources in URMe. SO_2/H_2SO_4, NH_3, amines, VOCs/HOMs, and NOx as gas compounds or precursors significantly affect NPF under relevant atmospheric conditions. Meanwhile, many of these compounds are pronounced during pollution episodes in URMe. NPF in polluted urban areas has been recognized since the 1990s (Hämeri et al., 1996), but still requires extensive study in different environmental conditions, especially in relation to the Asian polluted environment (Bousiotis et al., 2019; Chu et al., 2019; Kulmala et al., 2017; Nieminen et al., 2018; Vu et al., 2015). Because the contributing vapors and nucleation mechanisms vary with location and with atmospheric conditions even at the same location (Chu et al., 2019) and Asian countries like India have minimal numbers of work on it. NPF (known as the in-situ or secondary formation of UFP), growing either by homogeneous or heterogeneous nucleation under more specific atmospheric conditions (Kerminen et al., 2018; Kulmala et al., 2017, 2012), refers to the conversion of atmospheric gaseous precursors due to nucleation and subsequent growth process via physicochemical interaction, which involves the following steps: 1) chemical reactions in the gas phase to produce low-volatile vapor(s) of low volatility, 2) cluster formation from gaseous vapor, 3) nucleation or barrierless nucleation, 4) activation of clusters with the second group of vapors to form a critical nucleated particle, and 5) subsequent condensational growth of nucleated particles to detectable sizes or even larger (Chu et al., 2018; Kerminen et al., 2018; Kulmala et al., 2017; M Kulmala et al., 2004; Nieminen et al., 2018; Vu et al., 2015). Particle formation rate (FR), growth rate (GR), condensation sink (CS), coagulation sink (CoagS), condensation vapor concentration (Cv), and source rate of condensation vapors (Q) are the important variables for establishing the theory of any nucleation process in any environment (as URMe) (Chu et al., 2018; Kerminen et al., 2018; Kulmala et al., 2017; Kulmala et al., 2004; Nieminen et al., 2018; Vu et al., 2015) (Table 2.1). Unfortunately, despite having no specific mathematical model and unique definition in the context of NPF, (Dal Maso et al., 2005; Kulmala et al., 2012). NPF classification with identification and particle growth in clean and polluted environments in Asia and Europe is highly compliant (Zhang et al., 2021). The appearance of a

distinctly new mode of particles with a diameter of less than 20 nm and subsequent steady growth of the particles over several hours consecutively indicates that a characteristic NPF event showed a "banana" shaped aerosol growth, a distinctly new mode of particle number distribution (Dal Maso et al., 2005; Kulmala et al., 2012). Such events are usually caused by low pre-existing aerosol concentrations and high photochemical production of precursor vapors. However, in urban environments, NPF can still occur at high aerosol concentrations due to less efficient nanometer scavenging of clusters and/or the rapid growth of those clusters (Kulmala et al., 2017; Peng et al., 2017).

Table 2.1: Important variable for the NPF events (Chu et al., 2018)

Parameter	**Description**	**Calculated from**
FR	Formation rate of particles ($cm^{-3}s^{-1}$)	Temporal variation of particle size distribution
GR	Growth rate (nm/hr)	Temporal variation of particle size distribution
CS	Condensation sink ($\#S^{-1}$)	Particle Size Distribution
CoagS	Coagulation sink	Particle Size Distribution
Cv	Condensation vapor concentration	Growth rate of particle
Q	Source rate of condensation vapors	Condensation sink and Condensation vapor concentration

For many years, NPF events were thought not to take place in heavily polluted urban areas (i.e., URMe) as the effect of increased condensation sink was considered crucial in suppressing the formation and growth of new particles because NPF theory was based on the European country clean environment (Kerminen et al., 2018; Kulmala et al., 2016,

2014; Manninen et al., 2010; Mönkkönen et al., 2005; Nieminen et al., 2018). Recent long-term analysis has shown (i.e., China and India) that this is not the case and nowadays an increasing number of studies reported the occurrence of NPF events in polluted urban areas (Deng et al., 2020; Kulmala et al., 2017; Vu et al., 2015; Z. Wang et al., 2017; Yu et al., 2017; Zhang et al., 2021). Moreover, the high intensity of URMe emissions in China & India, compared to the dominant role of biogenic precursors at cleaning sites, has led to a greater diversity of pollutant species involved in the nucleation of NPF and subsequent development (Rönkkö and Timonen, 2019). Now China and India have become hotspots of NPF events (Yu et al., 2017).

For particle size distribution and its evolution in the context of NPF in most URMe of China and India, particle measurement did on particles larger than 10 nanometers, while nanoparticles 3 to 10 or larger nm have also been used in recent years. But these studies are found more in China than in India (Chu et al., 2019; Kanawade et al., 2020b; Z. Wang et al., 2017; Yu et al., 2017). There is a chance that the NPF growth rate may look like a vehicular emissions of sub 10 nm particles event and thus underestimate the NPF (Hietikko et al., 2018; Rönkkö et al., 2017; Rönkkö and Timonen, 2019). Compared to photochemically induced nucleation (Brines et al., 2015, 2014; Dall'Osto et al., 2012; Hama et al., 2017), attributed a greater portion of nucleation mode particles to vehicular emissions. To avoid the overestimation of NPF in URMe, one should consider the particle size (Hofman et al., 2016), the ratio of number concentrations of in the nucleation-mode particles to those of fine particles (Jung et al., 2013; Peng et al., 2017), the time of duration of NPF events (Zhu et al., 2017), and the correlation of the particle number concentration with other gaseous pollutant concentrations and meteorology conditions (Wang et al., 2014). But a recent observation showed that nanoclusters aerosol particle originating from traffic is notable in urban air at size 1.3–3.0 nm, which may pose new concerns regarding the origins of aerosol nanoclusters in semi-urban roadside environments (Rönkkö et al., 2017). In URMe, the biggest challenge in identifying NPF is the interference of primary emitted particles from newly combustion sources (Chu et al., 2019). In the first 1-2 second of exhaust cooling and dilution, for example, the formation and quick growth of vehicular particles always result in a 10 - 20 nm nucleation mode (Banerjee and Christian, 2018; Lee et al., 2015; Vu et al., 2015). Particularly if the instruments do not have a low particle size detection limit (such as particles larger than

10 nm). In that case, particle growth is necessary to distinguish an NPF from particles associated with local emission sources as traffic (Chu et al., 2019). Wang et al. (2014) show the difference between spikes of PNC, which are generally associated with combustion emissions and photochemically indued NPF.

2.3.1.1 Important factors responsible for formation of UFP

In different environments and seasons, NPF events vary with different frequencies ranging from less than 10% to more than 50% observed (Chu et al., 2019), due to the variation of CS value, condensable vapor concentration, Temperature, RH, air masses load, solar radiation, and a photochemical level process, wind properties, and anthropogenic emissions (Shen et al., 2011; Wu et al., 2007; Yue et al., 2009). Literature reviews summarise the recorded NPF event frequencies in China and India based on season, observation site type, and area, but ignoring observations of too short time, such as less than one month in China, but including the shot-term observation in India due to a smaller number of studies. There is no significant difference between China region's urban, suburban, and rural sites. The clean environment shows fewer NPF frequencies, and while the rural and urban site of the same region, NPF frequencies are higher in the urban site (Liu et al., 2014; Yue et al., 2013). Despite the similar frequencies of NPF in the context of the polluted area, higher FR (up to 220%), GR (up to 50%) and CS (up to 60%) were observed at the urban site than corresponding background site (Wang et al., 2013a; Yue et al., 2009). As a result, compared to rural areas, the higher pollution level in Chinese cities usually results in stronger NPF (Chu et al., 2019; Kanawade et al., 2014; Siingh et al., 2013). In Delhi, all monitoring is usually performed in the winter season; only one study, April-May analysis, was aimed at night-time new particle formation. Among them, the minimum occurrence of NPF events ranges from 30 % to 87 % at most, but most of them have a period of monitoring of less than one month. Kanawade et al. (2020) reported that 82% particle burst occurs, including NPF, in which Aitken mode contributes > 50% particle fraction in a condition of relatively high concentration of pre-existing particles. Long-term observation of ambient air pollution, meteorological parameters, and nanoparticles, and their precursors, is required to identify the primary factor affecting NPF events and their frequencies in URMe. Such as, Cai et al. (2017) found that the frequency of NPF events in Beijing was fundamentally determined by the

Fuchs surface area (a representative coagulation scavenging parameter based on kinetic theory and is proportional to CS) and Jayaratne et al. (2017) mentioned that the Fuchs' surface area has a strong correlation with the concentration of $PM_{2.5}$ mass, and no NPF event observed when the daily mean concentration of $PM_{2.5}$ was greater than 43 μgm^{-3} in Beijing in the winter of 2015. Despite all these facts coming to light, we cannot say that it is equally applicable to all NPF events because all these parameters are interconnected in a very complex manner. The simplification of the effect of anyone is not easy, such as the precursor vapors and photochemical activity, which may also play an essential role in driving NPF (Gong et al., 2010). In addition, occurrences of NPF were not very responsive to levels of common gas pollutants, including O_3, SO_2, NO_2 in China, in addition to the condensation sink (An et al., 2015; Zhu et al., 2013). However, in some cases, the CS or the average coagulation sinks during NPF events were not significantly lower compared to other times when new particles were not formed, indicating that other factors. Kanawade et al. (2020) mentioned that ammines influence NPF in Delhi, and Kanpur, India. SO_2 does not appear to be a significant limiting factor for NPF. Although, in heavily polluted conditions, there is enough SO_2 for NPF to occur. A similar conclusion could be drawn for sulfuric acid in a polluted urban area. Furthermore, NPF patterns may differ depending on whether there is a lot of SO_2 or not. High concentrations of SO_2 in polluted air masses typical of urban (heavy traffic emission) or power-plant plumes resulted in stronger nucleation but slower particle growth, despite similar CS with lower SO_2 concentrations (Gao et al., 2009; Gong et al., 2010; Herrmann et al., 2014; Qi et al., 2015; Young et al., 2013; Yu et al., 2016; Yue et al., 2010). In context to the seasonal effect on the NPF event, spring has high frequencies. It may be due to low CS, RH, Temperature, and high solar radiation. But in the case of the Indian seasonal effect on NPF events in URMe, there is a lack of long observation. The lowest NPF events in the North China Plain in the summer could relate to high RH and stagnant and contaminated air masses causing high CS. Usually observed low frequencies of the NPF event in winter could be due to the weak solar radiation and the typically high pollution levels at that time of year (Qi et al., 2015; Wu et al., 2007; Zhu et al., 2013).

Different loads of air masses from different directions can also affect NPF frequencies in URMe (Wu et al., 2007). The conventional concept of clean air masses with low CS makes that direction has had higher NPF frequencies(An et al., 2015; Peng et al., 2017;

Zhu et al., 2013). Still, NPF has been observed especially under the low-wind-speed conditions during the summertime in Beijing, when the wind changes its direction toward more polluted areas (Zhang et al., 2011). There is another example of it in different regions (Guo et al., 2012; Lv et al., 2018; Wang et al., 2013b). Qi et al. (2015) found the lower FR in clean air masses and higher GR in a polluted air mass plume direction in the duration of NPF. However, wind direction did not significantly influence the NPF frequency when the study occurred inside the densely populated urban area like Delhi for a short period on a small scale. As the above-mentioned influencing factor and their sources are similar and connected in URMe, getting one of the influencing factors is not so straightforward when other factors work like OH radicals and topography (Chu et al., 2019). An additional challenge is the lack of long-term specific studies in URMe.

In context to FR, which is categorized based on of particle size; “real FR” is considered a critical cluster that occurs down to a particle diameter of about 1.5 nm and "apparent FR," which is inferred indirectly only by measuring the particle formation rate at some larger size in most NPF studies (Kerminen and Kulmala, 2002; Lehtinen et al., 2007). Due to measurement limitation in India and China, FR is mostly calculated based on of ‘Apparent FR’. FR can range from less than 0.1 cm^{-3} s^{-1} at particle sizes larger than 10nm to about 10^3 cm^{-3} s^{-1} at particle sizes below 2 nm and it can differ by 2 orders of magnitude due to the different environmental conditions at a certain particle size (Chu et al., 2019). For example, many studies reported the FR of 3nm particles ranging from less than 1 to several tens of cm^{-3} s^{-1} (Chu et al., 2019).

As mentioned earlier, FR (inversely proportional to CS) usually shows a higher value like NPF frequencies in a polluted urban environment than in the regional site despite having a high CS value, indicating much more abundant precursors for NPF (Wang et al., 2013a). Recently, Yao et al., (2018) reported a long-term continuous observation for NPF in urban Shanghai and observed 1 to 2 orders of magnitude higher FR than typical values in a clean atmosphere. Up to now, there are still quite limited investigations into the relation between FR and organics (VOCs/HOMs), NH_3 and amines in China and it is undoubtedly crucial for a better understanding of NPF in polluted areas(Chu et al., 2019; Yao et al., 2018, 2016; Zheng et al., 2015).

In the case of GR, it is a critical factor for NPF in URMe to distinguish between nucleation mode particle burst and environmental NPF. There are several methods for calculating GR, which may result in differences in GR estimation. Aside from that, GR can range from a few nanometers to several tens of magnitudes, as shown in China and India at 10 to > 20 nm/hr (Chu et al., 2018; Kanawade et al., 2014). More abundant condensing vapour in polluted cities raises GR on the urban side compared to the regional site. Still, there is little data on sulphuric acid and low volatile organic vapour concentration in India and China that could explain GR more insightfully about the influencing factor. With higher photochemical and biological activities, the summer season induces a higher concentration of condensable vapour, resulting in a higher rate of GR than in other seasons (Qi et al., 2015; Shen et al., 2011; Zhu et al., 2013). In general, sulfuric acid is thought to be the most important contributor to the growth of newly formed particles (< 3 nm diameter particles), but its percentage contribution became less and less important in the growth of larger particles (> 10 nm diameter particles). According to some studies, H_2SO_4 had a negligible effect on the growth of particles larger than 10 nm (Liu et al., 2014; Meng et al., 2015). According to Yu et al. (2016), high concentration of extremely low-volatility organic compounds is the key factor leading to a maximum in GR for very small particles (1.4–3 nm) in urban Nanjing. A model simulation study on NPF in Beijing also confirm that only a small fraction of organics contributes to the formation of new particles, and that these organics are primarily O_3 initiated (Wang et al., 2013a).

Indeed the observed urban NPF is a balance between the outcome of the competition of FR & GR (source, i.e., sulfuric acid and highly- oxidized organic compounds) and CS (sink, i.e., pre-existing particle load) (Kerminen et al., 2018; Kulmala et al., 2017; Z. Wang et al., 2017; Zhang et al., 2021). In the polluted urban area, CS can also range from 0.02 to 0.07 /sec (Kulmala et al., 2005; Zhang et al., 2021), but in some cases, it reaches up to 0.1 /sec (Xiao et al., 2015). Existing findings support this expectation, as the average CS value is seen as being lower at NPF case days at most measurement sites relative to non-event days (Asmi et al., 2011; Birmili et al., 2003; Dal Maso et al., 2007; Kanawade et al., 2014; Kerminen et al., 2018; Salma and Németh, 2019; Wu et al., 2007). Kanawade et al. (2014) stated that Kanpur has less PNC than Pune, but, in the case of condensation sink, it shows vice versa because the large particle size of Kanpur (mean

particle mode diameter ~1.8 factor greater than Pune) resulted in higher condensation sink (CS). In severely polluted environments, amines and strongly oxidized organic compounds also play an essential role in NPF cases (Kanawade et al., 2020b). The high CS in urban ensures that gaseous precursors, clusters, and freshly formed particles experience a high scavenger loss rate. Based on pollution load, the CS value in URMe can be placed in the category of 'polluted type' because, according to Wang et al. (2017), the NPF event has been categorized into two classes based on the CS value; 'Clean type' (~0.014 S^{-1}), 'Polluted type' (~0.038 S^{-1}).

The ratio of particle scavenging loss rate over condensational growth rate, which is proportional to the ratio of CS to GR, was used as a criterion to predict the occurrence of NPF events (Kuang et al., 2010; McMurry et al., 2005). It turned out that NPF frequently occurred in megacities in China when the ratio of CS (10^{-4} s^{-1}) to GR (nm h^{-1}) was above 200, whereas it only occurred when this same ratio was less than 50 under clean and moderately polluted conditions (Kulmala et al., 2017). Most of the observation data reported ratios of CS (10−4 s−1) to GR (nm h−1) between 200 and 500, while a few were less than 200 but consistently higher than 50. More importantly, many studies reported that NPF took place with this ratio higher than 500 at urban and suburban sites. There are several possible reasons for the higher threshold ratio of CS to GR in a highly polluted environment, including the overestimation of particle losses due to assuming a coagulation sticking probability of 1, the underestimation of GR in the sub-3 size range, and also unidentified nucleation and growth mechanisms relevant to a polluted atmosphere (Kulmala et al., 2017; Yu et al., 2017). (Peng et al., 2017; Wu et al., 2007; Yu et al., 2016) found that NPF mainly occurred when the PM2.5 concentration (CS) and gas pollutant concentrations, such as NO_2, CO and SO_2, were both low. The NPF leads directly to a burst of small nanoparticles and prominently increases the particle number concentration. While NPF usually tends to occur on clean days with low CS, particle number concentrations are generally much higher on NPF event days than on non-event days (An et al., 2015; Shen et al., 2016). An et al. (2015) observed that NPF events significantly affected Aitken- and nuclei-mode particle surface and volume concentrations, while limiting contributions to accumulation- and coarse-mode particles.

2.3.2 URMe's from traffic microenvironment

Studies have shown that when compared on or in the vicinity of roadways, the concentration of UFP is one order of magnitude higher than the ambient level (Westerdahl et al., 2005). People are exposed to UFP while using public transportation, but also while waiting, walking on pedestrians, and living in flats, homes, shops, and other public places near congested traffic roads. All these factors have put UFP under deep scrutiny. According to Rönkkö and Timonen, (2019), traffic generated UFP by combustion process or non-exhaust (such as break wear) is divided into the following categories of source process; 1) primary UFP formed at high temperature, 2) delayed primary particles formed as gaseous compounds nucleate during the cooling and dilution process and 3) secondary UFP formed from gaseous precursors via the atmospheric photochemistry.

URMe's primary UFP with a high PNC is generally generated in hot and undiluted vehicular emission (Giechaskiel et al., 2014; Rönkkö et al., 2017). As per their formation mechanism and physicochemical characteristic can group into two particles size mode; 1) Core particles (having particles mean diameter < 10 nm); 2) Soot particles (having particles diameter >10 nm with particles mean diameter 30 to 100 nm)(Alanen et al., 2015; Harris and Maricq, 2001; Heikkilä et al., 2009b; Lähde et al., 2009; Rönkkö et al., 2007; Rönkkö and Timonen, 2019; Sgro et al., 2012). Core particles with the tendency of particle growth into larger size in a tailpipe and especially during cooling and dilution of the exhaust, are mostly non-volatile compounds and consist of amorphous carbonaceous compounds and metallic ash compounds from fuel and lubricant oil (Alanen et al., 2015; Fushimi et al., 2011; Harris and Maricq, 2001; Heikkilä et al., 2009b; Lähde et al., 2014, 2009; Rönkkö et al., 2007; Seong et al., 2014; Sgro et al., 2012). Compared to the nanoparticles of this range (< 10 nm mean diameter) formed through semi-volatile or volatile precursors, core particles have more lifetimes in the atmosphere and significantly in the human body (Fushimi et al., 2011). Although core particles' physicochemical characteristics and their health effects did not solve completely if the core particle escapes from particle growth into a larger size in the atmosphere, is inhaled, then deposits into the upper human respiratory airways (Alanen et al., 2015; Rönkkö et al., 2007; Sgro et al., 2012). Soot particles, which aggregate like

chain or spherical, consist mainly of elemental carbon and some metallic compounds (Fujitani, 2013; Harris and Maricq, 2001). Fuel's choice, injection mechanism, and other factors affect the soot particle number concentration. For example, the technological improvements that decrease soot particle concentrations increased the emissions of small core particles in several studies on diesel engine exhaust particles (Fujitani, 2013; Harris and Maricq, 2001; Karjalainen et al., 2016; Lähde et al., 2011; Nousiainen et al., 2013; Rönkkö et al., 2014, 2007). Primary UFP (hot and undiluted exhaust) are affected by the driving conditions of the vehicle and the technological parameters used in vehicles, e.g., the fuel injection type, fuel injection timing and pressure (Lähde et al., 2011), use of exhaust gas recirculation (De Filippo and Maricq, 2008), fuel properties (Fushimi et al., 2016; Heikkilä et al., 2009b), lubricant oil properties and exhaust after- treatment such as diesel oxidation catalyst, selective catalytic reduction (Karjalainen et al., 2012), diesel particulate filter (DPF) (Lee et al., 2015), and partial DPF (Heikkilä et al., 2009a). For example, Higher fuel injection pressures and metallic additives of lubricant oil have been observed to increase the concentrations of core particles (Rönkkö and Timonen, 2019). Besides these UFP particles, when the initially hot exhaust is diluted and cooled in the atmosphere, the hot and undiluted engine exhaust contains gaseous compounds that appear to condense on particle surfaces or nucleate and form new particles due to sudden decrease in the pressure and expansion. Rönkkö and Timonen (2019) considered it as "Delayed particle formation," which occurs within 1 to 3 seconds from tailpipe to road environment (Banerjee and Christian, 2018). This is also known as the stage - I which modifies the exhaust particle size distribution and increase the PNC (Banerjee and Christian, 2018; Pirjola et al., 2015). In this stage, sulphuric acid formed through the oxidation of sulphur from fuel and lubricating oil is a key component of UFP and more details about this stage formation mechanism can be found in the review of Banerjee and Christian (2018). Interestingly, oxidative exhaust after treatment device of tailpipe increases the UFP formation and number concentration of this stage because it oxidizes the engine out sulphuric dioxide to sulphuric trioxide that reacts with exhaust's water and forms gaseous sulfuric acid (Arnold et al., 2012; Casati et al., 2007; Pirjola et al., 2015; Rönkkö et al., 2006; Vehkamaki et al., 2003). The diameter of the UFP formed in stage-I is usually in the range of 3-30 nm. Most particles formed during the I stage fall under nucleation mode (Banerjee and Christian, 2018). Fushimi et al. (2011) and Karjalainen

et al. (2016) elucidated that the low volatile organic compound from fuel and lubricating oil significantly influence of UFP formation. Although the chemical composition is uncertain, the UFP formed at this point is considered a liquid-like particle, more effectively dissolved than a solid UFP in the respiratory tract and its epithelium, and can evaporate or even disappear when the particles are aged in the atmosphere (Rönkkö and Timonen, 2019). Therefore fuel, lubricating oil sulfur, exhaust after-treatment devices, climatic conditions, and existing ambient particle affects its formation. Such as cold weather favors more particle formation in atmospheric vehicle exhaust. More detail can see in (Banerjee and Christian, 2018; Kumar et al., 2018; Morawska et al., 2008; Pirjola et al., 2015; Vehkamaki et al., 2003) and Table 2.2.

Stage II occurs when UFP leaves the vehicle wake and gets mixed into ambient atmosphere (Banerjee and Christian, 2018; Chang et al., 2009). In this stage, the UFP formed in stage I undergo further dilution and they began interacting with one another undergoing coagulation and adsorption as they grow in size. In this stage, particle numbers decrease slightly but their size continues to grow (Banerjee and Christian, 2018; Chang et al., 2009; Pirjola et al., 2015). The important chemical interaction in this stage involves condensable organic particles, non-volatile organics particles, and black carbon soot particles; those particles interact with the particles in stage I and further help in their size growth by providing them nuclei and acting as coagulant agents. The UFP grows up to a size of 300 nm. The growth rate is vastly affected by ambient environmental conditions like relative humidity, temperature etc. (Banerjee and Christian, 2018; Kumar et al., 2010). According to Al–Dabbous et al. (2017), fresh traffic emissions (range < 10 nm) and aged traffic emissions (range 10 to 30 nm) contribute 40 % and 27 % to the PNC in URMe, while industrial and regional emissions contribute 9 % respectively. A typical traffic emission shows a bimodal pattern in PNSD of UFP; the first peak is 5 to 12 nm (fresh traffic emission), and the second peak is ~60 nm (aged traffic emission (Rönkkö and Timonen, 2019). Rönkkö and Timonen (2019), depicted the difference in peaks among tailpipe exhaust particles, roadside exhaust particles and atmospherically aged exhaust particles. Due to variations in the structure of fleets, air quality management systems, route design, and driving behaviour, fuel & vehicle standard, and local meteorological parameter among the countries and their cities, UFP's PND and PNSD

can’t be generalized because there is no universal guideline and standard for it, unlike other criteria pollutant.

Table 2.2: Factor affecting UFP formation

Parameter	**Change in parameter condition**	**Effect on UFP formation**
Fuel Sulphur content	Increase	Increase the PNC and nucleation rate
Sulphur to sulphuric acid conversion	Increase	Increase in PNC and nucleation rate
Soot particle	Increase	Decrease in PNC, increase in particle size
Organics, COV, non-volatile particles	Increase	Increase in size of the particle, decrease in nucleation rate, a slight decrease in PNC
Ambient Temperature	Decrease	Increase in PNC
Relative humidity	Increase	Increase in PNC
Wind speed	Increase	Decrease in overall PNC, negligible increase in PNC of very small particles (11-30nm)
Precipitation	Raindrop <0.2nm Raindrop >0.4nm	Decrease in PNC Increase in PNC
Pre-existing pollutants	increases	Reduction in nucleation, favourable condition for condensation, larger size particles will form

2.3.2.1 Important factors responsible for formation of UFP

Sulphur content of fuel; sulphur when released from the fuel into the atmosphere, reacts with water present in the atmosphere and forms sulphuric acid. This sulphuric acid then undergoes a binary homogeneous nucleation process (Vehkamaki et al., 2003) and forms particles up to a size 5.5 nm (Pirjola et al., 2015). Hence, the more sulphur content in the fuel, the more nucleation rate will be (Vehkamaki et al., 2003) and more will be the number of UFP formed. Also, it has been found that as the sulphur content is reduced, the amount of UFP particles formed reduces too but it does not follow a linear variation. As per Banerjee and Christian (2018), for the same environmental condition as the fuel sulphur content is reduced from 350 ppm to 250 ppm, a very sharp decline in the PNC is observed, and when the fuel sulphur content is reduced to 150 ppm, the PNC of UFP (in the nucleation mode range) becomes almost negligible. As earlier mentioned, sulphur to sulphuric acid conversion efficiency affects the PNC of UFP but not all the sulphur that is present in the fuel gets converted into sulphuric acid. Higher the efficiency of the sulphur to sulphuric acid conversion will be a higher number of UFP formed. As per Vehkamaki et al (2003), a change in concentration of sulphuric acid by a factor of 10 can cause a 10 order change in the nucleation rate. As per a study it has been found that a slight increase from 1% to 4% in the conversion efficiency can cause a sharp rise in order of 6 in the PNC in nucleation mode while a sharp decline is seen in the number concentration of UFP when the sulphur to sulphuric acid conversion efficiency is decreased from 10% to 5% (Banerjee and Christian, 2018). Unlike sulphur and its sulphuric efficiency, the soot particle as carbon formed due to incomplete combustion of the hydrocarbons has an inverse relation with PNC of UFP. Soot particle impacts the formation of accumulation mode particles. These particles have a larger diameter and provide the nuclei for the other gases to condense on them. A higher concentration of soot particles results in the formation of larger size particulate, which further leads to a reduction of UFP numbers (Banerjee and Christian, 2018). Condensable Organic nucleation rate Vapours (COV), Organic Particles and non-volatile particles don't have a major significantly influence on the number of UFP formed, but they affected the size of UFP formed. The Presence of COV and non-volatile particles influences the size of particles formed as these particles acts as a core and allow those very small nucleation

modes (< 5.5 nm) to coagulate over them and allow them to grow in diameter (Pirjola et al., 2015; Rönkkö and Timonen, 2019).

Ambient temperature plays a significant role in the forming primary UFP, as condensation rate is highly affected by the ambient temperature i., e as temperature decreases rate of condensation increases, which results in formation of more UFP. Ambient temperature significantly determines the threshold concentration of sulphuric acid (i.e., the sulphuric acid concentration that produces a nucleation rate of $10^6/cm^3$ (Vehkamaki et al., 2003). As per Banerjee and Christian (2018), the particle number concentration decreases from 6.0×10^5 to 2.3×10^5 as the temperature increase from 263k to 273k for a fuel with a sulphur content of 330 ppm and conversion efficiency of 1% with RH of 20%. It has been shown in various studies conducted by Banerjee and Christian (2018), Kulmala et al. (2004) and Vehkamaki et al. (2003) that both ambient temperature and RH plays a vital role in the formation of UFP. UFP gets dispersed, diluted, and re-suspended in the atmosphere due to the action of wind direction and speed. The PNC of UFP is a function of distance from the roadway. One of the critical difficulties in understanding variations in UFP concentration in the near roadway environment is that the dispersion process differs for ambient background and vehicle emissions. The dispersion near the roadway is dominated by turbulence from vehicle motion. It is a rapid process that disperses the vehicle exhaust in short periods (e.g., minutes), while the dispersion from ambient emission sources is mainly governed by atmospheric turbulence that transports emissions from stationary sources (Zhang and Wexler, 2002; Zhang et al., 2004). Besides the dispersion related to atmospheric and vehicles, researchers also found that green infrastructure (e.g., noise barriers, sound walls and vegetation barriers) can be considered as one potential solution for reducing UFP concentrations (see the section 2.3.3). Wind speed does not directly influence on the formation of UFP, but it plays a major role in the dispersion of UFP in URMe. Wind tends to carry UFP from its source to other places. As a result, high wind speed means a higher dilution ratio. As per the study of Abdul-Khalek et al. (1999) and Charron and Harrison (2003), a higher dilution ratio leads to lower nucleation rate and PNC. Also, as per Charron and Harrison (2003), wind speed has a negligible effect on very small particles (11-30 nm) and as a result, strong wind speed shows a higher PNC for very fine particles (11-30 nm). Various studies have found that UFP concertation reduces to

minimum at wind speed > 5m/s, while for particles with a size >100 nm, their concentration shows a U-shape curve for speed (5-10m/s). This U-curve is due to the re-suspension of the settled particles back into the atmosphere due to the action of the high-speed wind (Banerjee and Christian, 2018; Charron and Harrison, 2003; Kumar et al., 2008). Distance from road increases the geomean diameter of UFP but decreases the PNC of UFP. Brugge et al. (2007) concluded from a review of cardiopulmonary health studies that the most critical human exposure zone near roadways extends to 30 m downwind. More detail can see in Table 2.3.

Table 2.3: The relationship between particle size distribution and distance

Distance from the downwind from the Road (m)	**Peak Diameter (nm)**	**PNC (cm^{-3})**
17 m	10 nm	$>3.2 \times 10^{5}$
20 m	10 nm	$\sim 2.4 \times 10^{5}$
30 m	30 nm	$>1.6 \times 10^{5}$
90 m	50 nm	$>0.6 \times 10^{5}$
150 m	60 nm	$>0.4 \times 10^{5}$

Table 2.4: The relationship between wind direction and particle concentration

Wind direction	**PNC of UFP**
Wind from the road towards the sampling points	The concentration of particles reached the maximum at 15 m and decreased to half of the maximum at 150 m.

Wind parallel to the road	Under the action of parallel wind, the particle concentration decays to half of the maximum value at 50–100 m.
Wind away from the road	The wind direction had little effect on the particle concentration.

Precipitation or rainfall plays a complex role in respect of UFP. In general rain-drops washes the pollutants (including PM) of the atmosphere, lowering their concentration, but as per studies by (Banerjee and Christian, 2018; Charron and Harrison, 2003; Easter and Peters, 1994), it has been found that for UFP, the effect of rain depends on the size of the raindrop. It has been observed that if the raindrop has a size < 0.2 mm, they reduce the concentration of UFP from the atmosphere, but if the size of a raindrop is > 0.4 mm then the concertation of UFP increases. Also, precipitation increases the RH while decreasing the ambient temperature resulting in increased PNC of UFP. As a result, it has been found that after the rain, the rate of formation of UFP increases, with the highest PNC being found after 1 hour of precipitation (Banerjee and Christian, 2018). The ambient environment plays a significant impact in UFP formation. It has been found that the PNC of UFP increases after the rain and during the winter season. This UFP concentration increase during winter is due to low temperature. Also, due to temperature inversion, the dispersion of pollutants become slow which further contribute to the increase in the PNC of UFP. Seasonal influence on the particle size growth and PNC from road distance still did not explore thoroughly, although winter or cold seasons have fewer changes in nucleation mode's PNSD and have not changed in accumulation mode's PNSD. The growth of ultrafine particles in the winter or summer explains by the more effective condensation of released semi-volatile or volatile compounds in these conditions.

The spatial distribution of UFPs is highly inhomogeneous across the city. This inhomogeneity is primarily due to a heterogeneous urban environment (e.g., local sources and urban morphology) (Kumar et al., 2014) and the dynamic of UFPs (e.g., condensation and evaporation) (Zhang and Wexler, 2002). The near roadway concentrations vary by 30 to 40% on most days due to variations in vehicle flow rate. In urban near roadway environments, diurnal variation of UFP concentrations was shown to be related to the

variation in vehicle flow rate. The maximum UFP concentrations occurred on weekdays during rush hours and were correlated with traffic patterns. The diurnal variations during weekdays had a concentration peak during morning and afternoon rush hour. On weekends, the peak concentrations occurred in the middle of the day (Hussein et al., 2004; Hietikko et al., 2018). The strong relationship between traffic patterns and UFP concentrations reinforces the fact that vehicle emissions are a major source of UFPs since larger particles (accumulation mode particles) are poorly correlated with traffic conditions (vehicle flow rate and speed) (Hussein et al., 2004; Hietikko et al., 2018; Bello-Salau et al., 2015). In addition to differences in the traffic patterns, the weekdays usually had higher UFP concentrations compared to Saturday and Sunday. This can be explained by the fact that weekdays have a higher percentage of heavy-duty vehicles (HDV%) that emit significantly more UFPs than light-duty vehicles (LDVs) (Wang et al., 2010). UFPs concentrations were also found to be lower during nighttime than daytime. Zhu et al. (2006) concluded that UFP concentrations were 20% lower at night than at day. While Xiang et al. (2019b) found that the measurements at night can be lower by a factor of three. One should expect lower UFP concentrations during night-time due to lower vehicle flow rate fewer trucks and lower background concentrations. Seasonal variation in UFP concentrations is a complex issue. Studies have focused on seasonal variations in UFP concentration related to the effect of temperature, relative humidity and atmospheric mixing height. Most of the studies reported higher UFP concentrations in winter than in summer. In winter, the lower temperature and relative humidity can increase nucleation of the exhaust emitted by vehicles and resulted in higher UFP concentrations (Zhu et al., 2004; Wang et al., 2018). Lower mixing heights during winter can also increase in UFP concentrations because of less atmospheric dispersion (Saha et al., 2018). Pirjola et al. (2006) and Saha et al. (2018) demonstrated that the average UFP concentrations were 2-3 times higher in winter than in summer. However, field measurements conducted by Mejia et al. (2007) showed that seasonal variation in UFP concentrations was not significant when there were no significant meteorological differences between summer and winter. McMurry and Woo (2002) found that although average UFP concentrations tended to be higher in winter, while concentrations of particles with a size range between 3–10 nm increased in the summer due to photochemical nucleation due to stronger solar radiation. Park et al., (2008) found similar

photochemical nucleation events with particles size between 10-30 nm in summer, while traffic and residential heating led to enhanced UFP concentrations with sizes between 50-80 nm in winter. Generally, the studies conducted in the Northern hemisphere showed that there are clear seasonal trends (McMurry and Woo, 2002; Zhu et al., 2004; Pirjola et al., 2006; Park et al., 2008; Saha et al., 2018; Wang et al., 2018), contrary to study conducted in the Southern Chemosphere in Brisbane, Australia (Mejia et al., 2007). This mainly because the studies conducted in the Northern Chemosphere were in areas with significant meteorological differences between the seasons (Morawska et al., 2008). Besides the factors mentioned above, anthropogenic activities like home heating can also affect seasonal variations in UFP concentrations. Rovelli et al. (2017) found that seasonal differences in mass concentration for particles smaller than 1.6 um can be up to 3.5 times higher during the heating season than in the non-heating season. However, there is a lack of information on the changing UFP number concentrations in house heating.

2.3.3 Role of vegetation barriers in UFP near URMe

Besides the ambient environment, the ambient topography (like vegetation, buildings etc.) also plays a significant role in the PNC of UFP near URMe (Al-Dabbous and Kumar, 2014; Kumar et al., 2010; Lin et al., 2016). Out of these topographical features, vegetative barriers are of particular interest as they have been successfully used as pollution abatement measures. Various studies have concluded that roadside vegetation acts as a barrier for the air pollutants (Baldauf, 2016) and prevents them from dispersing into the near URMe. The effectiveness of this vegetation to reducing the dispersion of UFP is still unknown and needs to be studied further before a conclusion can be reached, but as per a study by Lin et al., (2016) vegetation barrio can cause a reduction in PNC by 37.7-63.6% in downward wind condition when wind speed is $\geq$ 0.5m/s, while as per a study conducted by Neft et al., (2016), it was found that the thickness of vegetation directly impacts the abatement efficiency of it. In a study conducted by Al-Dabbous (Al-Dabbous and Kumar, 2014), it was also found that vegetation not only influences the PNC of UFP, but also have a significant impact on the Respirable Depository Dose (RDD), showing a reduction of 36 - 80 % depending on wind direction and speed. Many studies have concluded that the effect of vegetative barrier is more when they are placed downwind and can significantly reduce the exposure of people living in the URMe

proximity to the urban road microenvironment (Al-Dabbous and Kumar, 2014; Baldauf, 2016; Bhardawaj et al., 2017; Brantley et al., 2014; Lin et al., 2016).

2.3.4 URMe's UFP Model

In the field of aerosols and UFP, models are extensively used and one of the most commonly used models is Land Use Regression (LUR) model (1977 Brigs), used to analyse the pollution concentration at any location in the study area and to understand the spatial-temporal variation of pollutants. LUR combines monitoring of air pollution at various locations, spread over the study area and the development of stochastic models using predictor variables usually obtained through GIS (Hoek et al., 2008; Karroum et al., 2020; Lv et al., 2020). AERMOD (1998 AERMIC), a steady-state Gaussian dispersion model, is capable of simultaneously simulating many sources with different shapes, elevations and characteristics, emitting one or more pollutants and is also capable accounting for the non-homogeneous vertical structure of the boundary layer (Hanna et al., 2001; Lv et al., 2020), and has shown promises in the field of UFP (Ahmed, 2017). Another Gaussian model called ADMS5 based on ADMS (1993, CERC) is used extensively by researchers. It is a versatile model capable of calculating the concentration of atmospheric pollutants generated from point sources, line sources, area or volume sources and is capable of handling up to 300 sources. ADMS has a similar algorithm as that of AERMOD and has a sub-model created specifically for road pollution diffusion known as ADMS-Roads (Gulia et al., 2014; Hanna et al., 2001). National Environment Research Institute developed another Gaussian Plume model that is used extensively in UFP, Denmark, called OSPM (2000). An important feature of OSPM is modelling the turbulence in the street, while considering the meandering effects of the winds, which makes it suitable for studying UFP in an urban street canyon (Berkowicz, 2000; Ketzel and Berkowicz, 2004). Another widely used model for aerosols particle is WRF-Chem (2000, NOAA/ESRL/GSD). It stands for Weather Research Forecast and Chemistry and is a WRF-based inline atmospheric chemistry model. It comprises of two modules, the weather module and the Chemistry module, used for simulating the effect of both meteorological and chemical parameters on a pollutant simultaneously and provides a more realistic result for an accurate study of aerosols. Around the same time, Pirjola (2000) felts the need to develop a model specifically for UFP, which resulted in the

development of the MONO-32 and MULTIMONO model (Pirjola and Kulmala, 2000) developed to study the aerosol particles. These models can investigate the role of different emissions in determining the concentration and composition of the particles while considering both emissions of gases and particles as well as gas-phase chemistry. The model also considers the dry deposition losses, Nucleation (binary and ternary), condensation as well as inter-intra molecular coagulation. MONO-32 models are also vastly used in combination with other models (such as CFD (Computational Fluid Dynamics)) to form advanced hybrid models for studying UFP (Gidhagen et al., 2004). While in the recent year the model that is used most is R-line model designed by US-EPA to simulate the near road mobile source pollutant dispersion and to study the human exposure. It is highly suitable for exposure risk assessment as it is designed to predict pollutant concentration at receptors very close to road and to simulate primary, chemically inert pollutants with emphasis on near surface releases and near source dispersion. What makes this model unique in comparison to other line model is that it contains a wind meander algorithm that accounts for dispersion in all directions during light and variable winds and is extensively used today to study the human exposure to UFP (Ahmed, 2017; Snyder et al., 2013), while the last model on the list is GAM, developed by Hastie and Tibshirani in 1990, and was later optimized by wood (Wood, 2008; Wood et al., 2017), it acts as a hybrid model incorporating both LUR as well as R-line model, it allows the used to estimate time series or spatial characteristics while representing the non-linear relations of a response variable with explanatory variables without the need to pre-define model functions and has been used by many researchers for analysis of UFP (Gerling et al., 2021; Sartini et al., 2013), GAM models are usually fitted to UFP data from a single site or from mobile measurement campaigns with limited temporal coverage, but recently as per a study Gerling et al. (2021), shows that GAMs are able to represent important processes that contribute to the particle number concentration from the smooth functions, i.e. emission, dilution, nucleation, deposition and long-range transport, while offering flexibility and evaluation of the specific and synergistic contributions of different variables affecting UFP concentrations. With the advancement in the field of UFP, the nature of the relationship between the sources of UFP and parameters affecting the formation of UFP has become complex to be measured by current models. As a result, many scholars have now looked toward a more adaptive,

self-organizing models based on Artificial Neural Networks (ANN), which allows them to train a model for better understanding and predicting the characteristics of the pollutants (Lv et al., 2020). As shown in a recent study by Ganji et al. (2020), who have coupled GIS with Bayesian regularized ANN (BRANN) model to develop an air pollution prediction model to predict near-road air quality based on measurements of ultrafine particles (UFPs).

2.4 UFP's measurement and instrumentation at URMe

In contrast to uniformly formed manufactured or engineered nanoparticles, URMe's UFP, qUFP, or Nano-particles have a wide range of shape and size distributions, including irregular shapes, aggregates, and agglomerates, making monitoring and measurement difficult (Kwon et al., 2020; Nussbaumer et al., 2008; Obaidullah et al., 2012). However, no definitive protocol or standard has yet been established to address this problem, but in UFP measurements several effective instruments of specific principles are available (Giechaskiel, 2018a; Giechaskiel et al., 2014; Knibbs et al., 2011; Kumar et al., 2021, 2014a, 2010; Morawska et al., 2008). As mentioned in the above section, UFP concentrations vary in the context of far away from tailpipe emission on or around the roadside to a significant level with specific monitoring systems. However, in this regard, the UN-EC has launched a particle measurement programme to develop a universal new system or protocol for monitoring and measuring UFP/qUFP/Nano-particles (European commission, 2008). Aerodynamic diameter (Da), Stock's diameter (Ds), or Electrical mobility (De) are more commonly (Giechaskiel, 2018b; Hinds, 1982) used by research society for UFP's PNC measurement in dynamic ambient air of URMe than its mass concentration measurement. According to (Nussbaumer et al., 2008; Obaidullah et al., 2012), as the size of the particulate matter becomes smaller, technically its measurement becomes quite challenging and selective. This section aim is to comprehensively overview of UFP / qUFP / Nano-particles measurement and their instrumentations. The aim is not to compare and contrast instruments, especially commercially available instrument. As shown in Figure 2.2, UFPs measurement can be done into the following way; 1- Concentration of UFP; 2- Size distribution of UFP; 3- Physiochemical characteristics of UFP. It includes the name of the technique used for the completeness of the measurement section.

Figure 2.2 shows the overview of utilization of available instruments in monitoring and physiochemical characterization of UFP at URMe. The UFP monitoring and measurement in URMe, includes two parts: measurement and physiochemical characterization. The measurement section has the most used techniques for PNC, Mass, and PNSD for UFP estimation, while the physiochemical section is related to structural properties, elemental & organic composition, Growth kinetics, magnetic properties etc.

2.4.1 Concentration of UFP

The concentration of UFPs (the number and mass concentration of UFPs) and surface area are mostly measured using gravimetric, optical, and microbalance techniques. (Figure 2.2 and Table 2.5).

2.4.1.1 Gravimetric Technique

In general, the mass of UFP/qUFP/Nano particles is measured using specific filter paper (by Glass fiber, PTEF, and Quartz filter paper) in a cascade impactor that is weighted before and after particulate matter sampling. Many of it is used in the physiochemical characterization of UFPs using specialized instruments such as TEM (Transmission Electron Microscopy), SEM (Scanning Electron Microscope), ICP-MS (Inductively Coupled Plasma Mass Spectrometry), and many others (Amaral et al., 2015; Giechaskiel et al., 2019, 2018). Unless the particles of a specific size are removed or stopped by the cyclone or impactor, granulometric fractions (nucleation, accumulation, and coarse mode) of a wide range of particulate matter are normally collected on filter paper. In general, quasi UFP (> 250 nm to 1000 nm) is measured with a cascade impactor equipped with a specially arranged multiple impactor stage for mass concentration and size distribution, in which a specific size cutoff is opened at each stage, allowing the sampled air (loaded with particulates) to enter and collect on the filter papers or the impactor plate. The sample air flow then entered the lower size cutoff impactor stage. The cascade stage or their cutoff diameter may also differ and be customary (Giechaskiel et al., 2014; Nussbaumer et al., 2008). The SKC Siotus Personal sampler, for example, is a cascade impactor with four stages (250nm, 500nm, 1000nm, and 2500nm) and a single diaphragm pump that maintains a 9L/m flow of sampling air (Lin et al., 2005; Rohra et al., 2018; Xue et al., 2019). Some other scientific cascade impactors are detailed in Kumar et al.

(2021). This study provides non-real-time data and cannot give statistically enough data in a short period of sampling days. According to (Durand et al., 2014; Fonseca et al., 2016; Nussbaumer et al., 2008), Berner low-pressure impactor (BLPI), Dekati Low-pressure impactor (DLPI) are commonly used because their particle size ranges are customary in different ranges of 10 nm to 10 µm. More information is provided in the following section, titled ‘impactor.'

According to Vincent. (2007), a conventional cascade impactor is not favorable for measurement of > 0.4 µm at atmospheric temperature. There is another type of cascade impactor family to substitute the conventional cascade impactor, micro-orifice uniform distributed impactor (MOUDI), with a sampled flow rate of 10 to 100 L/Min, which can cover a broad range of particle sizes (> 30nm to < 2500nm) on Quartz plate. MOUDI does not use any filter paper during sampling. Particulate matter can be collected from the quartz plate to the respective filter paper or solution for further physiochemical analysis.

In this particle bouncing issues are minimal as compared to conventional cascade impactors. With the integration of Quartz Crystal Microbalance, MOUDI provides a real-time mass concentration of different sizes and their distribution (Alam et al., 2011; M. Chen et al., 2016; Durand et al., 2014; Fonseca et al., 2016; Giechaskiel et al., 2018; Kumar et al., 2021; Lin et al., 2005; Liu, 2015; Marple et al., 1991).

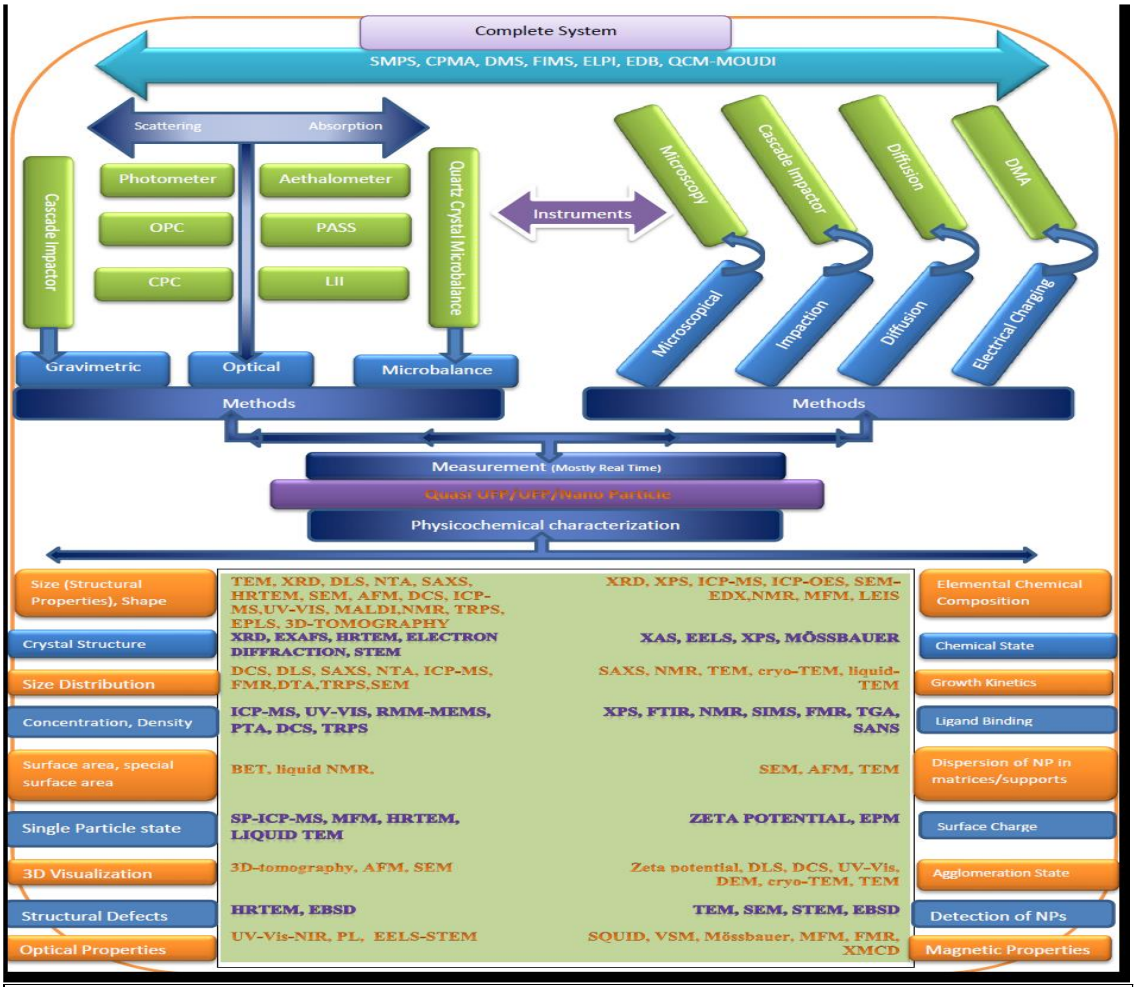

AFM :- Atomic force microscopy
BET :- Brunauer Emmett Teller
Cryo-TEM :- Cryo-electron microscopy
Cryo-TEM :- Cryo-electron microscopy
DCS :- Differential centrifugal sedimentation
DEM :- Differential electrochemical mass
DLS :- Dynamic light scattering

DSC :- Differential Scanning calorimetry
DTA :- Differential thermal analysis
ED :- Electron diffraction
EDX :- Energy dispersive X-ray
EELS :- Electron energy loss spectroscopy

EELS-STEM :- Electron energy loss spectroscopy – Scanning transmission electron microscopy
ELS :- Electrophoretic light scattering
EPLS :- Elliptically polarized light scattering
EPM :- Electrophoretic mobility
EPR :- Electron paramagnetic resonance
ESI :- Electrospray ionization
EXAFS :- Extended X-ray absorption fine structure
FMR :- Ferromagnetic resonance

FTIR :- Fourier transform infrared spectroscopy
HRTEM :- High-resolution Transmission electron microscopy
ICP-MS :- Inductively coupled plasma mass spectrometry
ICP-OES :- Inductively coupled plasma optical emission spectrometry
LEIS :- Low-energy ion scattering
Liquid NMR :- Liquid nuclear magnetic resonance
Liquid TEM :- Liquid transmission electron microscopy
MALDI :- Matrix-assisted laser desorption/ionization
MFM :- Magnetic force microscopy
NMR :- Nuclear magnetic resonance
NTA :- Nanoparticle tracking analysis
PL :- Photoluminescence
PTA :- Particle tracking analysis
RMM-MEMS :- Resonant mass measurement micro electro-mechanical system
SANS :- Small angle neutron scattering
SAXS :- Small-angle X-ray scattering
SEM :- Scanning electron microscope
SIMS :- Secondary ion mass spectrometry
SP-ICP-MS :- Single particle Inductively coupled plasma mass spectrometry
SQUID :- Superconducting quantum interference device

STEM :- Scanning transmission electron microscopy
TEM :- Transmission electron microscopy
TGA :- Thermal gravimetric analysis
TRPS :- Tunable resistive pulse sensing
TRPS :- Tunable resistive pulse sensing
UV-Vis :- Ultraviolet–visible spectroscopy
UV-Vis-NIR :- Ultraviolet–visible spectroscopy near infrared reflectance
VSM :- Vibrating sample magnetometry
XAS :- X-ray absorption spectroscopy

XMCD :- X-ray magnetic circular dichroism
XMCD :- X-ray magnetic circular dichroism

XPS :- X-ray photoelectron spectroscopy
XRD :- X-ray diffraction

Figure 2.2: Overview of UFP instrumentation for concentration and chemical characterization

2.4.1.2 Optical Technique

To measure the UFP/qUFP/Nano-particles in the ambient environment, the optical detection method employs the light beam scattering, absorption, and extinction principles (Belkacem et al., 2021; Giechaskiel et al., 2014). There are several instruments based on light scattering, absorption, and extinction principles, but light scattering-based instruments are more commonly used for real-time particulate matter measurement than absorption-based instruments because they are generally used for particulate matter measurement in the context of black carbon, whereas the use of extinction method is less common in the field of UFP (Amaral et al., 2015; Lonati et al., 2017).

2.4.1.2.1 Light scattering method

The light scattering method, according to (Giechaskiel et al., 2014), is "the light scattering pattern and intensity are strongly dependent on the particle size to the wavelength of incident light." When the sampled flow enters the light beam section, the photometer detector measures the scattered light by particles because light dispersion and scattering are particle-specific ensemble. In the optical particle counter, the aerosol is drowned through a light beam and light flushes, scattered by single particles, are received by a photodetector. The number concentration is determined from the count rate, and the particle's size is estimated from the pulse height. Commercially available instruments have various size ranges of particles ranging from a few nanometers to several hundred nanometers in diameter, with different measuring angles such as 30º, 45º, > 90º depending on customization and detection technology (Hinds, 1982). These are some following instruments for the light scattering method; DataRAM4 (Belkacem et al., 2021), WARS (Wide range aerosol spectrometer) from GRIMM Aerosol Technik model, Dust tracker (TSI model), PAMS (Kanomax model) (Lin et al., 2005; Liu, 2015). Proper maintenance and cleaning of the particle counting chamber can provide more reliable measurement data (Chowdhury et al., 2013; Kulkarni et al., 2011). In the light scattering method, optical particle counters and condensation particle counters are commonly used for real-time measurement of qUFp/UFP/Nano particles (Amaral et al., 2015). In general, the condensation particle counter (CPC), based on the light scattering method, is the most commonly used instrument for ultrafine particle number concentration. However, UFP

or Nano particles have a detection limit using the standard light scattering method due to their size. To accomplish this, a condensation chamber is used to grow the UFPs/Nano particles to photo detection level for use in the CPC detector (Amaral et al., 2015; Giechaskiel et al., 2014). Particle condensation occurs when the temperature of the sampled air drops in the chamber with the help of a condensation solution such as butanol or distilled water. Even though qUFPs exceed the lower size detection limit, optical particle counters are commonly used for mass or number concentration in real-time measurement of quasi-ultrafine particles (Giechaskiel et al., 2014). But CPC can be used on itself for total PNC of UFP (Morawska et al., 2008) and it is more effective in terms of particle size number distribution (PNSD) when combined with a differential mobility analyzer (DMA) or differential mobility spectrometer (DMS) (Kumar et al., 2010).

2.4.1.2.2 Light absorbing method

Because of a strong correlation between black carbon and light absorption, the main instruments used to measure black carbon in quasi UFP/qUFP/Nano particulate matter are light absorption. It is possible to do so using specific filter paper, such as a spotmeter for soot in engine exhaust smoke and an Aethalometer for black and elemental carbon (Hofman et al., 2018; Stapleton et al., 2018). The Photoacoustic Soot Sensor (PASS) and laser-induced Incandescence (LII) are advanced methods for measuring black carbon in diluted heated sampled flow in real-time (Aiken et al., 2016; Giechaskiel et al., 2014). These are mostly used to measure tailpipe or vehicular emissions (Giechaskiel, 2018a, 2018b; Giechaskiel et al., 2020, 2019, 2018, 2014).

2.4.1.3 Microbalance techniques

Microbalances are used to determine the mass of particulate matter collected on the surface of an oscillating element due to a change in the resonance frequency. The quartz crystal microbalance is explicitly designed for measuring fine and qUFP/UFP/Nano particles, which are electrostatically deposited on the thin quartz crystal resonator. The particle's mass can be calculated based on the decrease in resonance frequency. The measurement is hampered by temperature and humidity variations. QCM-MOUDI (Quartz crystal microbalance-micro-orifice uniform depositor impactor), TSI Model 140

is one of the advanced instruments that use a QCM and an impactor to overcome temperature and humidity variations. It is a real-time precision research-grade impactor with QCM sensors for real-time mass detection. The impactor has 2.5 µm inlet and 6 QCM stages with sharp efficiency curves and calibrated cut points of 960, 510, 305, 156, 74, and 45 nm at a 10L/min inlet flow rate, eliminating unwanted solid particle bounce. Particles collected on QCM can then be used for physiochemical analysis (Kumar et al., 2021; Segalin et al., 2020).

2.4.2 Size distribution measurement method

Size distribution is an important factor in studying the UFP/qUFP/Nano particle, which is represented by particle number concentration or mass concentration in different size channel bins and is primarily determined by particle properties such as geometric size, inertia, electrical mobility, and other particle properties. Size distribution is, in general, a combination of several measuring principles and their respective instruments. Size distribution usually takes place in three stages: 1) particle loading and charging or neutralisation; 2) particle size classification; and 3) detection. The following are some of the most used techniques for PNSD.

2.4.2.1 Microscopy technique

Microscopy is used to examine the morphology and size of a particle. In microscopy, particles are collected on specific filter paper with cascade impactor or MOUDI instruments, followed by filter preparation to improve visibility according to respective instruments TEM, SEM, and TCP-MS. For a wide range of information, image processing provides supportive and informative information on particle morphology, rotation radius, size distribution of primary particles, factual dimension, number of primary particles per aggregate, and size distribution of primary particles (Mourdikoudis et al., 2018). The main drawbacks are time consumption, off-site analysis or monitoring, and statistical inadequacy. It is suitable for solid particle analysis but not for semi-volatile particle analysis due to particle evaporation or loss during vacuum and electron beam heating (Giechaskiel et al., 2014; Vincent, 2007; Wentzel et al., 2003).

2.4.2.2 Impactor's technique

According to Hinds (1999), the cascade impactor operates based on particle inertial classification. The aerosol sample is routed through a series of stages, each directing the aerosol through an array of nozzles above a solid substrate (Vincent, 2007). Particles with aerodynamic diameters greater than the design cut-point are impacted, whereas smaller particles follow gas streamlines around the collection plate. The efficiency of impaction is proportional to Stoke's number. The finer the particles collected, the narrower the nozzle and the higher the air velocity. Because of their low inertia, the smallest particles passing through the final stage cannot be collected, but they are frequently collected onto a final filter. The traditional cascade impactor does not perform well with smaller particles (> 400nm aerodynamic diameter) (Kumar et al., 2021; Nussbaumer et al., 2008; Vincent, 2007). As a result, another type of modified cascade impactor family that can collect particles ranging from 30 nm to 10µm. Low-pressure cascade impactor (LPI), Dekati Low-pressure cascade impactor (DLPI), and Berner Low-Pressure Impactor are the impactors. Another cascade family that has minimised particle bouncing effects on impactors is the Micro-Orifice Uniform Depositor Impactor (MOUDI). With the addition of QCM, MOUDI has evolved into a real-time instrument for mass concentration and size distribution. More information can be found in the previous section on a microbalance. The Electrical Low-pressure Impactor (ELPI) is a high-tech real-time impactor in which unipolar corona charge charges the sampled aerosols before passing through a low-pressure cascade impactor with electrically isolated collection stages. It is based on three main principles: 1) corona charging; 2) inertial classification using a low-pressure cascade impactor; and 3) electrical detection of aerosol particles using a multi-channel electrometer. The Dekati electrical Low-pressure Impactor (DELPI) has a sampling time of 1s and a particle size range of ultrafine to coarse (7nm to 10 um). Particulate matter collected on the impactor can be analysed further for physio-chemical analysis (with the help of TEM, SEM, ICP-MS etc) (M. Chen et al., 2016; Corsini et al., 2019; Durand et al., 2014; Fonseca et al., 2016; Giechaskiel, 2018b; Giechaskiel et al., 2019, 2018; Kumar et al., 2021; Lin et al., 2005; Liu, 2015; Marple et al., 1991; Venkataraman and Rao, 2001).

2.4.2.3 Diffusion battery

According to Vincent (2007), using traditional instruments particles, less than 0.1 μm have little detectable response to gravitational and inertial forces. However, diffusion has a strong influence on the measurement of these particles. The Diffusion Battery (DB) is used to calculate the diffusion coefficient of particles through equivalent diameter in volume. Despite the fact that Fierz et al. (2011) stated that recent gravimetric and optical methods are insensitive to measuring nanoparticles and thus unsuitable for this task. However, diffusion batteries, with particle measurement ranges from 1nm to 100 nm, separate particles based on their mobility, which is determined by particle diffusion coefficients. In general, DB is used with a condensation particle counter and a switch valve to vary the effective length of the diffusion path. This resulted in the development of the 'electrical diffusion battery' (EDB), in which sampled particles are charged by a corona charger and then placed in the diffusion battery (which can be either tube or screen) (Amaral et al., 2015; Giechaskiel et al., 2014). According to (Vincent, 2007) the EDB collection efficiency is a function of the geometric properties of the tube or screen, the flow rate, and particle size.

2.4.2.4 Mobility analyser

Previously, a mobility analyzer was known as an 'Electrical Aerosol Analyzer (EAA),' in which particles were passed from electrical mobility after charging with a unipolar corona charger, which allows only particles below certain electrical mobility to pass and be measured with an electrometer. Currently, the differential mobility analyzer (DMA) is an advancement of the EAA in which a neutralizer (Bipolar diffusion charger) is used to provide a well-defined ‘Fuchs charge distribution.' The particles are then routed through an electrostatic classifier (which allows only narrow electrical mobility range particles to pass) and measured using a CPC or electrometer (Giechaskiel et al., 2020, 2019, 2014). The combination of DMA and CPC is known as a scanning mobility particle sizer. According to Wang and Flagan (1990), the applied voltage can be exponentially ramped to a scan over a particle diameter range in a few minutes. Fast scanning is incompatible with SMPS. It has been discovered in the literature that it can be customised based on research demand, such as the ‘Volatile Tandem Differential Mobility Analyzer

(VTDMA),' which has two nano DMA and two long DMA, as well as a heating tube and an ultrafine condensation particle counter for covering a wide range of aerosol particle size (Amaral et al., 2015; Giechaskiel et al., 2018, 2014; Maruf Hossain et al., 2012). In the aerosol monitoring committee, SMPS has a commercially diverse range of models. It is available in Short or Nano DMA (for smaller UFP/Nano particles) and Long DMA (for larger UFP/Nano particles), as well as CPC, which provides the size distribution with particle number concentration in different channels or size bins. DMA size range, size distribution channel or bin, and maximum concentration monitoring range differ between brands, such as TSI and Grimm models. The SMPS is a commonly used instrument for monitoring ambient UPF (Kumar et al., 2010).

2.4.2.5 Centrifugal Measurement of Particle Mass (CPMA)

According to the literature, CPMA has two specific electrodes (coaxial electrodes) that rotate at different speeds (the outer electrode rotates slightly slower than the inner electrode). As a result, when a charged particle passes between these electrodes, it is subjected to electrostatic and centrifugal forces that act in opposite directions. CPMA calculates the particle mass to charge ratio (which is measured by the difference between electrode voltage and rotation speed) (Giechaskiel et al., 2014; Johnson et al., 2013). The advantage of CPMA is that there is no need to collect dust for weighing while measuring particle mass. The Aerosol Particle Mass Analyzer (APM) works similarly to the CPMA, except that both electrodes rotate at the same angular velocity (Amaral et al., 2015).

2.4.2.6 Differential Mobility Spectrometer (DMS)

The particles are initially distributed in the DMS via unipolar charging via a corona wire diffusion charger. The sampled aerosol is then routed through the central rod's outer boundary (cylindrical electro-statistic classifier). It is made up of a series of electrically isolated rings that are linked to sensitive electrometers. The particle number distribution is measured by the deposition of charged particles on a ring electrode. DMS has lower particle sensitivity and size resolution than SMPS but higher sampling time resolution (0.1 to 1Hz), so it is more commonly used in vehicle exhaust monitoring with dilution

(Giechaskiel et al., 2014; Hosseini et al., 2010; Maruf Hossain et al., 2012; Nussbaumer et al., 2008).

2.4.2.7 Fast Integrated Mobility Spectrometer (FIMS)

Giechaskiel et al. (2014) and J. Wang et al. (2017) describes the FIMS composition as a charger, a size classifier, a condenser and a detector. (Kulkarni et al., 2011) and (Johnson et al., 2013; Olfert et al., 2008) state that the aerosol passes through a neutralizer thereby receiving a charge distribution of bipolar equilibrium. The aerosol passes through a mobility analyzer through which butanol saturated gas flows. Based on their electrical mobility, particles are separated into different paths in the field of the mobility analyzer. These classified particles enter the field-free condenser, where supersaturated butanol vapor increases their size by condensing over them. The laser beam illuminates the drops are illuminated by the at the exit, and a 10 Hz camera captures these images, which in turn provide particle concentration and particle mobility diameter (Amaral et al., 2015; Garg et al., 2000; Giechaskiel, 2018b; Giechaskiel et al., 2019; J. Wang et al., 2017).

Hence, there are some other principle-based instruments like Aerodynamic particle sizer, particle sizer Distribution, Aerosol Mass spectrometer for measurement of UFP/qUFP/Nano Particles such as SMPS, FMPS, ELPI, MOUDI, and OPC for UFP measurement uses according to their application.

The measurement characteristics of UFP/qUFP/nano particles are presented in Table 2.5, such as the detection limit, the size range and the accuracy of different techniques. Real-time sampling has an advantage over instruments that monitor non-real-time data in URMe. Size range and detection limit are essential factors for comparing instruments for particle size measurement. Accuracy measures the precision between the actual value and the measured value. With 30 percent accuracy, the Scatter Photometer is the most precise instrument. SMPS, FMPS, ELPI and OPC are necessary for measuring the UFP, which are necessary to consider of the impact of particulates on health issues. SMPS measures small particles better than FMPS; although low precision, the downside is that sampling data is unavailable in real-time. These two instruments cannot distinguish between coarse particles and UFP agglomerates, despite the usefulness of SMPS and ELPI, which is a defining difference for health problems.

Table 2.5: PM's instrument (Amaral et al., 2015; Giechaskiel et al., 2014)

Instrument	Real Time	Detection Limit	Size Range (nm)	A %	Advantages	Disadvantages
Filter	No	10 µg/m^3	D	5	Easy to handle, dependable, chemical analysis	Increased work
Scattering	Yes	10 µg/m^3	>50	30	No advantage as such	PM larges are measured
Spotmeter	No	25 µg/m^3	All	15	Measuring BC	Takes more time to response
PASS; LII	Yes	5 µg/m^3	>10	10	Measuring BC	Demand Calibration
Opacity	Yes	0.1 % opacity	>50	20	No advantage as such	Depends on many elements
TEOM	Yes	-	D	-	Goes well with filters	Filter must be changed for increased concentration
DLPI	No	-	30-10,000	-	Size range is large	Larger size particles are not suited
SMPS	No	100/cm^3	5-1000	15	Even few nm sized particles are detected	But range is limited, large sized particles are rejected

FMPS	Yes	1000 /cm^3	5.6-560	25	Fast, Changes made are indicated easily	SMPS is more accurate
ELPI	Yes	1000 /cm^3	7-10,000	25	Rugged; the range is large	Results can be affected due to wide channel plates
A=Accuracy,						

2.5 Health impact of UFP

In terms of health effects, there is less strong evidence of UFP compared to PM2.5, owing to a lack of long-term studies. While UFP has great potential for harming health, its precise function is still unknown in many diseases (Kumar et al., 2021; Kwon et al., 2020; Schraufnagel, 2020). As we have already discussed in the preceding section, the road microenvironment is one of the hotspots for UFPs in urban areas, as its concentration varies from the source place as a road to a nearby area, which is normally many times higher than the background concentration. Asians are exposed and at greater risk than in the European URMe region under this circumstance. More than 10^{12} ultrafine particles are ingested by a single person daily in Western countries. UFP effects on the respiratory system, the central, cardiovascular, cancer, diabetes, and deliberate population, such as children, and old (Kumar et al., 2021; Rönkkö and Timonen, 2019; Schraufnagel, 2020).

It is known that nanoparticles are efficiently deposited into the human respiratory system, but the deposition efficiencies are not uniform with respect to particle size. While the nanoparticles larger than ∼10 nm are deposited most efficiently into the alveolar region of the respiratory system, the smallest particles are deposited most efficiently to head airways (Yadav et al., 2019a). These areas contain potential paths for air pollution compounds deposited in the epithelium to be transported to the central nervous system, such as the olfactory bulb (EPA, 2008). Wang et al. (2019) suggested that the

combustion-originated nanoparticles of inhaled air can penetrate the human brain through the olfactory bulb and cause Alzheimer's disease and other brain diseases. The air pollution from traffic has also been associated with decreased cognitive function in older men (Peters and Helmholtz, 2015; Shi et al., 1999b; Solomon, 2012) reported associations between dementia incidence and local traffic pollution. However, they could not rule out environmental factors such as noise generated by traffic from their results. Meng et al. (2013) studied the small particles < 0.5μm with size-fractionated particle number concentration and their health effects. They reported that it has an adverse effects on daily mortality in Shenyang, China and explored the exponentially decreased particle size and an increased surface area having adverse toxicity exponentially as particulate matter's health effects (Meng et al., 2013). Due to increased / high surface area, UFPs can absorb the organic gases and heavy metal elements which further contribute to the larger particle growth through agglomeration. However, the toxicity of heavy metals and other pollutants as organic gases has already been explored. Lower mass, high surface area ratio, and high reactivity of nano-size particles show quite different physiochemical properties (Oberdörster et al., 2005; Singh and Nalwa, 2007). This property of UFPs makes its toxicity more complicated, complex and difficult compared to the conventional toxicity for the same (Terzano et al., 2010). There are three primary way of UFPs exposure (Cassee et al., 2002). Moreover, PM mainly enters our body through breathing (respiration process), but adsorption, metabolized distribution and excretion are the processes that govern the rate and fate of PM in the human body (Oberdörster et al., 2005); 1) Respiratory Tract; 2) Dermal Exposure; and 3) Ocular Exposure (Figure 2.3 and Figure 2.4)

UFP enters our lungs through the nasal cavity; inhalation is the main way to get UFPs exposure through respiration. The inhaled airborne UFPs go deeper into the downstream airway of the lung. Therefore, UFPs get more advantages in the initial interaction with lungs including trachea, bronchia and alveolus. This interaction can go beyond the tissue cell with mucosa (Dawson et al., 2009; Schmid et al., 2009; Thorley et al., 2014). Mucosa, a layer of mucus beyond tissue cells, is the human body's primary protective barrier for PM. Naturally, lungs do not have the ability to clean fine or UFPs thoroughly from deep in the site (Jiang et al., 2015). For the human body, there is a hypothesis that UFPs have the efficiency of pulmonary deposition and could reach deeper inside the

lungs because UFPs cannot be stopped or filtered by the nose and bronchioles. The human nose has a limitation for filtering UFPs. It can filter more than 80 % of 1 µm particles but less than 5% of 100 nm particles during the resting period of breathing (Anjilvel and Asgharian, 1995; Möller et al., 2008). The lungs are one of the most important parts of the respiratory system, having direct contact with the outer atmosphere. The lung has two parts- one is airways and the second is an alveolar structure has a larger epithelial surface area. The lung alveolar contains monolayer epithelial cells, which increases the possibility of UFPs to crossing the blood-gas barrier and deposit into the lungs. Even though UFPs have a nano-size particle, it is not capable of penetrating the light junction between cells. UFPs can enter only by translocation through the epithelial cell body. Further, due to passive diffusion, UFPs can transport (in or out) to the cellular cytoplasm. But in the case of larger particles (>100nm), the particles take entry into the cell primarily (via clathrin and also caveolin-mediated endocytosis), and these particles are stored or found in the endosomes or hydrosomes in the cytoplasm (Chen et al., 2016). After passing the blood-gas barrier UFPs could enter the circulation and contact 'extra -pulmonary tissue cell'. But the larger particles >100nm may be degraded with minimized toxic consequences in the circulation. The UFPs >100nm particles may get deposited in the cell membrane or the cell. This presence or deposition of UFPs may generate reactive oxygen species (ROS), which increases pro-inflammatory mediator's transcription via oxidative stress. Thus, UFP circulation makes it more toxic and inflammatory than fine particles (Pirjola et al., 2006). There is quite an effective deposition of certain UFPs in the respiratory system (nasopharyngeal, tracheobronchial, and alveolar region). The alveolar region has a high deposition efficiency of 20 nm with ~50%, and particles ranging >100 nm to 2.5 µm have 10 to 20% deposition efficiency due to the high deposition of UFP; alveolar faces more toxic effects on the lung by penetration of alveolar epithelium and UFP's circulation into the blood stream. With the help of a Multiple Path Particle Dosimeter (MPPD), the exact dose of UFPs can estimate, which is deposited in the lung. MPPD is developed initially for dose estimation in the lower respiratory tract (Yegambaram et al., 2015). According to Möller (2008), in the lung periphery and airway, there is a less quantity clearance of the UFP (inhaled >100nm) after respiration at a point of 24 hours.

There is no direct link or in vivo evidence supporting the penetration of UFPs through the skin, but we cannot fully reject this possibility. Because human skin has a larger surface area and works as a direct barrier to the outer environment, some research team suggested that it may go through two routes; intercellular trans-epidermal cell or diffusion through skin pores, penetrating or entering the human body (Bennat and Müller-Goymann, 2000; Boyes et al., 2012).

Ocular exposure is another way of UFP exposure in humans. It occurs in the eyes by floating particles or by transferring during rubbing eyes in high concentration area (high polluted area). UFPs could be retained in the nasal cavity by the drainage from the eye socket. Then, through the nose to the brain transport system, UFPs can reach into the brain. Further, there are more possibilities for the particle to enter the blood circulation and travel throughout the body. It may cross the biological barrier after entering into blood circulation. In this way, exposure may course ocular disease, such as discomfort eye syndrome (DES), by internal associations. Linking to taxi drivers disclosed this in potential exposure (Lee and Chang, 2000; Torricelli et al., 2011; Versura et al., 1999). Besides alveolar deposition, the UFPs deposition on the olfactory bulb surface is another principal issue for the health risk evaluation for uptake of UFPs through the respiratory system. This route of exposure (long-term exposure) of UFPs may produce neuro-degradation diseases (like Alzheimer's disease, Parkinson's disease (Knudsen et al., 2013; Liu et al., 2015). Toxicological studies have clearly explained the deposition in the nasal cavity, absorbed by olfactory bulb and translocated into brain (via blood-brain barrier).

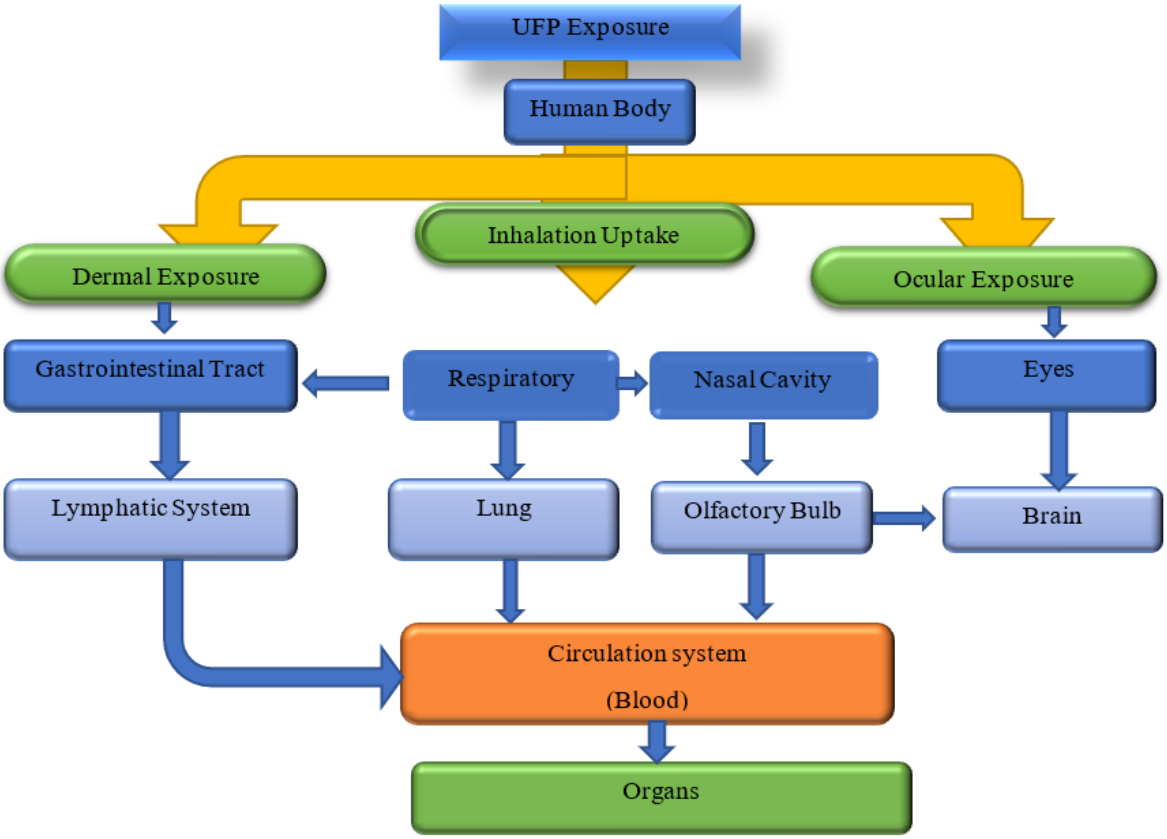

Figure 2.3: The possible penetration routes of airborne UFPs (Source; Chen et al., 2015)

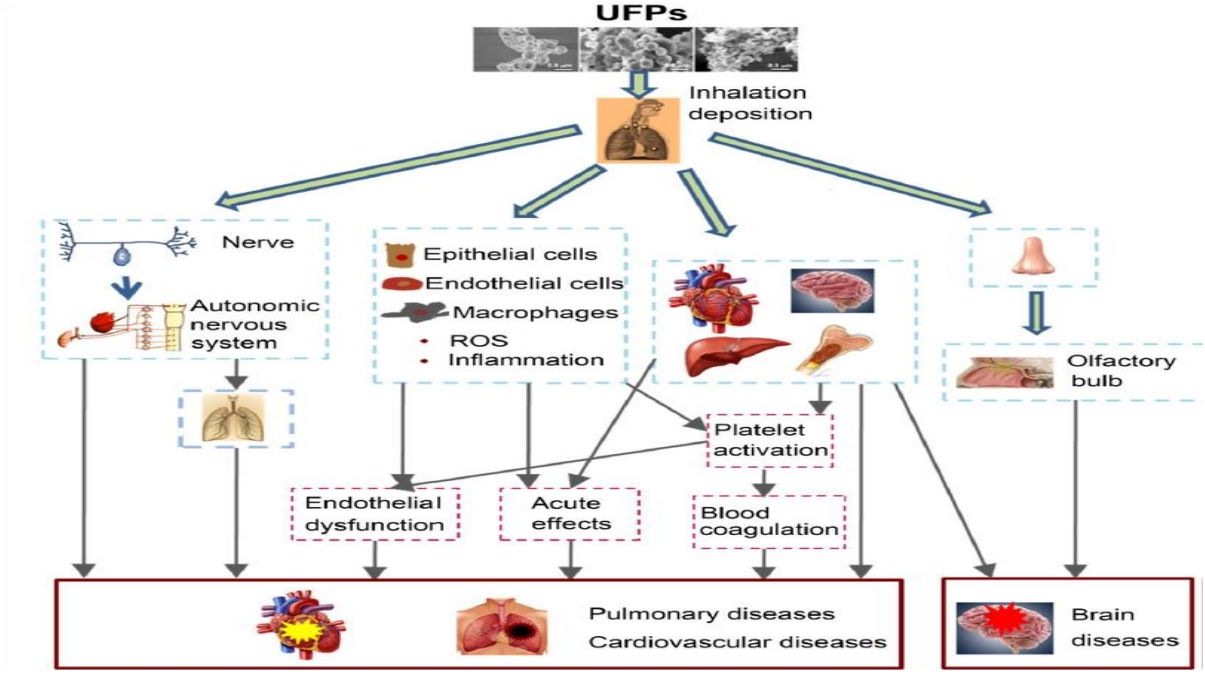

Figure 2.4: The potential toxicity mechanisms of UFPs (Source; Hu et al., 2015)

2.6 Status in Delhi

Table 2.6: List of research paper in concern of Delhi and India

Location	Type	Period	Size range (nm)	Num. Con. ($x10^3$ #/cm^{-3})	GR (nm/h)	Event (%)	Reference	Remark
New Delhi, India	Inside urban area	Dec. 2011 to Jan. 2013 (222 days)	5 nm to 32um	14.8	8.4	8.4 %	Jose et al., 2021	This study site is dominated by the Aitken mode particle, which follows a bimodal diurnal variation pattern, with peaks during morning and evening traffic hours. Accumulation mode particles are scarce over the study location except during the winter and post-monsoon days, when it shows a bimodal secondary peak along with the primary Aitken mode particle.

New Delhi, India	Inside urban area	2 to 9 Nov. 2016	10 to 800	25.52	1.6 to 30.3	87%	Kanawade et al., 2020	In their study they got higher GR rate also, but they got higher con of accumulation mode than Aitken mode which are not same in our condition
IITK, Kanpur, India	Inside urban area	30 Mar to 15 Apr 2013	4.45 to 736.5	10.195	3.2 to 6.7	82%	Kanawade et al., 2020	Thus, our findings emphasize the relevance of amines to secondary aerosol formation in severely polluted urban environments.
New Delhi, National Physical Laboratory	Inside urban area	Mar. &Apr. 2013; and Apr, 2014	4 to 661	-	5.64±3.03	-	Sarangi et al., 2018	Nucleation event at night-time

Ooty, India	Topographically 300 m above the valley	10 to 28 May, 2014	10.9 to 461.4	2.845 ±1.184	-	66%	Kompalli et al., 2018	The growth rate could not be determined because of the faster growth after the rapid burst of nucleated particles acting as a strong CS and ending the event
Mahaba-leshwar, India Physics Laboratory	Background 1348 m above mean sea level	Oct. to Nov. 2014	5 to 1000	21.800	0.96 to 1.9	8%	Leena et al., 2017	In tropical regions, such studies are limited, especially in the Indian region
Trivandrum, India	Background (10KM from	Jan. to Dec. 2013	15 to 15,000	~5.119 (±3.139)	~7.35 ± 2.93	Selective	Babu et al., 2016	the UFP bursts occurred during two distinct periods: First burst occurred soon after the onset and prevalence of land breeze close to late evening/midnight hours and the second

	urban area)							shortly after the sunrise and around the onset of the sea-breeze (between 06:00–09:00 h).
New Delhi, India National Physical Laboratory	Inside urban area	Nov. to Dec. 2011 (10 days)	9 to 425	37.2(event day 24.9(Non-event Day)	15.4 ± 11	30%	Sarangi et al., 2015	on an event day (November 4), particle mode peak size is increased with time, but the number concentration in the mode is systematically decreased.
Trivandrum, India	Background (10KM from urban area)	May to Jun. 2009	10 to 875	~15.900	~50	Selective	Kompalli et al., 2014	late evening/night hours

Hanle, India	Background (~300m above the surrounding	Aug. 2010	16 to 1364	~2.700	0.1 to 20	Selective	Kompalli et al, 2014	Day time event
IITK, Kanpur, India	Inside urban area	16 Apr. to 23 May, 2013	4 to 750	-	8.7 ± 3.2	14%	Kanawade et al., 2014	Despite lower particle number concentrations at Kanpur, larger particle sizes resulted in higher condensation sink than at Pune. The mean particle mode diameter at Kanpur was larger by a factor of ~1.8 than at Pune. Generally, the particle growth rates were higher at Kanpur, whereas the formation rates were higher at Pune.
IITM, Pune India	Outskirt of Urban area	16 Apr. to 23 May, 2012	14 to 750	-	(6.5 ± 1.2	26%	Kanawade et al., 2014	

IITK, Kanpur, India	Inside urban area	Dec.2006 to Nov. 2011	14 to 685	31.9 ± 29.7	-	-	Kanawade et al., 2014	
IITM, Pune	Outskirt of Urban area	Apr. 15 to May 31, 2010	0.46 to 50	-	3.1 ± 0.8 to 11.2 ± 3.5	36%	Siingh et al., 2013	Positive and Negative ions measurement
Mukteshwar or Mt. Norikura	Backgro und	late Nov. 2005 to late Jan. 2010	10 to 800	2.700	2.43	11.2 %	Neitola et al., 2011	The events were the most frequent in the spring months (March–June) when 97 event days were observed equating 81.5% of the events.

Gual Pahari Gurugaon, 25Km south of new Delhi	Background about	Dec. 2007 to Jan. 2009	4 to 850	22.600	-	70%	Hyvärinen et al., 2010	
Habitat Centre (IHC/TERI) New Delhi	inside urban area	26 Oct. to 9 Nov. 2002 (2 week)	3 to 800	62.8± 17.8	11.6 to 18.1	53% (13 % class 2 and 40% class 3	Mönkkönen et al., 2005	In this paper, it can take reference that GMD is higher for NU_10_25 in Delhi. Unfortunately, clear results on the connection between different trace gases and new particle formation cannot be achieved from our data set.

CHAPTER-3

3 METHODOLOGY

3.1 Introduction

Researchers and policymakers in Asia are becoming increasingly concerned about the deterioration of ambient air quality and their health impacts in massive urban areas such as the megacity Delhi, India. Because of their extreme variability in time and space, the urban population is subjected to a heterogeneous mixture of ambient air pollutants (Kumar et al., 2014, 2011; Mishra et al., 2019; Pandey et al., 2016; Singh et al., 2011). Profound implications such as climate change, poor visibility, and health issues are at high priority in Asian metro cities due to ambient air pollution (Kong et al., 2015; Kumar et al., 2016). The air quality of megacity Delhi over the last few years reached a more critical level in some specific periods (such as winter) and put pressure on the policy of the concerned agencies (Balakrishnan et al., 2019; Dholakia et al., 2013; Gurjar et al., 2016; Mukerjee and Shukla, 2016). Delhi, along with the National Capital Region (NCR), has an approximate population of 22.2 million in 2011, with a decennial increase of 7.96 % (Ministry of home affairs, 2011), the second-largest urban area in the world. However, in addition to the unique geographical and landlock conditions in Delhi, the low dispersion in the winter seasons worsens the ambient air quality (Chaudhari et al., 2016; Guttikunda et al., 2019; Kumar et al., 2017) and public health conditions (Health Effects Institute, 2019; Singh et al., 2019). For the reasons set out above, in November 2016, Kanawade et al. (2020) described it as a Sever Air Pollution Episode (SAPE), the Air Quality Index (AQI) reached an abysmal level (Sati and Mohan, 2014). At the early start of winter (October - November) every year, Diwali is celebrated by some people with great pomp and show, filling the sky with firecrackers burning neglecting associated pollution (Mandal et al., 2012). The Government, Semi-Government, and other concerned organizations have taken different measures to reduce air pollution, such as a ban on old vehicles (Goyal and Gandhi, 2016; Kumar et al., 2017), potential construction activities, biomass burning, diesel generators, Odd-Even scheme, and ban on Parali burning in and around Delhi (Srivastava and Jain, 2008). Although rapid urbanization

has resulted in a significant increase in the number of road vehicles in megacities such as Delhi over the last few decades, exposing residents to air pollution-related health risks, which are estimated to add 7 million unexpected losses a year (IQA AirVisual 2018). The total NCR area is 34,144 km^2, including Delhi city, with an area of 1483 km^2 (Kumar et al., 2017). Delhi city is known for the highest number of personal vehicles in India, with a total registered fleet of 2.9 million cars/jeeps and 6.1 million two-wheeler motor vehicles, which alone contributed to 93% of total registered vehicles (about 9.7 million), as on 31 March 2016 (Chandra et al., 2018). There are 11 million registered vehicles in Delhi and predicted to increase to 25.6 million by 2030 (Kumar et al., 2017). Two-wheelers comprise of nearly 56% (6.38 million) of total vehicles in Delhi in 2018 (Halder, 2019). As per the study of IIT Kanpur (2016), the contribution of the different sources towards $PM_{2.5}$ emissions in Delhi are road dust (38%), vehicles (20%), domestic sources (12%), industries (11%), concrete batching (6%), hotels/restaurants (3%), municipal sewage treatment (MSW) burning (3%), industries area (2%), construction (2%), diesel generators (2%), cremation (< 1%), and medical incinerators (< 1%) (Sharma and Dixit, 2015). The lower size particulate matter (ultrafine, quasi ultrafine, fine particles) shows more penetration and deposition than larger particulate matter in the human body with adverse health effects (Rönkkö and Timonen, 2019; Schraufnagel, 2020). The lower size particulate matter assessment is currently based on the Particle Number Concentration (PNC) with its particle size distribution instead of its mass concentration because of the negligible mass contribution. Specifically, the ultrafine particles (UFP), which are a subset of fine particles have caught the attention of researchers as they may further deteriorate the ambient air and induce health risks (Joshi et al., 2019, 2016; Kumar et al., 2012; Kwon et al., 2020; Schraufnagel, 2020; Yadav et al., 2019b). Transformation of UFP generated from various sources is being studied under different size modes; nucleation, coagulation, and accumulation (Banerjee et al., 2015; Dinoi et al., 2021; Segalin et al., 2020; Yadav et al., 2019b). These modes help explore and understand the UFP's Particle Number Size Distribution (PNSD). The emission sources, precursor gases, and meteorological parameters cause variability in the transformation of UFP (Chu et al., 2018; Kanawade et al., 2014; Murari et al., 2014; Tiwari et al., 2013; Wang et al., 2014, 2017). Emissions generated from vehicles and industries add majorly to the UFP levels.

Keeping the above points in mind, the methodology of this study is divided into two parts: the first part monitors and analyses the quantification, formation, and growth of UFP in the roadside microenvironment; the second part monitors and analyses major pollution episodes in Delhi, such as Diwali, and air pollution prevention schemes, such as Odd-even, in terms of UFP quantification and classification.

3.2 Site selection for the study

The monitoring site is located inside the Delhi Technological University campus, Delhi (28.75° N, 77.12° E, 223 m above the mean sea level). The first monitoring site is adjacent (8 meters away) to the roadside (the Bawana road; Figure 3.1), 12 km away from the Bawana industrial area, and is surrounded by residential building constructions. The experimental location receives considerable sample air from automobiles (an average hourly population of nearly 1300 vehicles passing during the peak hours on regular days) and other anthropogenic road emissions. However, the traffic during the experimental period dropped drastically (traffic reduced by 94%, >63%, and ~ 55% during different phases of the lockdown compared to the values in 2019 during a similar period) restrictions imposed during the lockdown. The experiments were carried out from April 2020 - June 2021.

The second monitoring site (Diwali and Background monitoring) is located inside the campus and >500 m far away from the roadside monitoring location. The google earth view of the location is depicted in Figure 3.2. The instrument was placed at a height of around 10 feet near the Central Pollution Control Board (CPCB) monitoring station inside the campus. The location was so selected that it covers residential and commercial areas, maintaining a homogeneous environment far away from road traffic (Figure 3.2). This way, we can minimize the vehicle-generated particle number concentration (PNC) related intervention, focusing on the background PNC in ambient air.

For Odd-even Scheme-II, the monitoring was carried out over Delhi at three different traffic corridors: Pitampura, Panchkuian Marg, and Najafgarh Road, respectively (Figure 3.3). The monitoring sites were selected in such a way so that they can cover a wide range of areas, i.e., industrial, commercial, residential, and institutional, in Delhi city (Mishra et al., 2019).

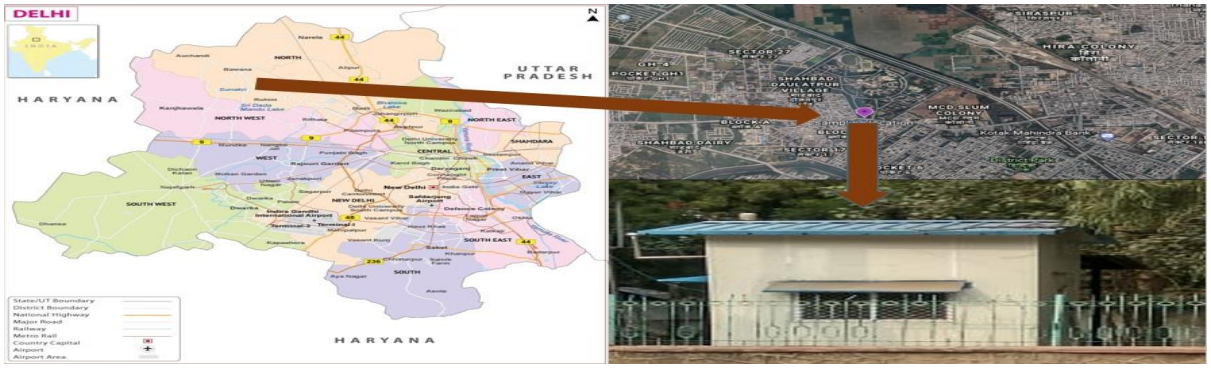

Figure 3.1: Monitoring location of road microenvironment at Delhi Technological University (DTU), New Delhi, India

Figure 3.2: Google earth view of Diwali and background monitoring station at DTU campus in New Delhi

Moreover, during the monitoring and assessment of the second phase of the Odd-Even scheme, 2016 for $PM_{2.5}$ & PM_1, similar locations were taken by Mishra et al. (2019). These locations provided the simultaneous data of our selected parameters for the periods considered in this study to be traffic-rich intercity traffic corridors. For example, Pitampura is a part of North-West Delhi, and it is an upscale residential, commercial and retail centre. The area is encompassed between Outer and Inner Ring Roads, NH-1, and Rohtak Road. Najafgarh is part of Southwest Delhi, primarily known as rural Delhi's economic and transport hub. It is situated on the outskirts of the Southwestern part of Delhi and borders the State of Haryana. Indira Gandhi International (IGI) Airport is the

nearest Airport to Najafgarh. Drivable roads well connect Najafgarh with significant destinations all over Delhi and Haryana. The Main Najafgarh Road (officially Shivaji Road) connects Najafgarh to New Delhi's city, while several other roads connect it to several villages along the Delhi-Haryana Border.

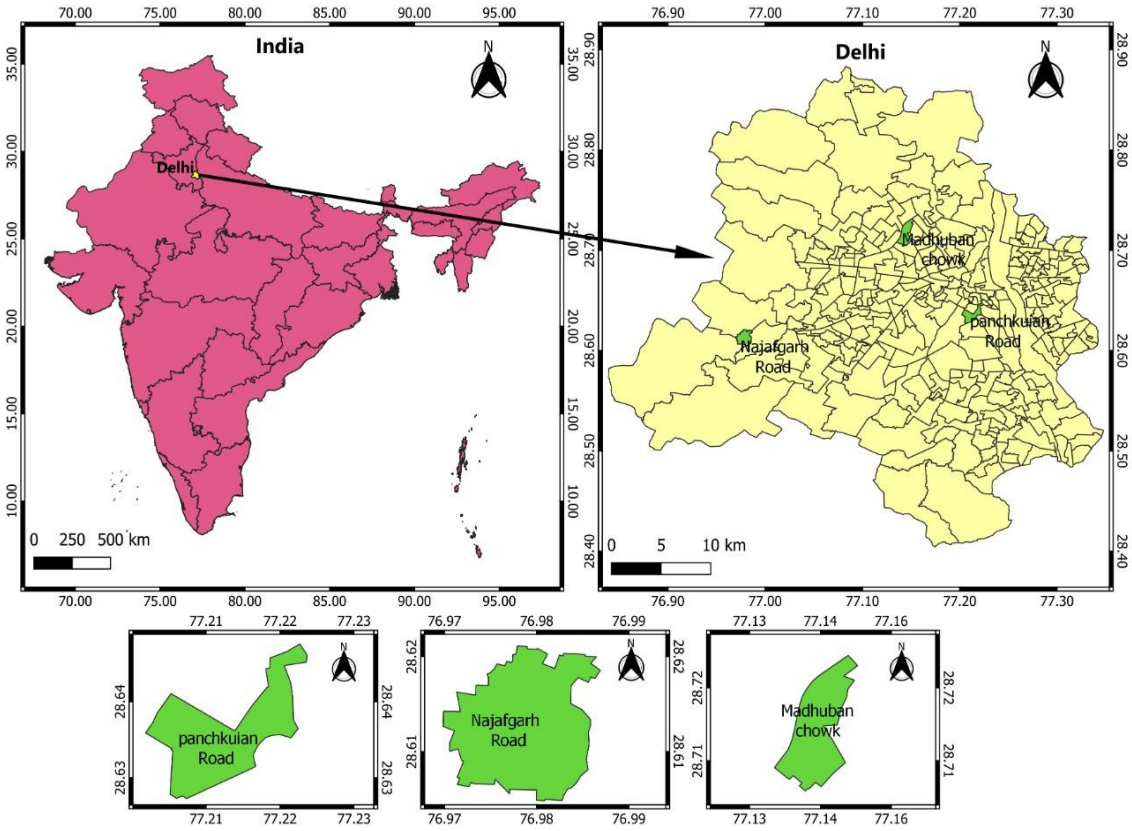

Figure 3.3: Monitoring location for the Odd-even Scheme-II in Delhi, India

3.3 Instrumentation

The measurement (UFP) of the particle number size distributions (PNSD) was carried out using a scanning mobility particle sizer with a condensation particle counter (SMPS + C) (Make: GRIMM Inc., Germany, Model: SMPS + C 5.403) in the size range of 10.2 to 1090 nm with a time span of ~7 min of each scan. The SMPS instrument uses the principle of 'differential mobility analysis' to size segregate aerosols into 45 size bins. The SMPS setup consists of an electrostatic classifier with a long differential mobility analyzer (LDMA) and n-butanol based condensation particle counter (Model: GRIMM,

SMPS + C 5.403), which counted the size-resolved particles. The particles were brought to an equilibrium charge distribution using a β-radioactive source (Ni-63) before they entered the classifier setup, and then these particles were classified according to their electrical mobility (Wiedensohler, 1988; Wang and Flagan, 1990; Collins et al., 2004). The ambient aerosols were drawn into the temperature-controlled laboratory from 3 meters height from the ground using conductive tubing of 0.8 cm diameter. A diffusion dryer was used to control higher RH conditions (Make: GRIMM Inc., Germany) with silica as a desiccant. The data is corrected for diffusion losses inside the sampling tubes and multiple charge correction using the software provided by the manufacturer.

The monitoring (for qUFP) was conducted with the portable instrument at all the selected locations. The instrument was placed at a horizontal distance of 8 m from the main road and at the height of 1.2 m from the ground. GRIMM™, Portable Aerosol Spectrometer (Optical Particle Counter), was used to monitor the data at all the selected locations. This instrument is based on real-time monitoring. It is a compact portable device built for continuous airborne particles measurement and measures the particle count distribution. Total inlet flow (1.2 L/min) is measured in an optical cell, and all optical and pneumatic components are self-tested to ensure high-quality standards. In this instrument, the monitored data was displayed as particle concentration in the unit particle/Liter and mass concentration in the unit $\mu g/m^3$. This instrument provides different size bins of particles and graphical representation with data correction.

Supporting the above, collocated real-time measurements of near-surface trace gases NO_x, O_3, SO_2, CO from trace gas analyzers and meteorological data (solar radiation, wind speed, wind direction, relative humidity, and air temperature) from automatic weather stations were used. The details of the instruments used in this experiment Table 3.1.

Table 3.1: Details of the instruments used in the present study

Parameter	**Instrument**	**Details**
Nano Aerosol	Scanning Mobility Particle Spectrometers with	Particle size range:10.2 nm to 1090 nm

number size distributions	Condensation Particle Counters (Model 5.403, GRIMM Aerosol Technik GmbH & Co. KG, Germany)	Size channels: 45 at standard 6.55 minutes interval
Particle Number count	Portable Aerosol Spectrometer (Optical Particle Counter) (Model 1.109, GRIMM Aerosol Technik GmbH & Co. KG, Germany)	This instrument has 31 equidistant sizes bins for particles ranging in size from 250 nm to 3200 nm.
Nitrogen oxide	NO_2/NO/NO_x Monitor Model 405 nm, 2B Technologies, In., USA)	Lower detectable limit: <1ppb 5.0 seconds interval
Ozone	Ozone monitor (Model 202, 2B Technologies, Inc., USA)	Lower detectable limit: <1.5ppb 5.0 seconds interval
Sulfur dioxide	Ambient SO_2 monitor (Model APSA-370, Horiba, Ltd., Japan)	Lower detectable limit: 0.5 ppb Zero drift: ±1.0 ppb/24-hour Linearity: ±1.0% of the full scale 5.0 minutes interval
Carbon Monoxide	Ambient CO monitor (Model APSA-370, Horiba, Ltd., Japan)	Lower detectable limit: 0.05 ppm Zero drift: ±0.1 ppm /24 hour Linearity: ±1.0% of the full scale

		3.0 minutes interval

3.4 Data statistics and equations

3.4.1 Data statistics

The dataset normality was tested using a combination of the Exploratory Data Analysis (EDA) plot and the Shapiro-Wilk (S-W) test. The Kruskal-Wallis (K-W) test, a nonparametric version of the ANOVA test, was performed on air quality data. The Kruskal Wallis test (rank-based nonparametric test) was used to determine the statistical differences between days (25^{th}, 26^{th}, $27^{th,}$ and 28^{th} November 2019) and independent variable pollutant (Nucleation mode, small Aitken mode, Large Aitken mode, Accumulation mode) of representative location in DTU campus in Delhi. Kruskal Wallis test denotes with H test.

$$\boldsymbol{H = \left[\frac{12}{n(n+1)}\sum_{j=1}^{c}\frac{T_i^2}{n_i}\right] - 3(n+1)} \qquad \textbf{3.1}$$

Where n= sum of sample size for all samples; c= number of samples; T_j=sum of rank in the j^{th} sample; n_j= size of the j^{th} sample. In particular, the H test examines whether the null hypothesis is valid and there are no statistical mean variations in population variances; if not true, then an alternative hypothesis is accepted. A 0.05 significance level was used in both cases. Therefore, if the p-value was lower than the significance threshold (< 0.05), the null hypothesis was rejected, and there was a statistically meaningful difference between the mean results.

3.4.2 Equations

3.4.2.1 Calculation of log-normal particle size distribution

An omnipresent primary mode (80-110 nm) in the Aitken and accumulation size regimes were present in all the observations. However, a distinct secondary mode, often open-

ended, was noticeable in the nucleation regime (< 25 nm) and the primary mode. The mean size distributions depicted flat or increased lower-size particle abundances confined to nucleation size regimes during the event periods. We have derived the modal parameters of the mean particle number size distributions during the event and non-event periods by fitting the observed size distributions to the analytical log-normal size distribution of the following form (Kompalli et al., 2018, 2020):

$$\frac{dN}{d\ ln\ D_p} = \sum_{j=1}^{n} \frac{N_k}{\sqrt{2\pi}\ ln\ \sigma_{m,j}} exp\left[-\frac{\left(ln\ D_p - ln\ D_{m,p,j}\right)^2}{2\ ln^2\ \sigma_{m,k}}\right] \quad \textbf{3.2}$$

(Where D_p is the particle diameter, n is the total number of the modes considered, $D_{m,p,j}$ is the mode diameter of the j^{th} mode, $\sigma_{m,j}$ is the corresponding width of the mode, and N_j is the particle number concentration (amplitude) of the j^{th} mode).

3.4.2.2 Calculation of growth rate (GR) and condensation sink (CS)

The growth rate (GR) represents the increase in particle size (nm/h) following their formation through nucleation. In this study, GR was calculated by the maximum concentration method described in (Kulmala et al., 2012). During an NPF event, due to a large influx of smaller particles, the mode of the PNSD shifts towards the lower size range. As the newly formed particles grow to larger sizes, this mode shifts towards the larger sizes. From the temporal evolution of the mode of the PNSD, the GR can be calculated. To derive the maximum particle concentration, the time series of the particle number concentrations in different size ranges were plotted. We estimated the GR from the slope of the best-fitted line on the graph of the mid-point diameter of particles versus the maximum concentration-time (Pierce et al., 2014; Dos Santos et al., 2015).

$$\boldsymbol{GR = (d_{p2} - d_{p1})/(t_2 - t_1)} \quad \textbf{3.3}$$

Where d_p is particle diameter in d_{p1} and d_{p2} and nm, and t is the respective time at t_1 and t_2.

The condensation sink (CS), defined as the rate at which condensable vapors condense on pre-existing particles, was calculated based on the following (Kulmala et al., 2001; Erupe et al., 2010; Kompalli et al., 2018, 2020).

$$\boldsymbol{CS = 2\pi D \sum_i \beta_i d_{pi} N_i} \qquad \textbf{3.4}$$

Where D is diffusion coefficient, β_i is the size-dependent transition correction factor, d_{pi} is the particle diameter in size-bin i, and N_i is the particle number concentration in that size bin. Further, the value of β_i was given by,

$$\boldsymbol{\beta_m = \frac{1 + K_n}{1+\left(\frac{4}{3\alpha_m}+0.337\right)K_n+\frac{4}{3\alpha_m}K_n^2}} \qquad \textbf{3.5}$$

Where α_m is the sticking coefficient (mass accommodation coefficient, taken as unity here), and K_n is the dimensionless Knudsen number, which is given by $K_n = 2\lambda / d_p$. Knudsen number is the ratio of λ (the effective mean free path) characterizing the gas concerning the transport of mass, and a length scale d_p characterizing the particle.

3.4.2.3 Estimation of sulfuric acid proxy concentrations

The most ubiquitous and key precursor for NPF is sulfuric acid (Kulmala et al., 2004, 2012; McMurry et al., 2005; Kulmala and Kerminen, 2008; Nieminen et al., 2009; Kerminen et al., 2018) due to its low vapor pressure under typical atmospheric conditions (e.g., <0.001 Torr at 300 K for pure H_2SO_4) (Kuang et al., 2008, 2010; Zhang et al., 2012). Gas-phase chemistry involving photo-oxidation of SO_2 produces sulfuric acid vapors that exceed the saturation vapor concentration over an aqueous solution (typically during the daytime) that can trigger NPF (e.g., Lee et al., 2019). The ambient concentration of sulfuric acid and freshly formed particles depict a strong correlation. Several studies have confirmed a strong correlation between the number concentrations of freshly formed particles and the ambient concentrations of sulphuric acid. Many studies proposed methods to estimate H_2SO_4 proxies (e.g., Petäjä et al., 2009; Mikkonen et al., 2011; Dada et al., 2020; Lu et al., 2019). In the present study, we have calculated a proxy for H_2SO_4 following the methodology of

Mikkonen et al. (2011), with an assumption that the production and loss of sulfuric acid are in pseudo-steady state, as below:

$$[\boldsymbol{H_2SO_4}] = \boldsymbol{8.21\ x\ 10^{-3}.k.Radiation.[SO_2]^{0.62}.[CS.RH]^{-0.13}} \quad \textbf{3.6}$$

where $[H_2SO_4]$ is sulfuric acid concentration, k is the reaction coefficient (1.03495), radiation is solar flux (W m^{-2}), $[SO_2]$ is the concentration of SO_2 (in ppb), CS is condensation sink (sec^{-1}), and RH is relative humidity (%).

3.4.2.4 Identification of nucleation events

We have adopted the criteria previously prescribed by Dal Maso et al. (2005) and explained in Kompalli et al. (2020, 2014a) to identify new particle formation events,. The criteria require (i) a clear appearance of a new mode in the nucleation size regime of the PNSD, which (ii) prevails for a few hours (> 1 hour), and (iii) subsequently grows to larger sizes. Well-defined nucleation events followed all the three criteria stated above, whereas the events that did not follow this criterion are classified as non-events. In some of the cases, though criteria (i) and (ii) are fulfilled, the growth of the nucleation mode, i.e., criteria (iii) did not meet, and such events are termed as an undefined class. Further, in an NPF event, if the particle formation and growth rates could be estimated without much ambiguity from the temporal evolution of PNSDs, it is classified as a 'Class I' event. However, due to rapid fluctuations in the concentrations, if the formation and growth rates could not be derived from the observations, it is a 'Class II' event. Among the Class I events, the event where the temporal evolution of the mode of the new particles is clearly distinguishable from the pre-existing background mode is called as 'Class Ia' event. Any event in the 'Class I' category, in which the temporal evolution new particle mode is obscured by or superimposed on the pre-existing PNSDs, is considered 'Class Ib'(Figure 3.4).

Further, we have also adopted by methodology prescribed by Zimmerman et al. (2020) to separate NPF events (nucleation followed by growth) and particle burst events (continuous bursts of nucleation mode particles that persisted for multiple hours while maintaining a constant geometric mean diameter. Also, during the burst events, there is

a discernible enhancement in NO_x concentrations, indicating the possible primary origin of the ultrafine particles.

Apart from the above, we have included the parameter odd-oxygen ($[Ox] \equiv [O_3]+[NO_2]$) in the analysis (Wood et al., 2010) in the analysis. The concentration of Ox describes oxidant capacity. It can be described as the sum of a regional (the O_3 background and NO_x-independent) and a local (linearly NO_x-dependent) contribution. Therefore, the association of oxidant Ox with NO_x helps to infer the atmospheric sources of Ox in the study area. As highlighted by Wood et al. (2010), odd-oxygen and the oxygenated component of organic aerosol (OOA) (which is a surrogate for secondary organics) have a better correlation when both species have similar spatial and time scales (< 8 hours) of formation. Thus, the events from localized pollution and those driven by photochemistry can be discerned.

3.4.2.5 Calculation of percentage change for Odd-even Scheme-II

Percentage change of pollutant in odd/even day with respect to normal day is calculated by:

$$\%\ \boldsymbol{Change\ of\ Con.} = \frac{\boldsymbol{Con.(odd\ or\ even\ day)} - \boldsymbol{Con.(normal\ day)}}{\boldsymbol{Con.(normal\ day)}} \boldsymbol{X\ 100} \qquad \mathbf{3.7}$$

Where, Con. (odd or even day) = concentration of pollutant on odd/even day of the scheme; Con. (normal day) = concentration of pollutant on a normal day of scheme. Statistical tool 'IBM-SPSS' software has been used in all statistical analyses.

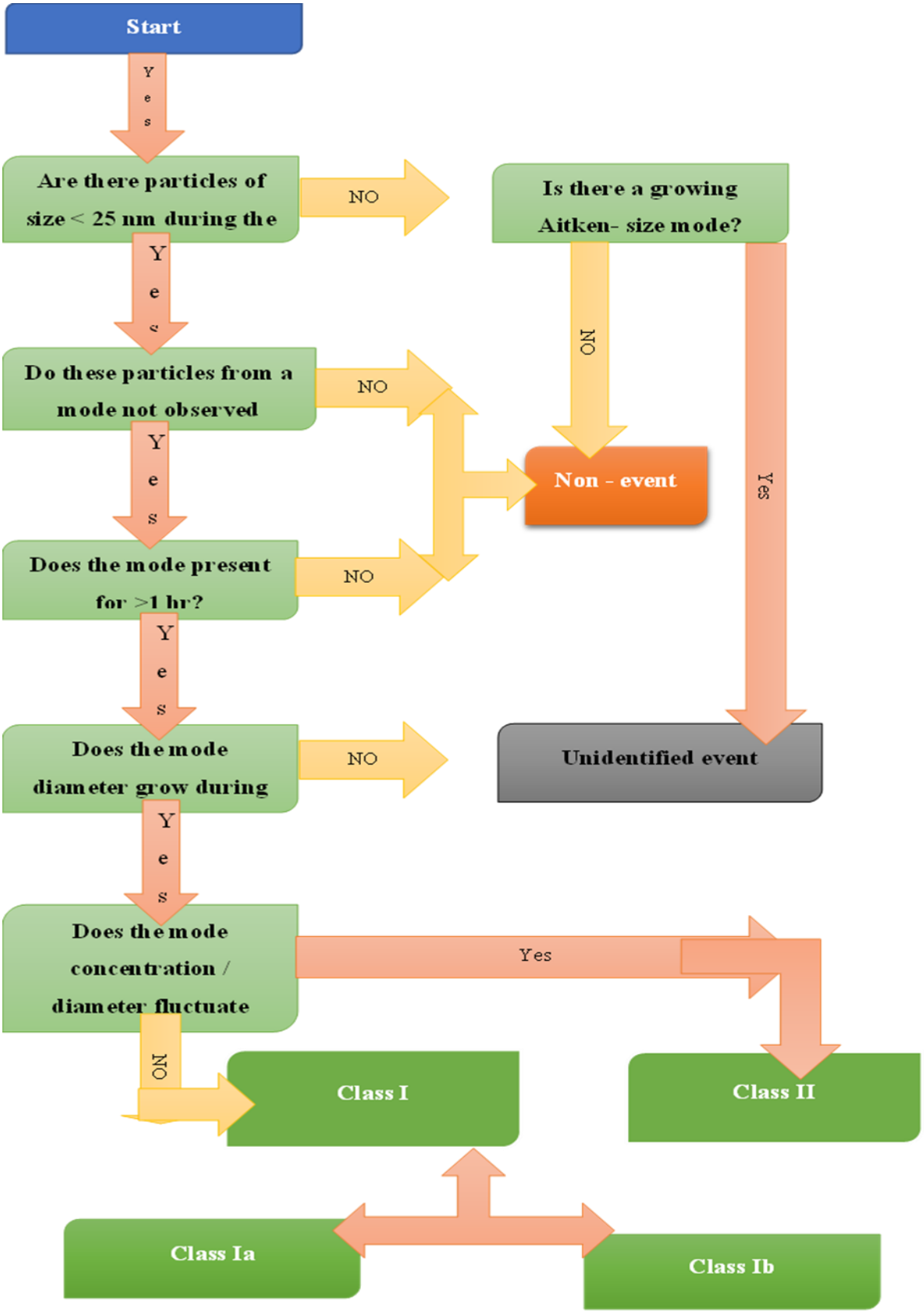

Figure 3.4: Flow chart of identification of nucleation event types

CHAPTER-4

4 RESULT AND DISCUSSION

4.1 Introduction

Due to a lack of space, the majority of the population in Delhi lives near the road microenvironment, and motorization is increasing day by day in Delhi, resulting in increased regular exposure to vehicular pollution and health risk. In today's highly urbanized cities, increasing the number of vehicles directly increases the city's ambient air pollution level. In recent years, ambient air pollution has become an essential aspect of the urban environment. Research Society is paying exploratory attention to atmospheric aerosols in the area of small size particulate matter. It is one of the significant sources of ultrafine particulate matter (UFP-less than 100 nm diameter) on the global and regional scale, affecting climate change, visibility, and cloud condensation nuclei (CCN) and other events. In a polluted city's environment, UFP becomes essential because it lacks a comprehensive study. UFP directly or indirectly affects human health, i.,e deep penetration and deposition into lungs, cardiorespiratory system to the terminal bronchioles and alveoli, bloodstream, and body organs such as brain, kidney and liver. However, UFP does not have an estimated and calculated health risk factor. PNC of UFP > 80% contributed by the road microenvironment in such cities where vehicular air pollution is one of the major sources of ambient air pollution. The advent of unregulated pollutants such as UFP has added an additional dimension to this already complex issue, while cities face challenges in addressing the problem of conventional air pollutants that are part of the current regulatory framework. Several experimental and numerical studies have advanced knowledge of the emission, formation, dispersion, exposure, and health effects of UFPs over the last decade. Most of these studies have been carried out in European cities, with only a few in developing Asian cities where most of the world's urban population resides. The present study focuses mainly on the outcome of data analysis of UFP in terms of classification and quantification in the road microenvironment. The study also covers the classification and quantification of UFP at certain events known as air pollution episodes in Delhi like Diwali and Odd-Even

Scheme - II. Data analysis (for Odd- Even Scheme -II) covers the particle size range of QuasiUFP (> 250 nm), as monitoring was conducted on the roadside at different locations in Delhi with the suitability of instrument (OPC), which covers the QuasiUFP size range.

This research focuses on particle size (10 nm > Dp <1000 nm), which is denoted as total PNC ('N_{total}'), and UFP is a subset of it. It has been classified into four modes for further investigation: the nucleation mode (10 nm > Dp <20 nm), the small Aitken mode (20 nm > Dp 50 nm), the large Aitken mode (50 nm > Dp <100 nm), and the accumulation mode (100 nm > Dp< 1000 nm). QuaiUFP (100 nm > Dp <500 nm) has also been discussed as needed.

The monitoring was conducted from 26th November 2019 to 31st June 2021 and covers 15 months (~75%) out of 20 total months. A background study was carried out in November and December of 2019, and a roadside study was carried out from April 2020 to June 2021. The "summary plot" graph (Figure 4.1) is a method of quickly summarising important aspects of data and provides a critical graphical and statistical overview. The plots in the left panel depict time series data, with blue indicating the presence of data and red indicating the absence of data. The daily mean values are also displayed in pale yellow scales to cover the data range from 0 to the maximum daily value. As a result, rather than conveying quantitative information, the daily deals indicate an overall trend. Overall summary include parameter, i.e., N total, UFP, Geo metric mean diameter of particle (GMD), nucleation mode, small Aitken mode, large Aitken mode, QuasiUFP, and accumulation mode) overall summary statistics. The percentage of data captured for each year is shown in green font. The distribution of each species is depicted using a histogram plot in the panels on the right. The mean, mode and 95th percentile of each calendar year of monitored data are mentioned on each panel. In left hand side of graph histogram shows the N total and UFP maximum concentration ranges from ~ 1.9 x 10^4 to 3.0 x 10^4 #/ cm^3 upto >50% and 0.5 x 10^4 to 1.5 x 10^4 #/cm^3 upto 40% respectively. While GMD maximum ranges from 30 nm to 80 nm > 60% during the monitoring period (Figure 4.1 and Figure 4.4). In calendar plot (Figure 4.2 and Figure 4.3) of UFP & GMD shows the average daily PNC through colour scaling. Summer and partially monsoon seasons show higher UPF concentration while GMD shows higher particle size in winter.

Figure 4.4 depicted that November and December 2019, as the background study shows, the higher GMD, which is > 60 nm diameter, and total PNC is higher than > 4.0 x 10^4 #/cm^3. But at the same time, it shows the minimum nucleation mode concentration, which is < 3.0 x 10^3 #/cm^3, while the accumulation mode is higher in December. This study investigates that background location has a higher size (GMD) particle number concentration compared to the roadside monitoring station. Although December has a higher value of PNC of all modes than November but in the case of the ratio of UFP/ $N_{total,}$ which is lower (0.59 ± 0.13) than November (0.64 ± 0.11) Table 4.1). More information on the variation of a PNC and GMD of particles by the time of day and day of week can be found in the figure (Figure 4.5 and Figure 4.6).

In the case of road microenvironment (April 2020 to June 2021)**,** PNC of N_{total} gradually increased from summer 2020 till early monsoon 2020 and sudden drop in October. Interestingly in winter 2020 & 2021**,** it retained the peak and gradually started to decrease in summer 2021 (Figure 4.4). On the contrary, GMD is low in **s**ummer and goes higher in the winter. However, it reached its highest peak >100 nm diameter in October 2020, while this month shows a decrement in all modes, which may be due to the monsoon month. Table 4.1 provides a detailed summary of each month's mean and standard deviation values. The PNC of the nucleation mode is greater in the summer than in the winter. Interestingly, the UFP/N total ratio exhibits a similar trend to the nucleation mode, indicating the importance of nucleation mode particles in new particle formation (NPF). This will be covered in the following section of this chapter.

The variation of a PNC of all modes and GMD of particles by the time of day and day of week of seasons (Summer, Winter, Monsoon) can be found in the figure (Figure 4.7, Figure 4.8, Figure 4.9, Figure 4.10, Figure 4.11, and Figure 4.12). In summer, N total and UFP start increase from morning 06:00 AM to 12:00 PM and 06:00 PM to 10:00 PM evening, which may be due to the photochemical reaction and vehicular emission with trans boundary condition, respectively. But in the case of accumulation mode, it started to decrease from 06:00 AM to 02-03:00 PM and then began to increase till late night of each day. There is no significant trend difference found between weeks in summer. Near afternoon time (~12:00 PM) shows the lowest GMD of days, which is a typical signature of photochemical reaction concerning new particle formation. N_{total} and UFP show the

same pattern in winter as summer, only the peaks are sharp and smooth. Importantly morning and evening peaks are almost the same, which is not in the case of summer, its morning peaks are always higher than evening peaks. Accumulation mode shows the same as summer, but its duration shrinks. In the case of GMD, interestingly, it does not show a smooth pattern like summer and gets a maximum drop before 12:00 noon unlike summer and keeps fluctuating till 05:00 PM, which indicate the hindrance in particle growth size. About the monsoon seasons, the variation of a PNC of all modes and GMD of particles by the time of day and day of the week can be found in the (Figure 4.7,Figure 4.8,Figure 4.9,Figure 4.10,Figure 4.11, Figure 4.12).

Table 4.1: A data summary of different modes in different seasons

Year	Month	Season		N_{total}	UFP	Nucleation	Small Aitken	large Aitken	Accumul - ation	GMD (nm)	UFP/ N_{total}
2019	November	Winter	Mean	2.79×10^4	1.83×10^4	2.45×10^3	7.19×10^3	8.70×10^3	9.58×10^3	69.22	0.64
			Std.	$\pm 1.62 \times 10^4$	$\pm 1.14 \times 10^4$	$\pm 1.39 \times 10^3$	$\pm 4.69 \times 10^3$	$\pm 6.85 \times 10^3$	$\pm 5.78 \times 10^3$	±31.36	±0.11
	December		Mean	4.30×10^4	2.66×10^4	2.71×10^3	9.77×10^3	1.41×10^4	1.64×10^4	78.23	0.59
			Std.	$\pm 2.98 \times 10^4$	$\pm 2.03 \times 10^4$	$\pm 3.22 \times 10^3$	$\pm 7.79 \times 10^3$	$\pm 1.30 \times 10^4$	$\pm 1.14 \times 10^4$	±33.51	±0.13

2020	April	Summer	Mean	2.38×10^4	1.78×10^4	4.59×10^3	6.38×10^3	6.81×10^3	6.00×10^3	58.14	0.72
			Std.	$\pm 1.18 \times 10^4$	$\pm 1.11 \times 10^4$	$\pm 6.70 \times 10^3$	$\pm 4.81 \times 10^3$	$\pm 4.10 \times 10^3$	$\pm 3.50 \times 10^3$	±21.89	±0.14
	May		Mean	3.15×10^4	2.23×10^4	4.79×10^3	7.91×10^3	9.57×10^3	9.24×10^3	65.51	0.68
			Std.	$\pm 1.87 \times 10^4$	$\pm 1.77 \times 10^4$	$\pm 9.96 \times 10^3$	$\pm 7.87 \times 10^3$	$\pm 5.87 \times 10^3$	$\pm 5.87 \times 10^3$	±23.21	±0.16
	June		Mean	3.84×10^4	3.28×10^4	8.69×10^3	1.39×10^4	1.03×10^4	5.52×10^3	47.17	0.83
			Std.	$\pm 2.12 \times 10^4$	$\pm 2.10 \times 10^4$	$\pm 1.15 \times 10^4$	$\pm 1.10 \times 10^4$	$\pm 4.48 \times 10^3$	$\pm 2.67 \times 10^3$	±15.45	±0.09
	July		Mean	4.08×10^4	3.61×10^4	1.17×10^4	1.47×10^4	9.69×10^3	4.68×10^3	41.36	0.86

		Monsoon	Std.	±2.65 x 10^4	±2.57 x 10^4	±1.43 x 10^4	±1.23 x 10^4	±4.97 x 10^3	±2.55 x 10^3	±12.94	±0.07
	October		Mean	2.76 x 10^4	1.35 x 10^4	2.56 x 10^3	4.95 x 10^3	5.97 x 10^3	1.42 x 10^4	99.12	0.46
			Std.	±1.44 x 10^4	±1.12 x 10^4	±4.90 x 10^3	±4.69 x 10^3	±3.82 x 10^3	±6.26 x 10^3	±32.14	±0.16
	November	Winter	Mean	3.62 x 10^4	2.02 x 10^4	4.54 x 10^3	7.37 x 10^3	8.27 x 10^3	1.60 x 10^4	87.27	0.52
			Std.	±2.05 x 10^4	±1.63 x 10^4	±7.44 x 10^3	±6.70 x 10^3	±6.24 x 10^3	±8.81 x 10^3	±35.31	±0.18
	December		Mean	4.19 x 10^4	2.52 x 10^4	4.76 x 10^3	8.96 x 10^3	1.14 x 10^4	1.68 x 10^4	80.57	0.56
			Std.	±2.71 x 10^4	±2.03 x 10^4	±7.85 x 10^3	±7.61 x 10^3	±1.02 x 10^4	±1.02 x 10^4	±27.17	±0.15

2021	January	Winter	Mean	4.29×10^4	2.70×10^4	5.09×10^3	9.71×10^3	1.22×10^4	1.59×10^4	76.92	0.59
			Std.	$\pm 2.69 \times 10^4$	$\pm 2.09 \times 10^4$	$\pm 8.53 \times 10^3$	$\pm 8.44 \times 10^3$	$\pm 9.73 \times 10^3$	$\pm 1.04 \times 10^4$	±27.00	±0.16
	February		Mean	3.60×10^4	2.31×10^4	5.86×10^3	8.60×10^3	8.60×10^3	1.29×10^4	74.77	0.60
			Std.	$\pm 2.18 \times 10^4$	$\pm 1.83 \times 10^4$	$\pm 9.04 \times 10^3$	$\pm 7.50 \times 10^3$	$\pm 6.72 \times 10^3$	$\pm 7.32 \times 10^3$	±29.81	±0.17
	March		Mean	3.51×10^4	2.64×10^4	8.90×10^3	1.04×10^4	7.13×10^3	8.68×10^3	56.51	0.71
			Std.	$\pm 2.05 \times 10^4$	$\pm 1.91 \times 10^4$	$\pm 1.15 \times 10^4$	$\pm 8.09 \times 10^3$	$\pm 4.77 \times 10^3$	$\pm 6.02 \times 10^3$	±26.01	±0.16
	April		Mean	3.05×10^4	2.22×10^4	7.52×10^3	8.39×10^3	6.31×10^3	8.32×10^3	60.13	0.70

		Summer	Std.	±1.61 x 10^4	±1.56 x 10^4	±1.01 x 10^4	±6.79 x 10^3	±3.54 x 10^3	±6.73 x 10^3	±30.52	±0.19
	May		Mean	2.26 x 10^4	1.68 x 10^4	4.78 x 10^3	6.69 x 10^3	5.32 x 10^3	5.83 x 10^3	58.05	0.70
			Std.	±1.25 x 10^4	±1.19 x 10^4	±6.22 x 10^3	±5.82 x 10^3	±3.30 x 10^3	±3.51 x 10^3	±22.78	±0.15
	June		Mean	2.47 x 10^4	1.99 x 10^4	6.48 x 10^3	8.26 x 10^3	5.20 x 10^3	4.77 x 10^3	50.29	0.76
			Std.	±1.59 x 10^4	±1.56 x 10^4	±8.37 x 10^3	±7.48 x 10^3	±3.05 x 10^3	±2.67 x 10^3	±20.05	±0.13

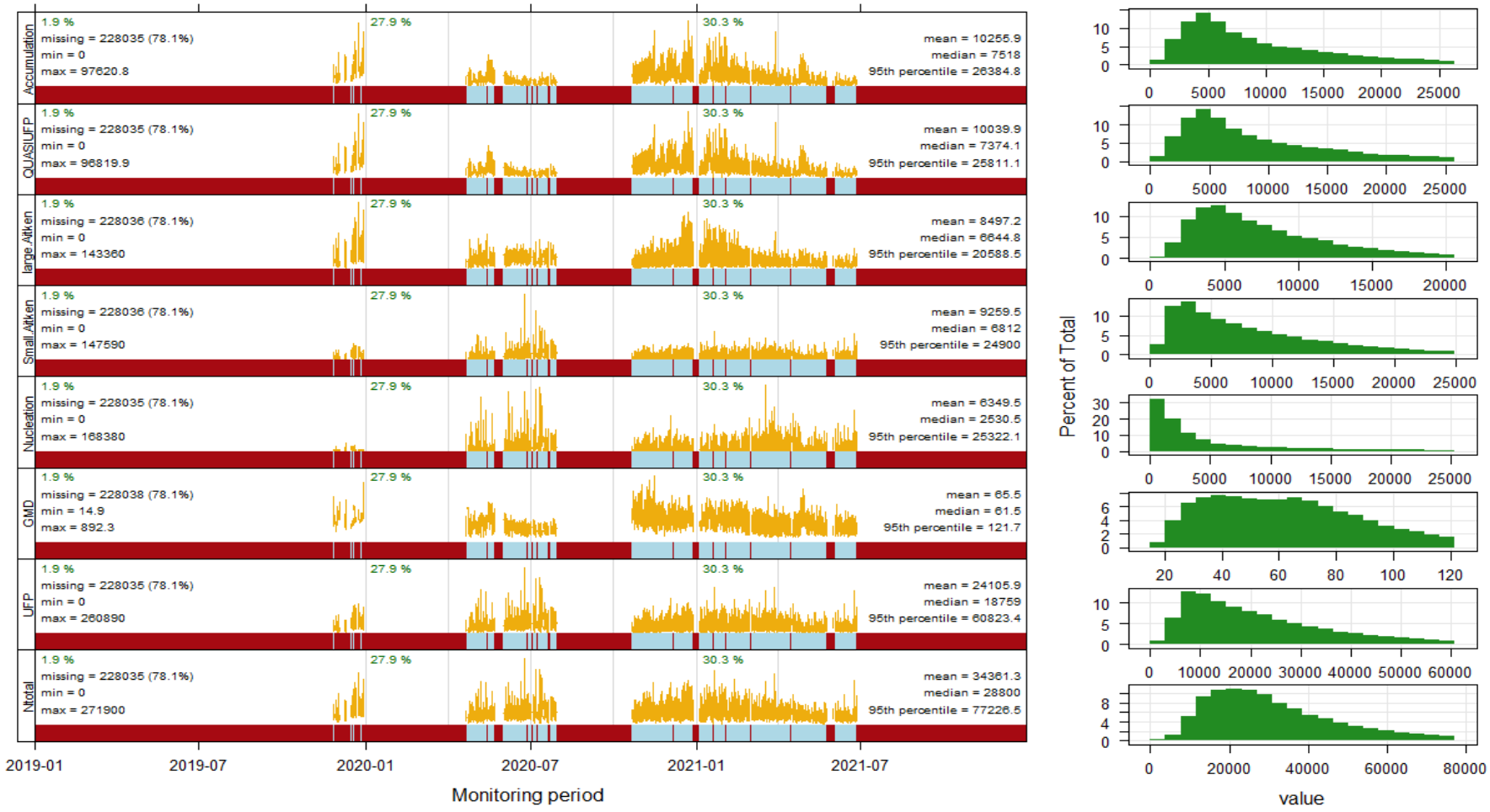

Figure 4.1: Summary plot of monitored data

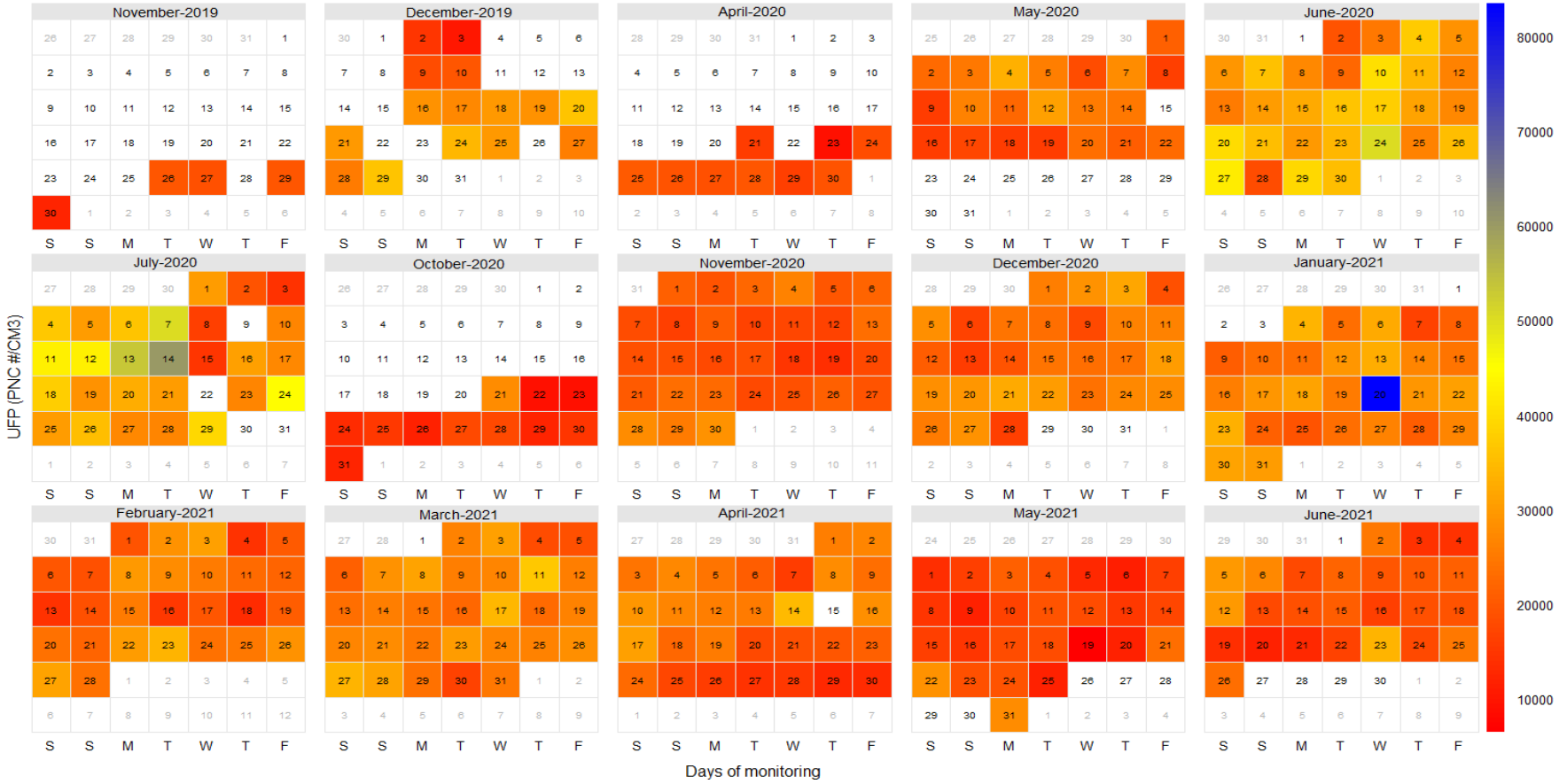

Figure 4.2: Calendar plot of UFP

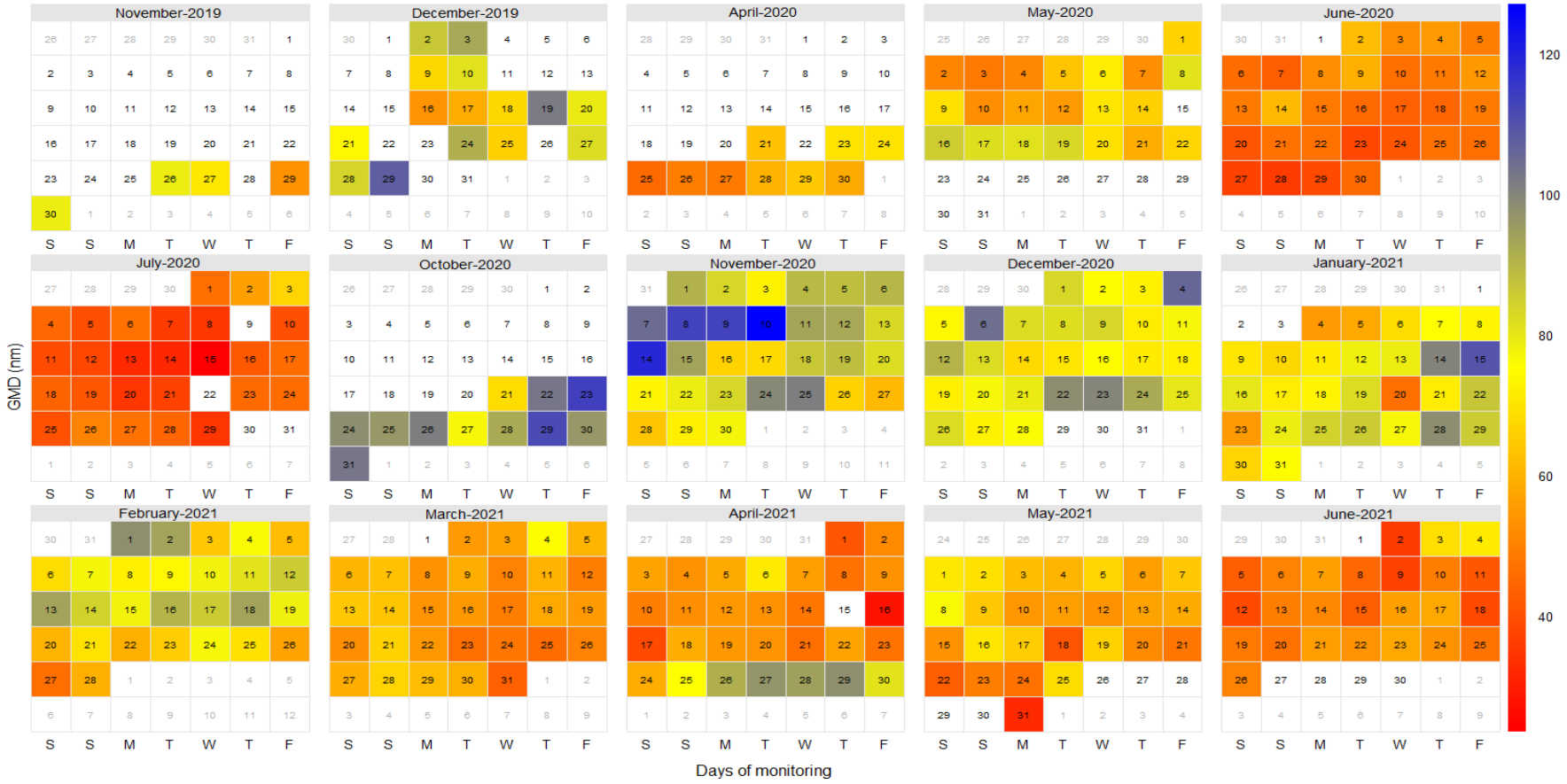

Figure 4.3: Calendar Plot of GMD

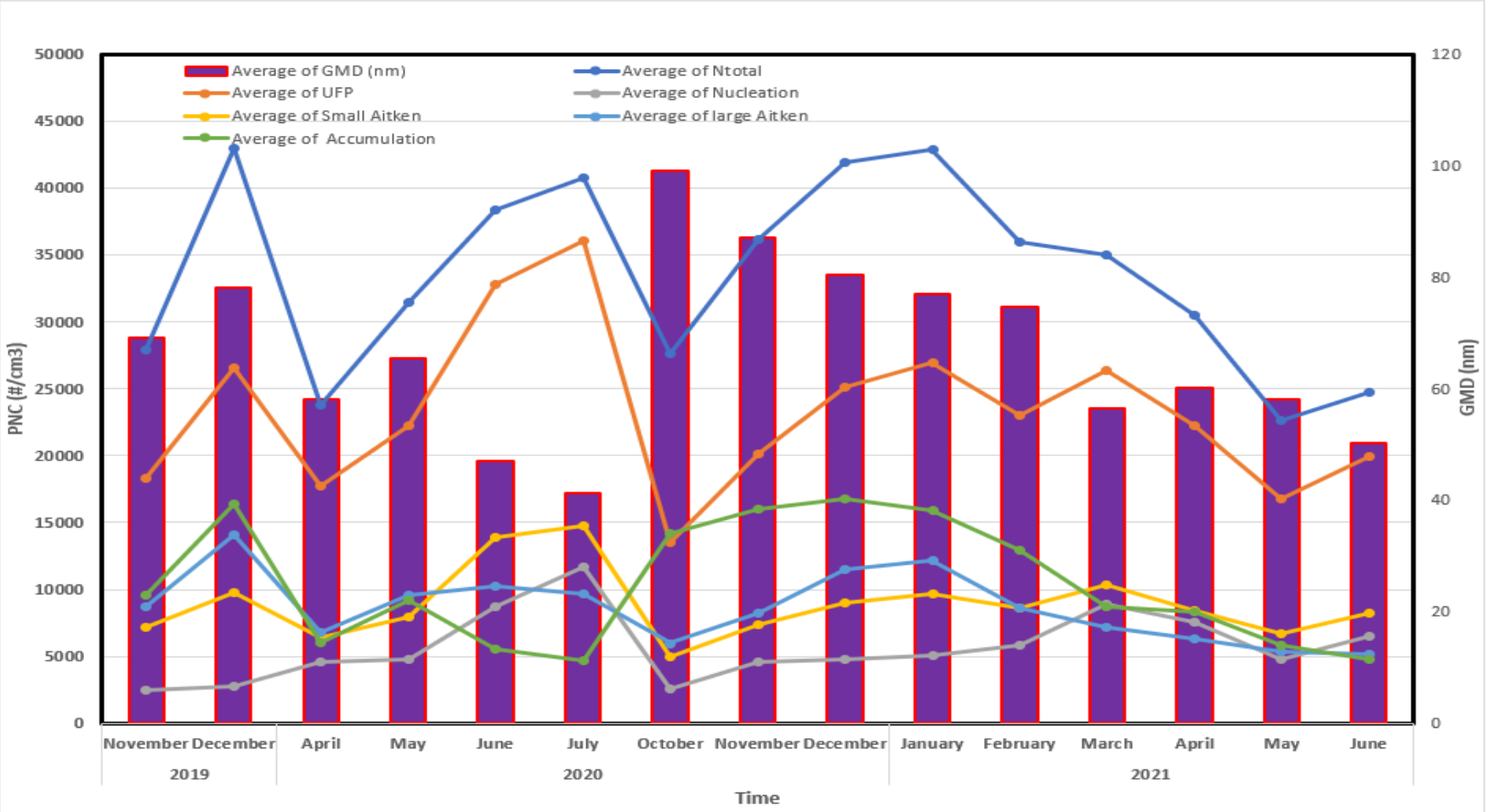

Figure 4.4: Time series of UFP and GMD

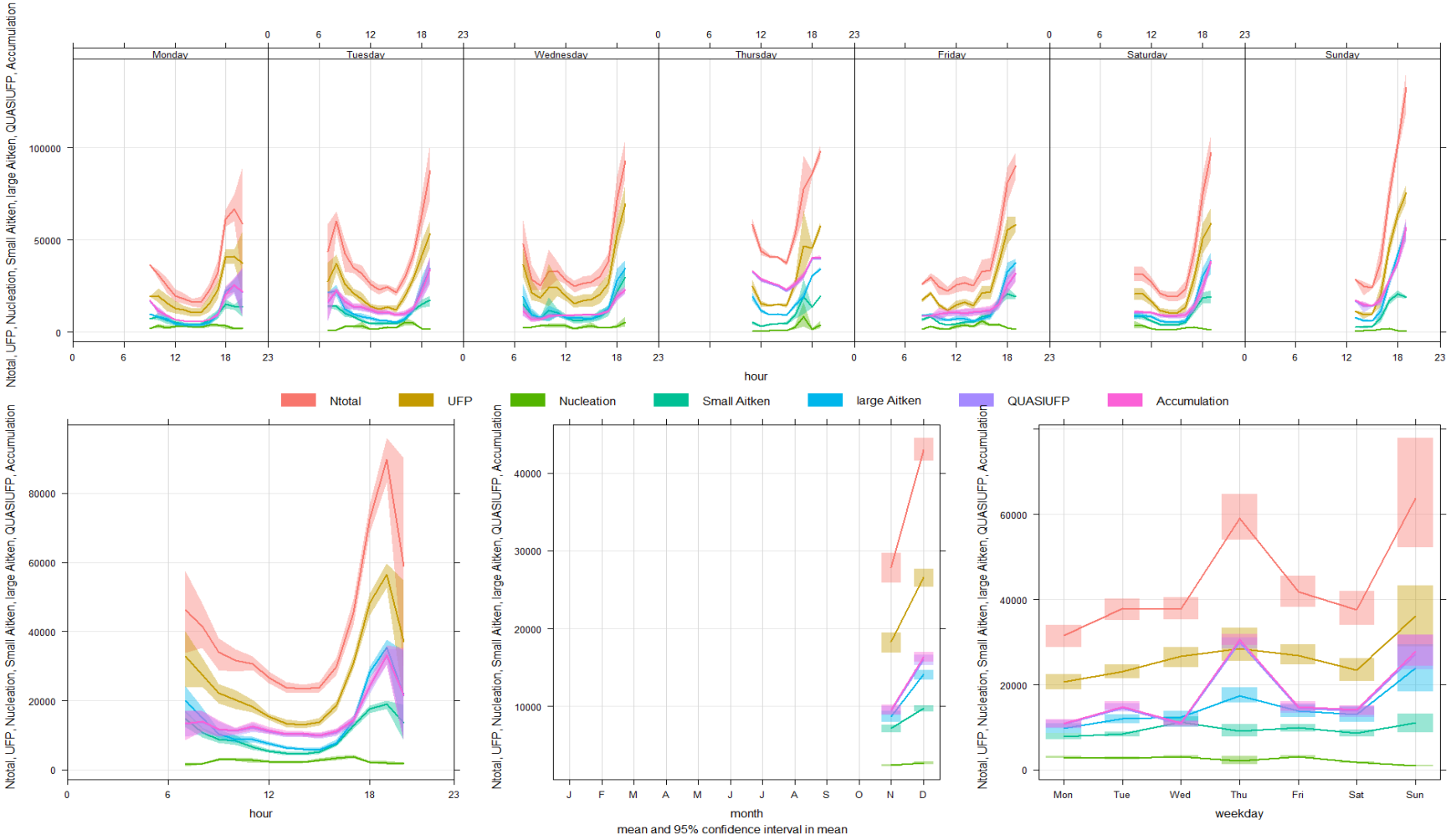

Figure 4.5: Time variation of PNC during background study

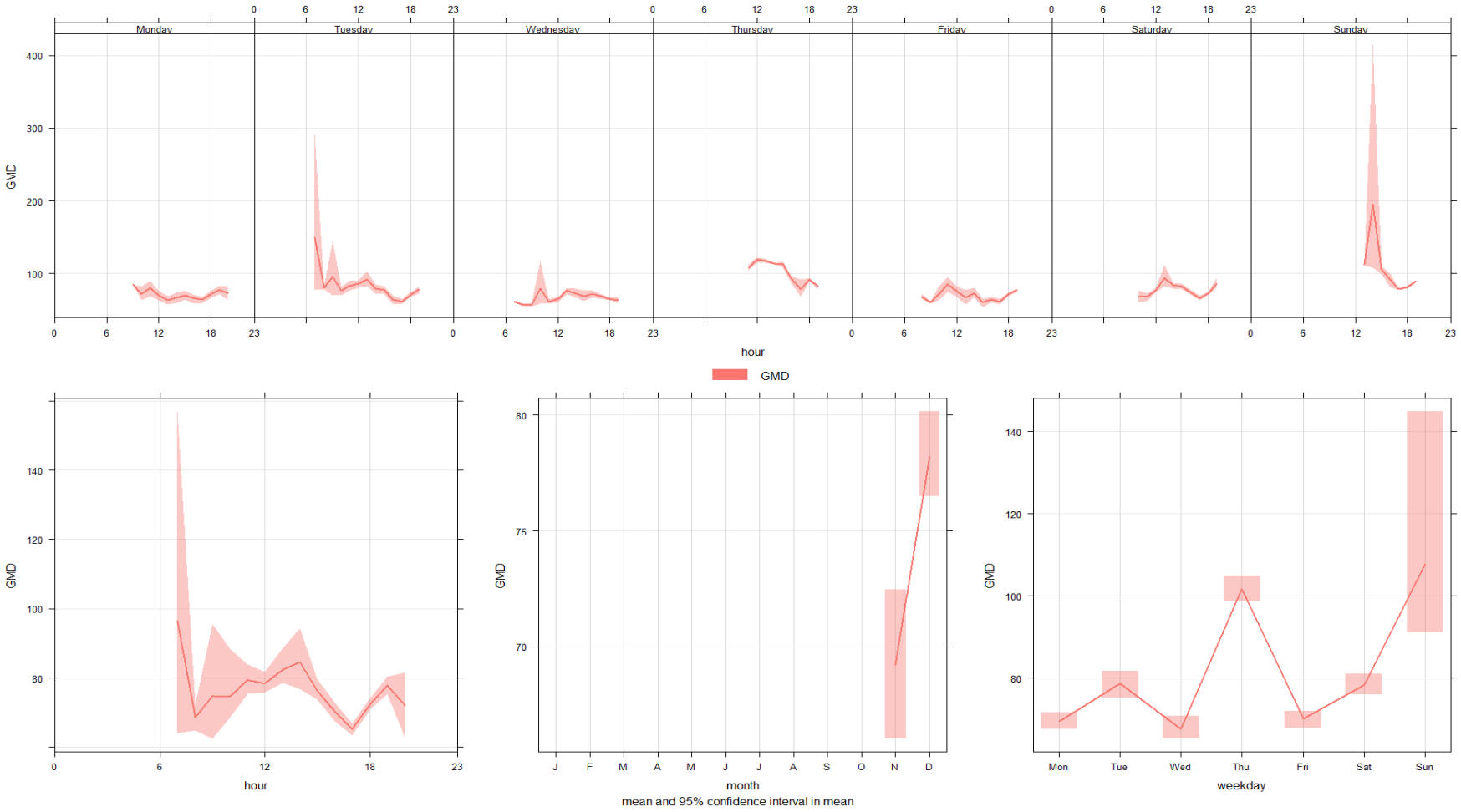

Figure 4.6: Time variation of GMD during background study

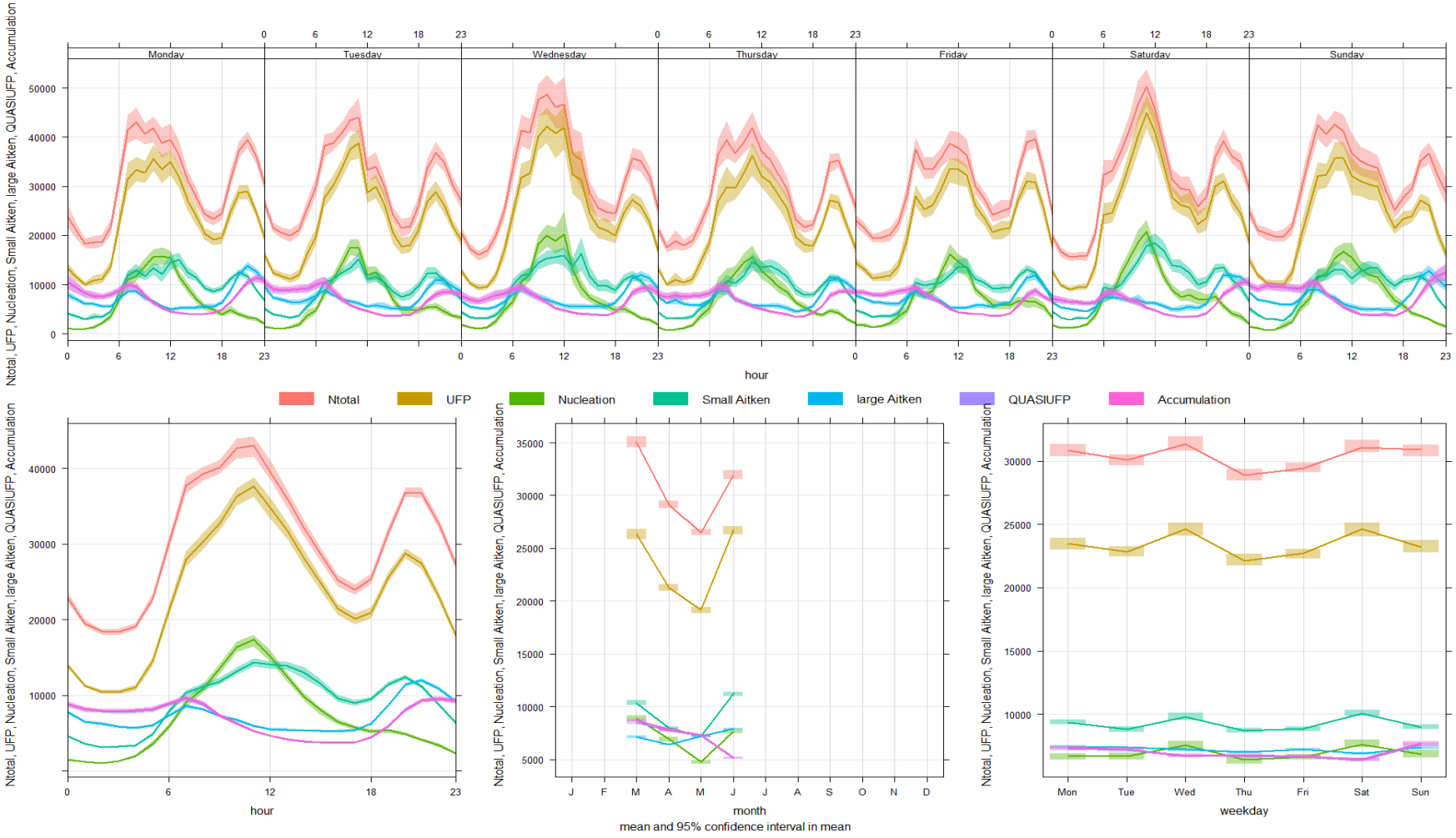

Figure 4.7: Time variation of PNC during summer season at road microenvironment

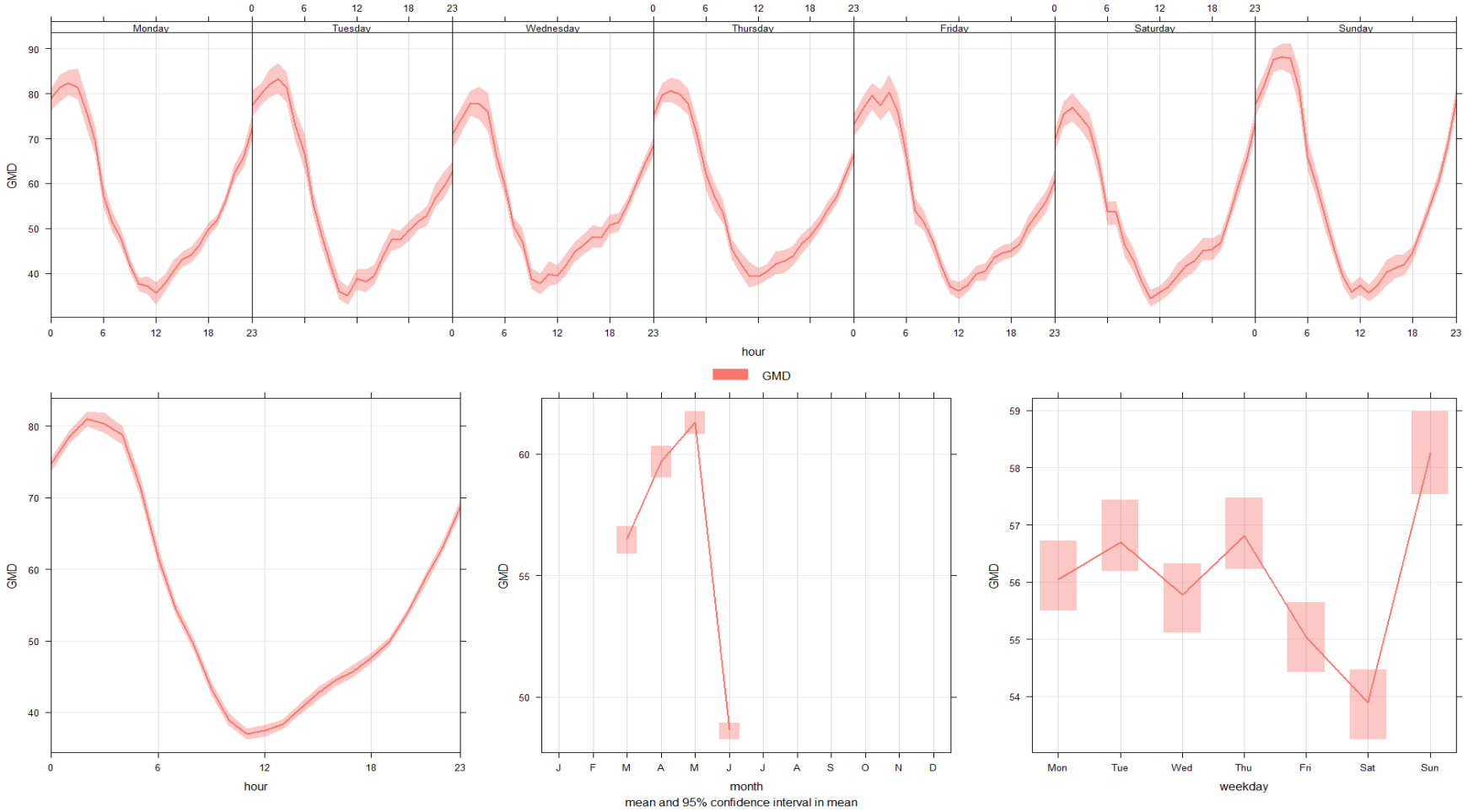

Figure 4.8: Time variation of GMD during summer season at road microenvironment

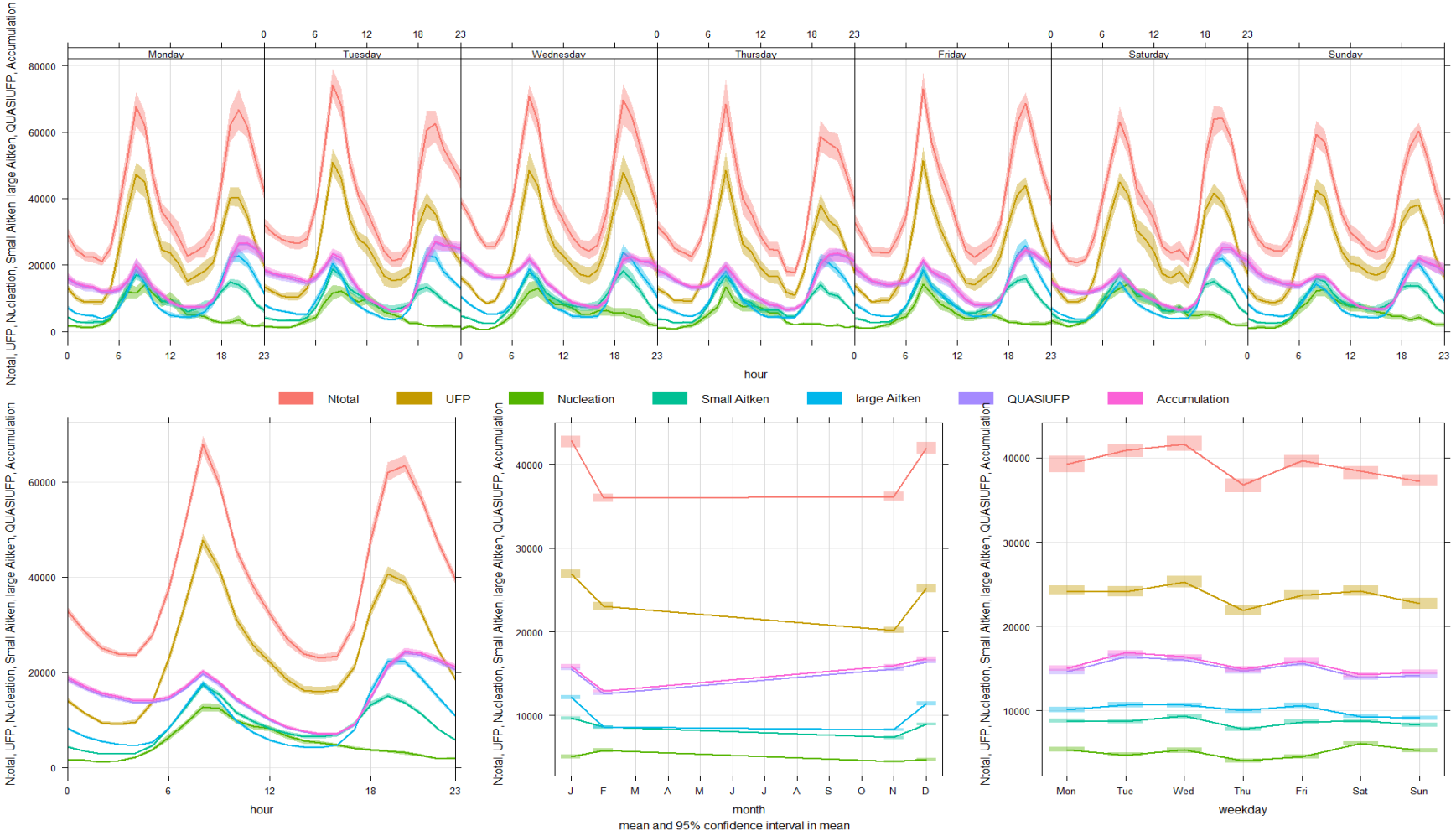

Figure 4.9: Time variation of PNC during winter season at road microenvironment

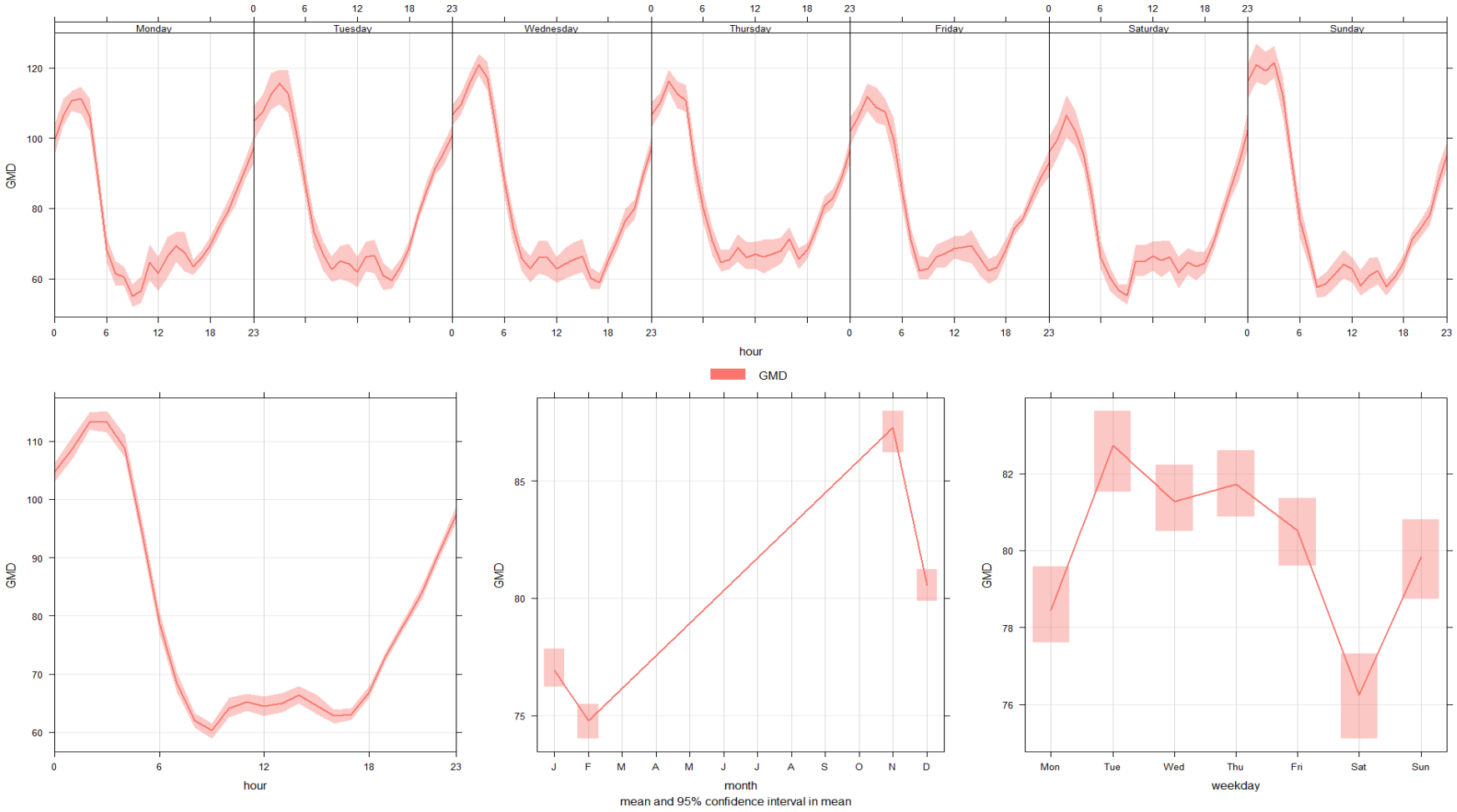

Figure 4.10: Time variation of GMD during winter season at road microenvironment

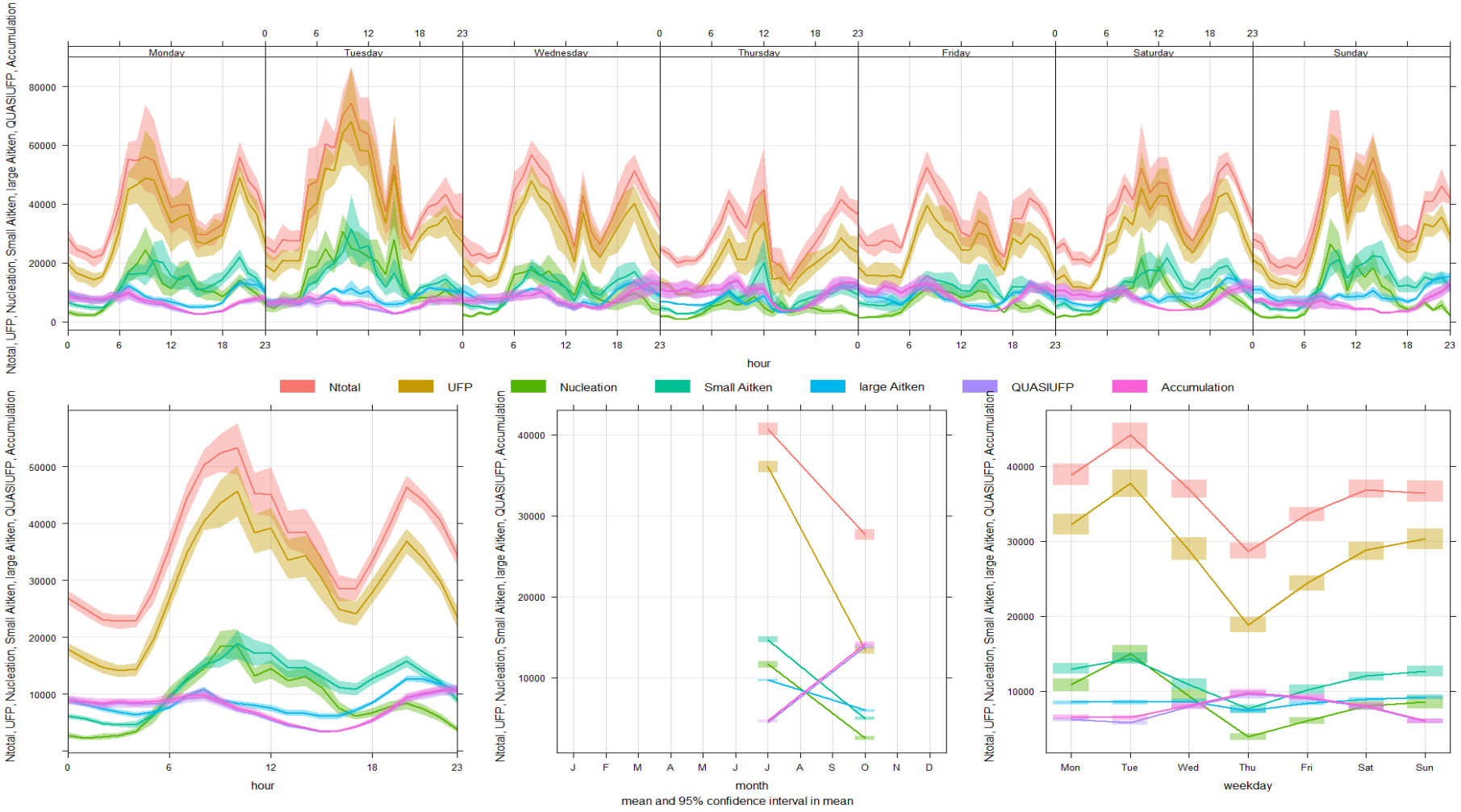

Figure 4.11: Time variation of PNC during monsoon season at road microenvironment

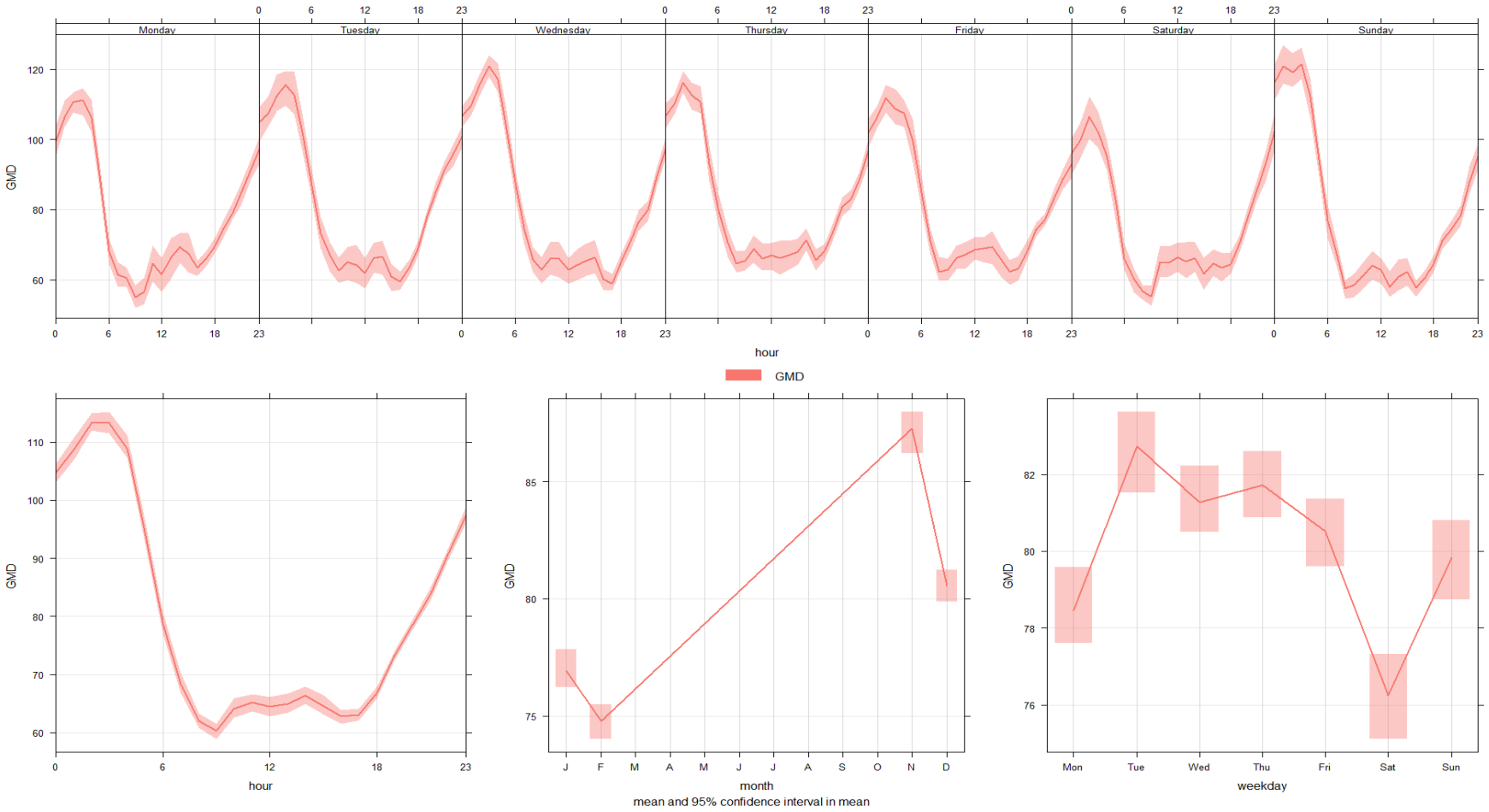

Figure 4.12: Time variation of GMD during monsoon season at road microenvironment

4.2 Number concentration and new particle formation events near road microenvironment in megacity Delhi.

The information on particle number size distributions (PNSD) is essential to understand aerosol direct (through scattering and absorption of incoming solar radiation) and indirect (through modification of cloud microphysics) radiative impacts on the earth's radiation balance (IPCC, 2013). Apart from the primary emissions, secondary aerosol formation through the gas to particle conversion mechanism also contributes significantly to the global aerosol burden in the atmosphere (Kulmala et al., 2004, 2012; Kulmala and Kerminen, 2008; Kerminen et al., 2018). While the impact of secondary aerosol formation mechanism on radiation balance (Giorgi and Lionello, 2008; Yu and Luo, 2009; Yu et al., 2012; Zhang et al., 2012; Ma and Yu, 2015; Wang et al., 2017; Lee et al., 2019), aerosol-cloud interactions (Kanakidou et al., 2005; Gordon et al., 2017) are major focus area. In recent years, the contribution coming from the fine and ultrafine (diameters D_p < 100 nm) to the ambient air pollution has also become a major concern (Kopanakis et al., 2018; Dinoi et al., 2021). New particle formation (NPF) involves the formation of molecular aggregates from precursor vapors, which grow to the size of a particle of 1 nm (Zhang et al., 2012; Kulmala et al., 2012, 2017; Hama et al., 2017; Kerminen et al., 2018). Once formed the nucleation mode (D_p < 25 nm) grow rapidly to larger Aitken (25< D_p < 100 nm) and accumulation mode (100< D_p< 1000 nm) sizes.

Globally, NPF is one of the intensely investigated topics in aerosol science as it occurs in distinct environments with different frequencies and intensities following different pathways of formation and growth (Birmili et al., 2000; O'Dowd et al., 2002; Kulmala et al., 2004, 2012, 2014; Tunved et al., 2006; Suni et al., 2008; Jeong et al., 2010; Meier et al., 2015; Babu et al., 2016; Chandra et al., 2016; Chu et al., 2018; Pétursdóttir et al., 2018; Kopanakis et al., 2018; Yao et al., 2018; Bousiotis et al., 2019; Kerminen et al., 2018; Nieminen et al., 2018; Lee et al., 2019; Kanawade et al., 2020b; Kompalli et al., 2020; Shen et al., 2020; Zhang et al., 2021). Though NPF over urban regions is thought to be difficult because of the large amounts of pre-existing particles acting as condensation sinks, thus deterring nucleation, several studies reported urban NPF events (Alam et al., 2003; Stanier et al., 2004; Wang et al., 2013, 2014; Yu et al., 2017). Urban NPF events are highly localized in nature and occur during conducive conditions

(photochemistry, local meteorological features), and these events significantly contribute to the fine particulate matter smaller than 2.5 μm ($PM_{2.5}$), which is one of the major species contributing to the degradation of air quality (McMurry, 1983; Mohan and Payra, 2009; Kumar et al., 2010). An enormous increase in ultrafine particles (UFP) concentrations in rapid time scales due to NPF can directly or indirectly affect human health (WHO, 2013; Schraufnagel, 2020) by causing cardiovascular and respiratory problems through deep penetration and deposition into the lungs (McCreanor et al., 2007; HEI Review Panel, 2013), the cardiorespiratory system (Rückerl et al., 2011), bloodstream (Bakand et al., 2012), body organs (Morris et al., 2003). The advent of unregulated pollutants such as UFP comes through direct emissions from traffic, biomass burning, and industrial sources (Kittelson, 1998; Alam et al., 2003; Kittelson et al., 2006; Morawska et al., 2008; Seigneur, 2009; Brines et al., 2015; Harrison et al., 2018) and from secondary formation mechanism, has added dimension to already complex urban air pollution issue (Kumar et al., 2012, 2018). To understand UFP concentrations and the various impacts of these aerosols over the urban regions, it is essential to delineate the contributions comes from primary and secondary sources. However, in the natural atmosphere, a convolution of multiple processes makes it difficult to demarcate the underlying processes.

Several experimental and numerical studies have advanced knowledge of the emission, formation, dispersion, exposure, and health effects of UFPs over the last decade. Most of these studies have been carried out in European cities (Kumar et al., 2013b), with only a few developing Asian cities where most of the world's urban population resides (Joodatnia et al., 2013). Especially the studies pertinent to NPF and its contribution to UFP concentrations over the urban regions in the Indian region are minimal (Siingh et al., 2013; Kanawade et al., 2014; Kompalli et al., 2014, 2018; Babu et al., 2016; Leena et al., 2017; Varghese et al., 2020).

The present study elucidates to understand secondary aerosol formation mechanism over a megacity, Delhi, India, when the primary sources are nearly cut-off due to the lockdowns imposed to tackle the spread of Coronavirus Disease 19 (COVID-19) pandemic. The Government of India has imposed the first phase of lockdown from March 24 to April 14, 2020. It was an extremely strict and complete clampdown on government

offices, commercial, private & industrial establishments, educational institutions, places of worship, and all air, water, and land transport services, barring on essential services such as healthcare, grocery shops, pharmacies, milk booths, banks, ATMs, petrol pumps, fire and emergency services. Following this, other phases of lockdown were also imposed in multiple phases: the second (April 15 to May 3, 2020), third (May 4 to May 17, 2020), and fourth (May 18 to May 31, 2020) phases. However, the vantage on restrictions has also been given phase-wise in terms of the mitigating human hardship and economic point of view (Indian Council of Medical Research, 2020; Ministry of Home Affairs, 2020). Therefore, every next phase of lockdown has seen an increase in some industrial activity and traffic density. Due to this, the Air Quality Index (AQI) of metro cities also gradually increased in every next 'Lockdown' Phase (Bera et al., 2020; Sahoo et al., 2020; Guttikunda, 2020).

New Delhi, the capital of India, is one of the largest cities in the world, experiences extreme pollution events due to multiple factors (complex sources and atmospheric conditions) (Kanawade et al., 2020b). Unlike the several previous studies carried out in New Delhi (e.g., Kulmala et al., 2005; Mönkkönen et al., 2005; Hyvärinen et al., 2010; Sarangi et al., 2015, 2018; Kanawade et al., 2020a, 2020b) during the normal circumstances, the lockdowns imposed to control the COVID-19 provided an opportunity to examine NPF during when near-complete cessation of the sources of primary aerosols (traffic emissions, industries, construction work, and reduced power generation) and some of the condensable vapors (e.g., volatile organic compounds; (Kanawade et al., 2020b)) occurred. It provided conditions akin to a natural laboratory examining particle concentrations, size distributions, and NPF events over such a megacity. In this context, the present study uses campaign mode observations conducted during the pre-monsoon (April-May) period and focuses on the following objectives: to understand the impact of the lockdown imposed due to COVID-19 on particle number concentrations in different size regimes, especially on UFP; to examine the frequency and intensity of the NPF events during the lockdowns of the different magnitude of restrictions; to identify the possible NPF pathways and delineate the impact of changing concentrations of the pre-existing particles and condensable vapors during the lockdown. It may be noted that during the present study, the direct measurements of precursor vapors such as H_2SO_4, and volatile organic compounds (VOCs) were not available.

Hence the exact nature of the species contributing to NPF through vapor phase gas-particle conversion could not be identified. Another limitation is that the lowest size bin measured in this study was 10.2 nm. Thus, there was no information on nascent new particles (sub-3 nm particles) or initial growth (1-10 nm).

As mentioned earlier, the present study was carried out during different phases (with varying relaxation to the anthropogenic activities) of the COVID-19 lockdown periods imposed by the government of India. The data was collected between April 21 and May 22, 2020. We have classified data into three different periods: Period- I (from April 21 to May 3, 2020, as Lockdown phase-2), Period- II (from May 4 to May 17, 2020, as lockdown phase-3), Period- III (from May 18 to May 22, 2020, as lockdown phase-4) to represent the gradual changes in sources of pollution.

4.2.1 Temporal variation of particle concentration

A stacked bar graph of the daily mean particle number concentrations in size regimes, nucleation (N_{Nuc}), Aitken (N_{Aitk}), and accumulation (N_{accu}) along with the geometric mean diameter (GMD; in nm diameter) of the PNSD is shown in Figure 4.13. The arrow marks below the figure indicate the days with NPF events. The shaded portions indicate different periods of the lockdown where successive relaxations lead to enhanced anthropogenic activities. The days with rainfall and the total accumulated rainfall for the day are also indicated in the figure. There was occasional rainfall during the study period (total accumulated rainfall of 32 mm and 2 mm during Period-1 and Period-2, respectively, and no rainfall occurred during Period-3).

The daily mean total concentrations ranged between 16014 cm^{-3} to 40717 cm^{-3}, and ultrafine particles dominated (50-88%) the total number concentrations during most days. The mean total particle concentrations (N_{total}) (± standard deviation) were ~25065 ± 13881 cm^{-3} and ~31681 ± 18776 cm^{-3} during Period-I and Period-II, respectively, which increased to ~31371 ± 16378 cm^{-3} for Period-III. Similarly, mean N_{accu} values doubled from Period-I (~ 6074 ± 3167 cm^{-3}) to Period-III (12306 ± 6596 cm^{-3}) through Period-II (8715 ± 5496 cm^{-3}). However, UFP concentrations (both N_{nuc} and N_{Aitk}) did not show any discernible trend, though they dominated the total particle number concentrations.

The dominance of UFP concentrations was explicit (> 70% of N_{total}) on the NPF event day compared to non-event days.

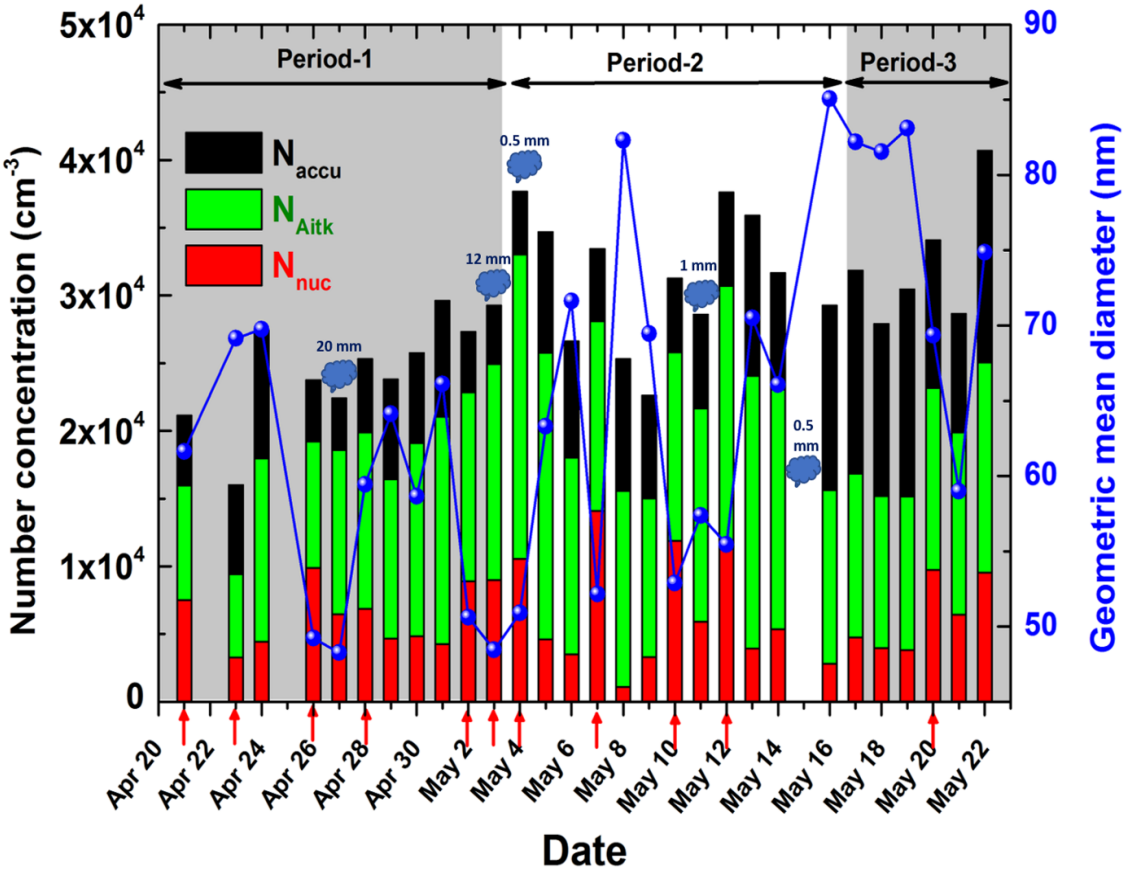

Figure 4.13 Stacked bar graph of daily mean number concentrations of nucleation (N_{nuc}), Aitken (N_{Aitk}), and accumulation (N_{accu}) particles (in cm^{-3}). The solid line shows the daily mean values of the geometric mean diameter (GMD) of the size distribution. The shaded portions indicate different periods of the lockdown, and the arrow marks indicate NPF event days. The days with rainfall and the total accumulated rainfall for the day are also indicated in the figure.

The contribution of N_{nuc} and N_{accu} to the N_{total} was in the range of 21-30% and 47-50%, respectively, during the non-event days, whereas N_{accu} was meagre (12-30%) on the event days. It is also highlighted by lower GMD values (50-60 nm) (marked in the figure) on the event days compared to the non-event days (65-85 nm). The mean value of GMD was lowest for Period-I (58.3 ± 20.2 nm) and highest for Period-III (73.4 ± 28.0 nm) due to shifting the existing particle sources, so that fraction of accumulation mode particles

(predominantly primary) was higher than the rest of the two phases. Typically, GMD goes down immediately after the nucleation events in the urban regions because of strong NPF bursts resulting in enhanced UFP concentrations (Kumar et al., 2014; Babu et al., 2016); However, during severe pollution events such as regional haze (which span across few days) NPF results in an increased GMD due to rapid secondary aerosol formation and growth (e.g., Guo et al., 2014; Zheng et al., 2021).

The mean values of particle concentrations, condensation sink values, meteorological parameters, precursors, and trace gas concentrations during the present study are given in Table 4.2. Here the values for the events and non-event days are shown separately. The values after ± describe standard deviation.

Table 4.2: Statistical summary of the particle number concentrations, condensation sink (CS), meteorological parameters, and traces gases during the event and non-event days

Parameter/	**Event day**			**Non-event**		
	Period I	**Period II**	**Period III**	**Period I**	**Period II**	**Period III**
	Particle number concentrations					
	Mean ± SD	Mean ± SD	Mean ± SD	Mean ± SD	Mean ± SD	Mean ± SD
N_{Total} (cm^{-3})	2.43 x 10^4 ± 1.71 x 10^4	3.50 x 10^4 ± 2.43 x 10^4	3.41 x 10^4 ± 2.38 x 10^4	2.64 x 10^4 ± 0.92 x 10^4	3.00 x 10^4 ± 1.31 x 10^4	3.06 x 10^4 ± 1.33 x 10^4

N_{nuc} (cm^{-3})	$7.81 \times 10^3 \pm 1.23 \times 10^4$	$1.19 \times 10^4 \pm 2.18 \times 10^4$	$9.73 \times 10^3 \pm 1.91 \times 10^4$	$4.58 \times 10^3 \pm 4.06 \times 10^3$	$4.07 \times 10^3 \pm 4.46 \times 10^3$	$5.37 \times 10^3 \pm 5.80 \times 10^3$
N_{Aitk} (cm^{-3})	$1.15 \times 10^4 \pm 7.68 \times 10^3$	$1.76 \times 10^4 \pm 1.07 \times 10^4$	$1.34 \times 10^4 \pm 7.89 \times 10^3$	$1.43 \times 10^4 \pm 6.41 \times 10^3$	$1.48 \times 10^4 \pm 8.25 \times 10^3$	$1.25 \times 10^4 \pm 6.94 \times 10^3$
N_{accu} (cmM^{-3})	$4.99 \times 10^3 \pm 2.45 \times 10^3$	$5.59 \times 10^3 \pm 3.82 \times 10^3$	$1.09 \times 10^4 \pm 5.62 \times 10^3$	$7.53 \times 10^3 \pm 2.32 \times 10^3$	$1.05 \times 10^4 \pm 5.71 \times 10^3$	$1.27 \times 10^4 \pm 6.80 \times 10^3$
Nuc fraction	0.40	0.40	0.41	0.24	0.21	0.30
N_{UFP}/N_{Total}	0.75 ± 0.13	0.80 ± 0.12	0.62 ± 0.19	0.70 ± 0.09	0.63 ± 0.14	0.58 ± 0.16
CS (sec^{-1})	0.034 ± 0.015	0.035 ± 0.012	0.07 ± 0.018	0.053 ± 0.024	0.072 ± 0.038	0.09 ± 0.048

Meteorological parameters						
AT(°C)	29.4 ± 3.3	28.7 ± 4.0	32.2 ± 5.3	30.9 ± 3.8	30.1± 4.4	32.5 ± 5.4
RH (%)	53.2 ± 12.2	52.4 ± 13.9	29.3 ± 9.0	51.2 ± 13.5	48.1 ± 14.4	33.2 ± 12.8
WS (m/s)	0.93 ± 0.78	0.83 ± 0.64	0.53 ± 0.21	0.68 ± 0.40	0.62 ± 0.32	0.59 ± 0.27
Trace Gases						
NO ($\mu g/m^3$)	5.56 ± 0.58	5.58 ± 0.74	5.38 ± 0.70	5.61 ± 0.73	5.77 ± 2.27	6.05 ± 2.23
NO_2 ($\mu g/m^3$)	17.17 ± 4.43	17.19 ± 6.23	21.40 ± 7.97	19.22 ± 4.20	22.17 ± 8.64	28.94 ± 14.55
NO_x ($\mu g/m^3$)	22.73 ± 5.02	22.77 ± 6.97	26.78 ± 8.67	24.83 ± 4.93	27.94 ± 10.91	34.99 ± 16.78
O_3 ($\mu g/m^3$)	95.25 ± 35.27	102.51 ± 41.15	112.22 ± 60.80	96.39 ± 47.09	90.64 ± 50.42	87.05 ± 56.61

CO ($\mu g/m^3$)	327.13 ± 198.21	384.63 ± 243.29	354.73 ± 388.53	482.83 ± 245.54	614.98 ± 366.78	686.43 ± 595.49
SO_2 ($\mu g/m^3$)	12.14 ± 3.29	12.09 ± 2.52	26.71 ± 16.94	12.93 ± 2.80	14.81 ± 5.03	25.12 ± 11.35
[Ox] ($\mu g/m^3$)	130.06 ± 14.33	136.41 ± 19.76	177.00 ± 23.91	110.38 ± 38.82	113.52 ± 43.22	117.31 ± 49.71
[H_2SO_4] (molec cm^{-3})	$1.55 \times 10^7 \pm 9.44 \times 10^6$	$1.30 \times 10^7 \pm 7.33 \times 10^6$	$4.27 \times 10^7 \pm 8.29 \times 10^6$	$4.61 \times 10^6 \pm 6.30 \times 10^6$	$5.37 \times 10^6 \pm 7.60 \times 10^6$	$1.02 \times 10^7 \pm 1.22 \times 10^7$

Considering only the non-event days, the mean total particle number concentrations gradually increased from Period-I ($2.64 \times 10^4 \pm 0.92 \times 10^4$ cm^{-3}) to Period-III ($3.06 \times 10^4 \pm 1.33 \times 10^4$ cm^{-3}) through Period-II ($3.00 \times 10^{-4} \pm 1.31 \times 10^4$ cm^{-3}). In contrast, the fraction of ultrafine particles gradually decreased from ~0.70 ± 0.09 during Period-I to 0.58 ± 0.16 during Period-III through ~ 0.63 ± 0.14 during Period-II. The values of nucleation mode particles were nearly 1.5 to 2 times higher on the event days compared to the non-event days, which is also reflected in the mean fractions of the ultrafine particle. However, the N_{accu} or N_{Aitk} did not show any such sharp contrast. They almost doubled from Period-I to Period-III, suggesting the impact of increased anthropogenic activities on particle concentrations on non-event days. Zimmerman et al. (2020) have

also reported a similar trend in particle number concentrations associated with lockdown and un-lock periods during the Covid-19 pandemic shut-down in North Carolina State University in Raleigh, NC, between April to June 2019 and November 2019 to May 2020. Another interesting aspect from Table 4.3 is the enhanced concentrations of proxies of the precursor vapors (both odd-oxygen [Ox] and [H_2SO_4] proxy) during the event days compared to non-event days. Considering the NPF event days, the mean concentrations of [H_2SO_4] proxy (which is the most ubiquitous precursor vapor for NPF) increased from 1.55 ± 0.94 x 10^7 molecules cm^{-3} during Period-1 to 4.27 ± 0.83 x 10^7 molecules cm^{-3} during Period-3, through moderate values 1.30 ± 0.73 x 10^7 molecules cm^{-3}. Even during the non-event days, the concentrations of [H_2SO_4] proxy (which are 2-4 times lower than the event day values) increased from Period-1 to Period-III. Similarly, the values of [Ox] (which is generally positively correlated with oxygenated organics) also showed an enhancement from Period-I (130.06 ± 14.33 μg m^{-3}) to Period-3 (177.00 ± 23.91 μg m^{-3}) during the event days, whereas [Ox] values did not show a significant difference during the non-event days.

A similar pattern is noticeable in the near surface-pollutant trace gases: NO_x, CO, and SO_2 concentrations, as evident from Figure 4.14 and Table 4.2. The phase-wise enhanced concentrations of NO_x (by > 40%), CO (by > 42%), and SO_2 (by > 95%) associated with the conditional relaxations from Period-I to Period-III further established the increased strength of primary emissions with progressive unlock relaxations. Further, the concentrations of trace species were higher during the non-event days compared to event days; e.g., the daily mean NO_x concentrations were in the range of 22-27 μg m^{-3} on the event days, whereas the concentrations were ~25-35 μg m^{-3} (with large variability) during the non-event days. But in the case of O_3, no significant difference from Period-I to Period-III was observed, but typically the mean values were higher during the event days compared to non-event days in all the phases of the lockdown. Recently, Srivastava et al. (2021) also reported similar trends in near-surface air pollutants over New Delhi during different phases of lockdown.

Interestingly, though slightly higher mean temperatures and lower RH conditions prevailed over the non-event days compared to the event days, the overall magnitudes were not different, and no statistically significant association was found between these

variables and nucleation events. However, gradually increasing air temperatures are relatively favourable for enhanced dispersion of air pollutants (Kompalli et al., 2014b), and any such dilution of the amounts of background particles reduces condensation sink throughout the vertical levels (Babu et al., 2016). We have not found any significant variation in the incoming solar flux during the event and non-event periods.

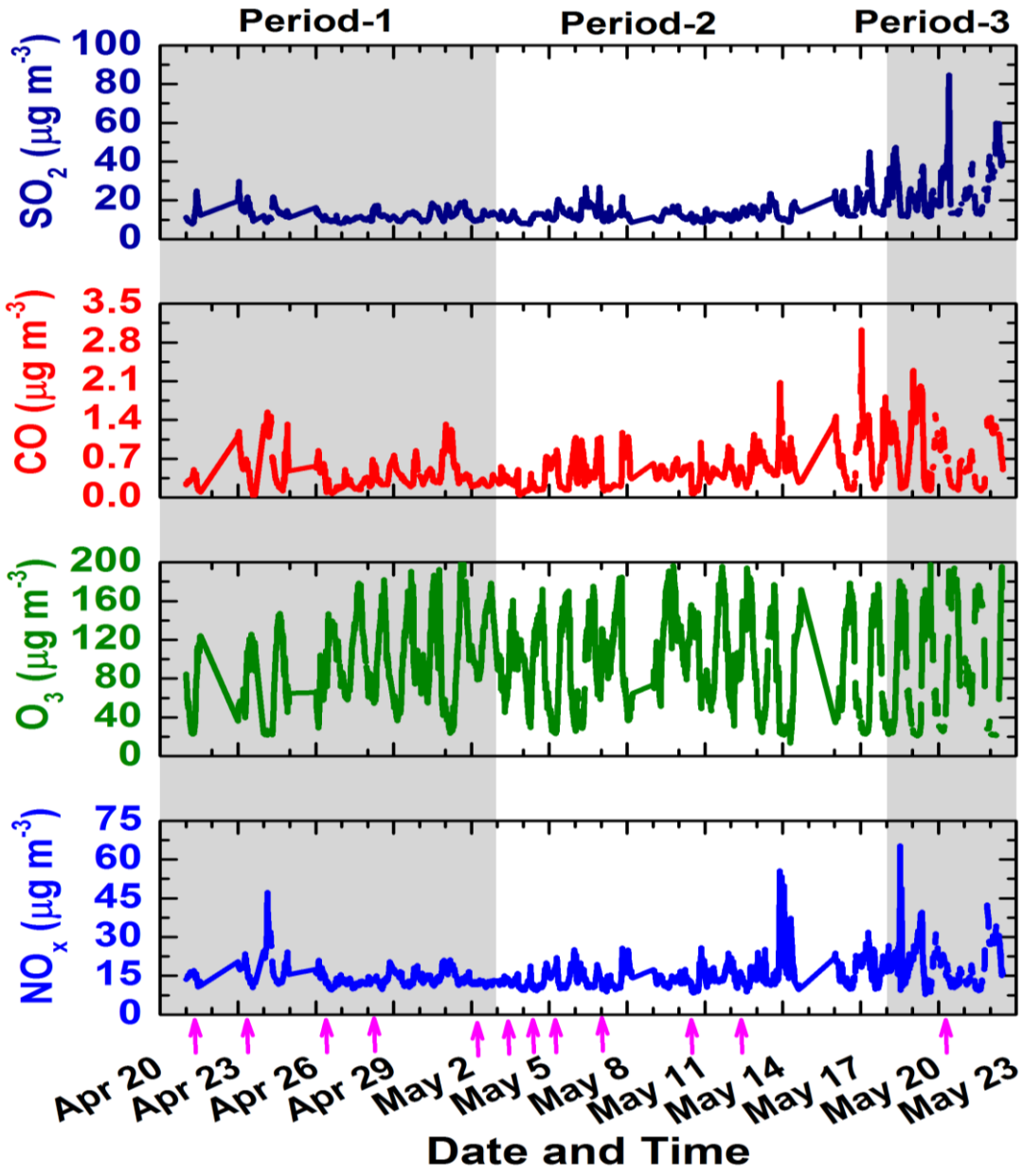

Figure 4.14: Temporal variation of trace gases (a) NOx, (b) Ozone, (c) CO, and (d) SO2 (all in µg m-3) during the present study

The mean N_{total} values (~2-3.5 x 10^4 cm^{-3}) observed in the present study are compared to the values reported over several urban locations (Stanier et al., 2004; Wehner et al., 2004; Hyvärinen et al., 2010; Siingh et al., 2013; Kanawade et al., 2014; Babu et al., 2016; Kerminen et al., 2018; Nieminen et al., 2018). Stanier et al. (2004) have reported N_{total} of the order of 10^3 to 10^5 cm^{-3} over the polluted urban areas. However, significantly higher numbers were reported in the urban areas of Asian countries compared to European countries (Hussein et al., 2004; Wehner et al., 2004; Siingh et al., 2013). The present values are significantly lower than the values previously reported over New Delhi (Mönkkönen et al., 2005; Hyvärinen et al., 2010; Sarangi et al., 2015, 2018; Kanawade et al., 2020a, 2020b), which highlights the effectiveness of cut-off sources in controlling primary pollutants. Srivastava et al. (2021) have noted that a significant improvement in air quality was observed across the countries due to COVID-19 induced lockdown, which is evident in our observations.

4.2.2 Temporal variation of particle number size distributions

Figure 4.15 shows the temporal variation of PNSDs during this study. The figure revealed several NPF events (marked with arrows) with a clear appearance of significant amounts (2-5 times increase from values before the event) of nucleation mode particles. Once formed, these particles rapidly grew into larger sizes (Aitken to accumulation modes); therefore, many of the events depicted a clear 'banana' pattern (Kulmala et al., 2012).

As described in the previous section, different classes of NPF events were observed during the present study. Typical examples of different classes of NPF events are shown in Figure 4.16, and Table 4.3 describes the details of various types of events observed in the present study. The overall frequency of the NPF events is ~ 41 % (among which 50% were Class Ia, 16.7% were Class Ib, 33.3% were Class II events) considering the entire study period. The NPF frequencies are 54.5%, 38%, and 20%, respectively, during Period-I (21-April to 03-May), Period-II (04-May to 17-May), and Period-III (18-May to 31-May). This emphasized that increasing anthropogenic primary emissions lead to a possible enhancement in the condensation sink, decreasing nucleation frequency.

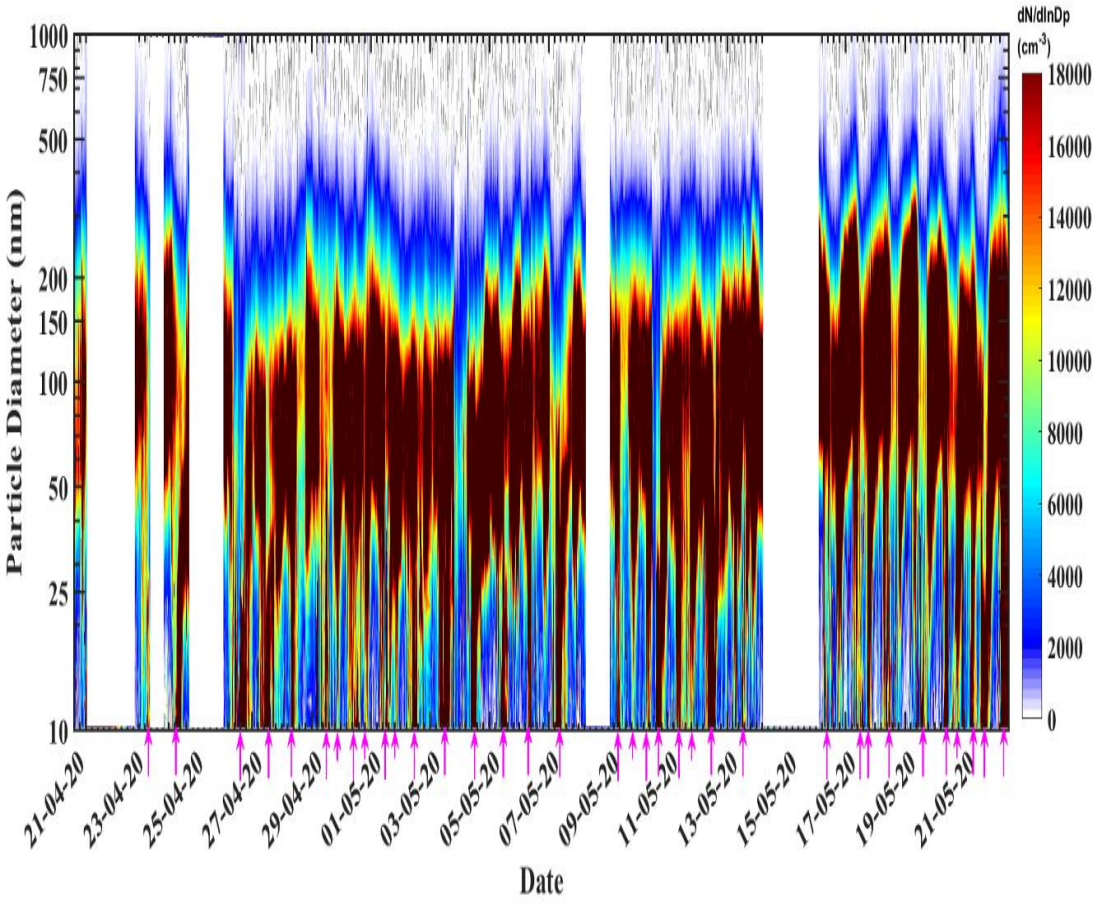

Figure 4.15: Temporal variation of particle number size distribution (PNSD) during the present study. The arrows on the bottom indicate the new particle formation events. The color bar indicates number concentrations, and the white portion indicates the data gap

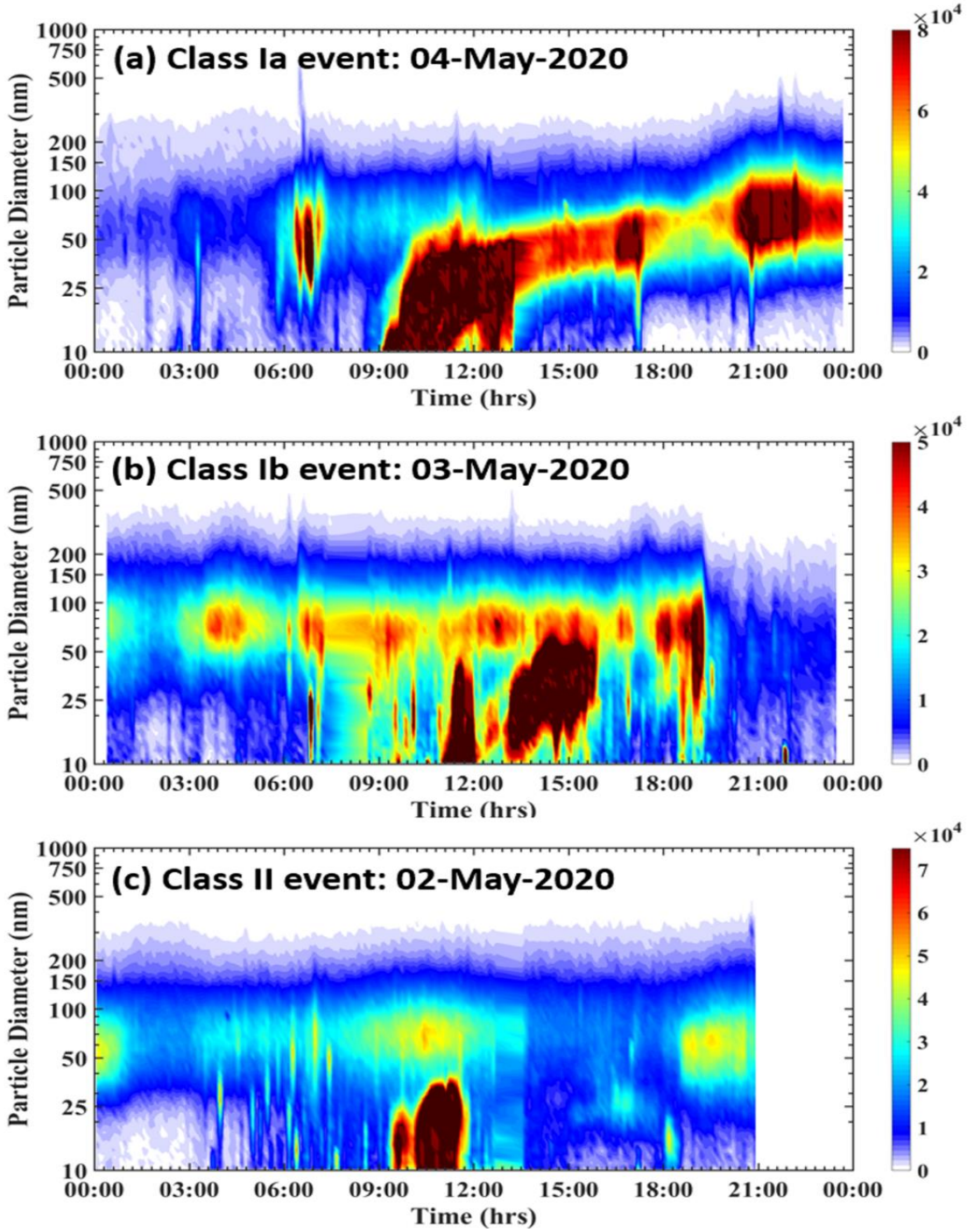

Figure 4.16: Typical example of Event day with event classification (Class Ia event, Class Ib, and Class II event) according to Typical example of Event day with event classification (Class Ia event, Class Ib, and Class II event) according to Dal Maso et al. (2005)

Table 4.3: New particle formation and their event classes along with their respective periods

Period	**Days with NPF event:** **Period wise** **% (days)**	**NPF event:** **whole campaign** **(%)**	**Event classes- no. of days**
Period I: 11 days 21/April/2020 to 03/May/2020	54.5% (6 days)	20.6%	Class Ia- 1 day Class Ib- 2 days Class II- 3 days Undefined: 2 days*
Period II: 13 days 04/May/2020 to 17/May/2020	38.4% (5 days)	17.2%	Class Ia- 5 days
Period III: 5 days 18/May/2020 to 31/May/2020	20.0% (1day)	3.4%	Class II-1 day
*Class Unit. =Undefined days (which contribute 8% Period wise and 6.8% overall monitoring.			

Earlier studies carried out over New Delhi (mostly during the colder months) reported different NPF frequencies (30-53%) (Mönkkönen et al., 2005; Sarangi et al., 2015; Kanawade et al., 2020a) compared to the present observations. These studies have suggested that such a high frequency of NPF events, despite the presence of a strong

condensation sink (because of the large amounts of pre-existing particles), would be possible due to the presence of substantial concentrations of condensable vapors. In such a case, the higher vapor source rates help to overcome the barrier posed by the CS (Kulmala et al., 2005; Mönkkönen et al., 2005) and result in NPF. The present NPF frequency (~ 41%) over New Delhi is comparable to the values reported in Asian urban cities like Beijing, China (40%) (Wu et al., 2007); Nanjing, China (44%) (Qi et al., 2015), and lower than the value (53%) reported by (Mönkkönen et al., 2005) over New Delhi. It may be noted that observing a consistent seasonal pattern of NPF events in an urban area is difficult (Vu et al., 2015), which explains this difference. Globally, Nieminen et al. (2018) reported that the events occur more frequently in March to May (~30% of the days) and least often in December to February (~10% of the days).

In our study, though most numbers of NPF events occurred during Period-I, the events belonged to different classes (Class Ia -1 day; Class Ib - 2 days; Class II - 3 days; undefined-2 days). In contrast, only well-defined Class Ia events were observed during Period-II, whereas only one event that occurred during Period-III was a Class II type event. Such differences among the events are possible due to the interplay between sources, sinks, and transformation processes of condensable vapors and pre-existing particles (Kulmala et al., 2004; Vu et al., 2015). These processes result in not only different frequencies, intensities of NPF events but different classes of the events as reported in several studies (Alam et al., 2003; Dunn et al., 2004; Stanier et al., 2004; Wehner et al., 2004; Jeong et al., 2004; Reche et al., 2011; Cheung et al., 2011; Gao et al., 2012). Compared to clean environments, the intensity of the events can be higher in polluted environments (Kulmala et al., 2004; Kerminen et al., 2018) due to the abundance of condensable vapors.

The particle number distributions are grouped separately for the nucleation event and non-event during different periods, and the mean PNSDs are shown in Figure 4.17.

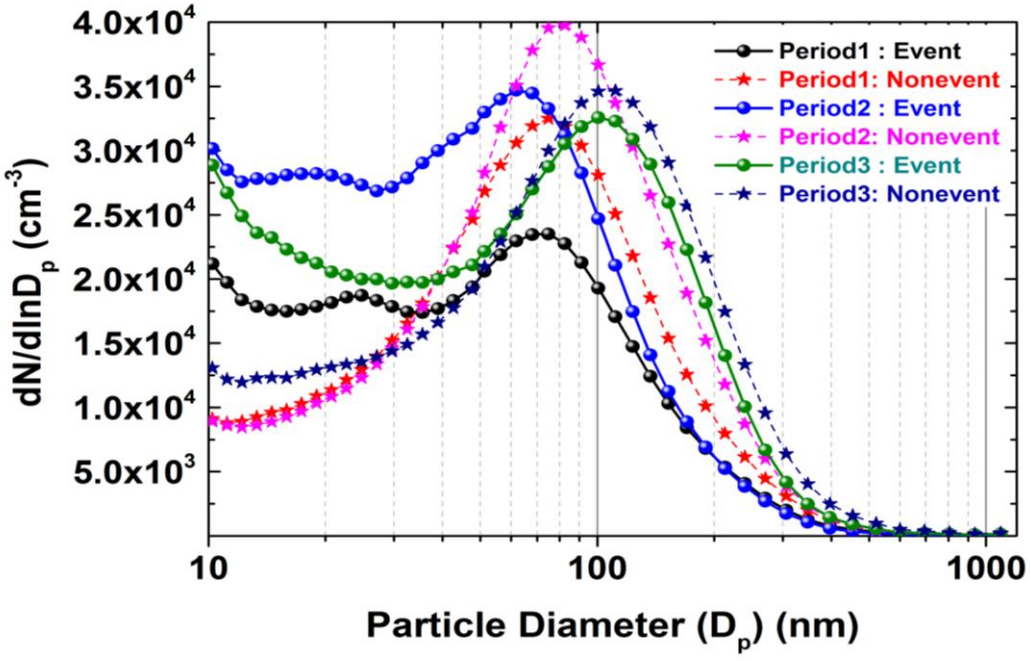

Figure 4.17: Average particle number size distributions for different periods during the event and non-event days

An omnipresent primary mode (80-110 nm) in the Aitken and accumulation size regimes were present in all the observations. However, a distinct secondary mode, often open-ended, was noticeable in the nucleation regime (< 25 nm) during the NPF event periods, along with the primary mode. The mean size distributions depicted flat or increased lower-size particle abundances confined to nucleation size regimes during the event periods. We have derived the modal parameters of the mean particle number size distributions during the event and non-event periods by fitting to the observed size distributions to the analytical log-normal size distribution of the following form (Kompalli et al., 2018, 2020):

$$\frac{dN}{d\ln D_p} = \sum_{j=1}^{n} \frac{N_k}{\sqrt{2\pi}\ln\sigma_{m,j}} \exp\left[-\frac{(\ln D_p - \ln D_{m,p,j})^2}{2\ln^2\sigma_{m,k}}\right] \quad (2)$$

(where D_p is the particle diameter, n is the total number of the modes considered, $D_{m,p,j}$ is the mode diameter of the j^{th} mode, $\sigma_{m,j}$ is the corresponding width of the mode, and N_j is the particle number concentration (amplitude) of the j^{th} mode).

The modal parameters for the PNSDs shown in Figure 4.17 are tabulated in Table 4.4.

Table 4.4: Modal parameters of the PNSDs during the present study

Period	Primary mode			Secondary mode		
	$D_{m,p,1}$ (nm)	$\sigma_{m,1}$	N_1 (cm^{-3})	$D_{m,p,2}$ (nm)	$\sigma_{m,2}$	N_2 (cm^{-3})
Period-I						
Event	78	1.14	2.32×10^4	Open mode		
Non-event	82	1.18	3.25×10^4	No mode	--	--
Period-II						
Event	69	1.16	3.25×10^4	Open mode		
Non-event	85	1.20	4.08 x 104	No mode	--	--
Period-III						
Event	105	1.08	3.21×10^4	Open mode		--
Non-event	111	1.27	3.39×10^4	No mode	--	

The gradual increase in primary mode peak concentrations with progressively eased-up restrictions is clear from Figure 4.17 are tabulated in Table 4.4. Interestingly the mode diameter of the primary mode also gradually shifted to larger values during both non-event (from 82 to 111 nm) and event (78 to 105 nm) periods, suggesting a considerable impact of lockdown cessation and unlock emissions on PNSDs. Another important aspect here is that the mode ~ 80 nm can originate from both primary and secondary (growth of newly formed particles) pathways. Some earlier studies have highlighted the importance of small exhaust plumes associated with vehicular traffic in UFP formation processes at local or regional scales (Bukowiecki et al., 2002; Kittelson et al., 2004; Rönkkö et al., 2006). Apart from the primary emissions, size transformation (due to condensation and coagulation) also results in an increased abundance of the larger-sized particles. It is possible that such aerosol transformation processes also contribute to the increased peak concentrations and larger mode diameters of the size spectra.

4.2.3 Characteristics of the nucleation events

All the NPF events observed in this study occurred during the daytime, unlike the night-time events reported by Sarangi et al. (2018). It suggests the strong role played by the photochemical process in prompting the nucleation process. The new particle formation in the atmosphere is determined by various factors, which include: (i) the nature and extent of availability of condensation vapors in supersaturated conditions, and (ii) the strength of the condensation sink (CS), which inhibits the nucleation process. From Table 4.2, it is clear that the CS values were higher during the non-event (0.07 - 0.09 sec^{-1}) days compared to the event (0.03 - 0.07 sec^{-1}) days, thus reiterating the importance of lower CS values to initiate nucleation (Dal Maso et al., 2005; Wang et al., 2017; Deng et al., 2020). The higher CS in urban regions ensures that gaseous precursors, molecular clusters, and freshly formed particles experience a high scavenger loss rate. The CS values during Period- I (0.052 sec^{-1}) < Period-II (0.072 sec^{-1}) < Period- III (0.09 sec^{-1}) of non-event days were typically greater than those seen on event days Period- I (0.034 sec^{-1}) < Period-II (0.035 sec^{-1}) < Period-III (0.07 sec^{-1}) respectively (Table 4.2). The present CS values are consistent with those reported over urban locations (Kanawade et al., 2014; Babu et al., 2016) over the Indian region and other urban areas (Guangzhou, China 0.035 -0.46 sec^{-1} (Yue et al., 2013), Shanghai, China (0.03- 0.10 sec^{-1}) (Xiao et al., 2015) and

Beijing, China (0.006- 0.06 sec^{-1}) (Wu et al., 2007). The details of all the events (duration, time of occurrences, growth rates, etc.) are provided in Table 4.5.

Table 4.5: Time of occurrence of NPF and growth (in Indian standard time: UT+ 05:30 hrs) and statistical summary of the events

Event Date	Nucleation period			Growth period					
	ST (hrs)	ET (hrs)	TT hrs	ST (hrs)	S_{GMD} (nm)	ET (hrs)	E_{GMD} (nm)	TT (hr)	GR (nm/hr)
21-Apr	9:55	13:36	3.68	10:50	19.5	13:36	31.0	2.76	3.31
23-Apr	14:30	15:32	1.03	14:44	15.4	15:46	46.71	1.03	-
26-Apr	13:48	17:51	3.81	14:29	14.9	18:05	39.99	3.6	6.58
28-Apr	08:15	09:59	1.76	08:49	22.95	14:01	67.79	5.2	7.76
02-May	09:24	11:42	2.3	10:40	23.02	11:56	47.43	1.2	-
03-May	11:08	11:57	0.85	11:29	19.35	14:49	45.06	3.0	6.57
04-May	09:10	14:00	4.83	10:12	22.45	20:06	69.1	9.9	4.33
05-May	10:33	11:56	1.38	10:40	23.14	15:50	69.95	5.16	5.82

07-May	06:50	09:50	3.00	7:18	15.84	12:01	44.14	4.7	6.22
10-May	14:34	18:43	4.15	15:09	16.69	20:48	44.85	5.6	4.58
12-May	09:54	14:19	4.21	11:10	20.48	15:56	50.34	4.8	8.37
20-May	08:26	11.05	2.50	09:28	22.18	11:05	42.02	1.6	-

ST = Start Time, ET = End Time, TT = Total Time, S_{GMD} = Start GMD, E_{GMD} = End GMD, GR = Growth Rate, GMD: Geometric mean diameter

Earlier studies (Kanawade et al., 2014; Babu et al., 2016; Kompalli et al., 2018) have reported NPF events over urban/polluted environments. Several earlier studies have suggested that secondary aerosol formation in the urban environment is somewhat less favoured (but not uncommon) due to larger background concentrations (Bukowiecki et al., 2002; Hussein et al., 2004; Reche et al., 2011). Generally, the primary ultrafine particles emitted along with the condensable vapors from anthropogenic activities (vehicular and industrial effluents) act as the potential condensation sink and inhibit NPF. However, a greater abondance of condensable vapors (semi-volatile organics and sulfur compounds) enables highly intense but localized NPF occasionally, even in urban locations (Väkevä et al., 2000; Alam et al., 2003; Stanier et al., 2004; Mönkkönen et al., 2005; Ahlm et al., 2012; Contini et al., 2012). Considering the present urban NPF events in this perspective, it is possible that the balance between enhanced emissions of gaseous precursors and primary particles decided the frequency, intensity, and shape of the NPF events.

It may be recollected that significant amounts of condensable vapors present in the urban atmosphere are considered to be the reason behind urban NPF events (Kerminen et al., 2018; Nieminen et al., 2018). Most of the NPF events reported earlier occurred during the daytime occurring due to photochemistry (Siingh et al., 2013; Ma and Birmili, 2015;

Sorribas et al., 2015; Lushnikov et al., 2017) and moderate levels of relative humidity (Hama et al., 2017; Lee et al., 2019), night-time events are not uncommon (Babu et al., 2016; Sarangi et al., 2018). Kanawade et al. (2014) have reported that NPF occurred during lower condensation sink, lower RH, greater solar radiation, and higher temperature conditions over polluted cities, Kanpur and Pune in India. Meteorological variables (temperature, relative humidity, solar radiation, and winds), atmospheric processes like photochemistry, local atmospheric boundary layer (ABL) dynamics, turbulence, etc. play a role in controlling that control the dynamics of the NPF pathways (Hussein et al., 2004; Kulmala et al., 2012; Babu et al., 2016; Kerminen et al., 2018; Kompalli et al., 2018, 2020). The varying CS values and meteorological conditions (lower RH and higher air temperatures during the event days) affect different types of NPF events. It is reflected in the statistics of the types of events in various periods of the present study.

Though the CS values during Period-I and II are nearly the same, all the events were seen during Period-I, whereas only Class Ia events were seen during Period-II. It highlighted a precise balance between the source strengths of the condensable vapors and pre-existing particles. Once formed, these particles can grow rapidly to larger sizes by consuming the same condensable vapors that initiated NPF or different vapors, which lead to different growth rates in different size regimes in varying environments. Understanding the growth rates of newly formed particles is essential for quantifying the impact of NPF on direct (light scattering by aerosols) and indirect (aerosol-cloud interactions). In this regard, we have estimated the particle growth rates for the nucleation events observed in the present study using Eq.3, and the values for each event are shown in Table 4.5. Interestingly, though NPF events are more frequent and well-defined during Period-II, lower particle growth rates (mean ~5.86 ± 1.44 nm h^{-1}) were observed during this period compared to Period-I (~6.05 ± 1.66 nm h^{-1}). Present GR values are comparable to the values reported by Kanawade et al. (2014) over the urban locations: Pune (~ 6.5 ± 1.2 nm h^{-1}), Kanpur (~ 8.7 ± 3.2 nm h^{-1}), and by Babu et al. (2016) (7.35 ± 2.93 nm h^{-1}) over a coastal semi-urban location, Thumba. Even higher GR values were reported by Mönkkönen et al. (2005) (11.6- 18.1 nm h^{-1}) and Sarangi et al. (2016) (15- 30 nm h^{-1}) over New Delhi for the winter period, when the concentrations of pollutants/condensable vapors were still higher.

4.2.4 Association between the particle concentrations, precursors, meteorological variables, and trace species

In order to establish the association between nucleation events and precursors and identify the potential species that contributed to the events, we have examined the variation of particle concentrations, precursors, and trace species during different periods. Figure 4.18 depicts the variation of concentrations of (a) N_{nuc} and odd oxygen [Ox], (b)N_{Aitk} and NO_x, (c) [H_2SO_4] proxy and GMD for Period-I, whereas Figure 4.19 and Figure 4.20 show the same for Period-2 and Period-3 respectively. The grey shaded portions in the figures indicate the NPF events, while cyan shaded portions indicate particle burst events (dissimilar to NPF with just enhancement in nucleation particle concentrations).

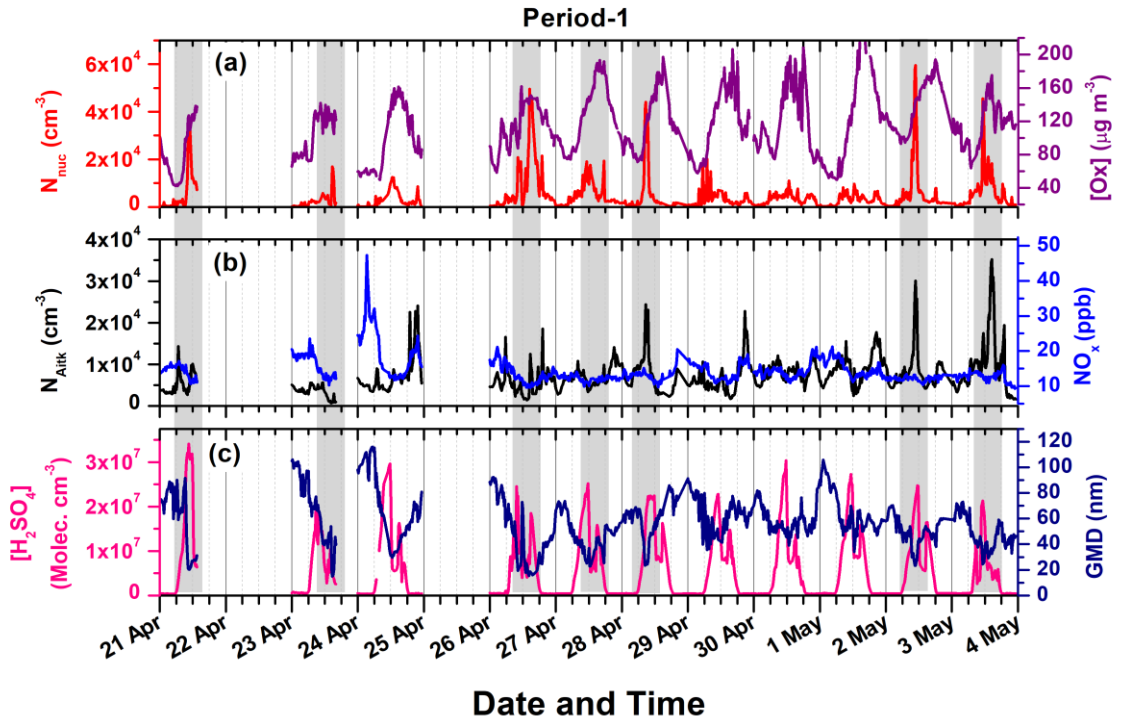

Figure 4.18: Temporal variation of (a) N_{nuc} and odd-oxygen [Ox] (b) N_{Aitk} and NO_x, (c) Sulfuric acid proxy concentration [H_2SO_4], and geometric mean diameter during Period-1. The grey-shaded portions indicate NPF events

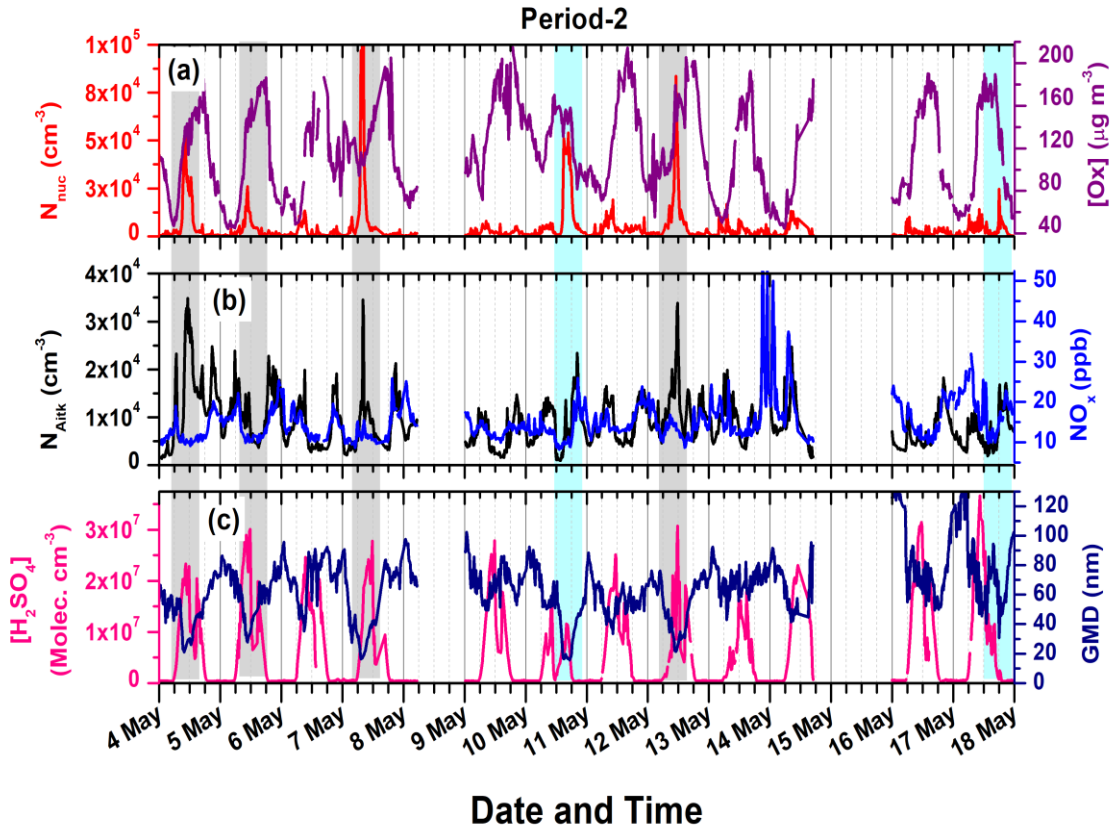

Figure 4.19: Temporal variation of (a) N_{nuc} and odd-oxygen [Ox] (b) N_{Aitk} and NO_x, (c) Sulfuric acid proxy concentration [H_2SO_4], and geometric mean diameter during Period-2. The grey-shaded portions indicate NPF events, whereas cyan-shaded portions indicate particle burst events

It is clear from Figure 4.18, Figure 4.19, andFigure 4.20 that all the nucleation events (where N_{nuc} increased by several orders of magnitude, as high as the values ~ 6.0-8.0 x 10^4 cm^{-3}) compared to non-event periods) are associated with a clear enhancement in the concentrations of [H_2SO_4] proxy (2 to 3.5 x 10^7 molecules cm^{-3}; ~ 2-3 orders higher than the non-event values). Such enhanced levels of gas-phase chemistry parameters, such as sulfuric acid proxy (Sipilä et al., 2010) provided evidence for the secondary formation of aerosols due to daytime photochemistry. Further, most of the events occurred during the daytime when [Ox] showed an increasing trend (daytime values are 4-5 times higher than nighttime values) (although there is no direct concurrent association between nucleation events and [Ox] for some cases). The concentrations of odd oxygen [Ox] are indicative

of the atmospheric oxidative capacity (Clapp and Jenkin, 2001), and these levels are strongly influenced by photochemical reactions, especially in polluted regions (Wood et al., 2010). As the oxygenated component of organic aerosols-

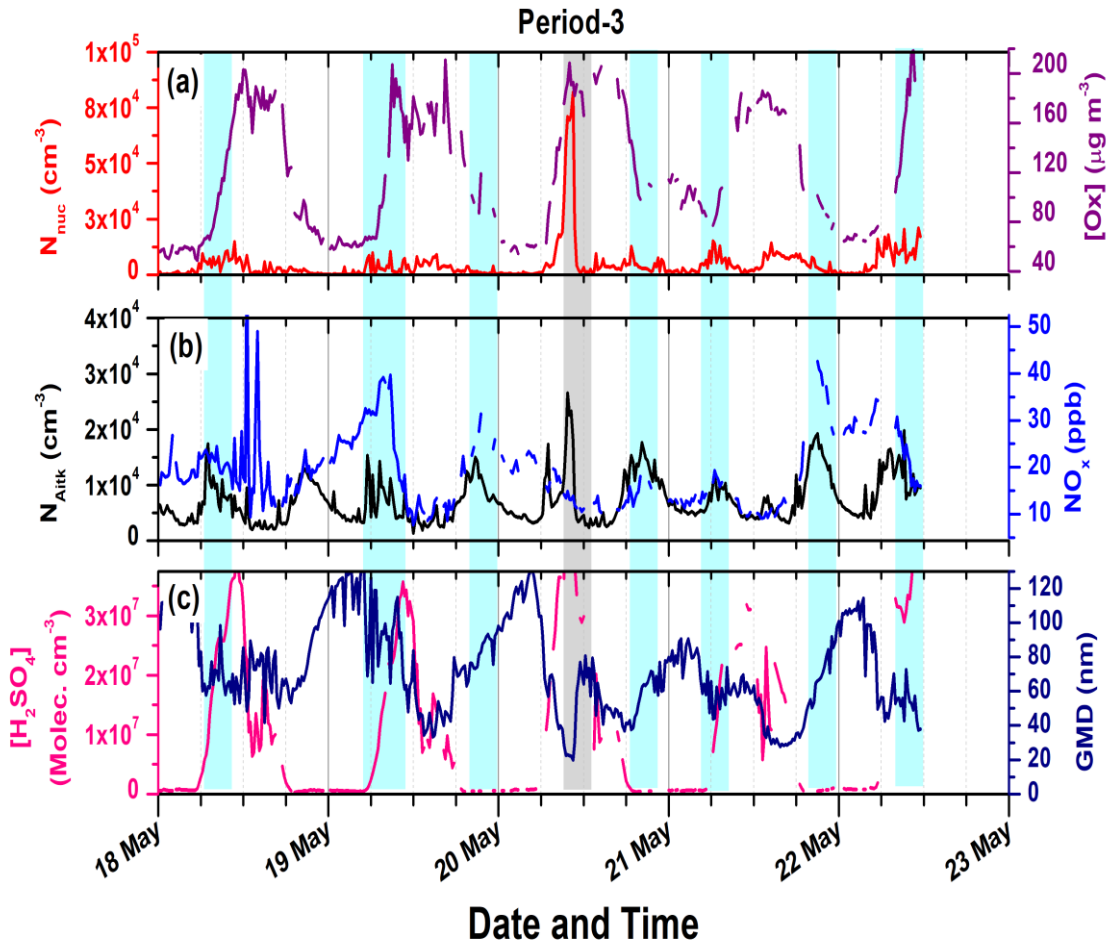

Figure 4.20: Temporal variation of (a) N_{nuc} and odd-oxygen [Ox] (b) N_{Aitk} and NO_x, (c) Sulfuric acid proxy concentration [H_2SO_4], and geometric mean diameter during Period-3. The grey-shaded portions indicate NPF events, whereas cyan-shaded portions indicate particle burst events

(OOA), which are mainly originated from secondary formation pathways from VOC precursors, show a strong association with [Ox], increased values of odd oxygen indirectly indicate nucleation events involving organic vapors. Therefore the current events may belong to the multi-component nucleation. However, [Ox] and [H_2SO_4]

proxy showed a typical diurnal variation pattern over the entire period; nucleation events did not occur during all the days (e.g., 29 April to 3 May in Figure 4.18). It became clearer from the marginal differences in the mean values of gas-phase chemistry parameters between the event and non-event days (Table 4.2). This suggested that enhancement in precursor levels is a necessary condition (but not sufficient) for NPF, but actual nucleation depends on several other factors. These include low scavenging rates of freshly formed embryos and particles (coagulation sink), lower condensation sink (Kuang et al., 2008, 2010), and higher insolation that drives photochemistry producing more OH radicals and condensable vapors (thereby creating conducive local super-saturation conditions for precursors) (Kulmala et al., 2004).

Further, as seen from the cyan-shaded portions in Figure 4.19 and Figure 4.20, the particle burst events (with enhanced N_{Aitk} and/or N_{nuc}) are typically associated with a clear increase in NO_x concentrations. Therefore, direct emissions from primary sources (traffic in this case) to the overall ultrafine particle abundance are also considerably present in this urban region. Incidentally, as the restrictions of COVID-19 lockdown were reduced, such events were noticed predominantly (most during Period-III (Figure 4.20) compared to Period-II (Figure 4.19), but none during Period-I with a strict lockdown). Figure 4.21, where the temporal variation of nucleation and Aitken mode particle concentrations color-mapped with NO_x concentrations (which is a proxy for traffic emissions), reiterated such an impact of road traffic emissions on UFP. The GMD values during such particle burst events did not depict any unambiguous drop (unlike the NPF events where GMD immediately dropped after the nucleation and subsequently displayed a definite growth).

Present [H_2SO_4] proxy values during the NPF events (2-3.5 x 10^7 molecules cm^{-3}) are lower than the values reported by Yu et al. (2016) over Nanjing, an urban region in China (3.6-3.9 molecules cm^{-3}), higher than those reported (1.2-2.1 x 10^7 molecules cm^{-3}) over the USA by Yu et al. (2014) and comparable to the values (2.5-2.9 molecules cm^{-3}) recently reported by Sebastian et al., (2021) over Hyderabad, an urban location in India.

Most of the current nucleation events during the afternoon/late noon period suggest the definitive role of photochemistry in producing the requisite conditions for NPF (Birmili et al., 2000). The present study period being hot summer with intense solar radiation

availability is conducive for NPF. During the daytime, the condensable vapors are chemically produced mostly due to oxidation reactions in the presence of sunlight. Such low volatile vapors emanating from high chemical reactivity species participate in the formation of the initial molecular cluster prerequisite for nucleation (Hussein et al., 2004). The high temperature and low RH conditions prevailing during the daytime further aid nucleation (Birmili et al., 2003; Hamed et al., 2007; O'Halloran et al., 2009; Suni et al., 2009; Kanawade et al., 2014; Salma et al., 2016; Dada et al., 2017; Pushpawela et al., 2018). The role of wind speeds is, generally, limited to cause the dispersion of the pollutants and pre-existing particles, thereby reducing the condensation sink values (Gómez-Moreno et al., 2011; Hofman et al., 2016; Hama et al., 2017). However, in the present study, we have not found any clear association between the magnitudes of T, RH, WS, and solar radiation with the intensity of nucleation (Kerminen et al., 2018). It underscores the complexity of nucleation in the real atmosphere, which occurs due to the convolution of multiple processes. One more vital point to note here is that since the nucleation is a competition between the condensable vapor source strength and condensation sink, varying strengths of emissions result in varying amounts of condensable vapors and pre-existing particles. Varying magnitudes of NPF from Period-I to Period-III highlights this aspect also.

Varying air masses can potentially affect the NPF phenomenon to varying precursor concentrations and meteorological variables (such as RH and T). To investigate this, we have examined the association between wind speeds and direction with particle concentrations (N_{nuc} and N_{Aitk}), NO_x (which is a proxy for local vehicular emissions), and [H_2SO_4] proxy concentrations (using eq. 3.6). The polar diagram of the wind speed and direction in Figure 4.22 shows the variations variables. The color scale (on the right-hand side of the figure) depicts the magnitude of concentrations.

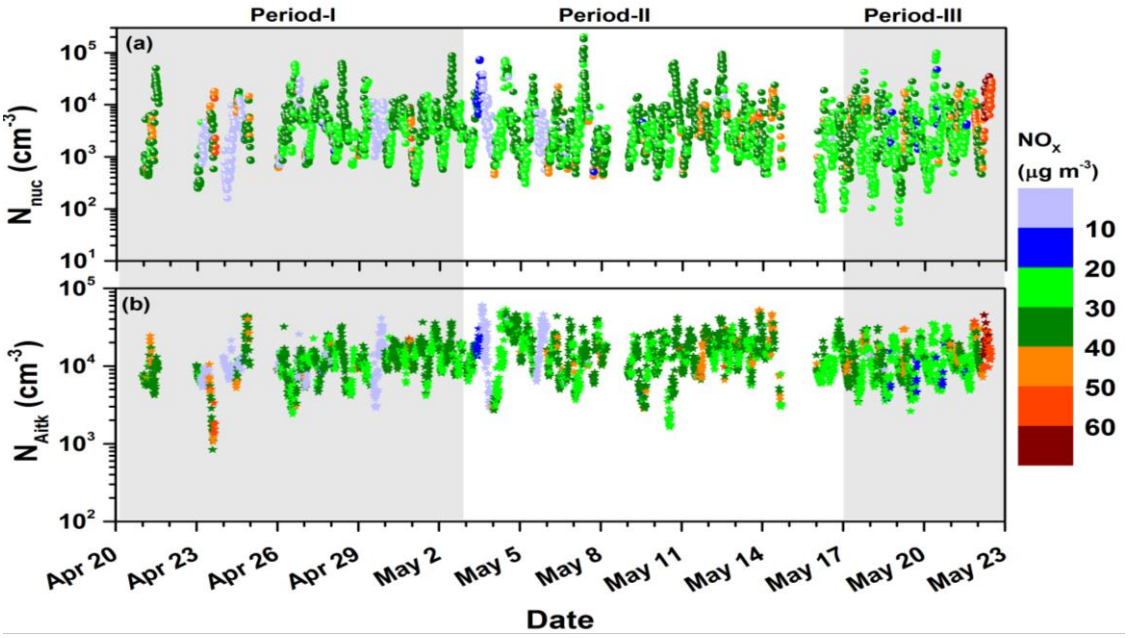

Figure 4.21: Temporal variation of nucleation and Aitken mode particle concentrations color-mapped with concurrent NO_x concentrations during the present study

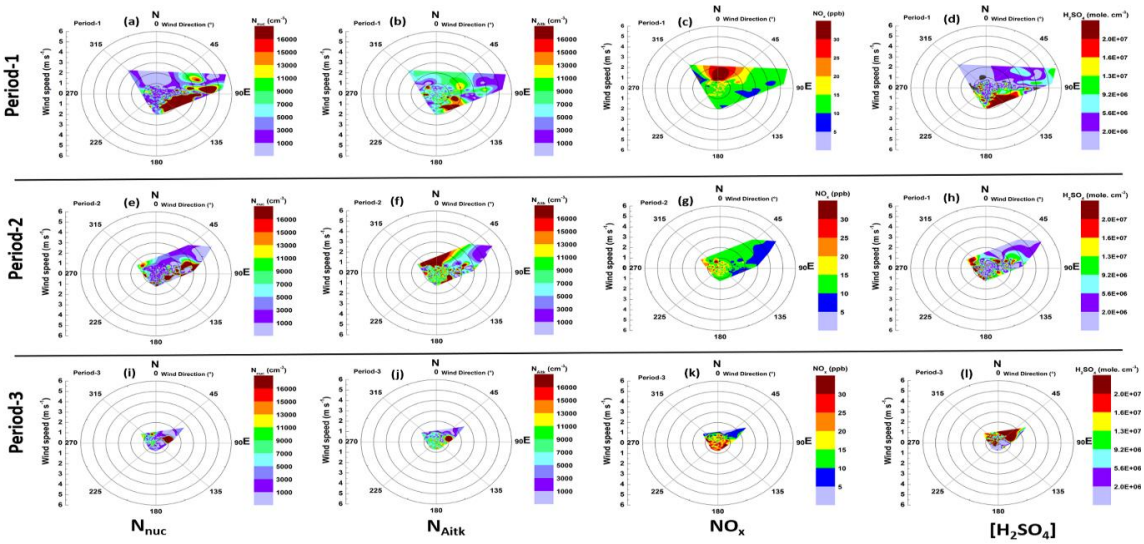

Figure 4.22: Association between wind speeds and direction with N_{nuc} (cm^{-3}), N_{Aitk} (cm^{-3}), NO_x (ppb), and sulfuric acid [H_2SO_4] concentration (molecules cm^{-3}) for Period-1 (a-d), Period-2 (e-h) and Period-3 (i-l). Color scale represents the magnitude of the quantity

From Figure 4.22, it is evident that higher amounts of N_{nuc} (>16000 cm^{-3}) were noticed predominantly when the air masses originated from the east-southeast sectors (panels a, e, i), while the values were relatively lower (2 to 4 times less) for the other wind sectors. Interestingly, elevated values of [H_2SO_4] proxy concentrations (panels d, h, l) ($\geq 2x10^7$ molecules cm^{-3}, which are nearly two orders of magnitude higher) were also seen when the winds were from these sectors compared to other sectors. This suggested the precursor-rich nature of the air masses from the east-southeast sectors. However, NO_x (which is predominantly anthropogenic in origin) was higher (>25 ppb) for the north-northeast sector (panels c, g) but lower (< 15 ppb) for the other wind sectors during Period-I and Period-II, whereas no clear air mass dependence of NO_x concentrations is perceptible during Period-3 (probably due to increased anthropogenic activities). Also, this supported that the nucleation mode particles were seen due to their formation from secondary pathways rather than primary vehicular emissions. Another important feature is the contrast between air mass dependence of N_{nuc} and N_{Aitk} (which matched with NO_x) during Period-II, thus suggesting a non-negligible contribution from direct traffic emissions (i.e., in-plume pollutants) to N_{Aitk} (this was clear even in Figure 4.19; cyan shaded portions). Nevertheless, such contribution from in-plume appears to be not significant during Period-I.

The enhancement in the concentrations of NO_x, SO_2, O_3, CO, which are criteria pollutants for the urban environment, highlighted the increased human activities with more relaxation in public movement (as seen in Table 4.2, which shows the highest concentration of these pollutants during Period-III). This is reflected even in the concentrations of pre-existing particles of predominantly primary origin.

4.2.5 Diurnal variation of particle concentrations

The diurnal variation of the pollutants (especially short-lived species) provides insights into the affinity between anthropogenic activities, meteorological conditions, ABL dynamics, and air pollution. Therefore, we have examined the diurnal variation pattern of the N_{total}, N_{nuc}, $N_{Aitk,}$ and N_{accu} to delineate the processes that affect particle concentrations in shorter timescales, which are shown in Figure 4.23 (for Period-I), Figure 4.24 (for Period-II), and Figure 4.25 (for Period-III). These figures highlighted a conspicuous pattern in different size regimes during the event and non-event days.

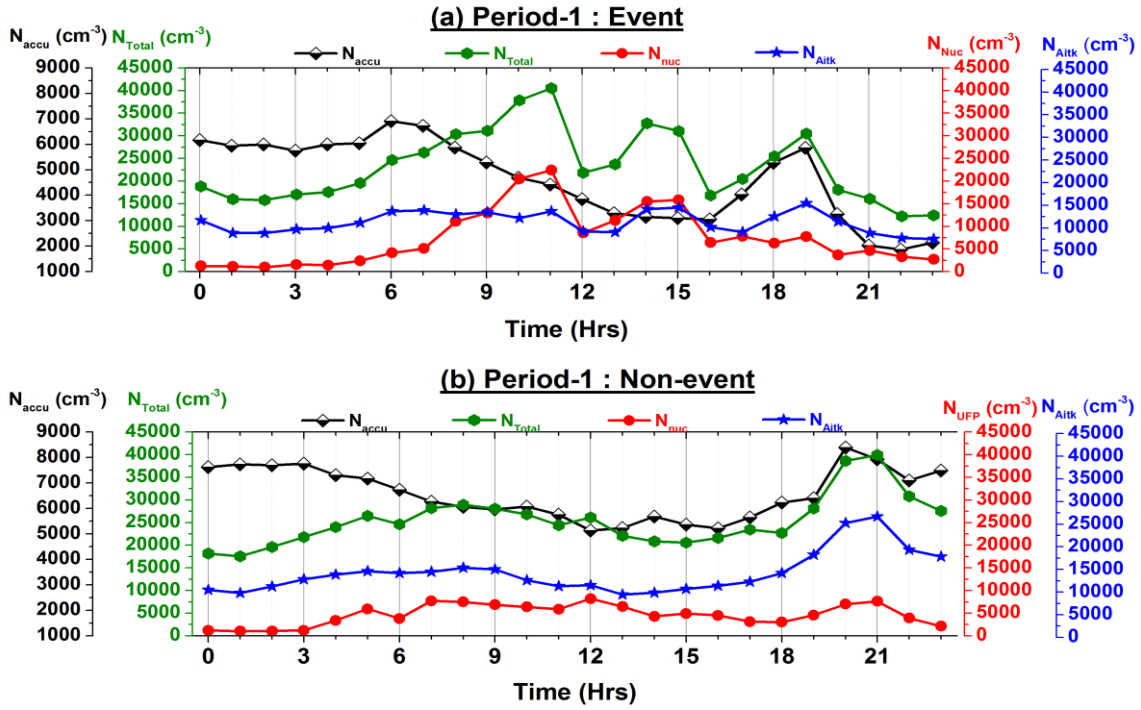

Figure 4.23: Diurnal variation of N_{Total}, N_{nuc}, N_{Aitk}, and N_{accu} during the event and non-event days of Period-1

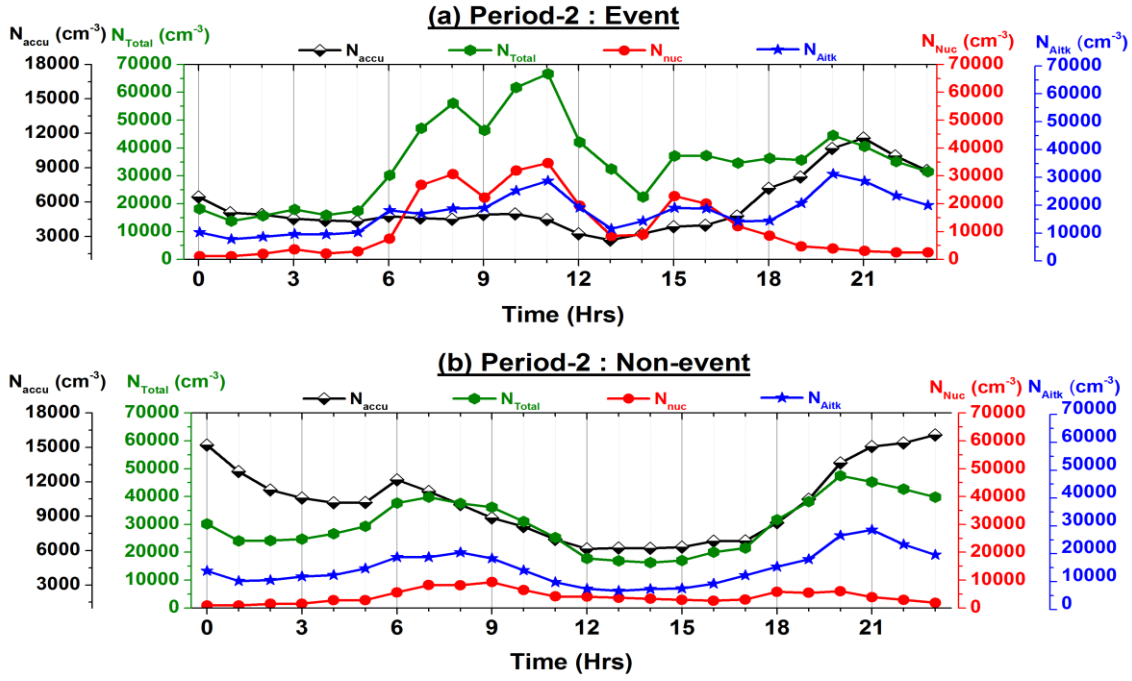

Figure 4.24: Same as Figure 10, but for Period-II

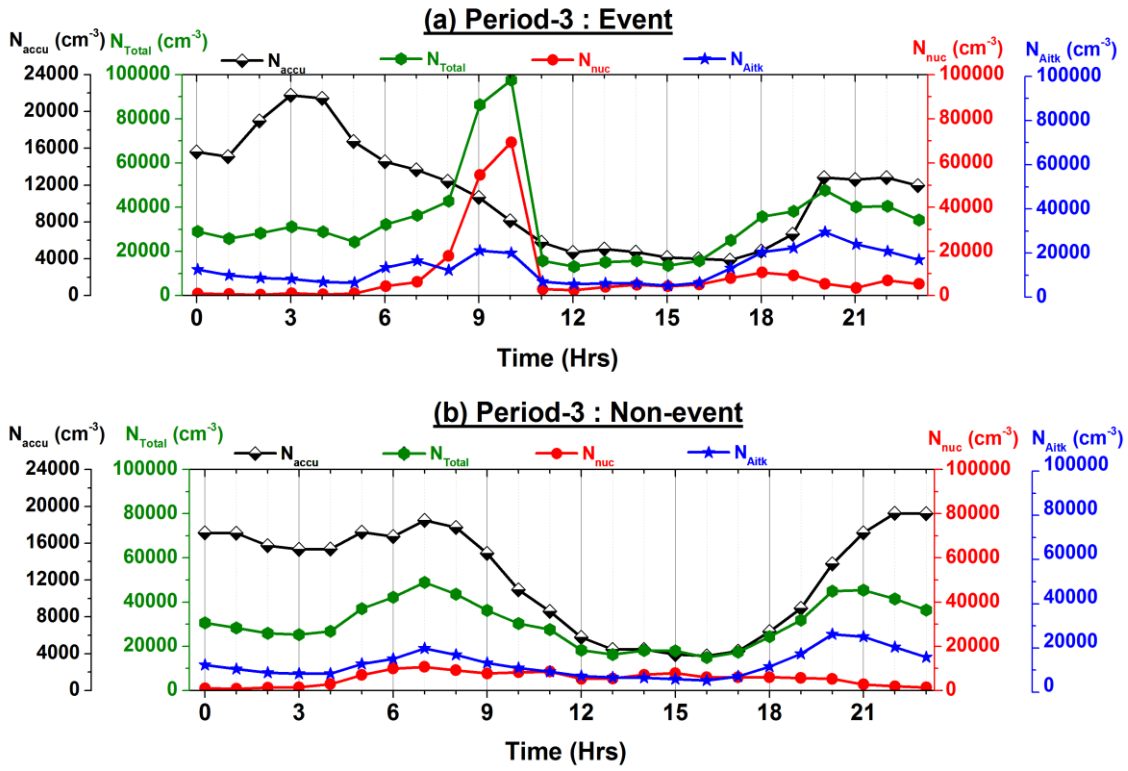

Figure 4.25: Same as Figure 10, but for Period-III

The diurnal variation of particle concentrations during the non-event days showed a typical double hump pattern governed by the local ABL dynamics and source/sink processes of aerosols (Kompalli et al., 2014a, 2014b; Babu et al., 2016). Two distinct peaks of varying magnitudes, the first one occurred about an hour after sunrise (07:00 - 08:00 hrs); the second and more prominent peak occurred during the late evening (20:00-23:00 hrs) with a trough during the daytime. The first peak occurs because thermals emanated after the sunrise breaking the nocturnal inversion and bringing the pollutants from the residual boundary layer to the surface. Following this, the daytime evolving convective boundary layer leads to sufficient ventilation of the pollutants; therefore, lower concentrations prevailed at the surface. Subsequently, as the sun sets, thermals cease to form, and stable atmospheric boundary layer conditions during the night-time confine the pollutants near the surface, resulting in a second and stronger peak. Several earlier studies have reported such a pattern of particle number concentrations (e.g., Hussein et al., 2004; Kompalli et al., 2014a; Babu et al., 2016). Besides this atmospheric dynamical phenomenon, varying source strengths during the day also contribute to the

observed diurnal pattern. Over urban locations, the contribution coming of rush-hour traffic to diurnal variation of the particle number concentrations is significant (Wu et al., 2008; Brines et al., 2015; Hama et al., 2017). An increase in traffic emissions, which are the main source of primary ultrafine particles, formed in the engine or the atmosphere after emission from the tailpipe (Shi et al., 1999; Charron and Harrison, 2003) reflected in N_{total} and N_{Aitk} concentrations in urban regions (Wang et al., 2014; Kopanakis et al., 2018). Primary particles related to traffic are emitted during the dilution and cooling of road vehicle exhaust (Charron and Harrison, 2003; Kittelson et al., 2006) or as carbonaceous soot agglomerates formed by fuel combustion (Kittelson, 1998; Shi et al., 2000; Banerjee and Christian, 2018; Rönkkö and Timonen, 2019).

Interestingly, the magnitude of the first and second peaks in N_{total}, $N_{Aitk,}$ and N_{accu} concentrations during the non-event days progressively increased from Period-I to Period-III, underlining the increased contributions from traffic emissions with the progressive unlocking of the activities. For example, the dominant second peak in N_{total} was seen at ~37500 cm^{-3} during the non-event days of Period-I, whereas for Period-III, it was at ~50000 cm^{-3}. Similar behaviour is observed in the case of N_{Aitk} and N_{accu} concentrations.

Such a typical pattern of diurnal variation is disturbed by frequent new particle formation events. As evident from the top panels from Figure 10-12, clear peak(s) is (are) noticed in the N_{nuc} and N_{total} during the daytime (09:00-15:00 hrs) of the event periods (Brines et al., 2015; Hama et al., 2017; Kompalli et al., 2018). The mean diurnal pattern of N_{nuc} depicted multiple peaks during the event days of Period-I (~10:00-11:00 hrs; 14:00-15:00 hrs and 18:00-19:00 hrs). During Period-II, the peaks occurred at 08:00 hrs and 11:00 hrs, whereas a single peak in N_{nuc} occurred at 10:00 hrs noticed during Period-III. It suggests different timings for the NPF events are mainly driven by photochemistry and reduced condensation sink values with enhanced dispersion of pre-existing particles. Further, atmospheric dynamical processes (such as variations in ABL heights and ventilation of the pollutants) have a definite impact on the diurnal variability of the primary and secondary aerosols (Kompalli et al., 2014a, 2014b). Also, the contribution from urban vehicular and anthropogenic emissions to the nucleation/Aitken mode

particles cannot be ruled out (Morawska et al., 2008; Kumar et al., 2014; Jayaratne et al., 2016; Hama et al., 2017; Kopanakis et al., 2018; Pushpawela et al., 2018).

In the urban regions, sulfuric acid -which is the most ubiquitous precursor for aerosol nucleation, is dominantly formed through secondary processes, i.e., from the combined effect of emitted gaseous precursors and photochemistry. It also emanates primarily from the hot vehicle exhaust (albeit not being a dominant source) that is converted rapidly to the particle phase. Also, the contribution of volatile organic compounds from traffic emissions over the urban regions to the secondary aerosol formation is significant, and it also depends on the prevailing meteorological conditions (Alam et al., 2003; Dunn et al., 2004; Stanier et al., 2004; Wehner et al., 2004; Jeong et al., 2004; Reche et al., 2011; Cheung et al., 2011; Gao et al., 2012; Kanawade et al., 2016). Primarily, photo-oxidation of organics (dominantly aromatic VOCs) originated from vehicular exhaust produces abundant precursors for secondary aerosol nucleation and subsequent growth to larger sizes (Ahlm et al., 2012; Zhang et al., 2012, 2015; Wang et al., 2015; Huang et al., 2016; Tröstl et al., 2016; Kerminen et al., 2018; Lee et al., 2019; Ling et al., 2019). These aspects are also reflected in the strength and timing of the observed NPF and growth events. Brines et al. (2015) categorize the aerosol size distribution in the urban areas (Brisbane-Australia, Madrid-Spain, and Barcelona- Spain) into three classes; 1) traffic- 44 to 63% of the day time, 2) Nucleation- 14 to 19%, and 3) Background pollution and specific cases 7 to 22%. Our pattern is similar to the one reported by Jeong et al. (2004), who found nucleation events in the morning (07:00 to 09:00 hrs) due to traffic emission and local pollution plumes in Rochester (NY), where the nucleation occurred between early afternoon and late afternoon. It is evident that during such events, the nucleation mode concentrations, which are highly subdued otherwise, increase by several orders (2-5) of magnitude (Wehner et al., 2004). However, prevailing background pollution levels play a crucial role in the particle number concentration in different size regimes, and they also strongly depend on the local meteorological factors (Hitchins et al., 2000; Morawska et al., 2008; Nicolás et al., 2009).

It may be noted that recently Srivastava et al. (2021) reported the diurnal variation of different near-surface pollutants (NO_x, Ozone, CO, PM2.5, and PM10) over New Delhi during the lockdown period. They observed an enhancement in the concentrations of each

pollutant with the progression of lockdown phases. We have not described the diurnal variation of trace gases in this manuscript because our observations/patterns are similar to their results.

The present study elucidated the atmospheric conditions controlling the NPF phenomenon using the unique opportunity available due to the COVID-19 lockdown. Since we did not measure particle concentrations below 10 nm, it is not possible to identify the Aitken mode particles originating from the growth of vapors + particles (which are primary in nature) and secondary aerosols from volatile organics/sulfuric acid emanated from traffic emissions. This work examined the impact of the photo-oxidation and condensation sink associated with the urban emissions on the intensity and frequency of the secondary aerosol formation process. Though reduced traffic emissions have resulted in decreased primary particles, it enhanced secondary aerosol formation, leading to highly elevated UFPs. This aspect needs to be considered to assess the overall impact of UFP on urban pollution, human health, and evolving suitable mitigation policies. The elevated precursors (perhaps, VOCs) from automobiles and decreasing pre-existing particle concentrations during the lockdown aided the efficient nucleation over the megacity; however, the exact species contributing to NPF is not identified, which forms the scope for a future study.

4.2.6 Summary

This study examined the impact of the COVID-19 lockdown and subsequent progressive relaxations of anthropogenic activities on particle number concentrations and number size distributions in the ultrafine and fine size range (10.2 to 1090 nm) over a megacity, New Delhi.

The mean total particle number concentrations gradually increased from Period-I (25065 ± 13881) with the strictest lockdown to Period-III (31681 ± 18776 cm^{-3}), where restrictions were eased up considerably. The fraction of ultrafine particles gradually decreased from ~0.70 ± 0.09 to 0.58 ± 0.16 during this period, with the doubling of the accumulation mode particle concentrations (N_{accu}). This highlighted the effect of intensified anthropogenic activities on particle number concentrations.

Several new particle formation events occurred with the nucleation mode particle concentrations (N_{nuc}) increasing by 3-8 times, which led to an enhancement in N_{total} by 2-5 times. Compared to the non-event days, N_{nuc} was ~1.5-2 times higher on the event days. Most of the NPF events occurred during the morning/afternoon hours of the day, demonstrating the role of photochemistry. However, there is no clear association between the prevailing meteorological conditions or trace gas concentrations and nucleation intensity.

The varying magnitudes of N_{nuc} and N_{UFP} on the event, non-event days established the competition between the strengths of the precursor vapor sources and condensation sink. Different classes of NPF events were identified with an overall NPF frequency of ~ 41 %. During Period-I, the NPF frequency is 20.6 %, with the occurrence of all classes of NPF events (Class Ia, Class Ib, and Class II), whereas NPF frequency of 17.2 % with only class Ia events were seen during Period- II. The lowest frequency (3.4 %) with only class II events during Period-III highlighted the role of urban primary emissions on UFP loading. Interestingly, while NPF events during Period-II are more frequent and well-defined, lower particle growth rates (mean ~5.86 ± 1.44 nm hr^{-1}) compared to the Period-I (~6.05 ± 1.66 nm hr^{-1}) have been observed during this period.

The condensation sink (CS) values on the non-event days during Period-I (0.053 sec^{-1}) < Period-II (0.072 sec^{-1}) < Period-III (0.09 sec^{-1}) were normally higher than those seen on event days of Period-I (0.034 sec^{-1}) < Period-II (0.035 sec^{-1}) < Period-III (0.07 sec^{-1}) < Period-III (0.07 sec^{-1}) respectively. It suggested that higher CS in the urban regions with a gradual increase in traffic ensures that gaseous precursors, molecular clusters, and newly formed particles experience a high loss rate. The frequency, intensity, and shape of the NPF events are determined by the competition between the CS and the strength of precursor vapor sources.

During the nucleation events, a clear enhancement in the concentrations of [H_2SO_4] proxy (2 to 3.5 x 10^7 molecules cm^{-3}; 2-3 orders higher than the non-event values) suggests the role of gas-phase photochemistry in NPF. Also, some of the NPF events were associated with increased odd oxygen concentrations [Ox], indicating the regional nature of the precursors and participation of VOC precursors in nucleation/growth.

However, particle burst events depicted NO_x enhancement, thereby suggesting contributions from traffic emissions to UFP abundance.

Almost all the NPF events occurred when the air masses originated from the east-southeast sectors, as evident from several times higher N_{nuc} and [H_2SO_4] proxy values compared to the other wind sectors. This suggested the precursor-rich nature of the air masses from the east-southeast sectors. However, NO_x, in general, was higher (>25 ppb) for the north-northeast sector but lower (< 15 ppb) for the other wind sectors, supporting the inference that the nucleation mode particles were formed from secondary pathways rather than primary vehicular emissions.

The diurnal pattern of N_{UFP} revealed a typical double hump pattern governed by the local atmospheric boundary layer dynamics and source/sink processes of aerosols during the non-event days. The magnitude of the first and second peaks in N_{total}, N_{Aitk}, and N_{accu} concentrations during non-event days gradually increased from Period-I to Period-III, underlining increased traffic emissions with the unlocking of activities. However, the mean diurnal pattern of N_{nuc} showed a distinct pattern during the events days with multiple peaks during the daytime of Period-I (~10:00-11:00 hrs; 14:00-15:00 hrs and 18:00-19:00 hrs), Period II (~08:00 hrs and 11:00 hrs) reiterating the role of photochemistry. Furthermore, the contribution of the urban vehicle and anthropogenic emissions to the particle nucleation mode cannot be excluded.

4.3 UFP and qUFP at selected location during specific events (pollution episodes) in megacity Delhi

Delhi's poor air quality has become well-known, particularly during the winter season and the Diwali festival. Keeping this in context, ultrafine particulate matter has been studied for Diwali 2019, as the government had banned conventional firecrackers in Delhi but has permitted the use of green crackers. The Delhi government implemented the odd-even scheme to reduce air pollution in the city, as it depends entirely on vehicle emission control. As a result, the Odd-Even Scheme -II (2019) has also been studied in the context of qUFP because vehicular emissions produce a significant amount of UFP in megacities.

4.3.1 Diwali event

Researchers and policymakers in Asia are becoming increasingly concerned about the deterioration of ambient air quality and their health impacts in massive urban areas such as the megacity Delhi, India. Because of their extreme variability in time and space, the urban population is subjected to a heterogeneous mixture of ambient air pollutants (Kumar et al., 2014, 2011; Mishra et al., 2019; Pandey et al., 2016; Singh et al., 2011). Profound implications such as climate change, poor visibility, and health issues are a high priority in Asian metro cities due to ambient air pollution (Kong et al., 2015; P. Kumar et al., 2016). Specifically, the ultrafine particles (UFP), which are a subset of fine particles have caught the attention of researchers as they may further deteriorate the ambient air and induce health risks (Joshi et al., 2019, 2016; Kumar et al., 2012; Kwon et al., 2020; Schraufnagel, 2020; Yadav et al., 2019b). Transformation of UFP generated from various sources is being studied under different size modes; nucleation, coagulation, and accumulation (Banerjee et al., 2015; Dinoi et al., 2021; Segalin et al., 2020; Yadav et al., 2019a). These modes help in explore and understand the UFP's Particle Number Size Distribution (PNSD). The emission sources, precursor gases, and meteorological parameters cause variability in the transformation of UFP (Chu et al., 2018; Kanawade et al., 2014; Murari et al., 2014; Tiwari et al., 2013; Wang et al., 2014, 2017). Emissions generated from vehicles and industries add majorly to the UFP levels. Besides this,

fireworks during public celebrations and festivals, e.g., Diwali in India, have the potential to create adverse air quality impacts on health, including emissions of UFP (Parkhi et al., 2016; Perrino et al., 2011; Rohra et al., 2018; Sati and Mohan, 2014; Srinivas et al., 2016; Yadav et al., 2019a). The burning of firecrackers enhances the manifold UFP concentration than the ambient background concentration such as in the Chinese Spring Festival (Zhang et al., 2010; Zhao et al., 2014), Diwali festival in India (Joshi et al., 2019, 2016; Majumdar and Nema, 2011; Monkkonen et al., 2004; Prakash et al., 2013; Yadav et al., 2019a), Millennium fireworks 2000 in Leipzig, Germany (Wehner et al., 2000); Milan, Italy during Italian football team wing FIFA cup 2006 (Pirker et al., 2020; Vecchi et al., 2008); Berlin, Germany (Dutschke et al., 2011); eastern Spanish festivals, Spain (Crespo et al., 2014); new year's eve festival in two European cities- Brno, Czech Republic & Graz, Austria (Tanda et al., 2019). For the 2006 Lantern Festival in Beijing, Wang et al. (2007) studied the chemical composition of atmospheric aerosols during the Lantern Festival in Beijing in 2006 and found that the chemical compositions (such as Ba, K, Sr, SO_4^{2-} and NO_3^-) were five times higher than in other nights. Joshi et al. (2019) investigated in a high-rise building of an Indian mega-city during the Diwali festival, the mass concentration of total suspended particulate matter on Diwali night was found to be 364 μgm^{-3} with an average particle number concentration for Diwali day (4.9×10^4 #/cm^3) and suggested that the best possible tracer group representing the fireworks could be Al, Ba, K, Sr, Cu. Yadav et al. (2019a) examined the fine particles ($PM_{2.5}$) for selected water-soluble inorganic components (WSIC), and discovered the manifold increment (K^+, 527%; Mg^{2+}, 175%; NO_3^-, 57%; Cl^-, 291%) in firework-specific ionic mass from pre-Diwali (D-2) to Diwali day depicts the contribution of firework emission of WSIC to ambient aerosols. The study of Vecchi et al. (2008) on chemical-physical properties of airborne particles (elements, ions, organic and elemental carbon and particles size distributions) collected during a fireworks episode in Milan (Italy) reported the elements typically emitted during pyrotechnic displays increased in 1 hr as follows: Sr (120 times), Mg (22 times), Ba (12 times), K (11 times), and Cu (6 times). To assess the impact of New Year's Eve fireworks on ambient air quality, chemically resolved size distributions of particles with diameters between 15 nm and 10 μm collected during fireworks episodes were compared to ones collected in normal winter weeks (Tanda et al., 2019). In conclusion, seven elements (Mg, Al, K, Cu, Sr, Ba and Bi) could be identified as strongly

influenced by New Year's Eve fireworks activities, both by optical inspection of the size-resolved element distribution patterns and via calculation of enrichment factors utilizing the newly identified fireworks specific maximum. Therefore, higher PNC of UFP due to firecracker bursting may have a significant level of health impact than other urban air pollution.

The air quality of megacity Delhi over the last few years has reached a more critical level during the Diwali period and puts pressure on the policy of the concerned agencies (Balakrishnan et al., 2019; Dholakia et al., 2013; Gurjar et al., 2016; Mukerjee and Shukla, 2016). Because Delhi, along with the National Capital Region (NCR), had an approximate population of 22.2 million in 2011, with a decennial increase of 7.96 % observed (Ministry of home affairs, 2011), the second-largest urban area in the world. A Judiciary prohibition was also implemented on firecrackers for buying, selling, and its bursting timing in and around the Delhi region in 2017 (TOI, 2016). The judicial ban on bursting crackers' timing also includes green and regular crackers (TOI, 2020). Eco-friendly crackers (green crackers) have been formulated by Indian scientists at the Council of Scientific and Industrial Research (CSIR) laboratories to minimize noise and air pollution emissions. As recorded by the CSIR, it reduces the PM_{10} & $PM_{2.5}$ through 30-35% emissions and sulphur and nitrogen oxides by 35-40% and has a sound level of less than 120 dB (decibel unit) (Srishti, 2016; TV Venkateswaran, 2019). The relevant reduction of these gases may be very important in reducing of secondary UFP formation because secondary aerosol consists of particles that are generated in the atmosphere through chemical processes when precursor gases oxidise and then condense into the particle phase. When these condensable species enter the particle phase, they can either condense onto existing particles or nucleate to form new particles (Yadav et al., 2021). However, this decrease in secondary UFP formation may compensate for the massive primary UFP emission caused by fireworks celebrations (Pirker et al., 2020). Relatively fewer studies investigated the evolution of number characteristics at the time of fireworks (Crespo et al., 2014; Dutschke et al., 2011; Izhar et al., 2018; Joshi et al., 2019, 2016; Pirker et al., 2020; Prakash et al., 2013; Zhang et al., 2010; Zhao et al., 2014). In recent work, particles emitted during the Diwali festival were found to be having multi-legged structures (Mishra et al., 2016). Some studies also quantified the modifications in background aerosol characteristics due to fireworks during celebratory activities

(Monkkonen et al. 2005; Zhang et al., 2010). The complexity of picking up characteristic number features of fireworks-induced aerosol emissions (during the Diwali festival) has been discussed in Joshi et al. (2016). In concern of Delhi's Diwali pollution there is not a such study based on particle number concentration and its PNSD.

Particulate emissions occurring at festivals lead to the deteriorated quality of ambient air (P. Kumar et al., 2016; Sarkar et al., 2010). Diwali event emissions are generally local and short-term (one or two-day celebration) but instigate the respiratory and health illness for a longer duration with the increased finer aerosols, e.g., UFP (Joshi et al., 2016; Singh et al., 2019). Scientists have been working on different aspects of firework-generated emissions, considering the significant impacts caused by them (Hirai et al., 2000; P. Kumar et al., 2016; Singh et al., 2010). PNSD of UFP from nucleation to accumulation mode passing through the Aitken modes and its size characterization during Diwali is discussed concerning traditional firecrackers bursting (Yadav et al., 2019a). Other Diwali-related research works highlight the behaviour of $PM_{10,}$ $PM_{2.5}$, $PM_{1,}$ and various gaseous pollutants (Attri et al., 2001; Parkhi et al., 2016; Ravindra et al., 2003; Sati and Mohan, 2014), but very little work is on the UFP. Dutschke et al. (2011) and Zhao et al. (2014) showed the PNSD of small nucleation mode to large Aitken and accumulation mode of the size range shifting. On the other hand, (Yadav et al., 2019a) concluded the inefficiency of connection between the temporal variation of PNC and the emission of fireworks, considering the more variability in it. Limited analysis has been done for PNC, PNSD, and relationship with meteorological factors, particularly (especially in concern of crackers) in urban cities like Delhi. UFP generation during the Diwali period as of intense firecracker burning follows quite distinctive patterns and composition compared to standard urban aerosols in the background, which needs analysis (M. Kumar et al., 2016). PNC related research may help to determine the Air Quality Index (AQI) in particle number count (Joshi et al., 2016). As far as India is concerned, recent studies conducted during Diwali, Joshi et al. (2019, 2016) and Yadav et al. (2019a) stated an apparent increase in UFP's PNC but lacked the effect of meteorological factors on PNC pattern and unclear source apportionment considering other (vehicular and industrial) emissions. This study was conducted to explain the following: PNSD of UFP and fine particles during pre, post, and Diwali day with diurnal variations of green crackers

bursting in Delhi; PNC of different size mode along with their geometric mean diameter (GMD) and influencing factor.

The instrument was placed at a height of around 10 feet near the Centre for Pollution Control Board (CPCB) monitoring station inside the campus (DTU). The location was so selected that it covers residential and commercial areas, maintaining a homogeneous environment far away from road traffic (Figure 3.2). This way, we can minimize the vehicle-generated particle number concentration (PNC) related intervention, and hence focusing on the fireworks emitted PNC in ambient air. Pre- and post-monitoring for Delhi's Diwali episode lasted for eight days for a minimum of 14 hours/day from 23rd to 30th October 2019. The data of days has been selected on the following statistical steps; 1) which have more than 80% continuous data (especially at peak time according to celebration timing), and 2) which have a significant difference between pre-and post-Diwali. The primary event day, i.e., the Diwali festival, was on 27th October 2019, while the bursting of firecrackers was mainly witnessed from 6:00 PM-10:00 PM on 26th - 28th October 2019. According to Joshi et al. (2016, 2019) and Yadav et al. (2019a) the day has been divided into different time slots (pre, post, and Diwali day) to get insights into fire bursting impacts during pre-Diwali and post-Diwali in comparison to the Diwali day.

The particle number size distribution (PNSD) and particle number concentration (PNC) were measured using a scanning mobility particle sizer with a condensation particle counter (SMPS + C) (Make: GRIMM Inc., Germany) in size range of 10.2 to 1090 nm for 7 minutes per scan and sample flow rate (ratio of sheath to aerosol flow rate=10) of 0.3 Lmin^{-1}. To size segregate aerosols into 45 size bins, the SMPS instrument employs the principle of 'differential mobility analysis.' To minimized the loss of particles, all the protocols were followed during the monitoring (Burkart et al., 2010; Joshi et al., 2012). The different size distributions, namely nucleation mode (10 nm < D_p < 20 nm), small-Aitken mode (20 nm < D_p < 50 nm), large- Aitken mode (50 nm < D_p < 100 nm), and accumulation mode (100 nm < D_p < 1000 nm) were observed during the experiment. PM_{10}, $PM_{2.5}$, SOx, NOx, CO, O_3, wind speed and relative humidity (RH) were also recorded for all the monitoring days using the data available from Central Pollution Control Board (CPCB) monitoring station at the DTU campus only.

The dataset normality was tested using a combination of the Exploratory Data Analysis (EDA) plot and the Shapiro-Wilk (S-W) test. The Kruskal-Wallis (K-W) test, a nonparametric version of the ANOVA test, was performed on air quality data. The Kruskal Wallis test (rank-based nonparametric test) was used to determine the statistical differences between days (25^{th}, 26^{th}, $27^{th,}$ and 28^{th} October 2019) and independent variable pollutant (Nucleation mode, small Aitken mode, Large Aitken mode, Accumulation mode) of representative location in DTU campus in Delhi. Kruskal Wallis test denotes with H test (Annexure - I). In particular, the H test examines whether the null hypothesis is valid i.e., there are no statistical mean variations in population variances; if not true, then an alternative hypothesis is accepted. A 0.05 significance level was used in both cases. Therefore, if the p-value was lower than the significance threshold (< 0.05), the null hypothesis was rejected, and there was a statistically meaningful difference between the mean results (Annexure - I).

4.3.1.1 Temporal variation of particle number concentration

The temporal variation of total aerosol concentration of particle number and their geometric mean diameter (GMD) during the study period are depicted in Figure 4.26. On the celebration day (27^{th} October 2019), a sudden rise in total PNC was observed from 6:00 PM-10:00 PM with an average of 1.29×10^5 # cm^{-3} (Table 4.6). In Figure 4.26, peak 'A' denotes the highest peak at ~7.30 PM with PNC of ~1.7×10^5 # cm^{-3} and GMD of ~39 nm, which reached the maximum at late night from 7:00 PM- 9:00 PM (with another peak after peak 'A'), which validates the maximum burning of firecrackers in this period. Even though this is shortly before the Government set the time (8:00 PM to 10:00 PM) for the green crackers to burst, it shows that people had already begun celebrating the event after being restricted (Jain, 2019). In contrast to previous studies (Joshi et al., 2016; Yadav et al., 2019a), it shows another peak as adjacent to peak 'A' at 9:50 pm with a PNC of 1.67 x10^5 # cm^{-3} and GMD of ~44 nm. This could explain the progressive impact of government rulings to end the celebration on time, causing the public to finish their green cracker. While Joshi et al. (2016) and Yadav et al. (2019a) studies describe the traditional firecracker bursting without any legal constraints, in which a single peak on Diwali day has PNC of ~1.2 x 10^5 for Mumbai (at ~ 10:10 PM) and ~4.5 x 10^4 for Varanasi (at ~7:50 PM). If we compare peak-related GMDs on Diwali evening time, it is 89 nm for Varanasi,

~51nm for Mumbai and 39 nm for Delhi. Whereas the PNC for Delhi (~1.7×10^5 # cm^{-3}) is greater than PNC in Mumbai (~1.2×10^5 # cm^{-3}) and Varanasi (4.5×10^4 # cm^{-3}). Here, it is to be noted that the above PNC and GMD for Mumbai and Varanasi correspond to traditional firecrackers, whereas the PNC and GMD in the case of Delhi pertain to the green crackers. Thus, it appears that the green crackers emit more particles in a lower size diameter in comparison to the traditional crackers. However, the timing of the event, the effect of meteorological conditions and geography vary between these locations. Nonetheless, the comparison of their Diwali emission is significant because the massive emission of firecrackers within a few hours on Diwali day degrades the air quality to a high level. As shown in Figure 4.26, while analyzing pre- and post- Diwali days, similar peaks were obtained with a peak PNC of ~1.0×10^5 and ~7.0×10^4 # cm^{-3} on 26th and 28th October 2019 during the evening event period (6:00 PM to 10:00 PM). This shows comparatively lesser burning of firecrackers these days, keeping the background concentration the same. The peaks for pre-and post-Diwali days were denoted by peaks ‘B’ and ‘C.’ Like other studies (Joshi et al., 2016; Yadav et al., 2019a); typically, pre and post-Diwali peaks have the similar trend of PNC. One day before Diwali, on October 26, 2019, is known as "Choti Diwali," and two days before, on October 25, 2019, is known as "Dhanteras." Dhanteras is well-known for its evening marketing, which causes massive traffic jams in major cities such as Delhi.

Table 4.6 Averaged (4 hr) PNC, GMD, and Ratio of different modes

		Nucleation mode (10-20 nm)		Small Aitken mode~ (20- 50 nm)		Large Aitken mode (50-100nm)		Accumulation mode (100-1000)		Ntotal	Diameter	UFP/Ntotal
Time Divisions	Days	PNC (#/cm^3)	GMD(nm)	PNC (#/cm^3)	GMD(nm)	PNC (#/cm^3)	GMD(nm)	PNC (#/cm^3)	GMD(nm)	PNC (#/cm^3)	GMD (nm)	Ratio
9:30 AM to 1:30 PM	25-Oct	7.89 x 10^3	14.6	1.03 x 10^4	32.2	5.14 x 10^3	71.2	7.27 x 10^3	198.0	3.06 x 10^4	48.9	0.76
	26-Oct	5.47 x 10^3	14.6	7.79 x 10^3	33.5	5.48 x 10^3	70.9	8.12 x 10^3	200.0	2.69 x 10^4	56.4	0.70
	27-Oct	1.60 x 10^4	13.7	9.36 x 10^3	32.0	6.37 x 10^3	72.3	1.41 x 10^4	232.0	4.59 x 10^4	51.4	0.69
	28-Oct	4.17 x 10^3	14.4	4.09 x 10^3	34.3	4.39 x 10^3	73.2	1.41 x 10^4	220.0	2.67 x 10^4	102.0	0.47
	25-Oct	1.73 x 10^3	15.2	5.42 x 10^3	34.0	4.07 x 10^3	72.7	7.18 x 10^3	192.0	1.84 x 10^4	72.9	0.61

2:00 PM to 06:00 PM	26-Oct	1.04 x 10^3	14.8	2.20 x 10^3	35.0	3.05 x 10^3	74.2	7.27 x 10^3	204.0	1.36 x 10^4	104.0	0.46
	27-Oct	7.08 x 10^3	13.5	4.56 x 10^3	32.2	4.29 x 10^3	73.2	7.05 x 10^3	228.0	2.30 x 10^4	50.1	0.69
	28-Oct	1.88 x 10^3	14.9	4.72 x 10^3	33.9	5.51 x 10^3	73.5	9.72 x 10^3	221.0	2.18 x 104	113.0	0.55
6:00 PM to 10:00 PM	25-Oct	6.89 x 10^3	15.5	1.32 x 10^4	36.2	1.75 x 10^4	72.1	1.97 x 10^4	174.0	5.73 x 10^4	74.1	0.66
	26-Oct	5.48 x 10^3	14.0	7.03 x 10^3	35.5	1.04 x 10^4	73.4	1.72 x 10^4	192.0	4.01 x 10^4	80.8	0.57
	27-Oct	4.51 x 10^4	13.6	2.74 x 10^4	32.1	2.06 x 10^4	72.2	3.61 x 10^4	224.0	1.29E+05	44.4	0.72
	28-Oct	5.59 x 10^3	14.5	1.08 x 10^4	35.9	1.37 x 10^4	73.1	2.14 x 10^4	225.0	5.15E+04	122.0	0.58

However, traffic jams occur on Choti Diwali, but to a lesser extent than on Dhanteras. It is a transition period between Diwali and Dhanteras, as firecracker celebrations take place in the evening, but much less than on Diwali. Figure 4.27,Figure 4.28,Figure 4.30. explains the PM_{10} and $PM_{2.5}$, particle number size distribution detail. Choti Diwali and Dhanteras have higher NO_X and CO concentrations due to traffic flow differences but lower PM concentrations due to less firecracker bursting than Diwali. More details about the diurnal pattern and affecting factors can be found in the next section. The meteorological factors/parameters did not significantly change between the pre and post-Diwali periods (Figure 4.27). However, it has been observed that the pre-Diwali peak 'B' has a higher PNC than the post-Diwali peak 'C.' This could be attributed to the people's excitement and preference to burst more crackers during pre-Diwali and Diwali period in comparison to post-Diwali period and also to the significant impact of the Government Ruling on Diwali crackers bursting related behaviour of people to mitigate the effects of air pollution.

The occurrence of other peaks ('D' at ~9:30 PM, 'E' at ~9:30 AM) on 25th and 27th October 2019 indicates the background concentration of particle number in ambient air, possibly from other sources like vehicular emission, commercial emission sources, and may be due to the influence of meteorological conditions (Zhao et al., 2017). During the morning hours of day's peaks were seen, which may contribute by boundary conditions, anthropogenic activities, and vehicular emissions (Joshi et al., 2016; Kangasniemi et al., 2019; Rönkkö et al., 2017; Rönkkö and Timonen, 2019; Wang et al., 2014; Yadav et al., 2019a). We have not discussed these peaks as they are not concerned with the scope of the study.

In Figure 4.26, the relationship is established between the PNC of UFP and its GMD, which describes that the number concentration maxima coincide with the GMD (nm) minima. The smaller, the finer aerosols' diameter, the larger their particle number concentrations. Similar trends for temporal variation of number concentration were shown by (Joshi et al., 2016; Yadav et al., 2019a). According to the pre-and post-Diwali day's GMD, peaks 'B' and 'C' clearly show that it lies in small- Aitken mode with ~35nm and ~25nm GMD respectively of well-established ultrafine particles range.

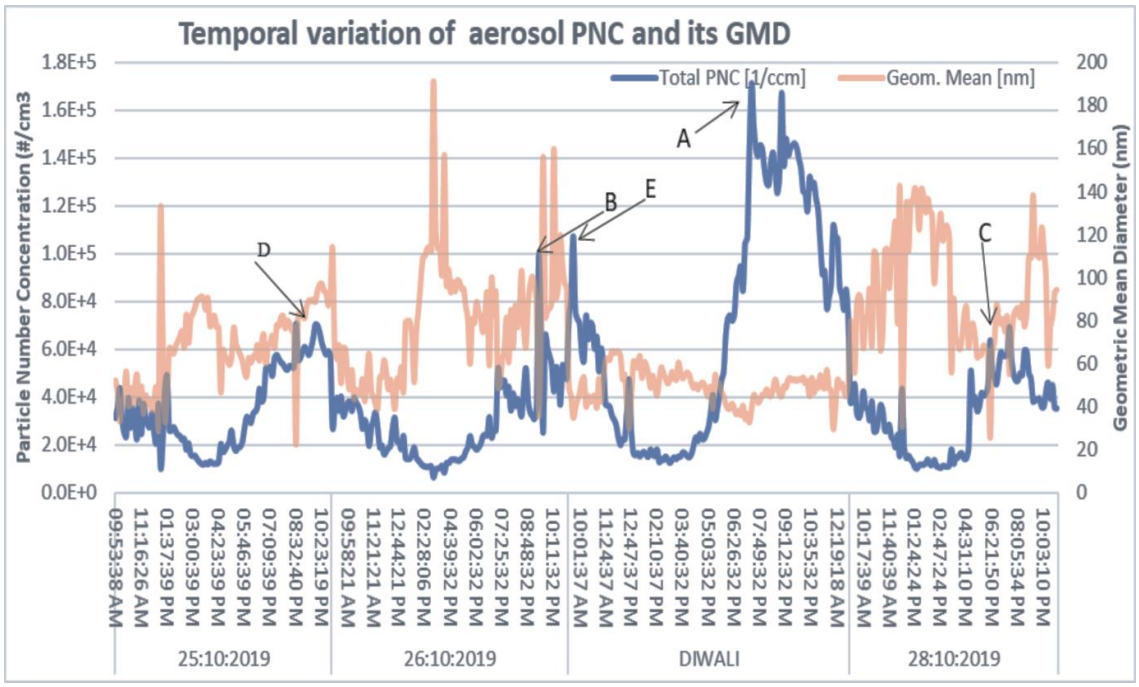

Figure *4.26*: The Temporal variation of aerosol PNC and its GMD during the study ('A,' 'B,' 'C,' 'D,' and 'E' show the peak of PNC)

Like other combustion processes, firework emissions are typically associated with particles in the accumulation mode. Yang et al. (2014) has reported Aitken and accumulation mode to account for 57% and 42% of the total PNC in China. In Beijing (China), a total PNC of 7.7 x 10^4 # cm^{-3} was reported during Spring festival fireworks, and the average particle diameter was observed to be 150 nm (Jing et al., 2014). Similarly, in Jinan (China), an average PNC of 2.5 x 10^4 cm^{-3} was reported during firework use, along with increased particles in the accumulation mode during the activity (Yang et al., 2014). In Germany, Wehner et al. (2000) also reported a dramatic increase in PNC in the accumulation range (> 100 nm) during a fireworks event. In a US-based study, Liu et al. (1997) have reported particle size variation between 0.3 and 1.9 µm. Whereas, in an experimental chamber, Betha & Balasubramanian (2013) have observed that between 60 to 85% of the particles from fireworks were in the ultrafine size range (i.e., particles with aerodynamic diameter <100 nm). The Nucleation and Aitken mode ratio calculated by us are given in Table 4.6 and discussed hereinafter Figure 4.31.

Meteorological factors such as wind speed and relative humidity are similar from 25th to 28th October 2019, including Diwali, with slight differences in wind speed and relative humidity. On Diwali Day, wind speed ranges from 0.2 to 0.3 m/s, which is lower than on other days from 1:00 PM to 5:00 PM but increases to 0.7 to 0.8 m/s after 6:30 PM and remains constant until late at night. During this time, RH is also lower. Lower RH and wind speed in urban areas are significant contributors to increased PNC in primary ultrafine emission (Chu et al., 2019; Dinoi et al., 2021; Rönkkö and Timonen, 2019; Tiwari et al., 2013; Wang et al., 2014). Polar plots show that the PNC of UFP is higher in the Southwest, where the residential area is located. On Diwali, residential areas are generally illuminated with electrical lights, candles, and oil feed lamps (Deepak) and the lighting of the firecracker bursting, resulting in a hotspot of air pollution during the event period (Figure 4.32, Figure 4.34,Figure 4.33, Figure 4.35, and Figure **4.36**).

4.3.1.2 Temporal variation of PMs and precursor gases and meteorological parameters

Figure 4.27 shows the diurnal pattern of PMs (PM_{10}, $PM_{2.5}$), gaseous (NOx, SOx, O_3, CO) and meteorological parameters (RH, Wind Speed) at the nearest monitoring station (DTU-CPCB) less than 10 m from 12th October to 11th November 2019 including Diwali celebration period. Monitoring duration has divided into pre-Diwali (12th to 24th October 2019), Diwali period (D-2; 25th October 2019-known as 'Dhanteras', D-1; 26th October 2019-known as 'Choti Diwali', Diwali; 27th October 2019, D+1; 28th October 2019, D+2; 29th October 2019), and post Diwali (30th October to 11th November 2019) for more insightfull investigation. On Diwali day on firecrackers celebration time (typically after 6 PM till late night), PMs concentration is much higher than on other day of monitoring at this time (e. g., ~1.4 times higher than on 'D-1') and after Diwali, $PM_{2.5}/PM_{10}$ ratio also incresed. The average $PM_{2.5}$ / PM_{10} ratio was found to be 0.81 during firecracker celebration time at Diwali day and at 'D+1' and 'D+2', which is a remarkably higher value. Such higher values are expected to be due to the high concentration of $PM_{2.5}$ and fine particles in the atmosphere of the Delhi region attributed mainly to the combustion (e.g., cracker bursting and lighting candle and oil- 'Deepak') during Diwali and one or two day after Diwali also. As mentioned in the section of the manuscript, the low-level

inversion layer is one of the important causes responsible for the higher concentration of $PM_{2.5}$ during winter (Fan et al., 2021; Tiwari et al., 2008). The $PM_{2.5}/PM_{10}$ ratio could be used identify their sources (Chan and Yao, 2008; Zhao et al., 2019). A higher ratio means the overwhelming contribution from $PM_{2.5}$, which is generally ascribed to primary pollution by anthropogenic activities and secondary particulate formation such as NO_3^-, SO_4^{2-}, NH_4^+, and organics, while a lower ratio is mainly contributed to fugitive dust or sand dust from long-distance transport (Chan and Yao, 2008). Since conventional Diwali celebration commences 1-2 days earlier of the festival day and continues for 1-2 days post-Diwali event, increased concentration of these pollutants is observed starting from pre-Diwali days and reaches its maximum on the event day (Diwali day) and continues to be high even a few days later of this event. But in the case of this Diwali (Green cracker) shows an interesting result: the gases (NOx, CO, O_3) have higher concentration before Diwali on 'D-2' and 'D-1'.

In concern of gases, NOx, interestingly, unlike on previous Diwali (conventional Diwali) (Ganguly et al., 2019; Mukherjee et al., 2018; Nigam et al., 2016; Pandey et al., 2016; Singh et al., 2010), it shows lower concentration than 'D-2', 'D-1' on Diwali day which may be due to huge traffic rush on evening time at 'D-2' and 'D-1' and the green crackers brusting on Diwali day, it may reduce 30 to 35 % NOx and SOx concencentration as per CSIR-NEERI claim. Therefore, SOx concentration does not show a major fluctuation in the concentration due to this festival. CO and O_3 show similar behaviour of mechanisms like typical Diwali period (Pratap et al., 2021). However, the concentrations of NOx, CO, O_3 after Diwali, start decreasing. Figure 4.27 depicts a variation of Ozone (O3) and Carbon monoxide (CO) during the Diwali event. Surface ozone is considered a vital secondary pollutant and its production is dependent on the intensity of solar radiation triggered by the presence of precursor gases like NOx, CO, and hydrocarbons. Ozone production is primarily controlled by the intensity of solar radiation during the daytime, when it is chemically removed by nitrogen monoxide (NO) and humid water vapor (Attri et al., 2001; Tiwari et al., 2014, 2015). During night-time on D-2, D-1, and Diwali nights, due to the traffic (massive on D-2, D-1) and burning of firecrackers on Diwali, a large amount of NO_2 is released into the atmosphere, which reacts with atmospheric oxygen to form nitric oxide (NO).

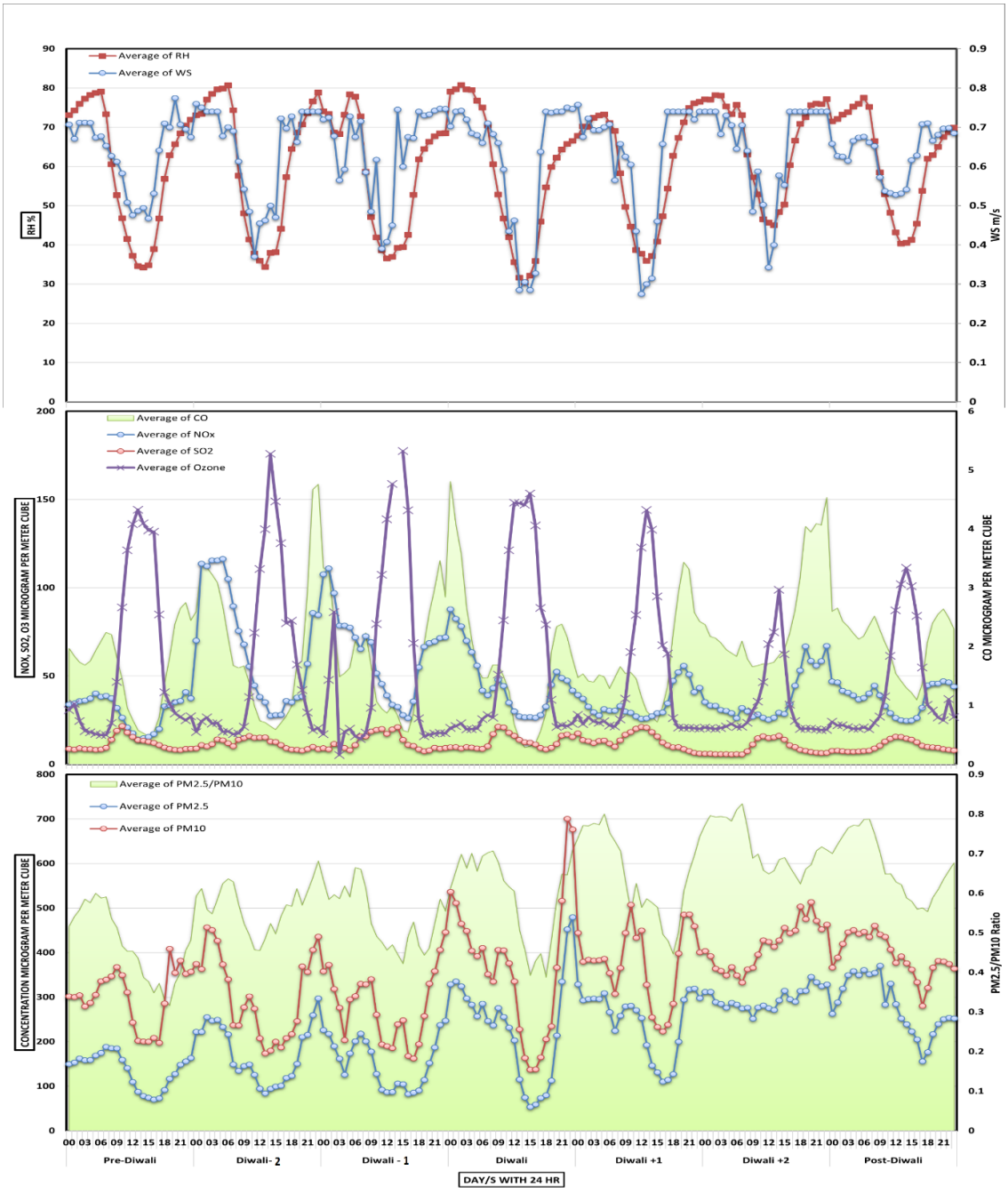

Figure 4.27: Diurnal pattern of PMs (PM_{10}, $PM_{2.5}$), $PM_{2.5}/PM_{10}$ ratio, gaseous (NOx, SOx, O_3, CO) and meteorological parameter (RH, Wind Speed) during 12th October to 11th November 2019

Therefore, NOx has a direct impression on O_3 formation. Wind speed and RH did not change at a significant level during the monitoring period. Regarding PNC of nucleation mode, small-Aitken mode, large Aitken mode, and accumulation mode's concentration

are higher through-out Diwali day but suddenly increase manifold at the time of firecracker celebration (Figure 4.28). Sporadic firecracker bursting on Diwali day before 6:00 PM (Ghei and Sane, 2018; Pratap et al., 2021) may be reasons for higher PNC (especially UFP) than on other days. As it can be observed, unfavourable dispersion conditions and stagnation of pollutants result in higher PNC levels in the morning time on Diwali. UFP/N_{total} ratio (ratio of UFP (10 nm to 100 nm diameter particle) and total PNC (10 nm to 1000 nm diameter particles)) ranges from 0.6 to 0.8 on Diwali day, which is higher than pre and post-Diwali day. UFP/ N_{total} reached a maximum ~0.8 at 6:00 to 8:00 PM, which is typical timing of firecrackers celebration, and this duration GMD was minimum of 38.0 to 42.0 nm, although whole day GMD ranges from38.0 to 58.0 nm which was lower than other day also. Interestingly nucleation mode shows the highest peak of PNC at 6 to 8:00 PM but did not indicate the new particle formation criteria (NPF) and particle growth formation (GR). It can be observed in Figure 4.29 that the particle burst with the absence of banana shape criteria of NPF and GR (Kerminen and Kulmala, 2002; Kulmala et al., 2017, 2012; Yadav et al., 2021). A similar result reported by Pirker et al. (2020) nanoparticle exposure due to fireworks during a football match inside stadium, shows the majority of the detected nanoparticles (UFPs) have a diameter between 20 to 200 nm with normalized concentration values reaching 1.4 x 10^5 #/cm^3 at firework celebration time (Zhang et al., 2010; Zhao et al., 2014). Firecracker bursting events are usually associated with an increase in the nanoparticle concentration, which is accompanied by a decrease in the mean particle size as most of the celebrations that are presented in the literature take place in big cities where the air is usually polluted with accumulation mode particles due to traffic, industry, and other sources (Joshi et al., 2019, 2016; Pirker et al., 2020; Yadav et al., 2019a).

4.3.1.3 Temporal variation of particle number size distribution

To better understand the size distribution of submicron aerosol particles during fireworks, the daily mean particle number size distributions (dN/dlogDp) representing the particle number concentrations in each channel for the overall size range are plotted in Figure 4.38. Except for Diwali day, which has a flat curve from 30 nm to 190 nm GMD, others have peaks of 75 nm, 100 nm, and 110 nm GMD for the 25th, 26th, and 28th

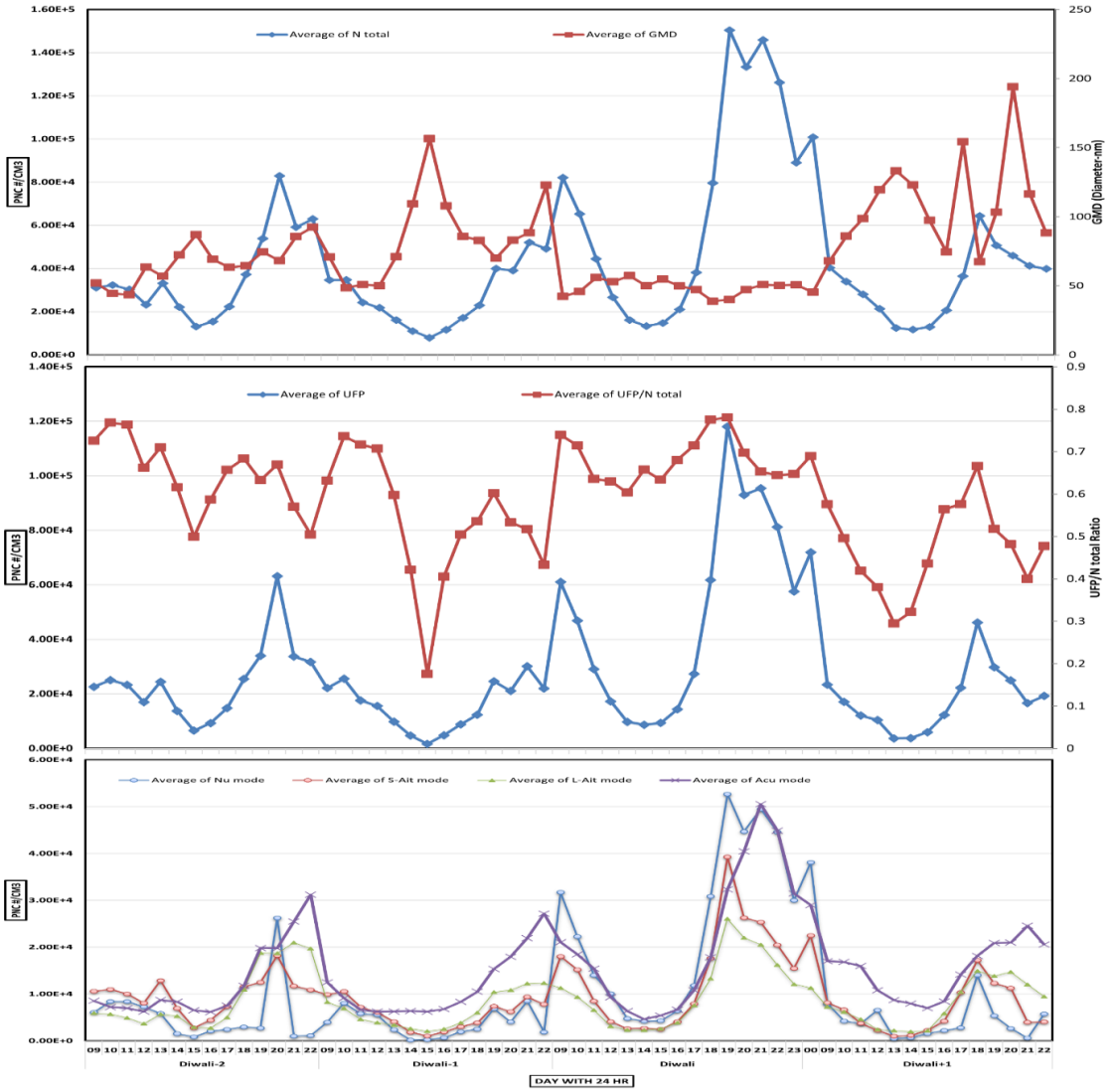

Figure 4.28: Diurnal pattern of different particle modes ((nucleation mode, small Aitken mode, large Aitken mode and accumulation mode) and N total PNC, ratio of UFP/Ntotal PNC, and GMD during 25th to 28th October 2019

of October 2019, respectively. The submicron particle size distribution exhibits a single peak, effectively covering a size range of 60–110 nm GMD. This indicates the dominance of large Aitken and accumulation mode particles. Aerosol concentrations were high for almost all size ranges on an eventful day, followed by pre-and post-Diwali days. Except for a moderate increase in small and large Aitken mode particles, the average particle number concentration could not identify any clear shift in the particle size distribution during extreme fireworks. However, when compared to non-

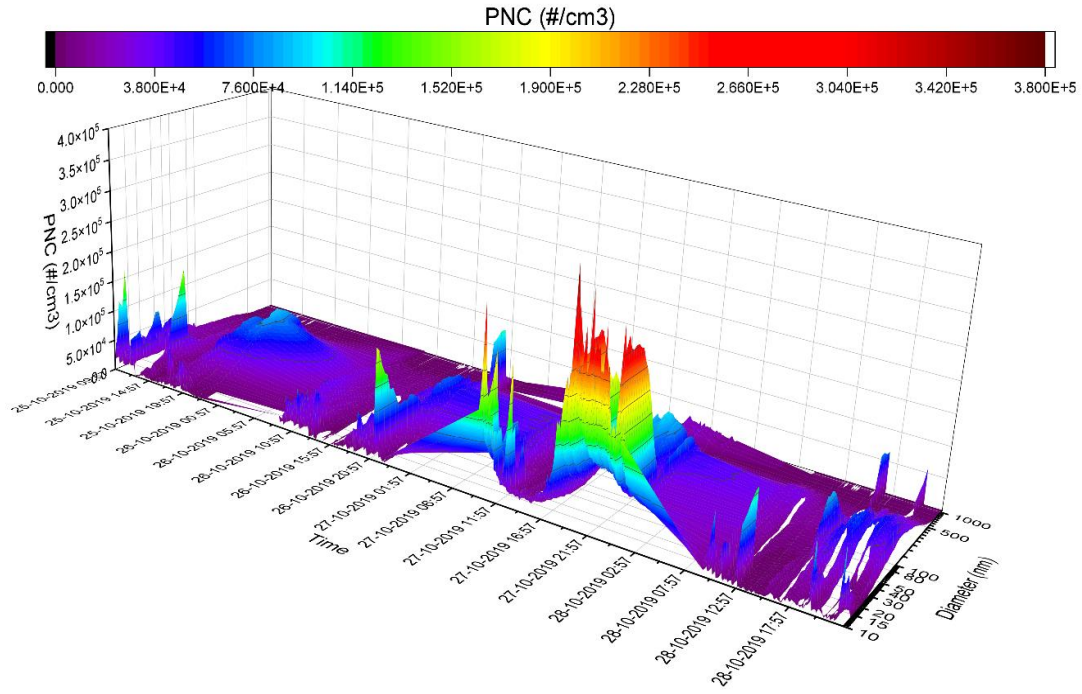

Figure 4.30: 3D surface plot of particle number size distribution during 25th to 28th October 2019

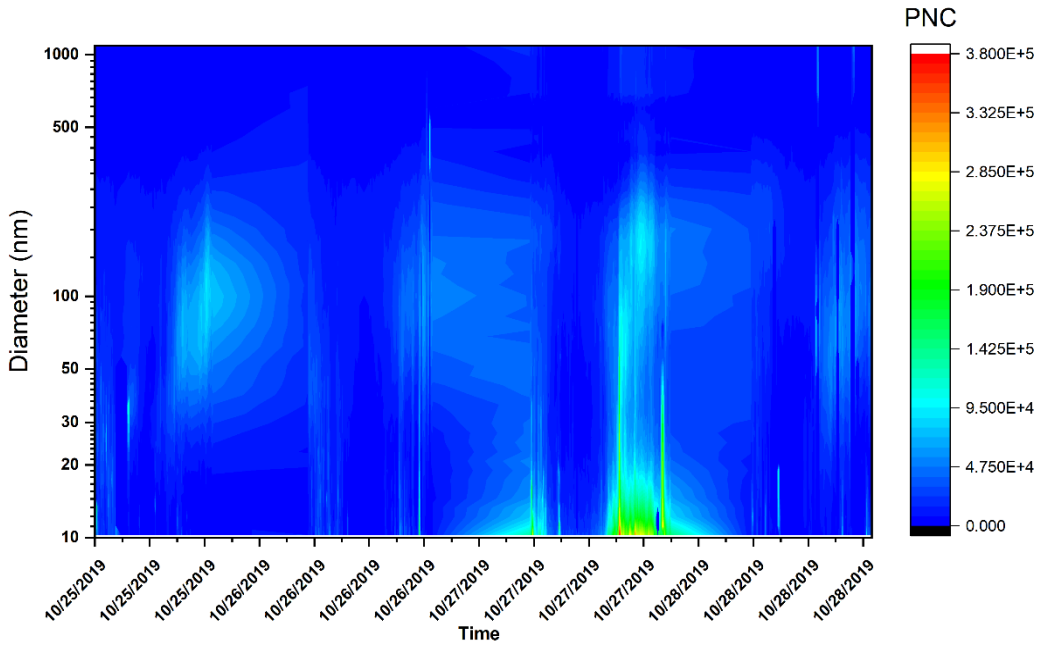

Figure 4.29: Contour plot of Particle number size distribution during 25th to 28th October 2019

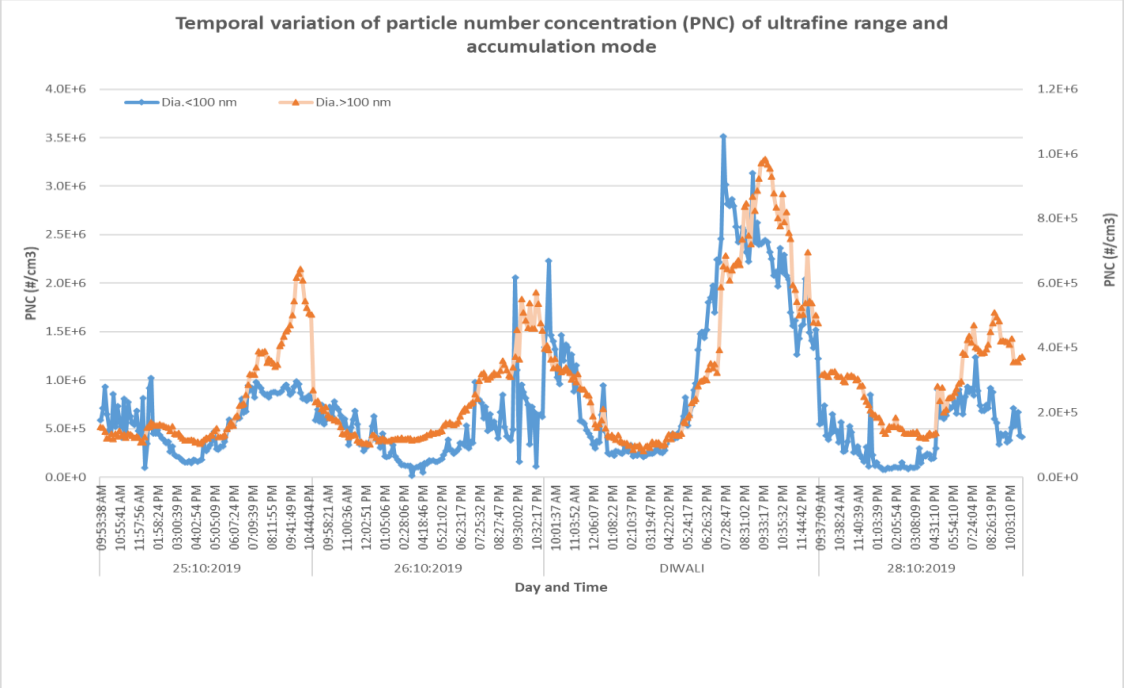

Figure 4.31: Temporal variation of UFP and Accumulation mode's PNC

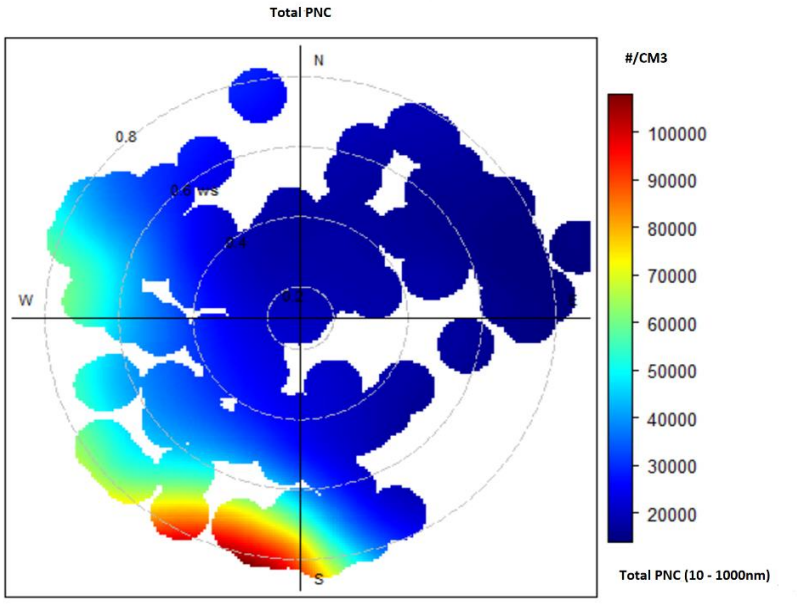

Figure 4.32: Polar Plot for N_{total} PNC (10 nm to 1000 nm)

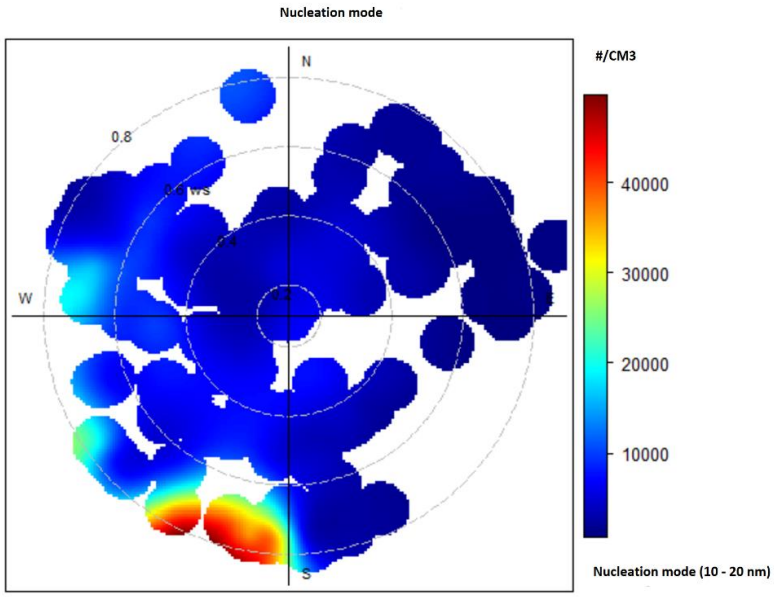

Figure 4.34: Polar Plot for Nucleation mode's PNC (10 nm to 20 nm)

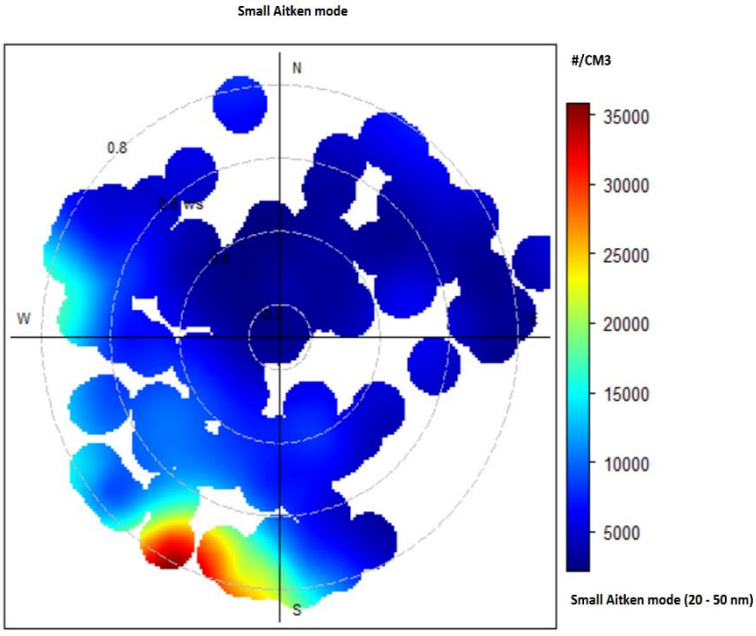

Figure 4.33: Polar Plot for Small Aitken mode's PNC (20 nm to 50 nm)

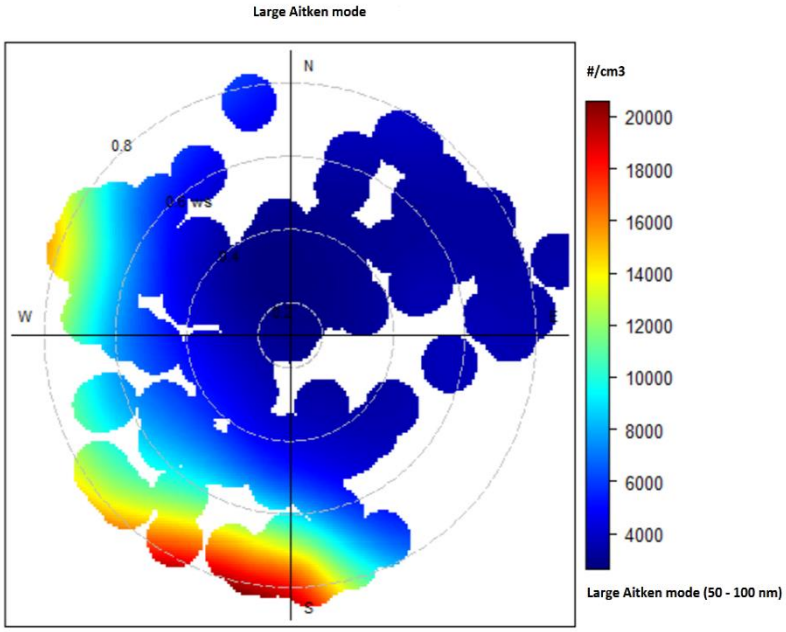

Figure 4.35: Polar Plot for Large Aitken mode's PNC (50 nm to 100 nm)

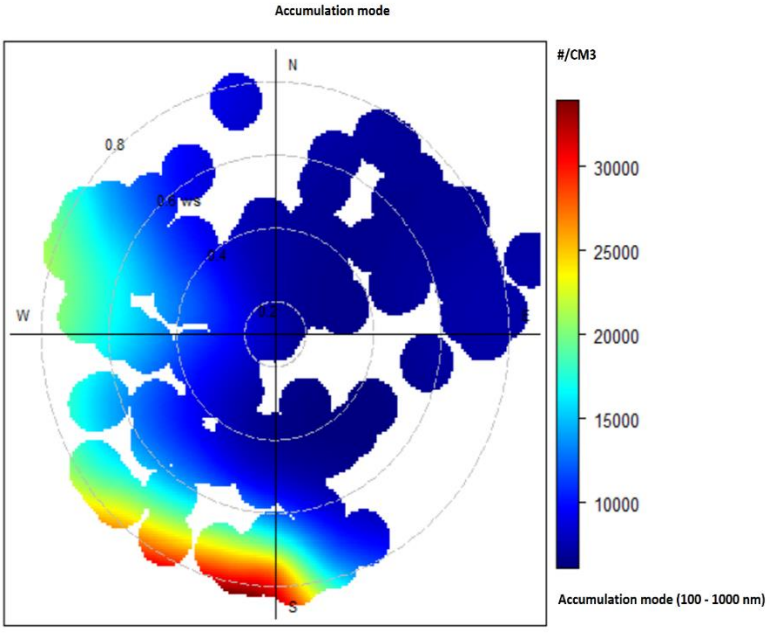

Figure 4.36: Polar Plot for Accumulation mode' PNC (100 nm to 1000 nm)

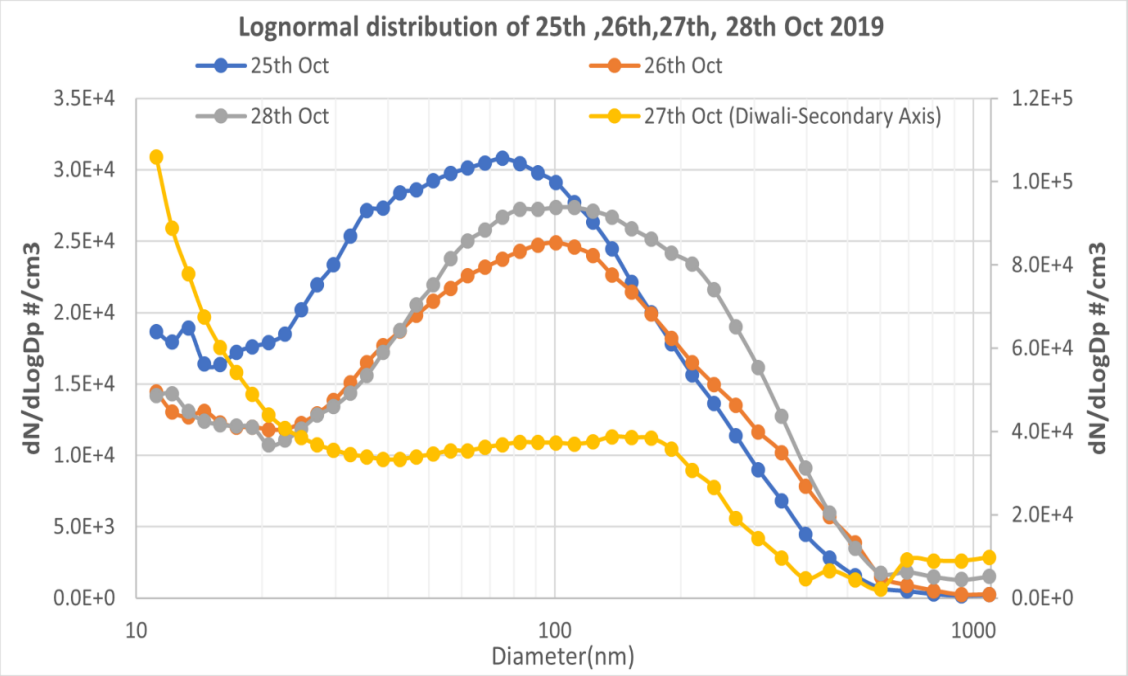

Figure 4.38: Average of aerosol particulates distribution of size during the experiment days

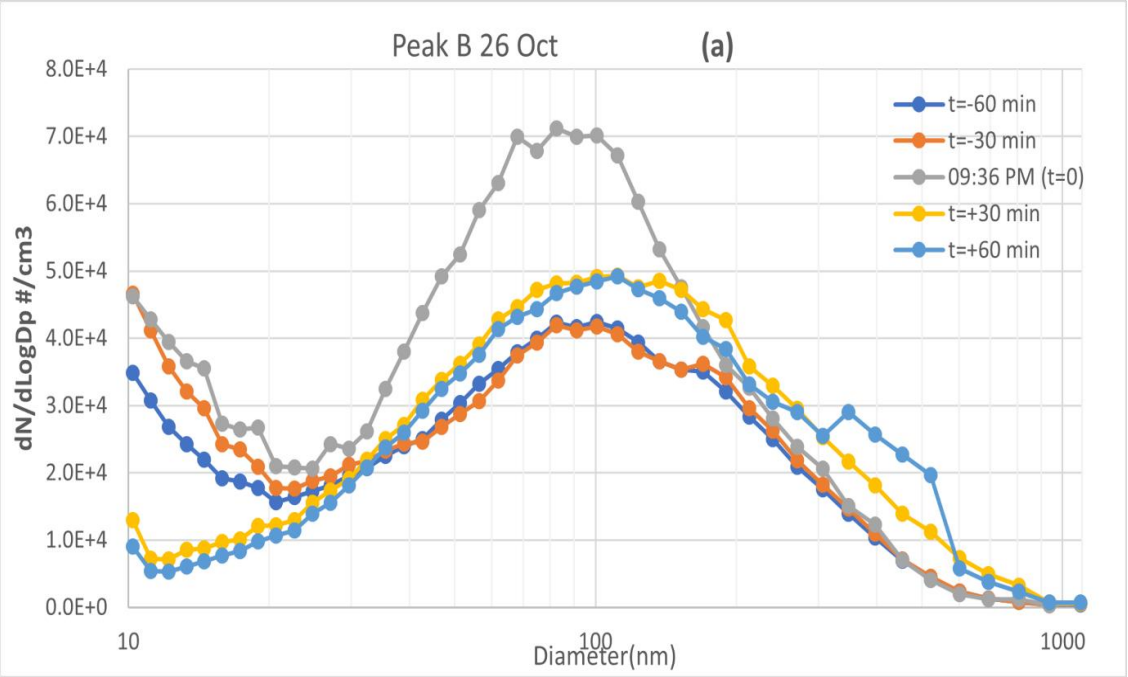

Figure 4.37: Progression of aerosol particulates in a resolved time manner during pre- Diwali days with peak 'B' reference.

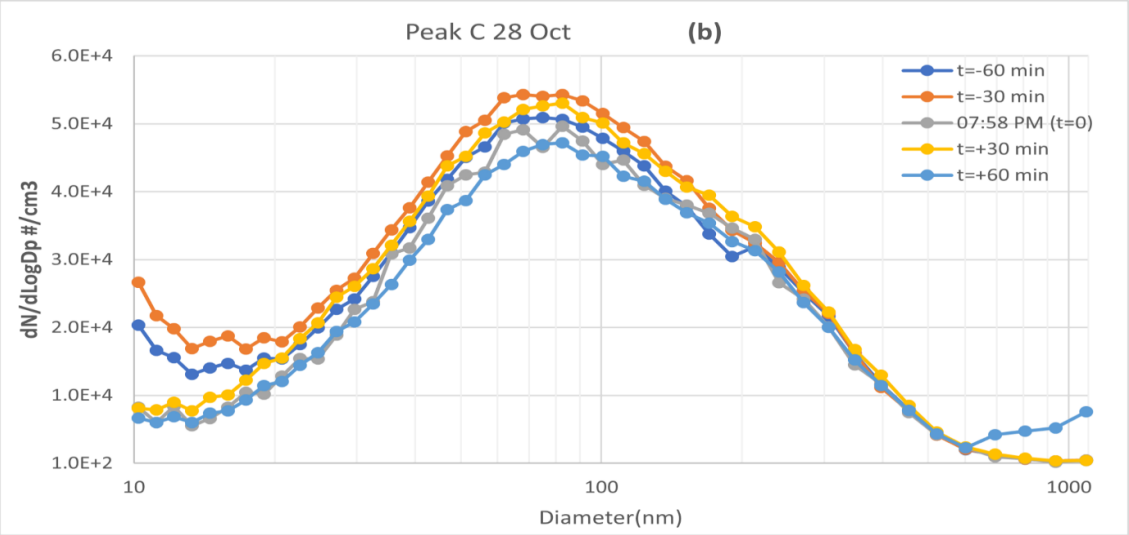

Figure 4.39: Progression of aerosol particulates in a resolved time manner during post- Diwali days with peak 'C' reference

-episodic days, nucleation mode particles accounted for the highest increase on Diwali day (% increase: pre-Diwali-25th October 313 %; post Diwali-28th October, 486 %), implying the formation of new particles during fireworks, which gradually coagulate and become part of background aerosols (Dal Maso et al., 2005; Zhao et al., 2017). As it can be observed, unfavourable dispersion conditions prevailed over India during the Diwali festival. The diurnal variation (Figure 4.28, Figure 4.40, Figure 4.41, Figure 4.42) of particle concentrations during Diwali day showed a typical double hump pattern governed by the local ABL dynamics and source/sink processes of aerosols (Kompalli et al., 2014a, 2014b; Babu et al., 2016). Two distinct peaks of varying magnitudes, the first one was occurred about an hour after sunrise (09:00 -10:00 hrs); the second and more prominent peak occurred during the late evening (18:00-23:00 hrs) with a trough during the daytime. The first peak occurs because thermals emanated after the sunrise breaking the nocturnal inversion and bringing the pollutants from the residual boundary layer to the surface. Following this, the daytime evolving convective boundary layer leads to sufficient ventilation of the pollutants; therefore, lower concentrations prevail at the surface. Subsequently, as the sun sets thermals cease to form, along with massive firecracker bursting and stable atmospheric boundary layer conditions during the

nighttime confine the pollutants near the surface, resulting in a second and stronger peak. Such a pattern of particle number concentrations has been reported in several earlier studies. Apart from this atmospheric dynamical phenomenon, varying source strengths (Sporadic firecracker bursting on Diwali day) during the day also contribute to the observed diurnal pattern (typically higer PNC throughtout the day on Diwali than on other day). Over urban locations, the contribution coming from traffic to diurnal variation of the particle number concentrations is significant (Wu et al., 2008; Brines et al., 2015; Hama et al., 2017).

For further analysis, we took the different distribution of size modes (in the span of 4 hrs each day) to gain more information on the particle size-shifting and other modes during the monitoring period in Diwali, as mentioned in Table 4.6. The 4 hrs span was chosen to differentiate the particle transformation from nucleation to accumulation mode in the morning (9:30 AM-1:30 PM), afternoon (2:00 PM-6:00 PM), and the night (6:00 PM-10:00 PM) during monitoring days (Kumar et al., 2016; Yadav et al., 2019a). The averages of 4 hrs (9:30 AM-1:30 PM, 2:00 PM-6:00 PM, and 6:00 PM-10:00 PM) for all the days are depicted in Figure 4.40, Figure 4.41, Figure 4.42. This time frame was chosen because of the ideal variation in atmospheric characteristics due to specific phenomena such as fireworks and meteorology (Joshi et al. 2016 and Yadav et al. 2019a). As expected, a shorter time frame in number concentration could resolve the periodic evaluation of particles under both firework-dominated and normal conditions. When the evening time (6:00 PM-10:00 PM) is compared for different particle number concentration modes on Diwali day, the PNC for nucleation mode is highest (4.5×10^4 # cm^3) (Table 4.6).

Consequently, except for small Aitken, large Aitken and accumulation mode showed the same flat curve resulting from green crackers bursting at night of Diwali day (Figure 4.42). Interestingly, the morning time frame also offers the same trend as night event time with less PNC. It appears that due to transboundary conditions, photochemically induced particle formation and the shift in the accumulation mode are due to the coagulation of freshly formed particles. Simultaneously, these particles disperse in the atmosphere. Finally, a fraction of particles from these sources survive in the atmosphere due to the combined action of coagulation and dispersion that forms a part of the

background aerosols (Anand and Mayya, 2011). A different trend was followed on pre and post-Diwali days in the different modes Figure 4.41and Figure 4.42, showing an increment of particles in size 45-50 nm range. Figure 4.42 shows a clear maximum increment in the nucleation mode and small-Aitken mode particles and a spike in accumulation mode particles on Diwali day (27th October 2019). Further analysis on Diwali day showed the increase in particle concentration from evening to midnight (6:00 PM-10:00 PM), which is nucleation (312%), and small Aitken (42%) mode particles against the pre-Diwali day (25th October 2019). On the Diwali day, overall averaged percentage contribution of nucleation, Aitken, and accumulation mode are 35%, 37%, and 28%, respectively, which is different from the traditional firecrackers; at Banaras 03.30%, 42.20%, & 54.41%, and Mumbai 14.78%, 45.5% & 41.75%, respectively.

In Table 4.6, a similar relationship is observed between small Aitken, Large Aitken mode particles, and the accumulation range particles. The growth of small and large Aitken particle formation matches the accumulation mode particle growth. From 6:00 PM-10:00 PM, there is a positive shift in the accumulation mode particles with a GMD of 223.7 nm for Diwali day (Table 4.6). To study this relationship more clearly, we have drawn a temporal variation graph in Figure 4.31 between ultrafine and accumulation mode particles.

The evolution of Ultrafine particles (dia <100nm) with the accumulation mode of particles (>100nm) is shown in Figure 4.31. Both particle ranges showed rising patterns during the extensive burning of firecrackers from 6:00 PM-10:00 PM, and both got parallel after some time. Both types of variations can be seen on pre-and post-Diwali days. The formation of large amounts of ultrafine particles leads to forming accumulation mode particles. They are dispersed into the atmosphere by getting sunk and coagulated in the background aerosol concentration, which is already present (Anand and Mayya, 2011). UFP/N_{total} ratio is higher than 0.7, while traditional fireworks have < 0.6, such as Varanasi – 0.45 and Mumbai – 0.58.

Also, it was done so that no hike in particle distribution was missed. In Figure 4.43, there is peak 'A' (3.41×10^5 # cm^{-3} at 7:21 PM) with GMD >20nm and peak 'D' (9.07×10^4/ cm^3 at 10:02 PM) with GMD ~111nm on the night of 27th and 25th October 2019 respectively to compare the firework emission and non-firework emission scenarios.

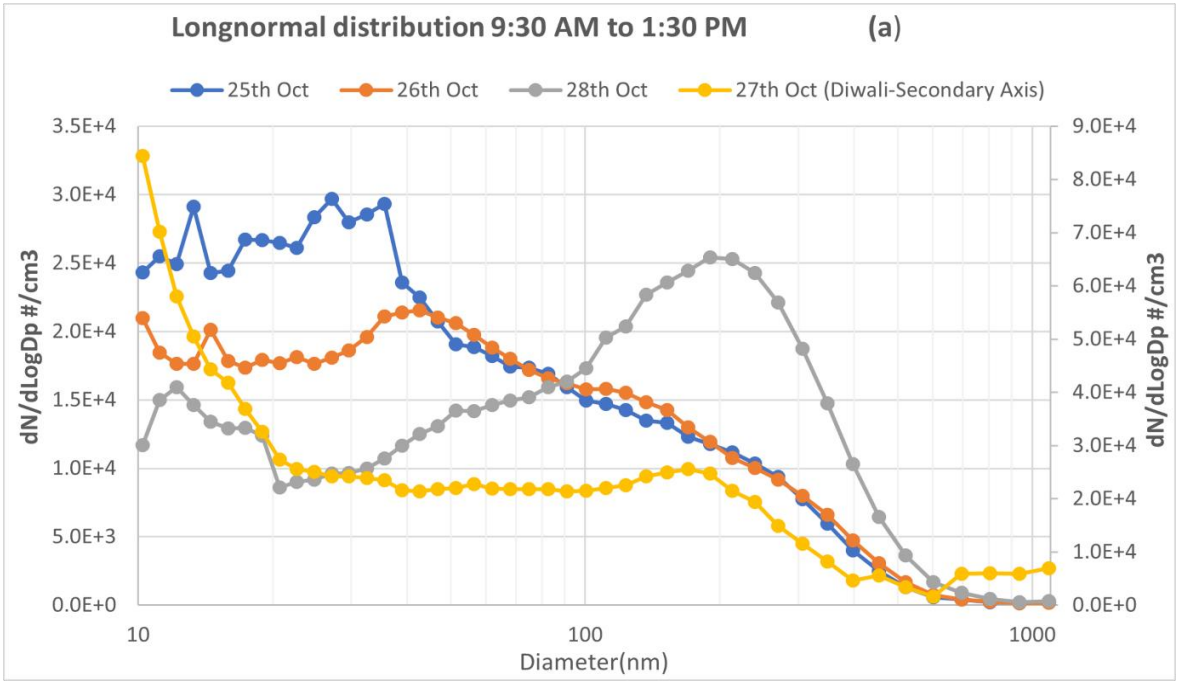

Figure 4.40: Average particle number size distribution during 9:30 AM to 1:30 PM

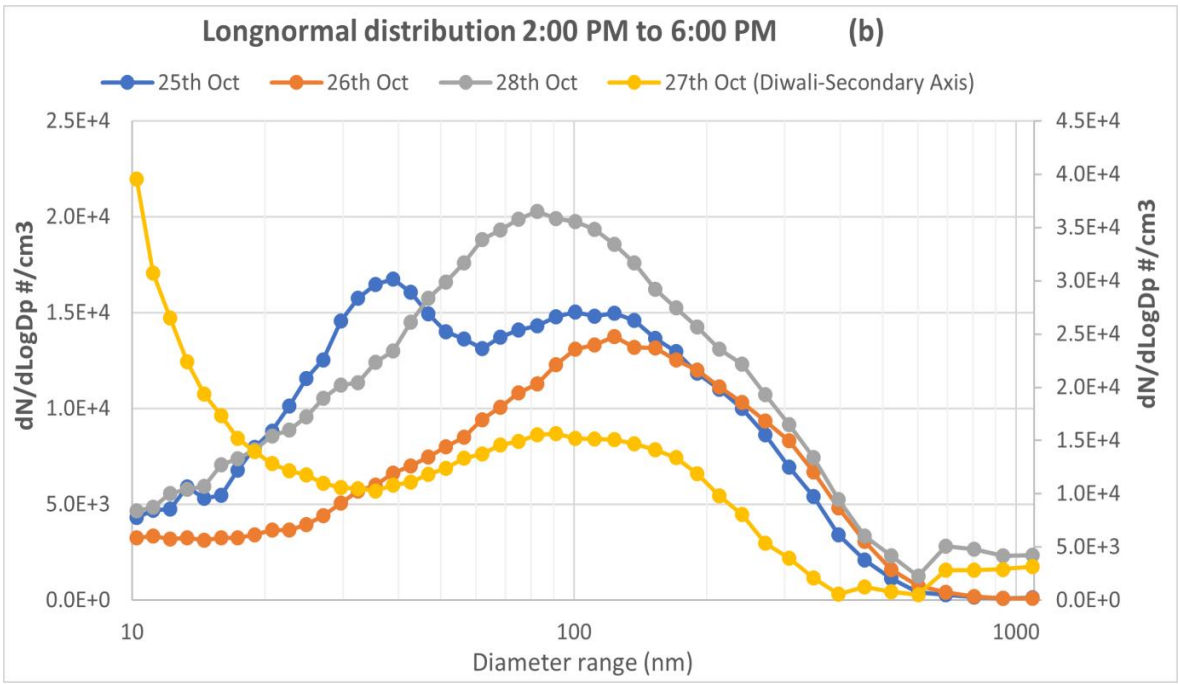

Figure 4.41: Average particle number size distribution during 2:00 PM to 6:00 PM

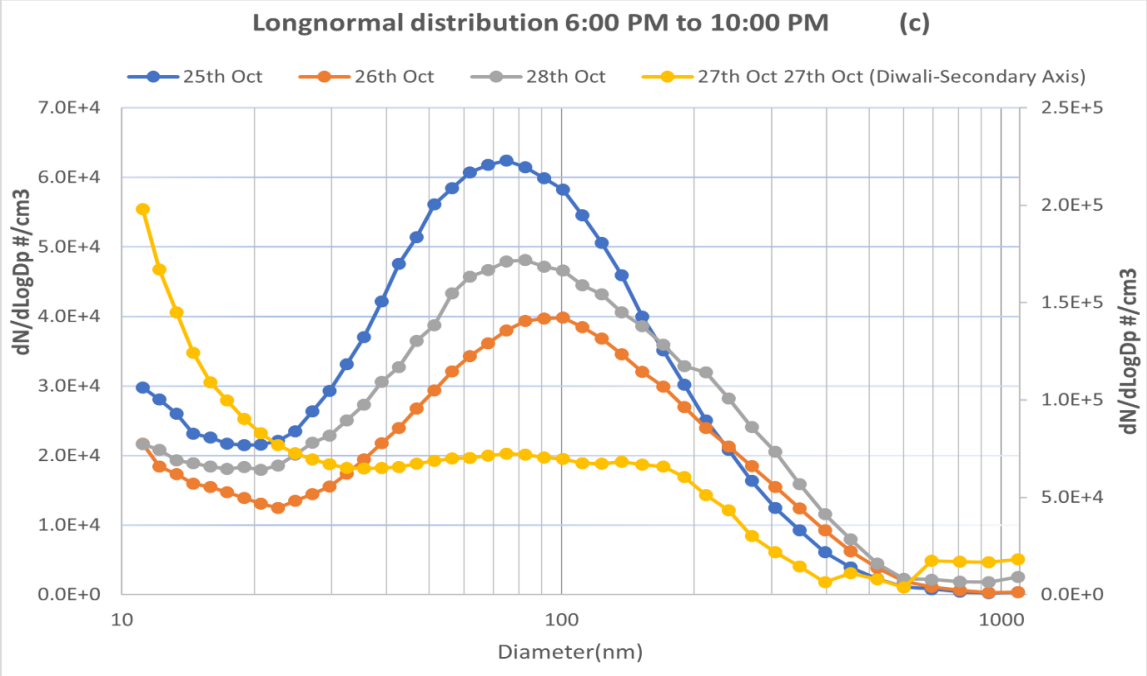

Figure 4.42: Average particle number size distribution during 6:00 PM to 10:00 PM

Peak's 'A' and 'D' are not similar in particle number concentration, but they are highest on their respective days. In Figure 4.43, a significant rise in the ultrafine particles' concentration (< 45nm) included nucleation, small and large- Aitken range particles from 6:00 PM-10:00 PM. Continuous formation of new particles in the UFP range indicated large firecrackers burning at night. The transition of particle formations from t = -360 min (background concentration) to reaching peak 'A' and reaching the background concentrations within 90 min of the peak attained has been shown. If we see the peak 'D' in Figure 4.44 (25th October 2019), it is observed that particle concentration evolution follows a different path than in Figure 4.43. Similar trends have also been shown in (Joshi et al., 2016). There was a clear transition from nucleation towards small and large Aitken modes. It contained all particle size distribution ranges from nucleation to accumulation range particles. The presence of spikes in the particles of accumulation range ~110 nm is noticed in Figure 4.44. Similarly, in other Figure 4.37, and Figure 4.39, there was a rise in the transition of particle number

concentration on pre-Diwali (26th October 2019) and post-Diwali day (28th October 2019). However, it was not the same as Diwali day, having low strength in particles' evolution. There was an increment of ultrafine particles in peak D of Figure 4.44. Still, after 60 mins, all the particle size range added up and showed a proper formation of accumulation particles. Peak C in Figure 4.39, it showed a similar rising particle number concentration pattern but without any other significant modes. Thus, from the above study, we can say that the bursting of firecrackers during festivals such as the Chinese New Year and Diwali can lead to the release of a significant amount of ultrafine and fine particles concentration, and accumulation range particle concentration also. These events can increase the background aerosol concentration, leading to short-term air quality deterioration, ultimately harming human health by deposition in the respiratory system's alveolar region (Manigrasso and Avino, 2012). It can be inferred from the present study that extreme burning of green firecrackers can increase the finer aerosol concentration on post-Diwali days. However, if emissions from various other sources in megacities like Delhi are to be considered, the complexity of different atmospheric processes requires a more prolonged study duration.

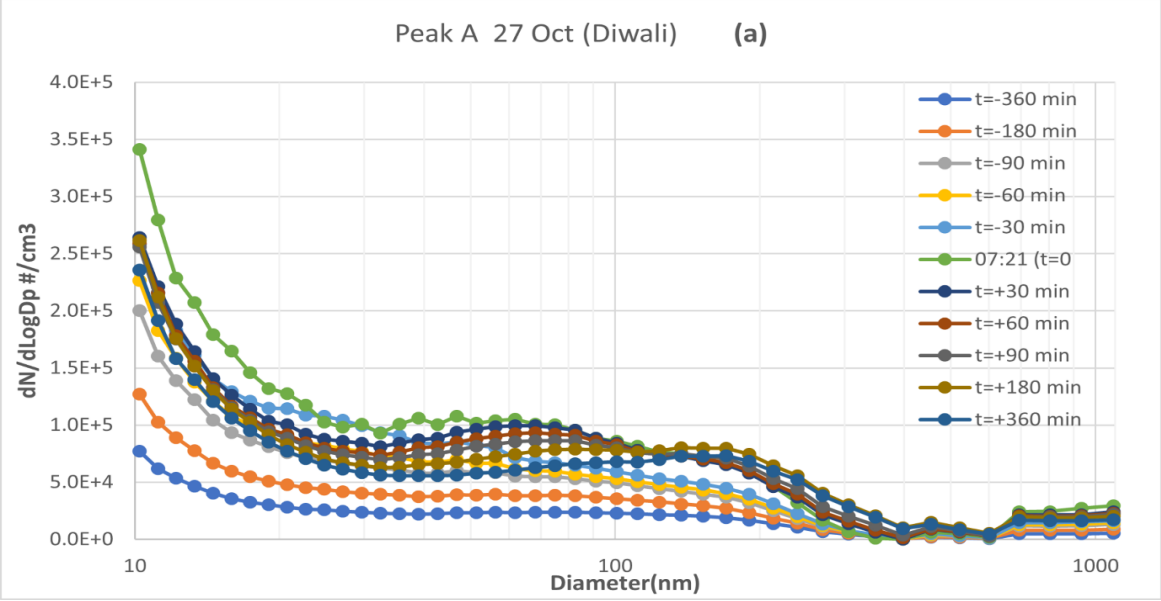

Figure 4.43: Progression of aerosol particulates in a resolved time manner during Diwali with peak 'A' reference

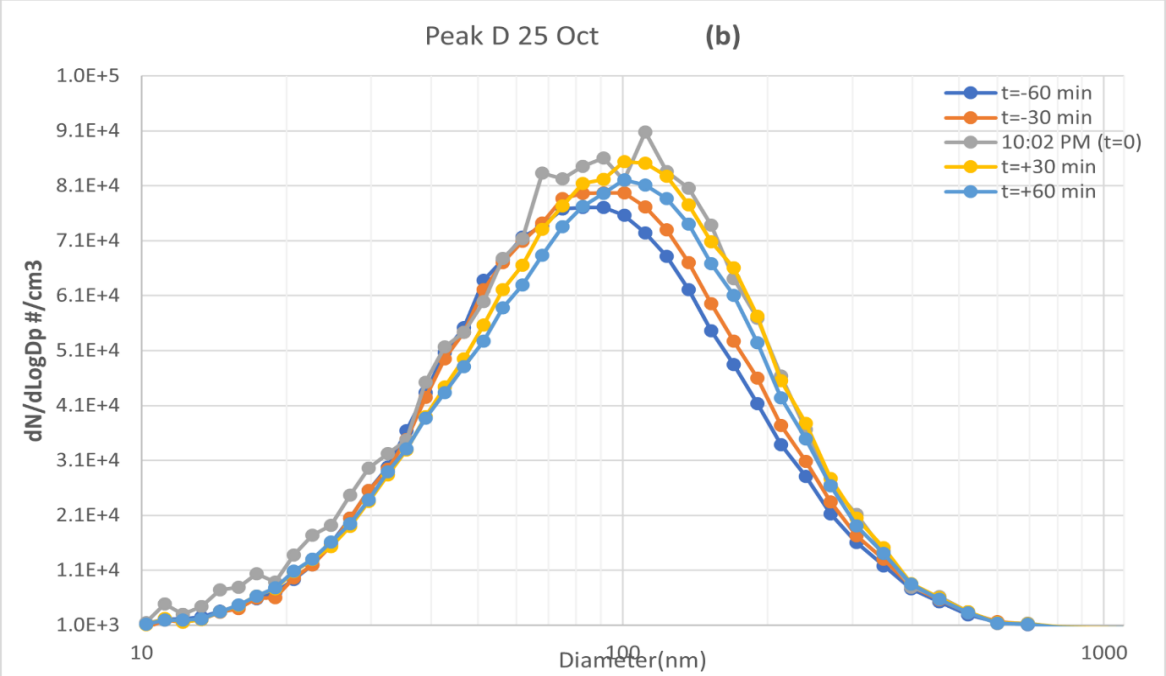

Figure 4.44: Progression of aerosol particulates in a resolved time manner during pre-Diwali days with peak 'D' reference

4.3.1.4 Summary

Following are the inferences drawn from the present study conducted on the Delhi Technological University campus to assess the impact of 'Green crackers' used for fireworks during the Diwali festival in 2019 to understand the formation of ultrafine particles (UFP's) and Particle Number Size Distribution (PNSD) in a better way:

Particle number concentration (PNC) reached a high of 1.29 x 10^5 # cm^{-3} with a geometric mean diameter (GMD) of ~44 nm during the Diwali celebration, with two peaks of 1.7 x 10^5 # cm^{-3} with a GMD of ~39 nm and 1.2 x 10^5 # cm^{-3} with a GMD of ~44 nm, respectively. During this event, the wind speed remained constant until late at night with a calm condition. The Southwest wind direction had the highest PNC of particles where the residential area is located.

Both peaks showed higher PNC than other pre-and post-Diwali peaks with 145.9 % and 97.9 % increase in PNC on Diwali day compared to pre-Diwali (26th October 2019) and post-Diwali (28th October 2019), respectively. This validates the effect of judicial regulation on fireworks celebrations to mitigate the impact of air pollution.

Interestingly, peak's GMD on Diwali evening time in case of Varanasi (GMD; 89 nm) and Mumbai (GMD; ~51nm) associated with traditional crackers are more than the Delhi (GMD; 39 nm) with green crackers, but PNC in case of Delhi (~1.7×10^5 # cm^{-3}) is more than the Mumbai (~1.2×10^5 # cm^{-3}) and Varanasi (4.5×10^4 # cm^{-3}). This indicates that green crackers emit more particles in a lower size diameter when compared to traditional crackers.

On Diwali day, there was an increase in PNSD, especially in nucleation 468% and 485% and small Aitken mode 147% and 110%, against the pre-Diwali day (26th October 2019) and post-Diwali (28th October 2019), respectively. Diwali day showed an increase in particle concentration from evening to midnight (6:00 PM-10:00 PM), which is nucleation (312%), and small Aitken (42%) mode particles against the pre-Diwali day (25th October 2019).

Except for Diwali day, which has a flat curve from 30 nm to 190 nm GMD, others have peaks of 75 nm, 100 nm, and 110 nm GMD for the 25th, 26th, and 28th of October 2019, respectively. The submicron particle size distribution exhibits a single peak effectively covering a size range of 60–110 nm GMD and indicates the dominance of large Aitken and accumulation mode particles. On Diwali day, however, the overall averaged percentage contribution of nucleation, Aitken, and accumulation mode are 35%, 37%, and 28%, respectively, which is different from the traditional firecrackers as in Banaras 03.30%, 42.20%, & 54.41%, and Mumbai 14.78%, 45.5% & 41.75%, respectively.

In the present case of green crackers, UFP/N_{total} ratio is higher than 0.7, while traditional fireworks have < 0.6, such as Varanasi (0.45) and Mumbai (0.58). Thus, Green cracker's emissions have a high ratio of UFP than traditional fireworks.

With Delhi's densely populated dynamics and other anthropogenic activities causing pollution, the locally produced Diwali emissions are felt to a larger extent as it affects the

respiratory system. This study may help assess the adverse health effects due to higher particle number concentration (PNC) caused by burning green firecrackers in megacities like Delhi and thus evaluate the relative impacts of traditional firecrackers and green firecrackers.

Until the particle number concentration (PNC) of ultrafine particles (UFPs) is reduced significantly, green crackers' health benefits remain questionable because the bursting of green crackers may result in exposure to and inhalation of the higher number of UFPs in comparison to traditional crackers.

4.3.2 Odd -Even events

In addition to Delhi, other cities worldwide have also implemented a driving prohibition scheme similar to Odd-Even in various forms to reduce urban air pollution. For the first time, the Odd-Even formula was implemented in Beijing in 2008, just before the summer Olympics. Initially, the Government called it temporary, but later, it became a permanent rule for the city when it was found effective. Some other places in the world like Paris, Bogota, and Mexico are plying road-rationing rules. China (Beijing) implemented air pollution reduction measurement when China's annual average concentration was 20% higher than the China National Ambient Air Quality Standards (CNAAQS) and 6% greater than WHO Air Quality Guidelines (WHO, 2005).

In contrast, the trial hit method policy for air pollution mitigation was adopted in India when pollution levels crossed several times (more than 50 times) with National Ambient Air Quality Standards (NAAQS) (Cai & Xie, 2010). Although this scheme cannot be considered a complete solution to combat air pollution, it can be implemented from time to time to reduce the pollution levels and associated impacts during excess peak time if it is shooting far beyond the normal levels. It may cause a shift in people's attitudes and raise awareness about environmental issues (Airy and Chandiramani, 2016).

The first phase of the Odd-Even scheme in India was implemented in 2016. The first phase of the Odd-Even driving scheme trial was enforced from 1 to 15 January 2016 in winter, and the second edition from 15 to 30 April 2016 in summer. Kumar et al. (2017) reported $PM_{2.5}$ was relatively low during the Odd-Even hours (11:00-20:00 hrs.) and high during non-Odd-Even hours (20:00-08:00 hrs.) when compared with the corresponding hours of the previous year of 2015. Mishra et al. (2019) found an average reduction in the ratios of PM_1 and $PM_{2.5}$ at selected monitoring locations, namely Pitampura-Madhuban Chowk (0.01), Panchkuian Road (0.1), and Najafgarh Road (0.11) during scheme days. Likewise, Sharma et al. (2016) reported a percentage reduction in the number of cars, i.e., 21% and 17%, in the first and second phases of the Odd-Even scheme, whereas the percentage increase in speeds, i.e., 18% and 13%, was observed during the first and second phase of scheme respectively. During

this study, they found that the average concentrations of PM_{10} were 1.8 - 4 times higher than permissible limits at five locations in the entire Delhi, whereas $PM_{2.5}$ levels were recorded 1.4 - 4.3 times greater than the prescribed standard during second phase of Odd-Even scheme.

The Delhi Government launched the third phase of the Odd-Even scheme from 4 to 15 November 2019 (12 days) to combat the national capital's hazardous air quality. During the Odd-Even days, the total number of buses on the road was 6681, including 3781- Delhi Transport Corporation (DTC), 2000 Cluster, and 900 Private buses. The number of private buses in the first (1-15 January 2016) and second (15-30 April 2016) phases of the Odd-Even scheme were 1400 and 500, respectively. In 2019 after implementing the third Odd-Even scheme in the capital, the Delhi passengers increased by 0.7 million. The female passenger's percentage increased by 40%. In DTC and cluster buses, the female passengers were found to be more because Delhi Government implemented free bus rides for female passengers on the occasion of Bhai-Duj (Hindu festival) on 29 October 2019, before the Odd-Even scheme. The ridership in Delhi Metro increased by 65-69%, and the metro trips also increased by 11% during the third Odd-Even scheme. The third phase of the Odd-Even scheme was scheduled from 8:00 am to 8:00 pm and to enforce the scheme very strictly, the Delhi Government has also kept a penalty of Rs. 4000/- in case of any violation of the scheme. However, this fine was Rs. 2000/- during the first and second phases of the Odd-Even scheme. During the implementation of the first and second phases of the scheme, exemptions were given to women drivers, commercial vehicles, two-wheelers, e-vehicles, and private CNG vehicles. However, in the third phase of this scheme implemented in 2019, private CNG vehicles were allowed to ply on the road due to the possibility of misuse of the exemption stickers given to vehicle owners.

The study has covered Odd-Even monitoring with PMs and its PNSD with particle number concentration in this phase. No literature has been found that has performed to date on the criteria listed above about the Odd-Even scheme expect some normal conditions (Apte et al., 2011; Saraswat et al., 2013b). This study aims to evaluate and analyze the impact of the third time implemented Odd-Even scheme on urban air quality in New Delhi. Currently, there are

no air quality standards in any part of the world to limit public exposure to atmospheric particles on a number basis since current regulations are based on mass concentrations of PM_{10} and $PM_{2.5}$ (Kumar et al., 2011). The objective of this study was; 1) To assess the PNC reduction for PM_1 due to the implementation of the Odd-Even scheme; the Odd-Even scheme's influence combined with other affecting factors on the PNC of PNSD's QuasiUFP, Sub-fine, Fine, and Coarse mode size range with a vehicle number change.

This Odd-Even study includes the monitoring at three different locations (Pitampura, Najafgarh, and Panchkuian) in Delhi, India, to find out the impact of the third Odd-Even scheme, as against normal day (normal day would be any day pre or post-Odd-Even scheme day when there was no restriction). Hundred percent monitoring for three days (odd day, even day and normal day) was covered at the Pitampura location. Still, the monitoring was interrupted at Najafgarh and Panchkuian locations due to drizzling in the evening time. Due to this, only 60.8% and 56.5% monitoring was covered at Najafgarh and Panchkuian locations, respectively. An overall 72.4% monitoring was covered during the Odd-Even scheme at all three locations across Delhi. A similar monitoring schedule and location selection were adopted by Mishra et al. (2019). But this study is based on the particle number concentration (PNC) of the different particle size distributions (PNSD) except for their mass concentration. In this study, despite the PNC of PM_1, it includes the study of different particle size modes such as; QuasiUFP (qUFP)- 250nm > qUFP < 500nm; Subfine- 500nm > Subfine < 1000nm of diameter. Additionally, it also includes higher size range than PM_1; fine particles- 1,000nm> Fine particles <25000nm; and Coarse particles- 25,000> Coarse <10,000nm of diameter. For getting more insight into lower size range particles, qUFP have further divided into qUFP-lower size range 250 nm > qUFP(L)<280nm, qUFP-higher size range 280 nm > qUFP(H) < 500nm.

A monitoring schedule at all three locations was prepared to cover the Odd-Even scheme's entire timing, i.e., from 8:00 am to 8:00 pm (12 hrs), as a guideline provided by the Government of Delhi. The monitoring includes one day before and two days during the Odd-Even of Phase III scheme and spanned between 1 -15 November 2019 (Table 4.7).

Table 4.7: Schedule of PM monitoring at selected traffic corridors

Schedule of PMs and their PNSD with PNC monitoring in Delhi city.			
Monitoring Station/Traffic Corridor		PM monitoring schedule – Pre-Odd-Even scheme (Before 4 November 2019)	PM monitoring schedule – During Odd-Even (4 -9 November 2019)
1.	Pitampura–Madhuban Chowk	1 November 2019	6 - 9 November 2019
2.	Panchkuian Road	2 November 2019	4 -5 November 2019
3.	Najafgarh Road	2 November 2019	4 - 5 November 2019

The dataset normality was tested using a combination of the Exploratory Data Analysis (EDA) plot and the Shapiro-Wilk (S-W) test. The Kruskal-Wallis (KW) test was performed on air quality data, a nonparametric version of the ANOVA test. The Kruskal Wallis test (rank-based nonparametric test) is used to determine if there are statistical differences between days (odd day, even day, and normal day) and independent variable pollutant (QuasiUFP, Subfine, Fine, Coarse, $PM_{0.5}$, PM_{1}, $PM_{2.5}$, PM_{10}) of representative location in Delhi. Kruskal Wallis test denotes with H test (eq. 1 and result table can be found in Annexure-II). Percentage change of Odd-Even has followed the eq. 3.7.

4.3.2.1 Temporal variation of particle number concentration

With a significance value of 0.05, the Kruskal Wallis test was performed on the parameters under consideration for the three locations. Parameters with a < 0.05 value rejecting the KW Test hypothesis have a statistically significant difference, but > 0.05 value has the opposite effect. In Annexure- II to IV, normal days with odd and even days have significant difference

for all parameters at all locations; however, the mean difference is not statistically significant between odd and even days for most parameters at all locations. Reduction in the PNC and vehicular count at all locations supports the Odd-Even scheme third phase (Figure 4.45, Figure 4.46 and Annexure- V to VII)

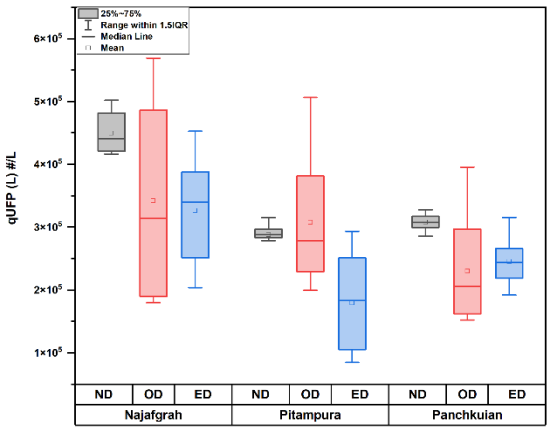

2(a)

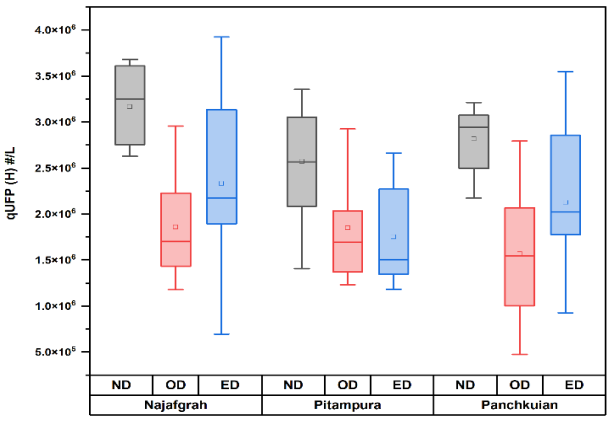

2(b)

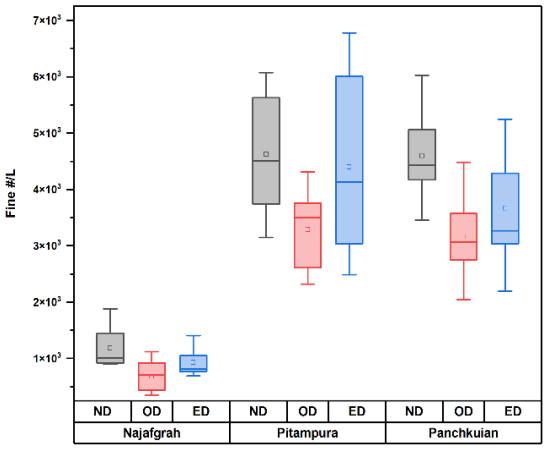

2(c)

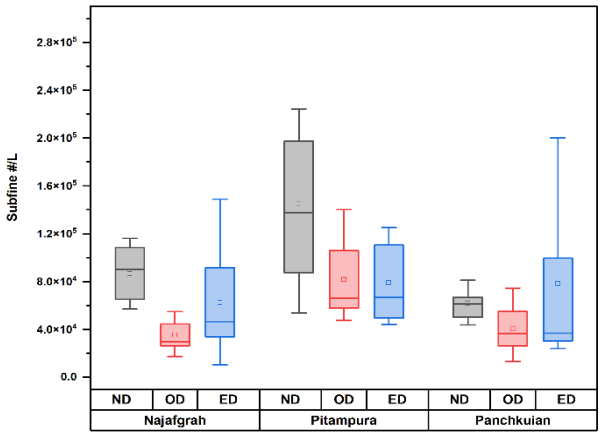

2(d)

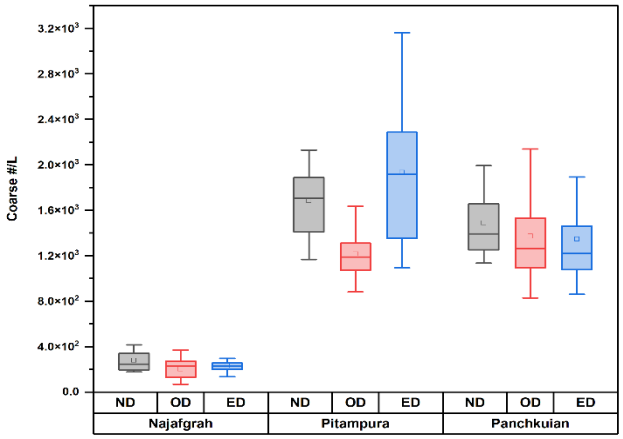

2(e)

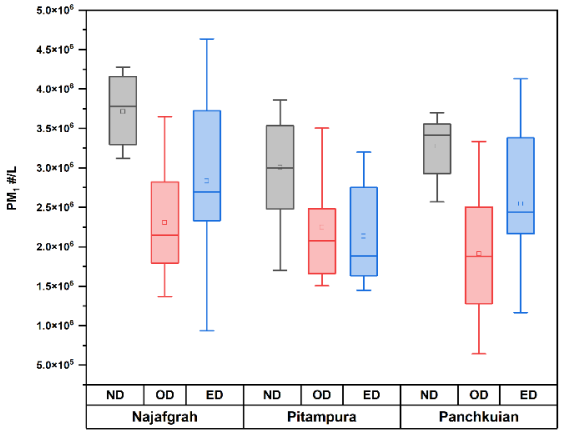

2(f)

Figure 4.45: Box plot showing variation in different PNC size range and PM_1 like 2(a) qUFP (L), 2(b) qUFP (H), 2(c) Fine, 2(d) Subfine, 2(e) Coarse, and 2(f) PM_1 during odd, even and normal day at Najafgarh, Pitampura, and Panchkuian respectively

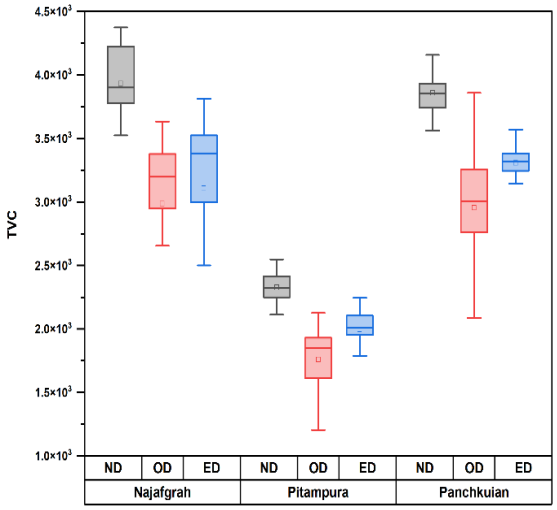

3(a)

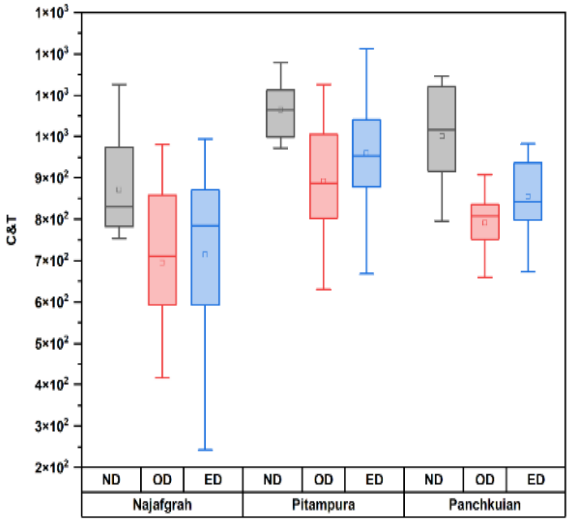

3(b)

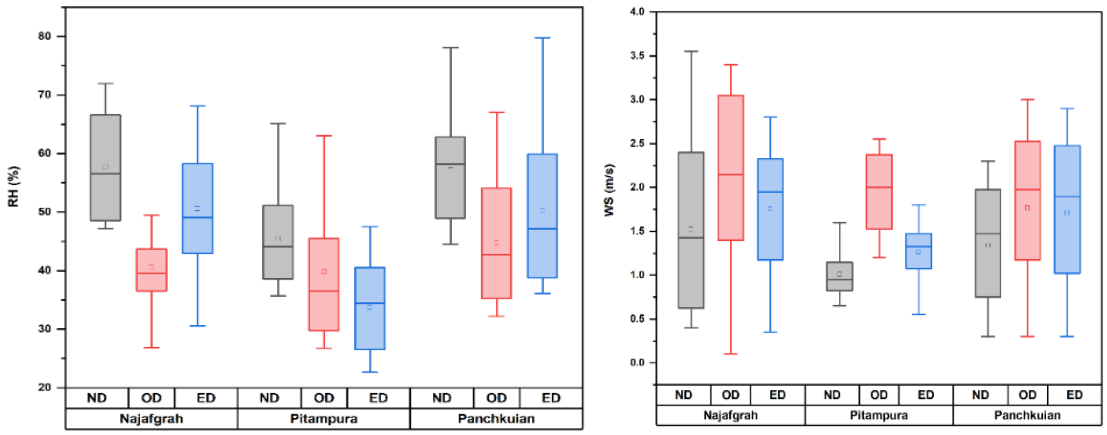

4(a) 4 (b)

Figure 4.46: Box plot showing variation in meterological parameters like 4(a) RH(%), and 4(b) Wind Speed (m/s) during Odd, Even and Normal day at Najafgarh, Pitampura, and Panchkuian

In previous years, during the first and second Odd-Even schemes, there has been found a minimal study on lower-sized particles such as PM_1. During this third phase of the study, the Odd-Even scheme's impact on particle number concentration of lower-sized (PM_1 and <PM_1) particles has been analyzed at all the selected locations. The impact analysis of the scheme was seen on different size bin particles i.e., QuasiUFP (0.25 µm>Dp<0.50 µm), subfine (0.50 µm>Dp<1.0 µm), fine (1.00 µm>Dp< 2.5 µm), Coarse (2.5 µm> Dp< 10.00 µm). Total Vehicle Count (TVC) and Car/Taxis (C&T) counting at the roadside monitoring location have also been done to establish the relationship between traffic volume and particle number concentration.

4.3.2.2 PM1 during Odd-Even scheme -II

According to the PM_1 series (Figure 4.47), the morning peak followed the decreasing trend from 1:00 pm to 2:00 pm than the afternoon period. However, the morning peak was observed to be higher than the afternoon peak during the Odd-Even scheme. PNC started decreasing from morning hour to afternoon during normal days. Again, PNC increases till

evening traffic peak hours (Figure 4.47) except Pitampura location, which showed a gradual decrement in the PNC after 2:30 pm. This decreasing trend of PNC at Pitampura may be due to drizzling effect, which started slowly from 2:30 pm to late evening. Total vehicle count includes the car/taxi, auto, two-wheeler, three-wheeler (Goods), bus, LCV (LCV), and heavy commercial vehicle (HCV). For a normal day, the total vehicle count (TVC) ranges from 3500 to 4500 vehicles per 30 minutes for Najafgarh and Panchkuian Road, but the Pitampura location ranges from 2000 -2500 vehicles per 30 minutes. In this sequence, the overall reduction on Odd-Even day for TVC at Panchkuian Road, Pitampura, and Najafgarh was 18.4%, 18.5% and 25.8%, respectively (Table 4.8).

Table 4.8: Percentage reduction during Odd-Even day

Location	**Day**	**Quasi UFP**	**Sub fine**	**Fine**	**Coarse**	**PM_1**	**TVC**	**Car & Taxi**
Najafgarh	Odd day reduction (%)	32.5	53.2	29.8	9.2	32.7	26.7	27.4
	Even day reduction (%)	15.9	32.2	18.3	10.1	16.5	24.9	24.8
	Overall reduction during study period (%)	24.2	42.7	24.1	9.7	24.6	25.8	26.1
Pitampura	Odd day reduction (%)	23.1	40.4	27.2	27.4	24	24.4	16.3
	Even day reduction (%)	27.6	43.8	5.7	-13.3	28.4	12.7	8.5
	Overall reduction during study period (%)	25.4	42.1	16.5	7.1	26.2	18.5	12.4
Panchkuian	Odd Day reduction (%)	32.36	28.8	25.9	9.2	33.5	21.9	19.1
	Even day reduction (%)	15.59	23.2	18.6	11.5	16.2	14.8	13.2

	Overall reduction during study period (%)	24	26	22.3	10.4	24.8	18.4	16.1

Najafgarh corridor was observed with maximum PM_1 concentration peak during the even day, for the same minimum peak was observed on the odd-day at Panchkuian monitoring station. Compared to the even days, PNC reduction for all three locations reached the same level. Still, TVC reduction doesn't follow the same trend (Figure 4.47), which supports the hypothesis that other factors like wind speed (WS), and relative humidity (RH) also play an essential role in PNC reduction at the roadside. PNC of vehicular emission depends on various factors such as wind speed and direction, temperature, RH, and pre-existing particle concentration (Kulshrestha et al., 2009; Pérez et al., 2010).

As shown in Annexure - V to VII before the Odd-Even scheme days, maximum and minimum particle numbers of PM_1 were observed $4.2x10^6$ #/L at Najafgarh road and $1.6x10^6$ #/L at Pitampura location. In contrast, during the Odd-Even period, maximum and minimum particle number concentrations of PM_1 were recorded $4.63x10^6$ and $9.35x10^5$ #/L at Najafgarh road (Even day), but in the case of the Odd day, the maximum was at Pitampura ($4.18x10^6$ #/L), whereas the minimum was at Panchkuian ($6.5x10^6$ #/L). The maximum total reduction of PM_1 number concentration reported at the Pitampura corridor of 26.2%, and a minimum reduction of PM_1 number concentration reported at Najafgarh of 24.6% during scheme days. Whereas during the second driving scheme, (Mishra et al., 2019) found a maximum reduction of PM_1 as 7.78% and a minimum of 2.69%, same at Pitampura location, respectively (in concern of particle mass concentration). Five different size bins have been classified to get more insightful observations for the particle number concentration at all three locations, which provide the overall effect of wind speed and relative humidity during the Odd-Even scheme.

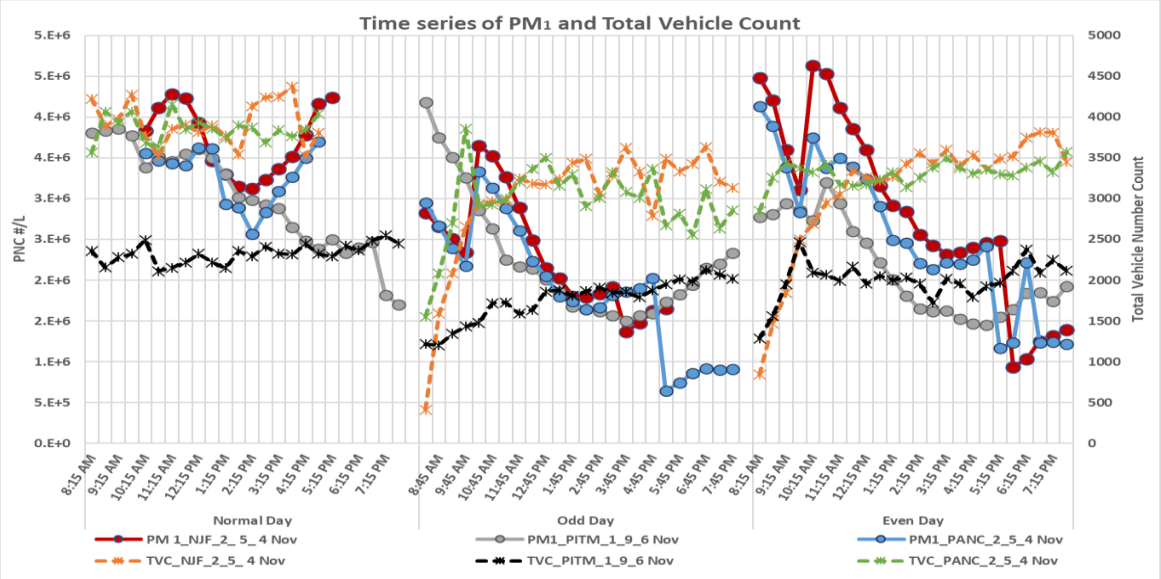

Figure 4.47: Time series of PM_1 and Total Vehicles Count

Note: - NJF- Najafgarh road, PITM- Pitampura road, PANC- Panchkuian Road, TVC- Total Vehicles Count *after location number are the date of monitoring in November

4.3.2.3 PNC at Najafgarh Road (NJF) during Odd-Even scheme-II

PNC, according to the KW, H test, follows a similar pattern in that there is a considerable mean difference in the concentrations between Odd/Even days compared to the normal day. However, for PNC, no such clear pattern could be seen (Annexure-III). Besides wind speed, a significant mean difference in the concentration has been found for different parameters such as RH, SR, TVC, etc. The results show that qUFP reduced steeply in the morning up to 1:00 pm during the odd day, but the reduction rate is comparatively low during the afternoon (Figure 4.47, Figure 4.48 and Figure 4.49). The percentage change compared to a normal day increased up to 1:00 pm (average increase of 26%). Afterward, the percentage change shows stagnation on an odd-day scheme. On an even day, qUFP's percentage change variation is not found so significant up to 2:00 pm; however, the variations were high after 2:00 pm. The percentage change was quite similar on both the odd and even day of the Odd-

Even scheme. On the odd day of the scheme, the particle size bin from sub-fine shows that the variations in percentage change are the same throughout the day, but on even day, variations in percentage change of sub-fine particles are observed high until noon (12:00 pm) and increased again after 2:00 pm.

The particle number concentration of fine particle size on the even-day of the scheme has been reduced; however, diurnal change in percentage is low throughout the day. On odd-day of the scheme, a reduction in percentage change in fine particle size observed with time from 40% to 19% (Table 4.8). Coarse particle size analysis on an odd day shows a reduction in pollutants until 1:00 pm; afterward, the concentration increased steeply. The same pattern was followed on an even day also. This expected change may be due to wind speed reduction.

Diurnal Meteorological data regarding time analysis unveiled that pollutant change is also affected by changes in a meteorological parameters such as wind speed and relative humidity (Rönkkö and Timonen, 2019). The increment in percentage change in the number concentration of particulate matter is expected due to high wind speed. The percentage change in wind speed is high on an odd day, increasing from morning 8:00 am to 1:00 pm, promoting the high dispersion of pollutants. Wind speed is reduced after 1:00 pm and shows less dispersion in pollutants. A similar pattern for wind speed is also followed on an even day. The wind speed trend concerning coarse particles shows that reducing the change in particulate matter percentage affected significantly due to the reduction in dispersion and accumulation of these particles in the surrounding. Diurnal variation in percentage change in relative humidity was found to be increased. The percentage change trend in particulate matter is explained by wind speed and total vehicle count but is less affected by relative humidity. Our study on the Odd-Even scheme at Najafgarh showed that particle number concentrations were comparatively high on normal days than on Odd-Even days. It may be because of lower traffic emissions on particle number concentration.

Variation in the particulate matter was also affected by total vehicle count percentage change, which was continuously reducing compared to normal days from 8:00 am to 1:00 pm on an odd day. The same pattern for total vehicle change was also followed on an even

day, showing that particulate matter variation depends on variation in total vehicle count. The present study on vehicle data showed a higher number of TVC and C&T in the morning, whereas less in the evening. Due to the Odd-Even scheme, the absolute reduction is estimated to be 25.8 % at the Najafgarh location in TVC. Similarly, an absolute reduction in C&T was much higher, 26%, due to the Odd-Even scheme. Higher particle number concentrations were observed for PM_1 followed by qUFP> subfine> fine. Najafgarh corridor observed a maximum reduction of 1µm by 42.7 % and a minimum reduction of coarse mode by 9.7 % in the ambient air across the corridor during the days of implementation of the scheme, which is the positive impact of the measure adopted toward the abatement of urban air pollution in the megacity of Delhi.

4.3.2.4 PNC at Pitampura Road during Odd-Even scheme-II

Similarly, Pitampura, follows a similar pattern there is a considerable mean difference in the concentrations between odd/even days compared to the normal day. However, for PNC, quasi and sub-fine follow the pattern of a significant difference on an odd/even day compared to a normal day. There isn't much difference in mean concentration on even and normal day; other than this, there is a difference observed, particularly between even and odd day concentrations.

The percentage change of qUFP at Pitampura station was slightly increased in the morning from 8:00 am–12:00 pm on an odd day. This change was not significant during 12:00–4:00 pm. During the time slot of 12:00–4:00 pm, in the beginning, the percentage change found increasing then shows the stagnation in percentage change. On an even day, in the 4:00–8:00 pm time slot, the percentage change reduced steeply, increasing particle concentration (Figure 4.47 and Figure 4.49). On an odd day, the percentage change of sub-fine particle size was observed with a high number concentration reduction in the morning (8:00 am–12:00 pm). However, variation in percentage change was not significant throughout the day. A similar trend was also seen on the even day of the scheme.

However, even day shows a reduction in percentage change in the morning time slot of 8:00 am-12:00 pm; then percentage change started slightly increasing. The percentage change was comparatively less during the time slot of 12:00 pm–4:00 pm. However, on an even day, the fluctuation in percentage change was observed throughout the day. The reduction in percentage change was significant during the time slot of 4:00 pm–8:00 pm. Percentage change in number concentration of coarse particles on an odd day shows that variations were not so high in the morning slot 8:00 am-12:00 pm, but in the evening from 4:00 pm-8:00 pm time slot, a slight reduction was observed. In the morning, from 8:00 am–12:00 pm, a high particle number concentration was recorded on the even day of the scheme.

Diurnal particle number concentrations showed a slight decrease in considered pollutants compared to a normal day, which seems to be associated with a decreased number of total vehicles on the road, especially cars and taxis, during the Odd-Even driving scheme days. This study on vehicle data has represented more TVC and C&T in the morning hours, less in the afternoon and evening on an odd day. Whereas on even day, higher numbers of vehicles were found to be in the afternoon and less in the morning and evening. Total vehicles were observed more on an even day than the odd day at Pitampura during scheme days.

Roadside particle number concentrations do not only depend on traffic density but also on meteorological parameters. High concentrations of PNC on a normal day at all the locations are expected due to higher traffic density, low wind speed, and relative humidity. Diurnal metrological data for time analysis (Figure 4.46) revealed that change in pollutants was also affected by changes in a meteorological parameter such as wind speed and relative humidity. The Pitampura corridor monitoring station was observed with a maximum and minimum wind speed peak at 7:15 pm and 11:45 am, respectively. Similar peaks were followed at 2:15 pm and minimum at 11:45 am–12:15 pm on an even day at the Pitampura monitoring station. Wind speed plays an important role in the percentage change of particulate matter due to the reduction in these particles' dispersion and accumulation in the surrounding.

During the Odd-Even scheme, the number of particles that contributed the maximum was PM_1 followed by qUFP> subfine> fine. PM_1 shows a 26.2% PNC reduction overall, including 24.0% on an odd day and 28.4% on an even day. Simultaneously, TVC indicates an overall decrease of 18.5%, including 24.4 % on an odd day and 18.5% on an even day. However, C&T was reduced by 12.4%. The maximum reduction in the number concentration of particles was 42.2% in the sub-fine, followed by 25.4% in qUFP, 16.5% in fine, and 7.1% in coarse size mode.

4.3.2.5 PNC at Panchkuian Road during Odd-Even scheme-II

For Panchkuian, nearly PNC exhibit a significant difference in mean concentration (odd/even day compared to normal day and even between odd and even day), except for $PM_{0.5}$, for which there is no significant difference between odd and even day concentrations. For PNC particles qUFP and Fine, there is a significant difference in mean concentrations for odd/even days compared to a normal day.

At Panchkuian road (Figure 4.47 and Figure 4.50) during the Odd-Even scheme study, percentage change on an odd day of the scheme for all size particle, the number concentrations showed a gradual decrease from 8:00 am till noon. Then percentage change for all sizes varies with changes after 12:00 noon significantly less in magnitude. However, a percentage change in number concentration was observed for all size particulate matter throughout the day, which shows that the PNC was less on scheme day than on the pre-scheme day. On an even day, the percentage change in number concentrations was almost in favor of the scheme. The percentage change for mostly all particulate size bins increased from morning to evening. Few size bins have shown a minor variation trend on even day such as coarse mode, and a sudden reduction in percentage change is observed at 12:15 pm for coarse particles and fine particles. Percentage change for size bin of fine was significantly less in the morning then increasing steeply throughout the day.

The wind speed and RH show the significance of PNC, and wind speed increases the dispersion and dilution of pollutants in the atmosphere. The increment in percentage change

in PNC was expected due to high wind speed. Wind speed and relative humidity were recorded higher on Odd-Even days than a pre-Odd-Even day at the Panchkuian location. For example, at the Panchkuian site, wind speed (mean ± standard deviation) was found to be 1.7 ± 0.8 on Odd-Even day and 1.3 ± 0.6 on the pre-Odd-Even day. Percentage change in wind speed was found to be high on the odd day which is increasing in morning slot 8:00 am-12:00 pm that promotes the high dispersion of pollutant and wind speed is reduced in afternoon slot 12:00 pm-4:00 pm whereas, evening slot 4:00 pm-8:00 pm shows less dispersion of pollutants. The same pattern for wind speed is followed on an even day. Variation in pollutants is also affected by the total vehicle count on the road during the scheme. TVC was found to be greater at 8:15 am on an odd day of the scheme, then continuously reducing in the morning slot 8:00 am-12:00 pm for the odd day of the scheme. Simultaneously, the maximum peak of C&T was found to be at 1:45 pm on an even day. However, TVC was observed less on odd days of the scheme than on even day and pre-Odd-Even day. During Odd-Even scheme days, a reduction in the total number of vehicles and C&T has been recorded as 18.3% and 16.1%, respectively, against the pre-driving scheme day. Like vehicles, at Panchkuian location recorded a significant drop in particle number concentrations as 24% in qUFP, 26.0% in sub-fine, 22.3% fine, and 10.4% in coarse, respectively. The highest contribution to particle number concentrations was observed for PM_1 at Punchkuiam road, followed by two other selected locations (Najafgrah and Pitampura).

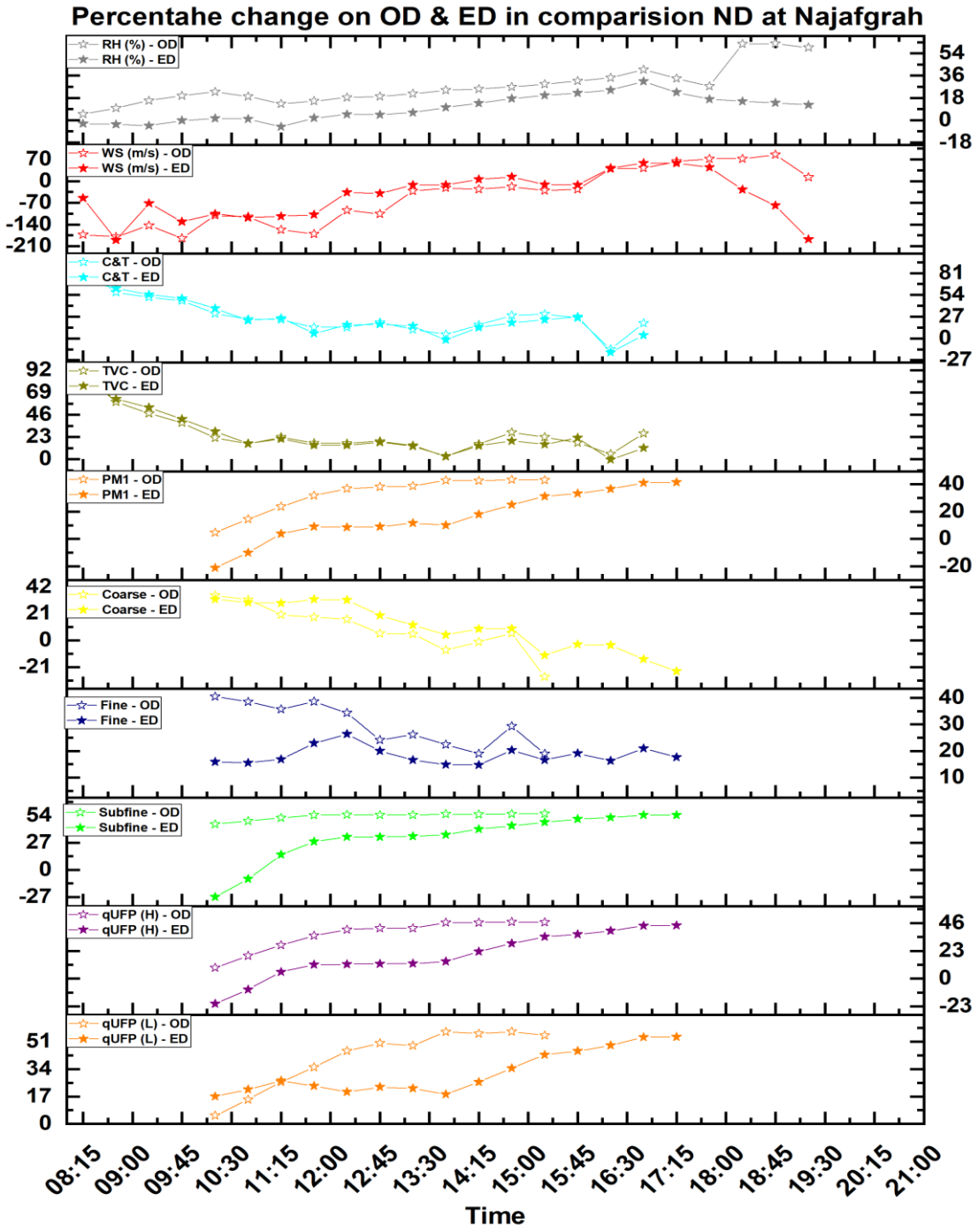

Figure 4.48: Percentage change of Odd day (5 November) and Even day (4 November) with respect to Normal day (2 November) at Najafgarh road

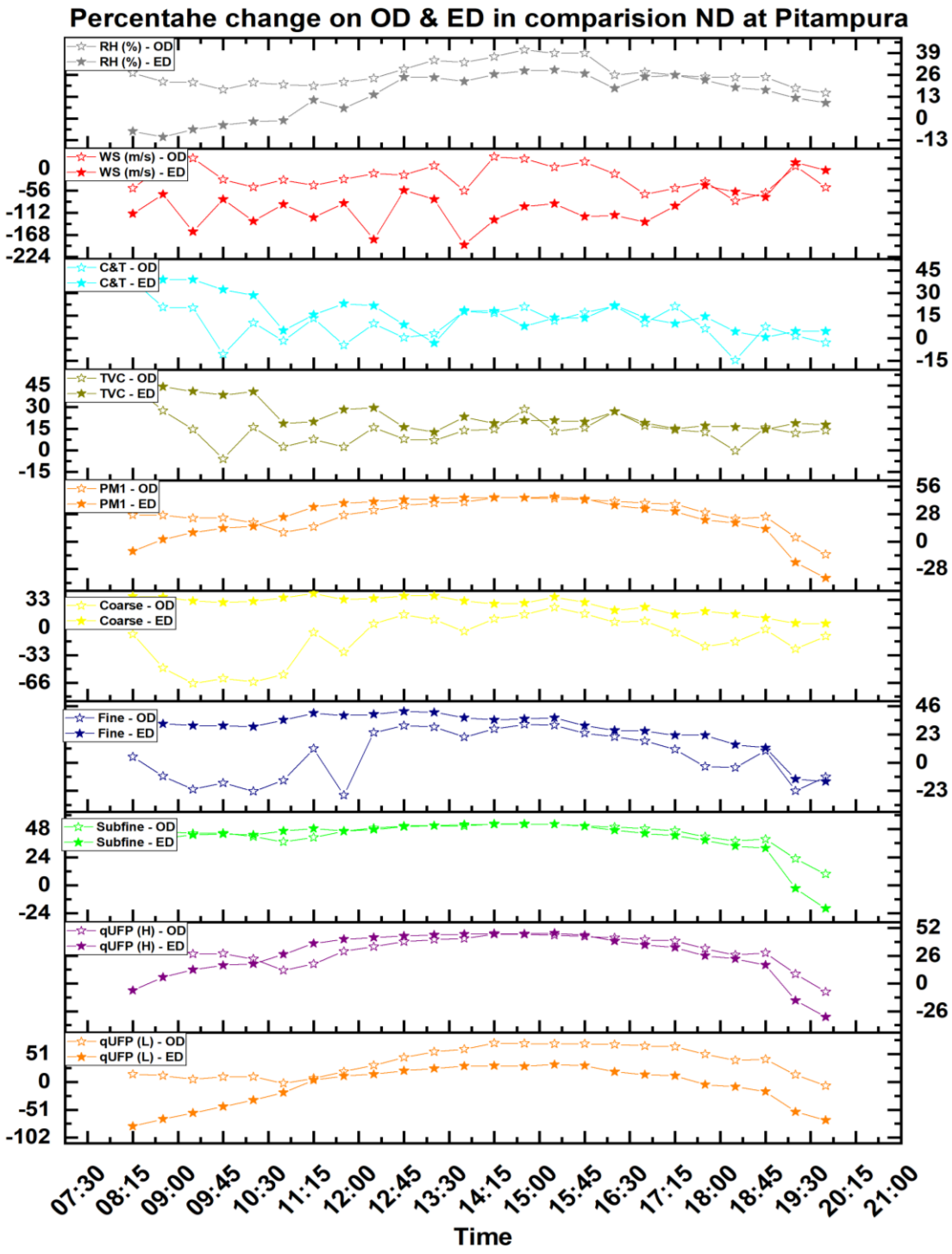

Figure 4.49: Percentage change of Odd day (9 November) with Even day (6 November) respective of Normal day (1 November) at Pitampura road

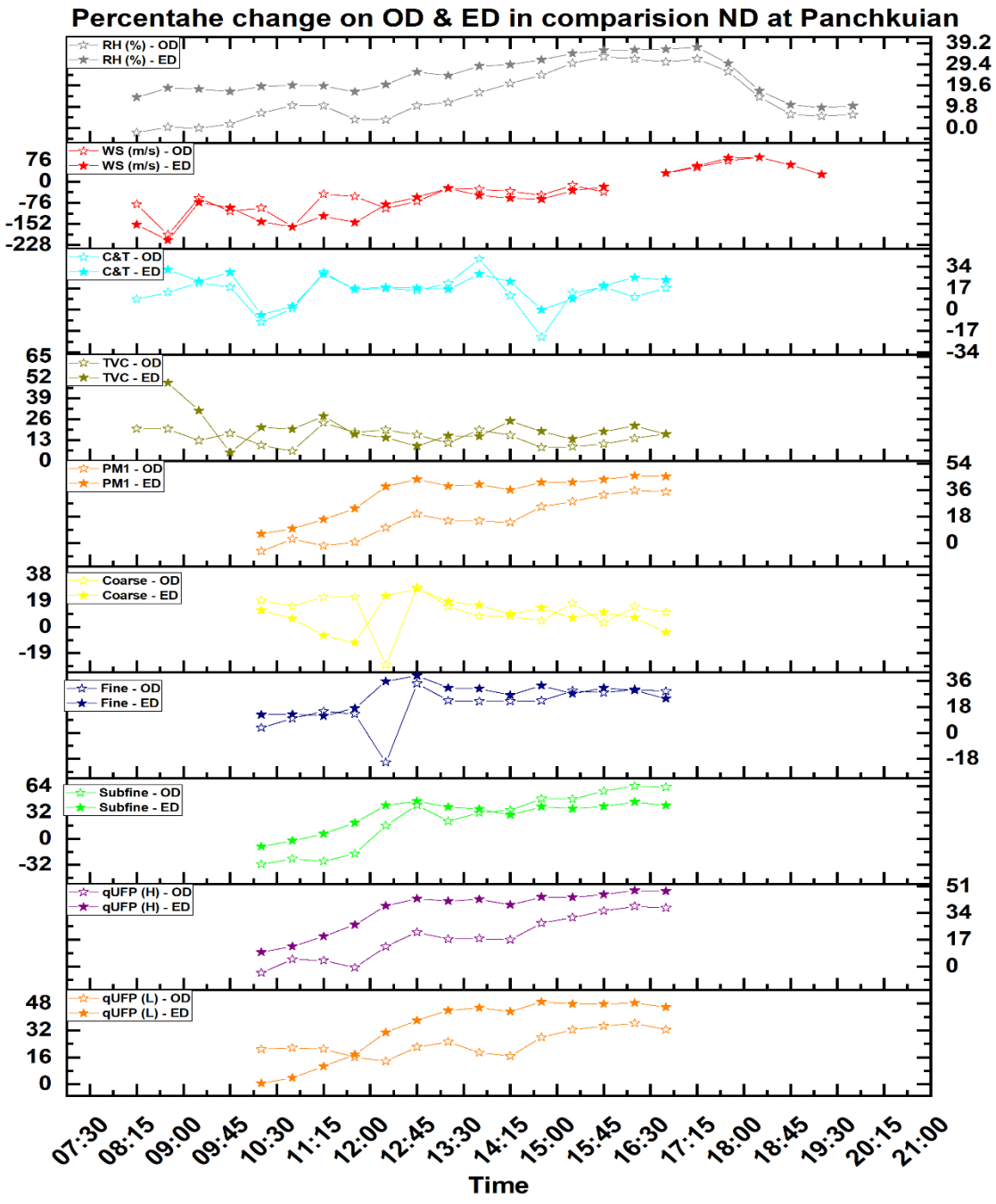

Figure 4.50: Percentage change of Odd day (5 November) with Even day (6 November) respective of Normal day (2 November) at Panchkuian road

4.3.2.6 Summary

It unveiled from the present study that the Odd-Even scheme has a positive result to combating air pollutant PM_1 number concentration in Delhi. The selected monitoring stations, namely, Najafgarh, Pitampura, and Pachukuian, revealed that PM_1 number concentration reduced during the Odd-Even scheme by 24.6%, 26.2%, and 24.8%, respectively. Compared to a normal day, Najafgarh's location shows a 32.7% reduction of PNC on an odd day, but on an even day, it showed a reduction of mostly half of the odd day (16.5%). The count of TVC led to a reduction of 26.7% and 24.9% for odd and even day, respectively, while 27.4% and 24.8% reduction occurred in C&T for odd and even day respectively. The concentration of PM_1 on Panchkuian road is higher on 'odd day' than 'even day' like Najafgarh road. At the same time, no significant difference was found in vehicle count reduction in TVC and C&T between odd and even day. In concern of PM_1, the PNC at Pitampura had shown a reduction of 24% for the odd day and 28.4% for even day. Pitampura and Panchkuian show almost the same PM_1 overall reduction (26.2%) at Najafgarh road. Although Pitampura's even day reduction is less (24.0%) and higher on an odd day (28.4%) compared to Najafgarh road 32.7% and 16.5%, respectively, which indicates that except for TVC and C&T reduction, other factors, including meteorological parameters, also have a significant effect on PNC.

CHAPTER-5

5 CONCLUSION

5.1 General

The entire study has covered various aspects (particle number size distribution, particle formation, particle growth, fate of PNC in different size modes such as nucleation mode, Aitken mode and accumulation mode) of UFP and qUFP in a specific context. The present study is based on the Capital City of India, Delhi in which sites are in the road microenvironment. The monitoring was conducted from 26th November 2019 to 31st June 2021 and covered 15 months (~75%) out of the total 20 months. In addition, the study also covers the classification and quantification of UFP at certain events known as air pollution episodes in Delhi like Diwali and Odd-Even Scheme - II.

5.2 Quantification of UFPs classification based on selected microenvironment of Megacity Delhi.

The N total and UFP maximum concentration ranges from ~ 1.9 x 10^4 to 3.0 x 10^4 #/ cm^3 upto >50% and 0.5 x 10^4 to 1.5 x 10^4 #/cm^3 upto 40% respectively. While GMD maximum ranges from 30 nm to 80 nm > 60% during the monitoring period. Summer and partially monsoon seasons shows higher UPF concentration, while GMD shows higher particle size in winter. In summer N total and UFP start increasing from morning 06:00 AM to 12:00 PM and 06:00 PM to 10:00 PM evening, which may be due to the photochemical reaction and vehicular emission with trans boundary condition respectively. But the in case of accumulation mode, it started to decrease from 06:00 AM to 02-03:00 PM and then started to increase till the late night of each day. There is no major trend difference found between weeks in summer. Near afternoon time (~12:00 PM) shows lowest GMD of days, which is a typical signature of photochemical reaction concerning new particle formation. N_{total} and UFP show the same pattern in winter as summer; only the peaks are sharp and smooth. Importantly morning and evening peaks are almost the same which is not the in case of summer. their morning peaks are always higher than evening peaks.

This study examined the impact of the COVID-19 lockdown and subsequent progressive relaxations of anthropogenic activities on particle number concentrations and number size distributions in the ultrafine and fine size range (10.2 to 1090 nm). The mean total particle number concentrations gradually increased from Period-I ($2.5 \times 10^4 \pm 1.3 \times 10^4$ cm^{-3}) with the strictest lockdown to Period-III ($3.1 \times 10^4 \pm 1.9 \times 10^4$ cm^{-3}), where restrictions were eased up considerably. The fraction of ultrafine particles gradually decreased from ~0.70 ± 0.09 to 0.58 ± 0.16 during this period, with the doubling of the accumulation mode particle concentrations (N_{accu}). This highlighted the effect of intensified anthropogenic activities on particle number concentrations.

5.3 Investigating the fate and transformation of UFPs from roadway.

Several new particle formation events occurred with the nucleation mode particle concentrations (N_{nuc}) increasing by 3-8 times, which led to an enhancement in N_{total} by 2-5 times. Compared to the non-event days, N_{nuc} was ~1.5-2 times higher on the event days. Most NPF events occurred during the morning/afternoon hours of the day, demonstrating the role of photochemistry. However, there is no clear association between the prevailing meteorological conditions or trace gas concentrations and nucleation intensity.

The varying magnitudes of N_{nuc} and N_{UFP} on the event and non-event days established the competition between the strengths of the precursor vapor sources and the condensation sink. Different classes of NPF events were identified with an overall NPF frequency of ~ 41 %. During Period-I, the NPF frequency is 20.6 %, with the occurrence of all classes of NPF events (Class Ia, Class Ib, and Class II), whereas NPF frequency of 17.2 % with only class Ia events was seen during Period- II. The lowest frequency (3.4 %) with only class II events during Period-III highlighted the role of urban primary emissions on UFP loading. Interestingly, while NPF events during Period-II are more frequent and well-defined, lower particle growth rates (mean ~5.86 ± 1.44 nm hr^{-1}) compared to the Period-I (~6.05 ± 1.66 nm hr^{-1}) have been observed during this period.

The condensation sink (CS) values on the non-event days during Period-I (0.053 sec^{-1}) < Period-II (0.072 sec^{-1}) < Period-III (0.09 sec^{-1}) were normally higher than those seen on event days of Period-I (0.034 sec^{-1}) < Period-II (0.035 sec^{-1}) < Period-III (0.07 sec^{-1}) <

Period-III (0.07 sec^{-1}) respectively. It suggested that higher CS in the urban regions with a gradual increase in traffic ensures that gaseous precursors, molecular clusters, and newly formed particles experience a high loss rate. The frequency, intensity, and shape of the NPF events are determined by the competition between the CS and the strength of precursor vapor sources.

5.4 Correlation of UFPs with NOx, and SOx under variable, meteorological conditions

During the nucleation events, a clear enhancement in the concentrations of [H_2SO_4] proxy (2 to 3.5 x 10^7 molecules cm^{-3}; 2-3 orders higher than the non-event values) suggests the role of gas-phase photochemistry in NPF. Also, some of the NPF events were associated with increased odd oxygen concentrations [Ox], indicating the regional nature of the precursors and participation of VOC precursors in nucleation/growth. However, particle burst events depicted NO_x enhancement, thereby suggesting contributions from traffic emissions to UFP abundance.

Almost all the NPF events occurred when the air masses originated from the east-southeast sectors, as evident from several times higher N_{nuc} and [H_2SO_4] proxy values compared to the other wind sectors. This suggested the precursor-rich nature of the air masses from the east-southeast sectors. However, NO_x, in general, was higher (>25 ppb) for the north-northeast sector but lower (< 15 ppb) for the other wind sectors, supporting the inference that the nucleation mode particles were formed from secondary pathways rather than primary vehicular emissions.

The diurnal pattern of N_{UFP} revealed a typical double hump pattern governed by the local atmospheric boundary layer dynamics and source/sink processes of aerosols during the non-event days. The magnitude of the first and second peaks in N_{total}, N_{Aitk}, and N_{accu} concentrations during non-event days gradually increased from Period-I to Period-III, underlining increased traffic emissions with the unlocking of activities. However, the mean diurnal pattern of N_{nuc} showed a distinct pattern during the events days with multiple peaks during the daytime of Period-I (~10:00-11:00 hrs; 14:00-15:00 hrs and 18:00-19:00 hrs), Period II (~08:00 hrs and 11:00 hrs) reiterating the role of

photochemistry. Furthermore, the contribution of the urban vehicle and anthropogenic emissions to the particle nucleation mode cannot be excluded.

5.5 Quantification of UFPs/qUFP's classification based on other events of Megacity Delhi

This study covered two other events regarding quantifying UFP/ qUFP's classification.

5.5.1 Diwali 2019

Since the air pollution and noise generated from fireworks are related to air quality and human health, the regulatory bodies had implemented the eco-friendly "Green Crackers" in megacity Delhi, India, to celebrate Diwali 2019 with the permission of a specific time slot (8:00 PM to 10:00 PM). The present study was conducted on a residential educational institute campus to evaluate the particle number size distribution (PNSD) of green cracker emissions. During the Diwali event period, the high peak of particle number concentration (PNC) reached 1.7 x 105 # cm-3 with a geometric mean diameter (GMD) of ~44 nm. The average PNC increment on Diwali day was 138 % and 97 % compared to pre (26th October 2019) and post (28th October 2019) Diwali period, respectively, including 468 %, 142 %, 65 %, 75 % on pre-Diwali and 485 %, 110 %, 32 %, 26 % on post-Diwali 2019 period in terms of Nucleation mode (10 nm < Dp < 20 nm), Small Aitken mode (20 nm < Dp < 50 nm), Large Aitken mode (50 nm < Dp < 100 nm), and Accumulation mode (100 nm < Dp < 1000 nm), respectively. Unlike traditional firework emissions, green crackers had a high UFP/Ntotal ratio of 0.72, including Nucleation mode-0.35, Aitken mode-0.30, and Accumulation mode 0.35, distinguishing it from other pre-and post-Diwali particle number size distribution-dN/dlogDp curves. These observations indicate that green crackers emit more particles with smaller diameters than traditional crackers.

5.5.2 Odd-Even scheme – II, 2019

The Odd-Even scheme was implemented in Delhi in 2019 on vehicle movement to curb air pollution during the winter season. This study selected three locations, namely Najafgarh, Pitampura, and Panchkuian road, to evaluate the Odd-Even scheme 2019.

This study revealed a reduction of 24 to 26 % in PM_1 particle number concentration along with their particle number size distribution as QuasiUFP (24 to 25.4%), sub-fine (26 to 42.7%) and fine (16.5 to 24.1%) in particle number concentrations. This study also covers the coarse particle size, with the lowest reduction (7 to 10%) at all the selected locations. Car & taxi, on which Odd-Even scheme was effective, has shown 12.6 to 26.4% reduction.

5.6 Importance of the study

Around 75% of PNC produced in urban areas comes from vehicle emissions, and UFPs account for 90% of PNC. Road traffic is one of the primary sources of UFPs and has a significant impact on air concentrations close to a major highway. The emission of vehicle exhaust from the roadway and different climatic phenomena affect the concentration and formation of these particles. As a result, exposure to UFPs along busy roadways and other important thoroughfares is a crucial area that needs more study and attention. The research study has the following possible applications:

- It will enhance knowledge of the source, formation, and growth of UFPs in the megacity of Delhi and other Asian cities where automobile emissions are the major source of pollution. As NPF events "Period II" present the optimal transition situation for moderate or reduced pollution, this will also aid in adoption in European cities where vehicular pollution is not a significant concern (vehicular emission).

- It will help to investigate the effects of secondary formation on the fluctuations in particle number count (PNC) and the relationship between the local vehicle emission microenvironment and PNC.

- The study will aid in understanding the size and number distribution of UFPs in Delhi and other Asian cities during various outdoor environments and seasons. The study will improve knowledge of the number of fine particles in a megacity as well as the application of EURO VI standards, which will employ the PNC as an emission standard.

• Based on the calculation of UFP exposure of residents close to roadside emissions, it will help policymakers make suitable strategies to reduce their exposure.

5.7 Future prospects of study

The present study aims to assess of the quantification, formation, and growth rate of UFP in selected microenvironments in Delhi. Based on the whole study and its results, here are some suggestions for future research.

This study aims to determine the quantity, generation, and growth rate of UFP in various microenvironments in Delhi. Following are some recommendations for further research based on the entire study and its findings. Long-term monitoring of UFP at various places within an urban region is required to determine PNC source apportionment. People and policymakers must pay close attention to vehicular pollution. There is a need to investigate the impact of URMe's UFP on human health when combined with biomarkers for exposure, so that the heterogeneity of passenger exposure may be linked to the number of particles in public transportation microenvironments. In the future, health risk assessments of school-aged children and comparative health assessments of commuters' exposures to black carbon, precursor gases, and UFP in urban and rural transport microenvironments will be possible.

5.8 Summary

The discussion in the conclusion section focused on the significant and key findings in relation to the purpose of these objectives, and the future prospects of the UFP study based on the findings of this study.

6 REFERENCES

Ababio-Donkor, A., Saleh, W., Fonzone, A., 2020. Understanding transport mode choice for commuting: the role of affect. Transp. Plan. Technol. 43, 385–403. https://doi.org/10.1080/03081060.2020.1747203

Abdul-Khalek, I., Kittelson, D., Brear, F., 1999. The influence of dilution conditions on diesel exhaust particle size distribution measurements. SAE Tech. Pap. https://doi.org/10.4271/1999-01-1142

Agustian, D., Rachmi, C.N., Indraswari, N., Molter, A., Carder, M., Rinawan, F.R., van Tongeren, M., Driejana, D., 2020. Feasibility of indonesia family life survey wave 5 (Ifls5) data for air pollution exposure–response study in indonesia. Int. J. Environ. Res. Public Health 17, 1–18. https://doi.org/10.3390/ijerph17249508

Ahlm, L., Liu, S., Day, D.A., Russell, L.M., Weber, R., Gentner, D.R., Goldstein, A.H., Digangi, J.P., Henry, S.B., Keutsch, F.N., Vandenboer, T.C., Markovic, M.Z., Murphy, J.G., Ren, X., Scheller, S., 2012. Formation and growth of ultrafine particles from secondary sources in Bakersfield, California. J. Geophys. Res. Atmos. 117, 1–13. https://doi.org/10.1029/2011JD017144

Ahmed, S., 2017. Modeling of Ultrafine Particle Emissions and Ambient Levels for the Near Roadside Environment. https://doi.org/10.15760/etd.3368

Aiken, A.C., McMeeking, G.R., Levin, E.J.T., Dubey, M.K., DeMott, P.J., Kreidenweis, S.M., 2016. Quantification of online removal of refractory black carbon using laser-induced incandescence in the single particle soot photometer. Aerosol Sci. Technol. 50, 679–692. https://doi.org/10.1080/02786826.2016.1173647

Air Quality Expert Group, 2018. Ultrafine Particles (UFP) in the UK 96.

Airy, A., Chandiramani, J., 2016. The Good and Bad of ‘ Odd-Even Formula ’: Case

Study of Delhi and Alternative Measures towards Sustainable Transport 3, 31–35.

Al-Dabbous, A.N., Kumar, P., 2015. Source apportionment of airborne nanoparticles in a Middle Eastern city using positive matrix factorization. Environ. Sci. Process. Impacts 17, 802–812. https://doi.org/10.1039/c5em00027k

Al-Dabbous, A.N., Kumar, P., 2014. The influence of roadside vegetation barriers on airborne nanoparticles and pedestrians exposure under varying wind conditions. Atmos. Environ. 90, 113–124. https://doi.org/10.1016/j.atmosenv.2014.03.040

Al–Dabbous, A.N., Kumar, P., Khan, A.R., 2017. Prediction of airborne nanoparticles at roadside location using a feed–forward artificial neural network. Atmos. Pollut. Res. 8, 446–454. https://doi.org/10.1016/j.apr.2016.11.004

Alam, A., Shi, J.P., Harrison, R.M., 2003. Observations of new particle formation in urban air. J. Geophys. Res. D Atmos. 108. https://doi.org/10.1029/2001jd001417

Alam, K., Blaschke, T., Madl, P., Mukhtar, A., Hussain, M., Trautmann, T., Rahman, S., 2011. Aerosol size distribution and mass concentration measurements in various cities of Pakistan. J. Environ. Monit. 13, 1944–1952. https://doi.org/10.1039/c1em10086f

Alanen, J., Saukko, E., Lehtoranta, K., Murtonen, T., Timonen, H., Hillamo, R., Karjalainen, P., Kuuluvainen, H., Harra, J., Keskinen, J., Rönkkö, T., 2015. The formation and physical properties of the particle emissions from a natural gas engine. Fuel 162, 155–161. https://doi.org/10.1016/j.fuel.2015.09.003

Amaral, S.S., de Carvalho, J.A., Costa, M.A.M., Pinheiro, C., 2015. An overview of particulate matter measurement instruments. Atmosphere (Basel). https://doi.org/10.3390/atmos6091327

An, J., Wang, H., Shen, L., Zhu, B., Zou, J., Gao, J., Kang, H., 2015. Characteristics of

new particle formation events in Nanjing, China: Effect of water-soluble ions. Atmos. Environ. 108, 32–40. https://doi.org/10.1016/j.atmosenv.2015.01.038

Anand, S., Mayya, Y.S., 2011. A simplified approach for solving coagulation-diffusion equation to estimate atmospheric background particle number loading factors contributed by emissions from localized sources. Atmos. Environ. 45, 4488–4496. https://doi.org/10.1016/j.atmosenv.2011.05.016

Anjilvel, S., Asgharian, B., 1995. A Multiple-Path Model of Particle Deposition in the Rat Lung. Fundam. Appl. Toxicol. 28, 41–50. https://doi.org/10.1006/FAAT.1995.1144

Apte, J.S., 2011. Commuter Exposure to Vehicle Air Pollution in New Delhi.

Apte, J.S., Kirchstetter, T.W., Reich, A.H., Deshpande, S.J., Kaushik, G., Chel, A., Marshall, J.D., Nazaroff, W.W., 2011. Concentrations of fine, ultrafine, and black carbon particles in auto-rickshaws in New Delhi, India. Atmos. Environ. 45, 4470–4480. https://doi.org/10.1016/j.atmosenv.2011.05.028

Arnold, F., Pirjola, L., Rönkkö, T., Reichl, U., Schlager, H., Lähde, T., Heikkilä, J., Keskinen, J., 2012. First online measurements of sulfuric acid gas in modern heavy-duty diesel engine exhaust: Implications for nanoparticle formation. Environ. Sci. Technol. 46, 11227–11234. https://doi.org/10.1021/es302432s

Arphorn, S., Ishimaru, T., Hara, K., Mahasandana, S., 2018. Considering the effects of ambient particulate matter on the lung function of motorcycle taxi drivers in Bangkok, Thailand. J. Air Waste Manag. Assoc. 68, 139–145. https://doi.org/10.1080/10962247.2017.1359217

Arub, Z., Bhandari, S., Gani, S., Apte, J.S., Hildebrandt Ruiz, L., Habib, G., 2020. Air mass physiochemical characteristics over New Delhi: impacts on aerosol

hygroscopicity and cloud condensation nuclei (CCN) formation. Atmos. Chem. Phys. 20, 6953–6971. https://doi.org/10.5194/acp-20-6953-2020

Asmi, E., Kivekäs, N., Kerminen, V.M., Komppula, M., Hyvärinen, A.P., Hatakka, J., Viisanen, Y., Lihavainen, H., 2011. Secondary new particle formation in Northern Finland Pallas site between the years 2000 and 2010. Atmos. Chem. Phys. 11, 12959–12972. https://doi.org/10.5194/acp-11-12959-2011

Attri, A.K., Kumar, U., Jain, V.K., 2001. Formation of ozone by fireworks. Nature 411, 1015. https://doi.org/10.1038/35082634

Babu, S.S., Kompalli, S.K., Moorthy, K.K., 2016. Aerosol number size distributions over a coastal semi urban location: Seasonal changes and ultrafine particle bursts. Sci. Total Environ. 563–564, 351–365. https://doi.org/10.1016/j.scitotenv.2016.03.246

Bakand, S., Hayes, A., Dechsakulthorn, F., 2012. Nanoparticles: A review of particle toxicology following inhalation exposure. Inhal. Toxicol. https://doi.org/10.3109/08958378.2010.642021

Balakrishnan, K., Dey, S., Gupta, T., Dhaliwal, R.S., Brauer, M., Cohen, A.J., Stanaway, J.D., Beig, G., Joshi, T.K., Aggarwal, A.N., Sabde, Y., Sadhu, H., Frostad, J., Causey, K., Godwin, W., Shukla, D.K., Kumar, G.A., Varghese, C.M., Muraleedharan, P., Agrawal, A., Anjana, R.M., Bhansali, A., Bhardwaj, D., Burkart, K., Cercy, K., Chakma, J.K., Chowdhury, S., Christopher, D.J., Dutta, E., Furtado, M., Ghosh, S., Ghoshal, A.G., Glenn, S.D., Guleria, R., Gupta, R., Jeemon, P., Kant, R., Kant, S., Kaur, T., Koul, P.A., Krish, V., Krishna, B., Larson, S.L., Madhipatla, K., Mahesh, P.A., Mohan, V., Mukhopadhyay, S., Mutreja, P., Naik, N., Nair, S., Nguyen, G., Odell, C.M., Pandian, J.D., Prabhakaran, D., Prabhakaran, P., Roy, A., Salvi, S., Sambandam, S., Saraf, D., Sharma, M., Shrivastava, A., Singh, V.,

Tandon, N., Thomas, N.J., Torre, A., Xavier, D., Yadav, G., Singh, S., Shekhar, C., Vos, T., Dandona, R., Reddy, K.S., Lim, S.S., Murray, C.J.L., Venkatesh, S., Dandona, L., 2019. The impact of air pollution on deaths, disease burden, and life expectancy across the states of India: the Global Burden of Disease Study 2017. Lancet Planet. Heal. 3, e26–e39. https://doi.org/10.1016/S2542-5196(18)30261-4

Baldauf, R., 2016. Recommendations for Constructing Roadside Vegetation Barriers to Improve Near-Road Air Quality. U.S. Environ. Prot. Agency 600/R–16/0.

Baldauf, R.W., Devlin, R.B., Gehr, P., Giannelli, R., Hassett-sipple, B., Jung, H., Martini, G., Mcdonald, J., Sacks, J.D., Walker, K., 2016. Ultrafine Particle Metrics and Research Considerations : Review of the 2015 UFP Workshop 1–21. https://doi.org/10.3390/ijerph13111054

Banerjee, T., Christian, R.A., 2018. A review on nanoparticle dispersion from vehicular exhaust: Assessment of Indian urban environment. Atmos. Pollut. Res. https://doi.org/10.1016/j.apr.2017.10.009

Banerjee, T., Murari, V., Kumar, M., Raju, M.P., 2015. Source apportionment of airborne particulates through receptor modeling: Indian scenario. Atmos. Res. https://doi.org/10.1016/j.atmosres.2015.04.017

Beig, G., Ghude, S.D., Deshpande, A., 2010. Scientific Evaluation of Air Quality Standards and Defining Air Quality Index for India. Indian Inst. Trop. Meteorol. 1–31.

Belkacem, I., Helali, A., Khardi, S., Chrouda, A., Slimi, K., 2021. Road traffic nanoparticle characteristics: Sustainable environment and mobility. Geosci. Front. In-Press, 101196. https://doi.org/10.1016/j.gsf.2021.101196

Belkacem, I., Khardi, S., Helali, A., Slimi, K., Serindat, S., 2020. The influence of urban

road traffic on nanoparticles: Roadside measurements. Atmos. Environ. 242, 117786. https://doi.org/10.1016/j.atmosenv.2020.117786

Bello-Salau, H., Aibinu, A., Onwuka, E., Dukiya, J., Bima, M., Onumanyi, A., Folorunso, T., 2015. A New Measure for Analysing Accelerometer Data towards Developing Efficient Road Defect Profiling Systems. J. Sci. Res. Reports 7, 108–116. https://doi.org/10.9734/jsrr/2015/16840

Bennat, C., Müller-Goymann, C.C., 2000. Skin penetration and stabilization of formulations containing microfine titanium dioxide as physical UV filter. Int. J. Cosmet. Sci. 22, 271–283. https://doi.org/10.1046/j.1467-2494.2000.00009.x

Bera, B., Bhattacharjee, S., Shit, P.K., Sengupta, N., Saha, S., 2020. Significant impacts of COVID-19 lockdown on urban air pollution in Kolkata (India) and amelioration of environmental health. Environ. Dev. Sustain. 1. https://doi.org/10.1007/s10668-020-00898-5

Berghmans, P., Bleux, N., Panis, L.I., Mishra, V.K., Torfs, R., Van Poppel, M., 2009. Exposure assessment of a cyclist to PM10 and ultrafine particles. Sci. Total Environ. 407, 1286–1298. https://doi.org/10.1016/j.scitotenv.2008.10.041

Berkowicz, R., 2000. Parameterised street pollution model 323–331.

Betha, R., Balasubramanian, R., 2013. Particulate emissions from commercial handheld sparklers: Evaluation of physical characteristics and emission rates. Aerosol Air Qual. Res. 13, 301–307. https://doi.org/10.4209/aaqr.2012.08.0208

Bhandari, S., Gani, S., Patel, K., Wang, D.S., Soni, P., Arub, Z., Habib, G., Apte, J.S., Hildebrandt Ruiz, L., 2020. Sources and atmospheric dynamics of organic aerosol in New Delhi, India: Insights from receptor modeling. Atmos. Chem. Phys. 20, 735–752. https://doi.org/10.5194/acp-20-735-2020

Bhardawaj, A., Habib, G., Kumar, A., Singh, S., Nema, A.K., 2017. A Review of Ultrafine Particle-Related Pollution during Vehicular Motion , Health Effects and Control 1, 268–288. https://doi.org/10.26502/jesph.96120024

Birmili, W., Berresheim, H., Plass-Dülmer, C., Elste, T., Gilge, S., Wiedensohler, A., Uhrner, U., 2003. The Hohenpeissenberg aerosol formation experiment (HAFEX): A long-term study including size-resolved aerosol, H2SO4, OH, and monoterpenes measurements. Atmos. Chem. Phys. 3, 361–376. https://doi.org/10.5194/acp-3-361-2003

Birmili, W., Wiedensohler, A., Plass-Dülmer, C., Berresheim, H., 2000. Evolution of newly formed aerosol particles in the continental boundary layer: A case study including OH and H2SO4 measurements. Geophys. Res. Lett. 27, 2205–2208. https://doi.org/10.1029/1999GL011334

Both, A.F., Westerdahl, D., Fruin, S., Haryanto, B., Marshall, J.D., 2013. Exposure to carbon monoxide, fine particle mass, and ultrafine particle number in Jakarta, Indonesia : Effect of commute mode. Sci. Total Environ. 443, 965–972. https://doi.org/10.1016/j.scitotenv.2012.10.082

Bousiotis, D., Dall'Osto, M., Beddows, D.C.S., Pope, F.D., Harrison, R.M., 2019. Analysis of new particle formation (NPF) events at nearby rural, urban background and urban roadside sites. Atmos. Chem. Phys. 19, 5679–5694. https://doi.org/10.5194/acp-19-5679-2019

Boyes, W.K., Chen, R., Chen, C., Yokel, R.A., 2012. The neurotoxic potential of engineered nanomaterials. Neurotoxicology 33, 902–910. https://doi.org/10.1016/j.neuro.2011.12.013

Brantley, H.L., Hagler, G.S.W., Deshmukh, P.J., Baldauf, R.W., 2014. Science of the

Total Environment Field assessment of the effects of roadside vegetation on near-road black carbon and particulate matter. Sci. Total Environ. 468–469, 120–129. https://doi.org/10.1016/j.scitotenv.2013.08.001

Brines, M., Dall'Osto, M., Beddows, D.C.S., Harrison, R.M., Gómez-Moreno, F., Núñez, L., Artíñano, B., Costabile, F., Gobbi, G.P., Salimi, F., Morawska, L., Sioutas, C., Querol, X., 2015. Traffic and nucleation events as main sources of ultrafine particles in high-insolation developed world cities. Atmos. Chem. Phys. 15, 5929–5945. https://doi.org/10.5194/acp-15-5929-2015

Brines, M., Dall'Osto, M., Beddows, D.C.S., Harrison, R.M., Querol, X., 2014. Simplifying aerosol size distributions modes simultaneously detected at four monitoring sites during SAPUSS. Atmos. Chem. Phys. 14, 2973–2986. https://doi.org/10.5194/acp-14-2973-2014

Brugge, D., Fuller, C.H., 2021. Ambient combustion ultrafine particles and health, Ambient Combustion Ultrafine Particles and Health.

Bukowiecki, N., Dommen, J., Prévôt, A.S.H., Richter, R., Weingartner, E., Baltensperger, U., 2002. A mobile pollutant measurement laboratory - Measuring gas phase and aerosol ambient concentrations with high spatial and temporal resolution. Atmos. Environ. 36, 5569–5579. https://doi.org/10.1016/S1352-2310(02)00694-5

Burkart, J., Steiner, G., Reischl, G., Moshammer, H., Neuberger, M., Hitzenberger, R., 2010. Characterizing the performance of two optical particle counters (Grimm OPC1.108 and OPC1.109) under urban aerosol conditions. J. Aerosol Sci. 41, 953–962. https://doi.org/10.1016/j.jaerosci.2010.07.007

Cai, H., Xie, S.D., 2010. A modelling study of air quality impact of odd-even day tra ffi

c restriction scheme before , during and after the 2008 Beijing Olympic Games 5135–5184.

Cai, R., Yang, D., Fu, Y., Wang, X., Li, X., Ma, Y., Hao, J., Zheng, J., Jiang, J., 2017. Aerosol surface area concentration: A governing factor in new particle formation in Beijing. Atmos. Chem. Phys. 17, 12327–12340. https://doi.org/10.5194/acp-17-12327-2017

Campagnolo, D., Cattaneo, A., Corbella, L., Borghi, F., Del Buono, L., Rovelli, S., Spinazzé, A., Cavallo, D.M., 2019. In-vehicle airborne fine and ultra-fine particulate matter exposure: The impact of leading vehicle emissions. Environ. Int. 123, 407–416. https://doi.org/10.1016/j.envint.2018.12.020

Carpentieri, M., Kumar, P., Robins, A., 2011. An overview of experimental results and dispersion modelling of nanoparticles in the wake of moving vehicles. Environ. Pollut. https://doi.org/10.1016/j.envpol.2010.11.041

Casati, R., Scheer, V., Vogt, R., Benter, T., 2007. Measurement of nucleation and soot mode particle emission from a diesel passenger car in real world and laboratory in situ dilution. Atmos. Environ. 41, 2125–2135. https://doi.org/10.1016/j.atmosenv.2006.10.078

Cassee, F., Muijser, H., Duistermaat, E., Freijer, J., Geerse, K., Marijnissen, J., Arts, J., 2002. Particle size-dependent total mass deposition in lungs determines inhalation toxicity of cadmium chloride aerosols in rats. Application of a multiple path dosimetry model. Arch. Toxicol. 76, 277–286. https://doi.org/10.1007/s00204-002-0344-8

Chan, C.K., Yao, X., 2008. Air pollution in mega cities in China. Atmos. Environ. https://doi.org/10.1016/j.atmosenv.2007.09.003

Chandra, B.P., Sinha, V., Hakkim, H., Kumar, A., Pawar, H., Mishra, A.K., Sharma, G., Pallavi, Garg, S., Ghude, S.D., Chate, D.M., Pithani, P., Kulkarni, R., Jenamani, R.K., Rajeevan, M., 2018. Odd-even traffic rule implementation during winter 2016 in Delhi did not reduce traffic emissions of VOCs, carbon dioxide, methane and carbon monoxide. Curr. Sci. 114, 1318–1325. https://doi.org/10.18520/cs/v114/i06/1318-1325

Chang, V.W.C., Hildemann, L.M., Chang, C.H., 2009. Dilution rates for tailpipe emissions: Effects of vehicle shape, tailpipe position, and exhaust velocity. J. Air Waste Manag. Assoc. 59, 715–724. https://doi.org/10.3155/1047-3289.59.6.715

Charron, A., Birmili, W., Harrison, R.M., 2008. Fingerprinting particle origins according to their size distribution at a UK rural site. J. Geophys. Res. Atmos. 113. https://doi.org/10.1029/2007JD008562

Charron, A., Harrison, R.M., 2003. Primary particle formation from vehicle emissions during exhaust dilution in the roadside atmosphere. Atmos. Environ. 37, 4109–4119. https://doi.org/10.1016/S1352-2310(03)00510-7

Chaudhari, P.R., Verma, S.R., Singh, D.K., 2016. Experimental Implementation of Odd-Even Scheme for Air Pollution Control in Delhi , India 2, 57–65.

Chauhan, V., Gupta, A., Parida, M., 2022. Evaluating service quality of Multimodal Transportation Hub (MMTH) in Delhi , India : A gender-based perspective. Case Stud. Transp. Policy. https://doi.org/10.1016/j.cstp.2022.04.007

Chen, M., Romay, F.J., Li, L., Naqwi, A., Marple, V.A., 2016. A novel quartz crystal cascade impactor for real-time aerosol mass distribution measurement. Aerosol Sci. Technol. 50, 971–983. https://doi.org/10.1080/02786826.2016.1213790

Chen, R., Hu, B., Liu, Y., Xu, J., Yang, G., Xu, D., Chen, C., 2016. Beyond PM2.5: The

role of ultrafine particles on adverse health effects of air pollution 1860, 2844–2855. https://doi.org/10.1016/j.bbagen.2016.03.019

Cheung, H.C., Morawska, L., Ristovski, Z.D., 2011. Observation of new particle formation in subtropical urban environment. Atmos. Chem. Phys. 11, 3823–3833. https://doi.org/10.5194/acp-11-3823-2011

Chowdhury, Z., Campanella, L., Gray, C., Al Masud, A., Marter-Kenyon, J., Pennise, D., Charron, D., Zuzhang, X., 2013. Measurement and modeling of indoor air pollution in rural households with multiple stove interventions in Yunnan, China. Atmos. Environ. 67, 161–169. https://doi.org/10.1016/j.atmosenv.2012.10.041

Chu, B., Kerminen, V.-M., Bianchi, F., Yan, C., Petäjä, T., Kulmala, M., 2018. Atmospheric new particle formation in China. Atmos. Chem. Phys. Discuss. 1–32. https://doi.org/10.5194/acp-2018-612

Chu, B., Matti Kerminen, V., Bianchi, F., Yan, C., Petäjä, T., Kulmala, M., 2019. Atmospheric new particle formation in China. Atmos. Chem. Phys. 19, 115–138. https://doi.org/10.5194/acp-19-115-2019

Collins, D.R., Cocker, D.R., Flagan, R.C., Seinfeld, J.H., 2004. The scanning DMA transfer function. Aerosol Sci. Technol. 38, 833–850. https://doi.org/10.1080/027868290503082

Colvile, R.N., Hutchinson, E.J., Mindell, J.S., Warren, R.F., 2001. The transport sector as a source of air pollution. Atmos. Environ. https://doi.org/10.1016/S1352-2310(00)00551-3

Contini, D., Donateo, A., Elefante, C., Grasso, F.M., 2012. Analysis of particles and carbon dioxide concentrations and fluxes in an urban area: Correlation with traffic rate and local micrometeorology. Atmos. Environ. 46, 25–35.

https://doi.org/10.1016/j.atmosenv.2011.10.039

Corsini, E., Marinovich, M., Vecchi, R., 2019. Ultrafine particles from residential biomass combustion: A review on experimental data and toxicological response. Int. J. Mol. Sci. https://doi.org/10.3390/ijms20204992

CPCB, 2014. National Air Quality Index. Cent. Pollut. Control Board 1–44.

Crespo, J., Yubero, E., Nicolás, J.F., Caballero, S., Galindo, N., 2014. Time evolution of atmospheric particle number concentration during high-intensity pyrotechnic events. Atmos. Environ. 96, 20–26. https://doi.org/10.1016/j.atmosenv.2014.06.063

Dada, L., Paasonen, P., Nieminen, T., Buenrostro Mazon, S., Kontkanen, J., Peräkylä, O., Lehtipalo, K., Hussein, T., Petäjä, T., Kerminen, V.M., Bäck, J., Kulmala, M., 2017. Long-term analysis of clear-sky new particle formation events and nonevents in Hyytiälä. Atmos. Chem. Phys. 17, 6227–6241. https://doi.org/10.5194/acp-17-6227-2017

Dal Maso, M., Kulmala, M., Riipinen, I., Wagner, R., Hussein, T., Aalto, P.P., Lehtinen, K.E.J., 2005. Formation and growth of fresh atmospheric aerosols: Eight years of aerosol size distribution data from SMEAR II, Hyytiälä, Finland. Boreal Environ. Res. 10, 323–336.

Dal Maso, M., Sogacheva, L., Aalto, P.P., Riipinen, I., Komppula, M., Tunved, P., Korhonen, L., Suur-uski, V., Hirsikko, A., Kurtén, T., Kerminen, V.M., Lihavainen, H., Viisanen, Y., Hansson, H.C., Kulmala, M., 2007. Aerosol size distribution measurements at four Nordic field stations: Identification, analysis and trajectory analysis of new particle formation bursts, in: Tellus, Series B: Chemical and Physical Meteorology. Blackwell Munksgaard, pp. 350–361. https://doi.org/10.1111/j.1600-0889.2007.00267.x

Dall'Osto, M., Beddows, D.C.S., Pey, J., Rodriguez, S., Alastuey, A., M. Harrison, R., Querol, X., 2012. Urban aerosol size distributions over the Mediterranean city of Barcelona, NE Spain. Atmos. Chem. Phys. 12, 10693–10707. https://doi.org/10.5194/acp-12-10693-2012

Dawson, K.A., Salvati, A., Lynch, I., 2009. Nanoparticles reconstruct lipids. Nat. Nanotechnol. 4, 84–85. https://doi.org/10.1038/nnano.2008.426

De Filippo, A., Maricq, M.M., 2008. Diesel nucleation mode particles: Semivolatile or solid? Environ. Sci. Technol. 42, 7957–7962. https://doi.org/10.1021/es8010332

Delfino, R.J., Sioutas, C., Malik, S., 2005. Potential role of ultrafine particles in associations between airborne particle mass and cardiovascular health. Environ. Health Perspect. https://doi.org/10.1289/ehp.7938

Deng, C., Fu, Y., Dada, L., Yan, C., Cai, R., Yang, D., Zhou, Y., Yin, R., Lu, Y., Li, X., Qiao, X., Fan, X., Nie, W., Kontkanen, J., Kangasluoma, J., Chu, B., Ding, A., Kerminen, V.M., Paasonen, P., Worsnop, D.R., Bianchi, F., Liu, Y., Zheng, J., Wang, L., Kulmala, M., Jiang, J., 2020. Seasonal Characteristics of New Particle Formation and Growth in Urban Beijing. Environ. Sci. Technol. https://doi.org/10.1021/acs.est.0c00808

Dey, S., Di Girolamo, L., van Donkelaar, A., Tripathi, S.N., Gupta, T., Mohan, M., 2012. Variability of outdoor fine particulate (PM 2.5) concentration in the Indian Subcontinent: A remote sensing approach. Remote Sens. Environ. 127, 153–161. https://doi.org/10.1016/j.rse.2012.08.021

Dholakia, H.H., Purohit, P., Rao, S., Garg, A., 2013. Impact of current policies on future air quality and health outcomes in Delhi, India 75, 241–248. https://doi.org/10.1016/j.atmosenv.2013.04.052

Dinoi, A., Weinhold, K., Wiedensohler, A., Contini, D., 2021. Study of new particle formation events in southern Italy. Atmos. Environ. 244. https://doi.org/10.1016/j.atmosenv.2020.117920

Dos Santos, V.N., Herrmann, E., Manninen, H.E., Hussein, T., Hakala, J., Nieminen, T., Aalto, P.P., Merkel, M., Wiedensohler, A., Kulmala, M., Petäjä, T., Hämeri, K., 2015. Variability of air ion concentrations in urban Paris. Atmos. Chem. Phys. 15, 13717–13737. https://doi.org/10.5194/acp-15-13717-2015

Dunn, M.J., Jiménez, J.L., Baumgardner, D., Castro, T., McMurry, P.H., Smith, J.N., 2004. Measurements of Mexico City nanoparticle size distributions: Observations of new particle formation and growth. Geophys. Res. Lett. 31. https://doi.org/10.1029/2004GL019483

Durand, T., Bau, S., Morele, Y., Matera, V., Bémer, D., Rousset, D., 2014. Quantification of low pressure impactor wall deposits during ziuc nanoparticle sampling. Aerosol Air Qual. Res. 14, 1812–1821. https://doi.org/10.4209/aaqr.2013.10.0304

Dutschke, A., Lohrer, C., Kurth, L., Seeger, S., Barthel, M., Panne, U., 2011. Aerosol emissions from outdoor firework displays. Chem. Eng. Technol. 34, 2044–2050. https://doi.org/10.1002/ceat.201100080

Easter, R.C., Peters, L.K., 1994. Binary homogeneous nucleation: temperature and relative humidity fluctuations, nonlinearity, and aspects of new particle production in the atmosphere. J. Appl. Meteorol. https://doi.org/10.1175/1520-0450(1994)033<0775:BHNTAR>2.0.CO;2

Erupe, M.E., Benson, D.R., Li, J., Young, L.H., Verheggen, B., Al-Refai, M., Tahboub, O., Cunningham, V., Frimpong, F., Viggiano, A.A., Lee, S.H., 2010. Correlation of aerosol nucleation rate with sulfuric acid and ammonia in Kent, Ohio: An

atmospheric observation. J. Geophys. Res. Atmos. 115. https://doi.org/10.1029/2010JD013942

EUROPEAN COMISSION, 2008. Commission Regulation (EC) No 692/2008. Off. J. Eur. Union 136.

Fan, H., Zhao, C., Yang, Y., Yang, X., 2021. Spatio-Temporal Variations of the PM2.5/PM10 Ratios and Its Application to Air Pollution Type Classification in China. Front. Environ. Sci. 9, 1–13. https://doi.org/10.3389/fenvs.2021.692440

Fierz, M., Houle, C., Steigmeier, P., Burtscher, H., 2011. Design, calibration, and field performance of a miniature diffusion size classifier. Aerosol Sci. Technol. 45, 1–10. https://doi.org/10.1080/02786826.2010.516283

Fonseca, A.S., Talbot, N., Schwarz, J., Ondráček, J., Ždímal, V., Kozáková, J., Viana, M., Karanasiou, A., Querol, X., Alastuey, A., Vu, T. V., Delgado-Saborit, J.M., Harrison, R.M., 2016. Intercomparison of four different cascade impactors for fine and ultrafine particle sampling in two European locations. Atmos. Chem. Phys. Discuss. 1–27. https://doi.org/10.5194/acp-2015-1016

Frampton, M.W., Brauer, M., Kleeman, M., 2013. HEI Perspectives 3 Executive Summary 1-15-2013. Underst. Heal. Eff. Ambient Ultrafine Part.

Franco, J.F., Gidhagen, L., Morales, R., Behrentz, E., 2019. Towards a better understanding of urban air quality management capabilities in Latin America. Environ. Sci. Policy 102, 43–53. https://doi.org/10.1016/j.envsci.2019.09.011

Fujitani, Y., 2013. Quantitative Determination of Composition of Particle Type by Morphology of Nanoparticles in Diesel Exhaust and Roadside Atmosphere. J. Civ. Environ. Eng. 01, 2. https://doi.org/10.4172/2165-784x.s1-002

Fushimi, A., Kondo, Y., Kobayashi, S., Fujitani, Y., Saitoh, K., Takami, A., Tanabe, K.,

2016. Chemical composition and source of fine and nanoparticles from recent direct injection gasoline passenger cars: Effects of fuel and ambient temperature. Atmos. Environ. 124, 77–84. https://doi.org/10.1016/j.atmosenv.2015.11.017

Fushimi, A., Saitoh, K., Fujitani, Y., Hasegawa, S., Takahashi, K., Tanabe, K., Kobayashi, S., 2011. Organic-rich nanoparticles (diameter: 10-30 nm) in diesel exhaust: Fuel and oil contribution based on chemical composition. Atmos. Environ. 45, 6326–6336. https://doi.org/10.1016/j.atmosenv.2011.08.053

Ganguly, N.D., Tzanis, C.G., Philippopoulos, K., Deligiorgi, D., 2019. Analysis of a severe air pollution episode in India during Diwali festival - A nationwide approach. Atmosfera 32, 225–236. https://doi.org/10.20937/ATM.2019.32.03.05

Gani, S., Bhandari, S., Patel, K., Seraj, S., Soni, P., Arub, Z., Habib, G., Hildebrandt Ruiz, L., Apte, J., 2020. Particle number concentrations and size distribution in a polluted megacity: The Delhi Aerosol Supersite study. Atmos. Chem. Phys. 1–30. https://doi.org/10.5194/acp-2020-6

Gani, S., Bhandari, S., Seraj, S., Wang, D.S., Patel, K., Soni, P., Arub, Z., Habib, G., Hildebrandt Ruiz, L., Apte, J., 2018. Submicron aerosol composition in the world's most polluted megacity: The Delhi Aerosol Supersite campaign. Atmos. Chem. Phys. Discuss. 5, 1–33. https://doi.org/10.5194/acp-2018-1066

Gani, S., Bhandari, S., Seraj, S., Wang, D.S., Patel, K., Soni, P., Arub, Z., Habib, G., Hildebrandt Ruiz, L., Apte, J.S., 2019. Submicron aerosol composition in the world's most polluted megacity: The Delhi Aerosol Supersite study. Atmos. Chem. Phys. 19, 6843–6859. https://doi.org/10.5194/acp-19-6843-2019

Ganji, A., Minet, L., Weichenthal, S., Hatzopoulou, M., 2020. Predicting Traffic-Related Air Pollution Using Feature Extraction from Built Environment Images. Environ.

Sci. Technol. 54, 10688–10699. https://doi.org/10.1021/acs.est.0c00412

Gao, J., Chai, F., Wang, T., Wang, S., Wang, W., 2012. Particle number size distribution and new particle formation: New characteristics during the special pollution control period in Beijing. J. Environ. Sci. 24, 14–21. https://doi.org/10.1016/S1001-0742(11)60725-0

Gao, J., Wang, T., Zhou, X., Wu, W., Wang, W., 2009. Measurement of aerosol number size distributions in the Yangtze River delta in China: Formation and growth of particles under polluted conditions. Atmos. Environ. 43, 829–836. https://doi.org/10.1016/j.atmosenv.2008.10.046

Garg, B.D., Cadle, S.H., Mulawa, P.A., Groblicki, P.J., Laroo, C., Parr, G.A., 2000. Brake wear particulate matter emissions. Environ. Sci. Technol. 34, 4463–4469. https://doi.org/10.1021/es001108h

Gerling, L., Wiedensohler, A., Weber, S., 2021. Statistical modelling of spatial and temporal variation in urban particle number size distribution at traffic and background sites. Atmos. Environ. 244. https://doi.org/10.1016/j.atmosenv.2020.117925

Ghei, D., Sane, R., 2018. Estimates of air pollution in Delhi from the burning of firecrackers during the festival of Diwali. PLoS One 13. https://doi.org/10.1371/journal.pone.0200371

Gidhagen, L., Johansson, C., Langner, J., Olivares, G., 2004. Simulation of NOx and ultrafine particles in a street canyon in Stockholm, Sweden. Atmos. Environ. 38, 2029–2044. https://doi.org/10.1016/j.atmosenv.2004.02.014

Giechaskiel, B., 2018a. Solid particle number emission factors of euro vi heavy-duty vehicles on the road and in the laboratory. Int. J. Environ. Res. Public Health 15.

https://doi.org/10.3390/ijerph15020304

Giechaskiel, B., 2018b. Real Driving Emissions (RDE): Particle Number (PN) Portable Measurement Systems (PEMS) calibration, JRC Technical Reports.

Giechaskiel, B., Bonnel, P., Perujo, A., Dilara, P., 2019. Solid particle number (SPN) portable emissions measurement systems (PEMS) in the european legislation: A review. Int. J. Environ. Res. Public Health. https://doi.org/10.3390/ijerph16234819

Giechaskiel, B., Lähde, T., Gandi, S., Keller, S., Kreutziger, P., Mamakos, A., 2020. Assessment of 10-nm particle number (Pn) portable emissions measurement systems (pems) for future regulations. Int. J. Environ. Res. Public Health 17. https://doi.org/10.3390/ijerph17113878

Giechaskiel, B., Lahde, T., Suarez-Bertoa, R., Clairotte, M., Grigoratos, T., Zardini, A., Perujo, A., Martini, G., 2018. Particle number measurements in the European legislation and future JRC activities. Combust. Engines 174, 3–16. https://doi.org/10.19206/ce-2018-301

Giechaskiel, B., Maricq, M., Ntziachristos, L., Dardiotis, C., Wang, X., Axmann, H., Bergmann, A., Schindler, W., 2014. Review of motor vehicle particulate emissions sampling and measurement: From smoke and filter mass to particle number. J. Aerosol Sci. 67, 48–86. https://doi.org/10.1016/j.jaerosci.2013.09.003

Giorgi, F., Lionello, P., 2008. Climate change projections for the Mediterranean region. Glob. Planet. Change 63, 90–104. https://doi.org/10.1016/j.gloplacha.2007.09.005

Goel, A., Kumar, P., 2016. Vertical and horizontal variability in airborne nanoparticles and their exposure around signalised traffic intersections. Environ. Pollut. 214, 54–69. https://doi.org/10.1016/j.envpol.2016.03.033

Goel, A., Kumar, P., 2015. Characterisation of nanoparticle emissions and exposure at

traffic intersections through fast-response mobile and sequential measurements. Atmos. Environ. 107, 374–390. https://doi.org/10.1016/j.atmosenv.2015.02.002

Gómez-Moreno, F.J., Pujadas, M., Plaza, J., Rodríguez-Maroto, J.J., Martínez-Lozano, P., Artíñano, B., 2011. Influence of seasonal factors on the atmospheric particle number concentration and size distribution in Madrid. Atmos. Environ. 45, 3169–3180. https://doi.org/10.1016/j.atmosenv.2011.02.041

Gong, Y., Hu, M., Cheng, Y., Su, H., Yue, D., Liu, F., Wiedensohler, A., Wang, Z., Kalesse, H., Liu, S., Wu, Z., Xiao, K., Mi, P., Zhang, Y., 2010. Competition of coagulation sink and source rate: New particle formation in the Pearl River Delta of China. Atmos. Environ. 44, 3278–3285. https://doi.org/10.1016/j.atmosenv.2010.05.049

Gordon, H., Kirkby, J., Baltensperger, U., Bianchi, F., Breitenlechner, M., Curtius, J., Dias, A., Dommen, J., Donahue, N.M., Dunne, E.M., Duplissy, J., Ehrhart, S., Flagan, R.C., Frege, C., Fuchs, C., Hansel, A., Hoyle, C.R., Kulmala, M., Kürten, A., Lehtipalo, K., Makhmutov, V., Molteni, U., Rissanen, M.P., Stozkhov, Y., Tröstl, J., Tsagkogeorgas, G., Wagner, R., Williamson, C., Wimmer, D., Winkler, P.M., Yan, C., Carslaw, K.S., 2017. Causes and importance of new particle formation in the present-day and preindustrial atmospheres. J. Geophys. Res. Atmos. 122, 8739–8760. https://doi.org/10.1002/2017JD026844

Goyal, M.K., Sharma, A., Surampalli, R.Y., 2020. Remote Sensing and GIS Applications in Sustainability, in: Sustainability. Wiley, pp. 605–626. https://doi.org/10.1002/9781119434016.ch28

Goyal, P., Gandhi, G., 2016. Assessment of Air Quality during the ‘Odd-Even Scheme’ of Vehicles in Delhi. Indian J. Sci. Technol. 9, 1–7.

https://doi.org/10.17485/ijst/2016/v9i48/105801

Gulia, S., Shiva Nagendra, S.M., Khare, M., 2014. Performance evaluation of ISCST3, adms-urban and aermod for urban air quality management in a mega city of India. Int. J. Sustain. Dev. Plan. 9, 778–793. https://doi.org/10.2495/SDP-V9-N6-778-793

Guo, H., Wang, D.W., Cheung, K., Ling, Z.H., Chan, C.K., Yao, X.H., 2012. Observation of aerosol size distribution and new particle formation at a mountain site in subtropical Hong Kong. Atmos. Chem. Phys. 12, 9923–9939. https://doi.org/10.5194/acp-12-9923-2012

Gurjar, B.R., Ravindra, K., Nagpure, A.S., 2016. Air pollution trends over Indian megacities and their local-to-global implications. https://doi.org/10.1016/j.atmosenv.2016.06.030

Guttikunda, S.K., Nishadh, K.A., Jawahar, P., 2019. Air pollution knowledge assessments (APnA) for 20 Indian cities. Urban Clim. 27, 124–141. https://doi.org/10.1016/j.uclim.2018.11.005

Hagan, D.H., Gani, S., Bhandari, S., Patel, K., Habib, G., Apte, J.S., Hildebrandt Ruiz, L., Kroll, J.H., 2019. Inferring Aerosol Sources from Low-Cost Air Quality Sensor Measurements: A Case Study in Delhi, India. Environ. Sci. Technol. Lett. 6, 467–472. https://doi.org/10.1021/acs.estlett.9b00393

Hakkim, H., Kumar, A., Sinha, B., Sinha, V., 2022. Air pollution scenario analyses of fleet replacement strategies to accomplish reductions in criteria air pollutants and 74 VOCs over India. Atmos. Environ. X 13, 100150. https://doi.org/10.1016/j.aeaoa.2022.100150

Halder, R., 2019. Odd-even scheme in Delhi: Exempting two-wheelers not wise idea, say experts | Delhi News - Times of India. The Times of India.

Hama, S.M.L., Cordell, R.L., Monks, P.S., 2017. Quantifying primary and secondary source contributions to ultrafine particles in the UK urban background. Atmos. Environ. 166, 62–78. https://doi.org/10.1016/j.atmosenv.2017.07.013

Hamed, A., Joutsensaari, J., Mikkonen, S., Sogacheva, L., Dal Maso, M., Kulmala, M., Cavalli, F., Fuzzi, S., Facchini, M.C., Decesari, S., Mircea, M., Lehtinen, K.E.J., Laaksonen, A., 2007. Nucleation and growth of new particles in Po Valley, Italy. Atmos. Chem. Phys. 7, 355–376. https://doi.org/10.5194/acp-7-355-2007

Hämeri, K., Kulmala, M., Aalto, P., Leszczynski, K., Visuri, R., Hämekoski, K., 1996. The investigations of aerosol particle formation in urban background area of Helsinki. Atmos. Res. 41, 281–298. https://doi.org/10.1016/0169-8095(96)00015-4

Hanna, S.R., Egan, B.A., Purdum, J., Wagler, J., 2001. Evaluation of the ADMS, AERMOD, and ISC3 dispersion models with the OPTEX, Duke Forest, Kincaid, Indianapolis and Lovett field datasets. Int. J. Environ. Pollut. 16, 301–314. https://doi.org/10.1504/ijep.2001.000626

Harris, S.J., Maricq, M.M., 2001. Signature size distributions for diesel and gasoline engine exhaust particulate matter. J. Aerosol Sci. 32, 749–764. https://doi.org/10.1016/S0021-8502(00)00111-7

Harrison, R.M., Mackenzie, A.R., Xu, H., Alam, M.S., Nikolova, I., Zhong, J., Singh, A., Zeraati-rezaei, S., Stark, C., Beddows, D.C.S., Liang, Z., Xu, R., Cai, X., Harrison, R.M., 2018. Diesel exhaust nanoparticles and their behaviour in the atmosphere. R. Soc. Publ. Proc.R.Soc, 1–20. https://doi.org/10.1098/rspa.2018.0492

Health Effects Institute, 2019. State of Global Air 2019. Heal. Eff. Institute. 24. https://doi.org/https://www.stateofglobalair.org/sites/default/files/soga_2019_repor

t.pdf

HEI Review Panel, 2013. Understanding the Health Effects of Ambient Ultrafine Particles. Heal. Eff. Inst. 122.

Heikkilä, J., Rönkkö, T., Lähde, T., Lemmetty, M., Arffman, A., Virtanen, A., Keskinen, J., Pirjola, L., Rothe, D., 2009a. Effect of open channel filter on particle emissions of modern diesel engine. J. Air Waste Manag. Assoc. 59, 1148–1154. https://doi.org/10.3155/1047-3289.59.10.1148

Heikkilä, J., Virtanen, A., Rönkkö, T., Keskinen, J., Aakko-Saksa, P., Murtonen, T., 2009b. Nanoparticle Emissions from a Heavy-Duty Engine Running on Alternative Diesel Fuels. Environ. Sci. Technol. 43, 9501–9506. https://doi.org/10.1021/es9013807

Herrmann, E., Ding, A.J., Kerminen, V.M., Petäjä, T., Yang, X.Q., Sun, J.N., Qi, X.M., Manninen, H., Hakala, J., Nieminen, T., Aalto, P.P., Kulmala, M., Fu, C.B., 2014. Aerosols and nucleation in eastern China: First insights from the new SORPES-NJU station. Atmos. Chem. Phys. 14, 2169–2183. https://doi.org/10.5194/acp-14-2169-2014

Hetland, R.B., Refsnes, M., Myran, T., Johansen, B. V., Uthus, N., Schwarze, P.E., 2000. Mineral and/or metal content as critical determinants of particle-induced release of IL-6 and IL-8 from A549 cells. J. Toxicol. Environ. Heal. - Part A 60, 47–65. https://doi.org/10.1080/009841000156583

Hietikko, R., Kuuluvainen, H., Harrison, R.M., Portin, H., Timonen, H., Niemi, J. V., Rönkkö, T., 2018. Diurnal variation of nanocluster aerosol concentrations and emission factors in a street canyon. Atmos. Environ. 189, 98–106. https://doi.org/10.1016/j.atmosenv.2018.06.031

Hinds, W.C., 1999. Aerosol technology: properties, behaviour, and measurement of airborne particles.

Hinds, W.C., 1982. Aerosol technology: properties, behaviour, and measurement of airborne particles. 483.

Hirai, K., Yamazaki, Y., Okada, K., Furuta, S., Kubo, K., 2000. Acute Eosinophilic Pneumonia Associated with Smoke from Fireworks. Intern. Med. 39, 401–403. https://doi.org/10.2169/internalmedicine.39.401

Hitchins, J., Morawska, L., Wolff, R., Gilbert, D., 2000. Concentrations of submicrometre particles from vehicle emissions near a major road. Atmos. Environ. 34, 51–59. https://doi.org/10.1016/S1352-2310(99)00304-0

Hoek, G., Beelen, R., Hoogh, K. De, Vienneau, D., Gulliver, J., Fischer, P., Briggs, D., 2008. A review of land-use regression models to assess spatial variation of outdoor air pollution. Atmos. Environ. 42, 7561–7578. https://doi.org/10.1016/j.atmosenv.2008.05.057

Hofman, J., Samson, R., Joosen, S., Blust, R., Lenaerts, S., 2018. Cyclist exposure to black carbon, ultrafine particles and heavy metals: An experimental study along two commuting routes near Antwerp, Belgium. Environ. Res. 164, 530–538. https://doi.org/10.1016/j.envres.2018.03.004

Hofman, J., Staelens, J., Cordell, R., Stroobants, C., Zikova, N., Hama, S.M.L., Wyche, K.P., Kos, G.P.A., Van Der Zee, S., Smallbone, K.L., Weijers, E.P., Monks, P.S., Roekens, E., 2016. Ultrafine particles in four European urban environments: Results from a new continuous long-term monitoring network. Atmos. Environ. 136, 68–81. https://doi.org/10.1016/j.atmosenv.2016.04.010

Hosseini, S., Li, Q., Cocker, D., Weise, D., Miller, A., Shrivastava, M., Miller, J.W.,

Mahalingam, S., Princevac, M., Jung, H., 2010. Particle size distributions from laboratory-scale biomass fires using fast response instruments. Atmos. Chem. Phys. 10, 8065–8076. https://doi.org/10.5194/acp-10-8065-2010

Hussein, T., Hämeri, K., Aalto, P.P., Paatero, P., Kulmala, M., 2005. Modal structure and spatial-temporal variations of urban and suburban aerosols in Helsinki - Finland. Atmos. Environ. 39, 1655–1668. https://doi.org/10.1016/j.atmosenv.2004.11.031

Hussein, T., Puustinen, A., Aalto, P.P., Mäkelä, J.M., Hämeri, K., Kulmala, M., 2004. Urban aerosol number size distributions. Atmos. Chem. Phys. 4, 391–411. https://doi.org/10.5194/acp-4-391-2004

Hyvärinen, A.P., Lihavainen, H., Komppula, M., Panwar, T.S., Sharma, V.P., Hooda, R.K., Viisanen, Y., 2010. Aerosol measurements at the Gual Pahari EUCAARI station: Preliminary results from in-situ measurements. Atmos. Chem. Phys. 10, 7241–7252. https://doi.org/10.5194/acp-10-7241-2010

Indian Council of Medical Research, 2020. Press Release [WWW Document]. Indian Counc. Med. Res. Gov. India. URL https://main.icmr.nic.in/press-release (accessed 12.9.20).

Integrated Review Plan for the National Ambient Air Quality Standards for Particulate Matter, n.d.

IQA AirVisual, 2018. 2018 World Air Quality Report-Region & City. IQA AirVisual 1, 22.

IQAir, 2019. World Air Quality Report. 2019 World Air Qual. Rep. 1–35.

Iqbal, Q., Musarat, M.A., Ullah, N., Alaloul, W.S., Rabbani, M.B.A., Al Madhoun, W., Iqbal, S., 2022. Marble Dust Effect on the Air Quality: An Environmental Assessment Approach. Sustainability 14, 3831. https://doi.org/10.3390/su14073831

Izhar, S., Rajput, P., Gupta, T., 2018. Variation of particle number and mass concentration and associated mass deposition during Diwali festival. Urban Clim. 24, 1027–1036. https://doi.org/10.1016/j.uclim.2017.12.005

Jain, A., 2019. Diwali 2019: Time Slots For Bursting Crackers In Delhi, Tamil Nadu And Other States [WWW Document]. HuffPost none. URL https://www.huffpost.com/archive/in/entry/diwali-2019-time-slots-bursting-crackers-delhi-tamil-nadu_in_5dafeac9e4b0f34e3a7e8f12 (accessed 5.30.21).

Jain, N., Bhatia, A., Pathak, H., 2014. Emission of air pollutants from crop residue burning in India. Aerosol Air Qual. Res. 14, 422–430. https://doi.org/10.4209/aaqr.2013.01.0031

Jayaratne, R., Pushpawela, B., He, C., Li, H., Gao, J., Chai, F., Morawska, L., 2017. Observations of particles at their formation sizes in Beijing, China. Atmos. Chem. Phys. 17, 8825–8835. https://doi.org/10.5194/acp-17-8825-2017

Jeong, C.H., Hopke, P.K., Chalupa, D., Utell, M., 2004. Characteristics of Nucleation and Growth Events of Ultrafine Particles Measured in Rochester, NY. Environ. Sci. Technol. 38, 1933–1940. https://doi.org/10.1021/es034811p

Jiang, X., Miclăuş, T., Wang, L., Foldbjerg, R., Sutherland, D.S., Autrup, H., Chen, C., Beer, C., 2015. Fast intracellular dissolution and persistent cellular uptake of silver nanoparticles in CHO-K1 cells: implication for cytotoxicity. Nanotoxicology 9, 181–189. https://doi.org/10.3109/17435390.2014.907457

Jing, H., Li, Y.F., Zhao, J., Li, B., Sun, J., Chen, R., Gao, Y., Chen, C., 2014. Wide-range particle characterization and elemental concentration in Beijing aerosol during the 2013 Spring Festival. Environ. Pollut. 192, 204–211. https://doi.org/10.1016/j.envpol.2014.06.003

Johnson, T.J., Symonds, J.P.R., Olfert, J.S., 2013. Mass-mobility measurements using a centrifugal particle mass analyzer and differential mobility spectrometer. Aerosol Sci. Technol. 47, 1215–1225. https://doi.org/10.1080/02786826.2013.830692

Joodatnia, P., Kumar, P., Robins, A., 2013. The behaviour of traffic produced nanoparticles in a car cabin and resulting exposure rates. Atmos. Environ. 65, 40–51. https://doi.org/10.1016/j.atmosenv.2012.10.025

Jose, S., Mishra, A.K., Lodhi, N.K., Sharma, S.K., Singh, S., 2021. Characteristics of Aerosol Size Distributions and New Particle Formation Events at Delhi: An Urban Location in the Indo-Gangetic Plains. Front. Earth Sci. 9, 1146. https://doi.org/10.3389/feart.2021.750111

Joshi, M., Khan, A., Anand, S., Sapra, B.K., 2016. Size evolution of ultrafine particles: Differential signatures of normal and episodic events. Environ. Pollut. 208, 354–360. https://doi.org/10.1016/j.envpol.2015.10.001

Joshi, M., Nakhwa, A., Khandare, P., Khan, A., Mariam, Sapra, B.K., 2019. Simultaneous measurements of mass, chemical compositional and number characteristics of aerosol particles emitted during fireworks. Atmos. Environ. 217, 116925. https://doi.org/10.1016/j.atmosenv.2019.116925

Joshi, M., Sapra, B.K., Khan, A., Tripathi, S.N., Shamjad, P.M., Gupta, T., Mayya, Y.S., 2012. Harmonisation of nanoparticle concentration measurements using GRIMM and TSI scanning mobility particle sizers. J. Nanoparticle Res. 14, 1–14. https://doi.org/10.1007/s11051-012-1268-8

Junaid, M., Syed, J.H., Abbasi, N.A., Hashmi, M.Z., Malik, R.N., Pei, D.S., 2018. Status of indoor air pollution (IAP) through particulate matter (PM) emissions and associated health concerns in South Asia. Chemosphere 191, 651–663.

https://doi.org/10.1016/j.chemosphere.2017.10.097

Jung, J., Miyazaki, Y., Kawamura, K., 2013. Different characteristics of new particle formation between urban and deciduous forest sites in Northern Japan during the summers of 2010-2011. Atmos. Chem. Phys. 13, 51–68. https://doi.org/10.5194/acp-13-51-2013

Kaminsky, J.A., Gaskin, E.A.L.M., Matsuda, M., Miguel, A.H., 2009. In-Cabin commuter exposure to ultrafine particles on commuter roads in and around Hong Kong's Tseung Kwan O Tunnel. Aerosol Air Qual. Res. 9. https://doi.org/10.4209/aaqr.2008.09.0041

Kanakidou, M., Seinfeld, J.H., Pandis, S.N., Barnes, I., Dentener, F.J., Facchini, M.C., Van Dingenen, R., Ervens, B., Nenes, A., Nielsen, C.J., Swietlicki, E., Putaud, J.P., Balkanski, Y., Fuzzi, S., Horth, J., Moortgat, G.K., Winterhalter, R., Myhre, C.E.L., Tsigaridis, K., Vignati, E., Stephanou, E.G., Wilson, J., 2005. Organic aerosol and global climate modelling: A review. Atmos. Chem. Phys. https://doi.org/10.5194/acp-5-1053-2005

Kanawade, V.P., Srivastava, A.K., Ram, K., Asmi, E., Vakkari, V., Soni, V.K., Varaprasad, V., Sarangi, C., 2020a. What caused severe air pollution episode of November 2016 in New Delhi? Atmos. Environ. 222, 117125. https://doi.org/10.1016/j.atmosenv.2019.117125

Kanawade, V.P., Tripathi, S.N., Chakraborty, A., Yu, H., 2020b. Chemical Characterisation of Sub-micron Aerosols During New Particle Formation in an Urban Atmosphere. Aerosol Air Qual. Res. 1–12. https://doi.org/10.4209/aaqr.2019.04.0196

Kanawade, V.P., Tripathi, S.N., Siingh, D., Gautam, A.S., Srivastava, A.K., Kamra,

A.K., Soni, V.K., Sethi, V., 2014. Observations of new particle formation at two distinct Indian subcontinental urban locations. Atmos. Environ. 96, 370–379. https://doi.org/10.1016/j.atmosenv.2014.08.001

Kangasniemi, O., Kuuluvainen, H., Heikkilä, J., Pirjola, L., Niemi, J. V., Timonen, H., Saarikoski, S., Rönkkö, T., Maso, M.D., 2019. Dispersion of a traffic related nanocluster aerosol near a major road. Atmosphere (Basel). 10. https://doi.org/10.3390/atmos10060309

Karjalainen, P., Ntziachristos, L., Murtonen, T., Wihersaari, H., Simonen, P., Mylläri, F., Nylund, N.O., Keskinen, J., Rönkkö, T., 2016. Heavy Duty Diesel Exhaust Particles during Engine Motoring Formed by Lube Oil Consumption. Environ. Sci. Technol. 50, 12504–12511. https://doi.org/10.1021/acs.est.6b03284

Karjalainen, P., Ronkko, T., Lahde, T., Rostedt, A., Keskinen, J., Saarikoski, S., Aurela, M., Hillamo, R., Malinen, A., Pirjola, L., Amberla, A., 2012. Reduction of Heavy-Duty Diesel Exhaust Particle Number and Mass at Low Exhaust Temperature Driving by the DOC and the SCR. SAE Int. J. Fuels Lubr. 5, 1114–1122. https://doi.org/10.4271/2012-01-1664

Karroum, K., Lin, Y., Chiang, Y.Y., Ben Maissa, Y., El Haziti, M., Sokolov, A., Delbarre, H., 2020. A Review of Air Quality Modeling. Mapan - J. Metrol. Soc. India 35, 287–300. https://doi.org/10.1007/s12647-020-00371-8

Kerminen, V.M., Chen, X., Vakkari, V., Petäjä, T., Kulmala, M., Bianchi, F., 2018. Atmospheric new particle formation and growth: Review of field observations. Environ. Res. Lett. 13. https://doi.org/10.1088/1748-9326/aadf3c

Kerminen, V.M., Kulmala, M., 2002. Analytical formulae connecting the “real” and the “apparent” nucleation rate and the nuclei number concentration for atmospheric

nucleation events. J. Aerosol Sci. 33, 609–622. https://doi.org/10.1016/S0021-8502(01)00194-X

Ketzel, M., Berkowicz, R., 2004. Modelling the fate of ultrafine particles from exhaust pipe to rural background: An analysis of time scales for dilution, coagulation and deposition. Atmos. Environ. 38, 2639–2652. https://doi.org/10.1016/j.atmosenv.2004.02.020

Kittelson, D.B., 1998. Engines and nanoparticles: A review. J. Aerosol Sci. https://doi.org/10.1016/S0021-8502(97)10037-4

Kittelson, D.B., Hotel, W.G., Angeles, L., 2006. Ultrafine Particle Formation Mechanisms. South Coast Air Qual. Manag. Dist. Conf. Ultrafine Part. Sci. , Technol. , Policy Issues 37.

Kittelson, D.B., Watts, W.F., Johnson, J.P., 2004. Nanoparticle emissions on Minnesota highways. Atmos. Environ. 38, 9–19. https://doi.org/10.1016/j.atmosenv.2003.09.037

Knibbs, L.D., Cole-hunter, T., Morawska, L., 2011. A review of commuter exposure to ultra fi ne particles and its health effects. Atmos. Environ. 45, 2611–2622. https://doi.org/10.1016/j.atmosenv.2011.02.065

Knudsen, K.B., Northeved, H., Ek, P.K., Permin, A., Andresen, T.L., Larsen, S., Wegener, K.M., Lam, H.R., Lykkesfeldt, J., 2013. Differential toxicological response to positively and negatively charged nanoparticles in the rat brain. Nanotoxicology 8, 1–33. https://doi.org/10.3109/17435390.2013.829589

Kompalli, S.K., Babu, S.S., Udayasoorian, C., Jayabalakrishnan, R.M., 2018. Role of anthropogenic emissions and meteorology on ultrafine particle bursts over a high altitude site in Western Ghats during pre-monsoon. J. Atmos. Solar-Terrestrial Phys.

179, 378–388. https://doi.org/10.1016/j.jastp.2018.09.001

Kompalli, S.K., Nair, V.S., Jayachandran, V., Gogoi, M.M., Babu, S.S., 2020. Particle number size distributions and new particle formation events over the northern Indian Ocean during continental outflow. Atmos. Environ. 238, 117719. https://doi.org/10.1016/j.atmosenv.2020.117719

Kompalli, S.K., Suresh Babu, S., Krishna Moorthy, K., Gogoi, M.M., Vijayakumar S Nair, Jai Prakash Chaubey, 2014. The formation and growth of ultrafine particles in two contrasting environments: a case study. Ann. Geophys. 32, 817–830. https://doi.org/10.5194/angeo-32-817-2014

Kong, S., Li, X., Li, L., Yin, Y., Chen, K., Yuan, L., Zhang, Y., Shan, Y., Ji, Y., 2015. Variation of polycyclic aromatic hydrocarbons in atmospheric PM2.5 during winter haze period around 2014 Chinese Spring Festival at Nanjing: Insights of source changes, air mass direction and firework particle injection. Sci. Total Environ. 520, 59–72. https://doi.org/10.1016/j.scitotenv.2015.03.001

Kopanakis, I., Chatoutsidou, S.E., Glytsos, T., Lazaridis, M., 2018. Impact from local sources and variability of fine particle number concentration in a coastal sub-urban site. Atmos. Res. 213, 136–148. https://doi.org/10.1016/j.atmosres.2018.06.002

Kuang, C., Riipinen, I., Sihto, S.L., Kulmala, M., McCormick, A. V., McMurry, P.H., 2010. An improved criterion for new particle formation in diverse atmospheric environments. Atmos. Chem. Phys. 10, 8469–8480. https://doi.org/10.5194/acp-10-8469-2010

Kulkarni, P., Baron, P.A., Willeke, K., 2011. Aerosol Measurement: Principles, Techniques, and Applications: Third Edition, Aerosol Measurement: Principles, Techniques, and Applications: Third Edition. Wiley.

https://doi.org/10.1002/9781118001684

Kulmala, M., Kerminen, V.M., 2008. On the formation and growth of atmospheric nanoparticles. Atmos. Res. 90, 132–150. https://doi.org/10.1016/j.atmosres.2008.01.005

Kulmala, M., Kerminen, V.M., Petäjä, T., Ding, A.J., Wang, L., 2017. Atmospheric gas-to-particle conversion: Why NPF events are observed in megacities? Faraday Discuss. 200, 271–288. https://doi.org/10.1039/c6fd00257a

Kulmala, M., MASO, M.D., MÄKELÄ, J.M., PIRJOLA, L., VÄKEVÄ, M., AALTO, P., MIIKKULAINEN, P., HÄMERI, K., O'DOWD, C.D., 2001. On the formation, growth and composition of nucleation mode particles. Tellus B 53, 479–490. https://doi.org/10.1034/j.1600-0889.2001.d01-33.x

Kulmala, M., Petäjä, T., Ehn, M., Thornton, J., Sipilä, M., Worsnop, D.R., Kerminen, V.M., 2014. Chemistry of atmospheric nucleation: On the recent advances on precursor characterization and atmospheric cluster composition in connection with atmospheric new particle formation. Annu. Rev. Phys. Chem. 65, 21–37. https://doi.org/10.1146/annurev-physchem-040412-110014

Kulmala, M., Petäjä, T., Kerminen, V.M., Kujansuu, J., Ruuskanen, T., Ding, A., Nie, W., Hu, M., Wang, Z., Wu, Z., Wang, L., Worsnop, D.R., 2016. On secondary new particle formation in China. Front. Environ. Sci. Eng. 10, 8. https://doi.org/10.1007/s11783-016-0850-1

Kulmala, M., Petäjä, T., Mönkkönen, P., Koponen, I.K., Dal Maso, M., Aalto, P.P., Lehtinen, K.E.J., Kerminen, V.M., 2005. On the growth nucleation mode particles: Source rates of condensable vapor in polluted and clean environments. Atmos. Chem. Phys. 5, 409–416. https://doi.org/10.5194/acp-5-409-2005

Kulmala, M., Petäjä, T., Nieminen, T., Sipilä, M., Manninen, H.E., Lehtipalo, K., Dal Maso, M., Aalto, P.P., Junninen, H., Paasonen, P., Riipinen, I., Lehtinen, K.E.J., Laaksonen, A., Kerminen, V.M., 2012. Measurement of the nucleation of atmospheric aerosol particles. Nat. Protoc. 7, 1651–1667. https://doi.org/10.1038/nprot.2012.091

Kulmala, M, Vehkamäki, H., Petäjä, T., Dal Maso, M., Lauri, A., Kerminen, V.M., Birmili, W., McMurry, P.H., 2004. Formation and growth rates of ultrafine atmospheric particles: A review of observations. J. Aerosol Sci. https://doi.org/10.1016/j.jaerosci.2003.10.003

Kulmala, M., Vehkamäki, H., Petäjä, T., Dal Maso, M., Lauri, A., Kerminen, V.M., Birmili, W., McMurry, P.H., 2004. Formation and growth rates of ultrafine atmospheric particles: A review of observations. J. Aerosol Sci. 35, 143–176. https://doi.org/10.1016/j.jaerosci.2003.10.003

Kulshrestha, A., Satsangi, P.G., Masih, J., Taneja, A., 2009. Metal concentration of PM2.5 and PM10 particles and seasonal variations in urban and rural environment of Agra, India. Sci. Total Environ. 407, 6196–6204. https://doi.org/10.1016/j.scitotenv.2009.08.050

Kumar, M., Singh, R.K.S., Murari, V., Singh, A.K., Singh, R.K.S., Banerjee, T., 2016. Fireworks induced particle pollution: A spatio-temporal analysis. Atmos. Res. 180, 78–91. https://doi.org/10.1016/j.atmosres.2016.05.014

Kumar, P., Fennell, P., Britter, R., 2008. Effect of wind direction and speed on the dispersion of nucleation and accumulation mode particles in an urban street canyon. Sci. Total Environ. 402, 82–94. https://doi.org/10.1016/j.scitotenv.2008.04.032

Kumar, P., Gulia, S., Harrison, R.M., Khare, M., 2017. The influence of odd–even car

trial on fine and coarse particles in Delhi. Environ. Pollut. 225, 20–30. https://doi.org/10.1016/j.envpol.2017.03.017

Kumar, P., Gurjar, B.R., Nagpure, A.S., Harrison, R.M., 2011. Preliminary estimates of nanoparticle number emissions from road vehicles in megacity Delhi and associated health impacts. Environ. Sci. Technol. 45, 5514–5521. https://doi.org/10.1021/es2003183

Kumar, P., Jain, S., Gurjar, B.R., Sharma, P., Khare, M., Morawska, L., Britter, R., 2013a. New Directions: Can a "blue sky" return to Indian megacities? Atmos. Environ. https://doi.org/10.1016/j.atmosenv.2013.01.055

Kumar, P., Kalaiarasan, G., Porter, A.E., Pinna, A., Kłosowski, M.M., Demokritou, P., Chung, K.F., Pain, C., Arvind, D.K., Arcucci, R., Adcock, I.M., Dilliway, C., 2021. An overview of methods of fine and ultrafine particle collection for physicochemical characterisation and toxicity assessments. Sci. Total Environ. https://doi.org/10.1016/j.scitotenv.2020.143553

Kumar, P., Khare, M., Harrison, R.M., Bloss, W.J., Lewis, A.C., Coe, H., Morawska, L., 2015. New directions: Air pollution challenges for developing megacities like Delhi. Atmos. Environ. https://doi.org/10.1016/j.atmosenv.2015.10.032

Kumar, P., Kumar, A., Lead, J.R., 2012. Nanoparticles in the Indian environment: Known, unknowns and awareness. Environ. Sci. Technol. https://doi.org/10.1021/es302308h

Kumar, P., Kumar, R., Yadav, S., 2016. Water-soluble ions and carbon content of size-segregated aerosols in New Delhi, India: direct and indirect influences of firework displays. Environ. Sci. Pollut. Res. 23, 20749–20760. https://doi.org/10.1007/s11356-016-7313-x

Kumar, P., Morawska, L., Birmili, W., Paasonen, P., Hu, M., Kulmala, M., Harrison, R.M., Norford, L., Britter, R., 2014a. Ultrafine particles in cities. Environ. Int. 66, 1–10. https://doi.org/10.1016/j.envint.2014.01.013

Kumar, P., Morawska, L., Birmili, W., Paasonen, P., Hu, M., Kulmala, M., Harrison, R.M., Norford, L., Britter, R., 2014b. Ultrafine particles in cities. Environ. Int. 66, 1–10. https://doi.org/10.1016/j.envint.2014.01.013

Kumar, P., Patton, A.P., Durant, J.L., Frey, H.C., 2018. A review of factors impacting exposure to PM2.5, ultrafine particles and black carbon in Asian transport microenvironments. Atmos. Environ. https://doi.org/10.1016/j.atmosenv.2018.05.046

Kumar, P., Pirjola, L., Ketzel, M., Harrison, R.M., 2013b. Nanoparticle emissions from 11 non-vehicle exhaust sources - A review. Atmos. Environ. https://doi.org/10.1016/j.atmosenv.2012.11.011

Kumar, P., Robins, A., Vardoulakis, S., Britter, R., 2010. A review of the characteristics of nanoparticles in the urban atmosphere and the prospects for developing regulatory controls. Atmos. Environ. https://doi.org/10.1016/j.atmosenv.2010.08.016

Kwon, H.S., Ryu, M.H., Carlsten, C., 2020. Ultrafine particles: unique physicochemical properties relevant to health and disease. Exp. Mol. Med. https://doi.org/10.1038/s12276-020-0405-1

Lähde, T., Rönkkö, T., Happonen, M., Söderström, C., Virtanen, A., Solla, A., Kytö, M., Rothe, D., Keskinen, J., 2011. Effect of fuel injection pressure on a heavy-duty diesel engine nonvolatile particle emission. Environ. Sci. Technol. 45, 2504–2509. https://doi.org/10.1021/es103431p

Lähde, T., Rönkkö, T., Virtanen, A., Schuck, T.J., Pirjola, L., Hämeri, K., Kulmala, M., Arnold, F., Rothe, D., Keskinen, J., 2009. Heavy duty diesel engine exhaust aerosol particle and ion measurements. Environ. Sci. Technol. 43, 163–168. https://doi.org/10.1021/es801690h

Lähde, T., Virtanen, A., Happonen, M., Söderström, C., Kytö, M., Keskinen, J., 2014. Heavy-duty, off-road diesel engine low-load particle number emissions and particle control. J. Air Waste Manag. Assoc. 64, 1186–1194. https://doi.org/10.1080/10962247.2014.936985

Layale, 2014. Determinants of in-Cabin Exposure To Vehicle-.

Lee, S.C., Chang, M., 2000. Hong Kong 41, 0–4.

Lee, S.H., Gordon, H., Yu, H., Lehtipalo, K., Haley, R., Li, Y., Zhang, R., 2019. New Particle Formation in the Atmosphere: From Molecular Clusters to Global Climate. J. Geophys. Res. Atmos. https://doi.org/10.1029/2018JD029356

Lee, S.H., Kwak, J.H., Lee, S.Y., Lee, J.H., 2015. On-road chasing and laboratory measurements of exhaust particle emissions of diesel vehicles equipped with aftertreatment technologies (DPF, urea-SCR). Int. J. Automot. Technol. 16, 551–559. https://doi.org/10.1007/s12239-015-0056-8

Lee, S.H., Uin, J., Guenther, A.B., de Gouw, J.A., Yu, F., Nadykto, A.B., Herb, J., Ng, N.L., Koss, A., Brune, W.H., Baumann, K., Kanawade, V.P., Keutsch, F.N., Nenes, A., Olsen, K., Goldstein, A., Ouyang, Q., 2016. Isoprene suppression of new particle formation: Potential mechanisms and implications. J. Geophys. Res. 121, 14621–14635. https://doi.org/10.1002/2016JD024844

Leena, P.P., Anil Kumar, V., Dani, K.K., Sombawne, S.M., Murugavel, P., Pandithurai, G., 2017. Evidence of new particle formation during post monsoon season over a

high-altitude site of the Western Ghats, India. Toxicol. Environ. Chem. 99, 652–664. https://doi.org/10.1080/02772248.2016.1274031

Lehtinen, K.E.J., Dal Maso, M., Kulmala, M., Kerminen, V.M., 2007. Estimating nucleation rates from apparent particle formation rates and vice versa: Revised formulation of the Kerminen-Kulmala equation. J. Aerosol Sci. 38, 988–994. https://doi.org/10.1016/j.jaerosci.2007.06.009

Li, X., Dallmann, T.R., May, A.A., Stanier, C.O., Grieshop, A.P., Lipsky, E.M., Robinson, A.L., Presto, A.A., 2018. Size distribution of vehicle emitted primary particles measured in a traffic tunnel. Atmos. Environ. 191, 9–18. https://doi.org/10.1016/j.atmosenv.2018.07.052

Lin, C.C., Chen, S.J., Huang, K.L., Hwang, W.I., Chang-Chien, G.P., Lin, W.Y., 2005. Characteristics of metals in nano/ultrafine/fine/coarse particles collected beside a heavily trafficked road. Environ. Sci. Technol. 39, 8113–8122. https://doi.org/10.1021/es048182a

Lin, M.Y., Hagler, G., Baldauf, R., Isakov, V., Lin, H.Y., Khlystov, A., 2016. The effects of vegetation barriers on near-road ultrafine particle number and carbon monoxide concentrations 553, 372–379. https://doi.org/10.1016/j.scitotenv.2016.02.035

Lingard, J.J.N., Agus, E.L., Young, D.T., Andrews, G.E., Tomlin, A.S., 2006. Observations of urban airborne particle number concentrations during rush-hour conditions: Analysis of the number based size distributions and modal parameters. J. Environ. Monit. 8, 1203–1218. https://doi.org/10.1039/b611479b

Liu, D.Y., Rutherford, D., Kinsey, M., Prather, K.A., 1997. Real-Time Monitoring of Pyrotechnically Derived Aerosol Particles in the Troposphere. Anal. Chem. 69, 1808–1814. https://doi.org/10.1021/ac9612988

Liu, F., Huang, Y., Zhang, F., Chen, Q., Wu, B., Rui, W., Zheng, J.C., Ding, W., 2015. Macrophages treated with particulate matter PM $_{2.5}$ induce selective neurotoxicity through glutaminase-mediated glutamate generation. J. Neurochem. 134, 315–326. https://doi.org/10.1111/jnc.13135

Liu, Q., 2015. Ultrafine particle generation and measurement. Virginia Commonwealth University.

Liu, X.H., Zhu, Y.J., Zheng, M., Gao, H.W., Yao, X.H., 2014. Production and growth of new particles during two cruise campaigns in the marginal seas of China. Atmos. Chem. Phys. 14, 7941–7951. https://doi.org/10.5194/acp-14-7941-2014

Lonati, G., Ozgen, S., Ripamonti, G., Signorini, S., 2017. Variability of black carbon and ultrafine particle concentration on urban bike routes in a Mid-Sized City in the Po Valley (Northern Italy). Atmosphere (Basel). 8, 40. https://doi.org/10.3390/atmos8020040

Loxham, M., Woo, J., Singhania, A., Smithers, N.P., Yeomans, A., Packham, G., Crainic, A.M., Cook, R.B., Cassee, F.R., Woelk, C.H., Davies, D.E., 2020. Upregulation of epithelial metallothioneins by metal-rich ultrafine particulate matter from an underground railway. Metallomics 12, 1070–1082. https://doi.org/10.1039/d0mt00014k

Lushnikov, A.A., Zagaynov, V.A., Lyubovtseva, Y.S., 2017. Formation of aerosols in the lower troposphere. Russ. J. Earth Sci. 17, 69–96. https://doi.org/10.2205/2017ES000604

Lv, G., Sui, X., Chen, J., Jayaratne, R., Mellouki, A., 2018. Investigation of new particle formation at the summit of Mt. Tai, China. Atmos. Chem. Phys. 18, 2243–2258. https://doi.org/10.5194/acp-18-2243-2018

Lv, Y., Chen, X., Wei, S., Zhu, R., Wang, B., Chen, B., Kong, M., Zhang, J. (Jensen), 2020. Sources, concentrations, and transport models of ultrafine particles near highways: a Literature Review. Build. Environ. https://doi.org/10.1016/j.buildenv.2020.107325

Ma, N., Birmili, W., 2015. Estimating the contribution of photochemical particle formation to ultrafine particle number averages in an urban atmosphere. Sci. Total Environ. 512–513, 154–166. https://doi.org/10.1016/j.scitotenv.2015.01.009

Ma, X., Yu, F., 2015. Seasonal and spatial variations of global aerosol optical depth: Multi-year modelling with GEOS-Chem-APM and comparisons with multiple-platform observations. Tellus, Ser. B Chem. Phys. Meteorol. 67, 25115. https://doi.org/10.3402/tellusb.v67.25115

Majumdar, D., Nema, P., 2011. Assessment of fine particle number profile in fugitive emissions from firecrackers. J. Sci. Ind. Res. (India). 70, 225–229.

Mandal, P., Prakash, M., Bassin, J.K., 2012. Impact of Diwali celebrations on urban air and noise quality in Delhi City, India. Environ. Monit. Assess. 184, 209–215. https://doi.org/10.1007/s10661-011-1960-7

Manigrasso, M., Avino, P., 2012. Fast evolution of urban ultrafine particles: Implications for deposition doses in the human respiratory system. Atmos. Environ. 51, 116–123. https://doi.org/10.1016/j.atmosenv.2012.01.039

Manninen, H.E., Nieminen, T., Asmi, E., Gagné, S., Häkkinen, S., Lehtipalo, K., Aalto, P., Vana, M., Mirme, A., Mirme, S., Hõrrak, U., Plass-Dülmer, C., Stange, G., Kiss, G., Hoffer, A., Töro, N., Moerman, M., Henzing, B., De Leeuw, G., Brinkenberg, M., Kouvarakis, G.N., Bougiatioti, A., Mihalopoulos, N., O'Dowd, C., Ceburnis, D., Arneth, A., Svenningsson, B., Swietlicki, E., Tarozzi, L., Decesari, S., Facchini,

M.C., Birmili, W., Sonntag, A., Wiedensohler, A., Boulon, J., Sellegri, K., Laj, P., Gysel, M., Bukowiecki, N., Weingartner, E., Wehrle, G., Laaksonen, A., Hamed, A., Joutsensaari, J., Petäjä, T., Kerminen, V.M., Kulmala, M., 2010. EUCAARI ion spectrometer measurements at 12 European sites-analysis of new particle formation events. Atmos. Chem. Phys. 10, 7907–7927. https://doi.org/10.5194/acp-10-7907-2010

Markandeya, Verma, P.K., Mishra, V., Singh, N.K., Shukla, S.P., Mohan, D., 2021. Spatio-temporal assessment of ambient air quality, their health effects and improvement during COVID-19 lockdown in one of the most polluted cities of India. Environ. Sci. Pollut. Res. 28, 10536–10551. https://doi.org/10.1007/s11356-020-11248-3

Marple, V.A., Rubow, K.L., Behm, S.M., 1991. A microorifice uniform deposit impactor (moudi): Description, calibration, and use. Aerosol Sci. Technol. 14, 434–436. https://doi.org/10.1080/02786829108959504

Maruf Hossain, A.M.M., Park, S., Kim, J.S., Park, K., 2012. Volatility and mixing states of ultrafine particles from biomass burning. J. Hazard. Mater. 205–206, 189–197. https://doi.org/10.1016/j.jhazmat.2011.12.061

Mazaheri, M., Lin, W., Clifford, S., Yue, D., Zhai, Y., Xu, M., Rizza, V., Morawska, L., 2019. Characteristics of school children's personal exposure to ultrafine particles in Heshan, Pearl River Delta, China – A pilot study. Environ. Int. 132, 105134. https://doi.org/10.1016/j.envint.2019.105134

McCreanor, J., Cullinan, P., Nieuwenhuijsen, M.J., Stewart-Evans, J., Malliarou, E., Jarup, L., Harrington, R., Svartengren, M., Han, I.-K., Ohman-Strickland, P., Chung, K.F., Zhang, J., 2007. Respiratory Effects of Exposure to Diesel Traffic in

Persons with Asthma. N. Engl. J. Med. 357, 2348–2358. https://doi.org/10.1056/nejmoa071535

McMurry, P.H., 1983. New particle formation in the presence of an aerosol: Rates, time scales, and sub-0.01 μm size distributions. J. Colloid Interface Sci. 95, 72–80. https://doi.org/10.1016/0021-9797(83)90073-5

McMurry, P.H., Fink, M., Sakurai, H., Stolzenburg, M.R., Mauldin, I.L., Smith, J., Eisele, F., Moore, K., Sjostedt, S., Tanner, D., Huey, L.G., Nowak, J.B., Edgerton, E., Voisin, D., 2005. A criterion for new particle formation in the sulfur-rich Atlanta atmosphere. J. Geophys. Res. Atmos. 110, 1–10. https://doi.org/10.1029/2005JD005901

Meng, H., Zhu, Y., Evans, G.J., Jeong, C.H., Yao, X., 2015. Roles of SO2 oxidation in new particle formation events. J. Environ. Sci. (China) 30, 90–101. https://doi.org/10.1016/j.jes.2014.12.002

Meng, X., Ma, Y., Chen, R., Zhou, Z., Chen, B., Kan, H., 2013. Size-fractionated particle number concentrations and daily mortality in a Chinese City 121, 1174–1178. https://doi.org/10.1289/ehp.1206398

Ministry of home affairs, 2011. Census of India Website : Office of the Registrar General & Census Commissioner, India. Govenment of India.

Ministry of Home Affairs, 2020. Circulars for Covid-19 | Ministry of Home Affairs | GoI [WWW Document]. Minist. Home Aff. Gov. India. URL https://www.mha.gov.in/notifications/circulars-covid-19 (accessed 12.9.20).

Mishra, R.K., Pandey, A., Pandey, G., Kumar, A., 2019. The effect of odd-even driving scheme on PM 2.5 and PM 1.0 emission. Transp. Res. Part D Transp. Environ. 67, 541–552. https://doi.org/10.1016/j.trd.2019.01.005

Mohan, D., Tiwari, G., Goel, R., Lahkar, P., 2017. Evaluation of odd-even day traffic restriction experiments in Delhi, India. Transp. Res. Rec. 2627, 9–16. https://doi.org/10.3141/2627-02

Mohan, M., Payra, S., 2009. Influence of aerosol spectrum and air pollutants on fog formation in urban environment of megacity Delhi, India. Environ. Monit. Assess. 151, 265–277. https://doi.org/10.1007/s10661-008-0268-8

Möller, W., Felten, K., Sommerer, K., Scheuch, G., Meyer, G., Meyer, P., Häussinger, K., Kreyling, W.G., 2008. Deposition, Retention, and Translocation of Ultrafine Particles from the Central Airways and Lung Periphery. Am. J. Respir. Crit. Care Med. 177, 426–432. https://doi.org/10.1164/rccm.200602-301OC

Mönkkönen, P., Koponen, I.K., Lehtinen, K.E.J., Hämeri, K., Uma, R., Kulmala, M., 2005. Measurements in a highly polluted Asian mega city: Observations of aerosol number size distribution, modal parameters and nucleation events. Atmos. Chem. Phys. 5, 57–66. https://doi.org/10.5194/acp-5-57-2005

Monkkonen, P., Koponen, I.K., Lehtinen, K.E.J., Uma, R., Srinivasan, D., 2004. Death of nucleation and Aitken mode particles : observations at extreme atmospheric conditions and their theoretical explanation 35, 781–787. https://doi.org/10.1016/j.jaerosci.2003.12.004

Morawska, L., Ristovski, Z., Jayaratne, E.R., Keogh, D.U., Ling, X., 2008. Ambient nano and ultrafine particles from motor vehicle emissions: Characteristics, ambient processing and implications on human exposure. Atmos. Environ. https://doi.org/10.1016/j.atmosenv.2008.07.050

Morris, M.E., Lee, H.J., Predko, L.M., 2003. Gender differences in the membrane transport of endogenous and exogenous compounds. Pharmacol. Rev.

https://doi.org/10.1124/pr.55.2.1

Mourdikoudis, S., Pallares, R.M., Thanh, N.T.K., 2018. Characterization techniques for nanoparticles: Comparison and complementarity upon studying nanoparticle properties. Nanoscale 10, 12871–12934. https://doi.org/10.1039/c8nr02278j

Mukherjee, T., Asutosh, A., Pandey, S.K., Yang, L., Gogoi, P.P., Panwar, A., Vinoj, V., 2018. Increasing potential for air pollution over megacity New Delhi: A study based on 2016 diwali episode. Aerosol Air Qual. Res. 18, 2510–2518. https://doi.org/10.4209/aaqr.2017.11.0440

Murari, V., Kumar, M., Barman, S.C., Banerjee, T., 2014. Temporal variability of MODIS aerosol optical depth and chemical characterization of airborne particulates in Varanasi, India. Environ. Sci. Pollut. Res. 22, 1329–1343. https://doi.org/10.1007/s11356-014-3418-2

Nagpure, A.S., Sharma, K., Gurjar, B.R., 2013. Traffic induced emission estimates and trends (2000-2005) in megacity Delhi. Urban Clim. 4, 61–73. https://doi.org/10.1016/j.uclim.2013.04.005

Neft, I., Scungio, M., Culver, N., Singh, S., 2016. Aerosol Science and Technology Simulations of aerosol filtration by vegetation: Validation of existing models with available lab data and application to near-roadway scenario Simulations of aerosol filtration by vegetation: Validation of existing models w. https://doi.org/10.1080/02786826.2016.1206653

Neitola, K., Asmi, E., Komppula, M., Hyӧvarinen, A.P., Raatikainen, T., Panwar, T.S., Sharma, V.P., Lihavainen, H., 2011. New particle formation infrequently observed in Himalayan foothills-why? Atmos. Chem. Phys. 11, 8447–8458. https://doi.org/10.5194/acp-11-8447-2011

Nicolás, J.F., Yubero, E., Pastor, C., Crespo, J., Carratalá, A., 2009. Influence of meteorological variability upon aerosol mass size distribution. Atmos. Res. 94, 330–337. https://doi.org/10.1016/j.atmosres.2009.06.007

Nieminen, T., Kerminen, V., Petäjä, T., Aalto, P.P., Arshinov, M., Asmi, E., Baltensperger, U., Beddows, D.C.S., Beukes, J.P., Collins, D., Ding, A., Harrison, R.M., Henzing, B., Hooda, R., Hu, M., Hõrrak, U., Kivekäs, N., Komsaare, K., Krejci, R., Kristensson, A., Laakso, L., Laaksonen, A., Leaitch, W.R., Lihavainen, H., Mihalopoulos, N., Németh, Z., Nie, W., O'Dowd, C., Salma, I., Sellegri, K., Svenningsson, B., Swietlicki, E., Tunved, P., Ulevicius, V., Vakkari, V., Vana, M., Wiedensohler, A., Wu, Z., Virtanen, A., Kulmala, M., 2018. Global analysis of continental boundary layer new particle formation based on long-term measurements. Atmos. Chem. Phys. Discuss. 1–34. https://doi.org/10.5194/acp-2018-304

Nigam, S., Kumar, N., Mandal, N.K., Padma, B., Rao, S., 2016. Real Time Ambient Air Quality Status during Diwali Festival in Central, India. J. Geosci. Environ. Prot. 04, 162–172. https://doi.org/10.4236/gep.2016.41017

Nousiainen, P., Niemi, S., Rönkkö, T., Karjalainen, P., Keskinen, J., Kuuluvainen, H., Pirjola, L., Saveljeff, H., 2013. Effect of injection parameters on exhaust gaseous and nucleation mode particle emissions of a tier 4i nonroad diesel engine, in: SAE Technical Papers. SAE International. https://doi.org/10.4271/2013-01-2575

Nussbaumer, T., Czasch, C., Klippel, N., Johansson, L., Tullin, C., 2008. Particulate emissions from biomass combustion in IEA countries, in: 16th European Biomass Conference and Exhibition. p. 40.

O'Dowd, C.D., Aalto, P., Hämeri, K., Kulmala, M., Hoffmann, T., 2002. Atmospheric

particles from organic vapours. Nature 416, 497–498. https://doi.org/10.1038/416497a

O'Halloran, T.L., Fuentes, J.D., Collins, D.R., Cleveland, M.J., Keene, W.C., 2009. Influence of air mass source region on nanoparticle events and hygroscopicity in central Virginia, U.S. Atmos. Environ. 43, 3586–3595. https://doi.org/10.1016/j.atmosenv.2009.03.033

Obaidullah, M., Bram, S., Verma, V.K., De Ruyck, J., 2012. A review on particle emissions from small scale biomass combustion. Int. J. Renew. Energy Res. 2, 147–159. https://doi.org/10.20508/ijrer.15633

Oberdörster, G., 2000. Pulmonary effects of inhaled ultrafine particles. Int. Arch. Occup. Environ. Health. https://doi.org/10.1007/s004200000185

Oberdörster, G., Oberdörster, E., Oberdörster, J., 2005. Nanotoxicology: An emerging discipline evolving from studies of ultrafine particles. Environ. Health Perspect. https://doi.org/10.1289/ehp.7339

Oberdörster, G., Sharp, Z., Atudorei, V., Elder, A., Gelein, R., Kreyling, W., Cox, C., 2004. Translocation of inhaled ultrafine particles to the brain, in: Inhalation Toxicology. pp. 437–445. https://doi.org/10.1080/08958370490439597

Olfert, J.S., Kulkarni, P., Wang, J., 2008. Measuring aerosol size distributions with the fast integrated mobility spectrometer. J. Aerosol Sci. 39, 940–956. https://doi.org/10.1016/j.jaerosci.2008.06.005

Pacheco, M.T., Parmigiani, M.M.M., de Fatima Andrade, M., Morawska, L., Kumar, P., 2017. A review of emissions and concentrations of particulate matter in the three major metropolitan areas of Brazil. J. Transp. Heal. https://doi.org/10.1016/j.jth.2017.01.008

Pandey, A., Mishra, R.K., Shukla, A., 2016. Study on air pollution trends (2010-2015) due to fireworks during Diwali festival in Delhi , India 03, 1–10. https://doi.org/10.14456/ssstj.2016.5

Parkhi, N., Chate, D., Ghude, S.D., Peshin, S., Mahajan, A., Srinivas, R., Surendran, D., Ali, K., Singh, S., Trimbake, H., Beig, G., 2016. Large inter annual variation in air quality during the annual festival “Diwali” in an Indian megacity. J. Environ. Sci. (China) 43, 265–272. https://doi.org/10.1016/j.jes.2015.08.015

Patel, K., Bhandari, S., Gani, S., Campmier, M.J., Kumar, P., Habib, G., Apte, J., Hildebrandt Ruiz, L., 2021. Sources and Dynamics of Submicron Aerosol during the Autumn Onset of the Air Pollution Season in Delhi, India. ACS Earth Sp. Chem. 5, 118–128. https://doi.org/10.1021/acsearthspacechem.0c00340

Patton, A.P., Laumbach, R., Ohman-Strickland, P., Black, K., Alimokhtari, S., Lioy, P.J., Kipen, H.M., 2016. Scripted drives: A robust protocol for generating exposures to traffic-related air pollution. Atmos. Environ. 143, 290–299. https://doi.org/10.1016/j.atmosenv.2016.08.038

Peng, Y., Liu, X., Dai, J., Wang, Z., Dong, Z., Dong, Y., Chen, C., Li, X., Zhao, N., Fan, C., 2017. Aerosol size distribution and new particle formation events in the suburb of Xi’an, northwest China. Atmos. Environ. 153, 194–205. https://doi.org/10.1016/j.atmosenv.2017.01.022

Pérez, N., Pey, J., Cusack, M., Reche, C., Querol, X., Alastuey, A., Viana, M., 2010. Variability of particle number, black carbon, and PM10, PM 2.5, and PM1 Levels and Speciation: Influence of road traffic emissions on urban air quality, in: Aerosol Science and Technology. Taylor & Francis Group, pp. 487–499. https://doi.org/10.1080/02786821003758286

Perrino, C., Tiwari, S., Catrambone, M., Torre, S.D., Rantica, E., Canepari, S., 2011. Chemical characterization of atmospheric PM in Delhi, India, during different periods of the year including Diwali festival. Atmos. Pollut. Res. 2, 418–427. https://doi.org/10.5094/APR.2011.048

Peters, A., Helmholtz, 2015. Health Effects of Ambient Ultrafine Particles – New Evidence on Short-Term Exposures Health Effects of Ambient Ultrafine Particles Multicenter time-series studies Evidence from the Beijing Olympics Health effects of personal exposure Summary and research.

Pétursdóttir, U., Kirkelund, G.M., Press-Kristensen, K., Hertel, O., Mikkelsen, T.N., 2018. Ultrafine particles in inhabited areas in the Arctic - From very low to high concentrations. Atmos. Pollut. Res. 9, 299–308. https://doi.org/10.1016/j.apr.2017.10.008

Pierce, J.R., Westervelt, D.M., Atwood, S.A., Barnes, E.A., Leaitch, W.R., 2014. New-particle formation, growth and climate-relevant particle production in egbert, canada: Analysis from 1 year of size-distribution observations. Atmos. Chem. Phys. 14, 8647–8663. https://doi.org/10.5194/acp-14-8647-2014

Pirjola, L., Karl, M., Rönkkö, T., Arnold, F., 2015. Model studies of volatile diesel exhaust particle formation: Are organic vapours involved in nucleation and growth? Atmos. Chem. Phys. 15, 10435–10452. https://doi.org/10.5194/acp-15-10435-2015

Pirjola, L., Kulmala, M., 2000. Aerosol dynamical model MULTIMONO. Boreal Environ. Res. 5, 361–374.

Pirjola, L., Paasonen, P., Pfeiffer, D., Hussein, T., Hämeri, K., Koskentalo, T., Virtanen, A., Rönkkö, T., Keskinen, J., Pakkanen, T.A., Hillamo, R.E., 2006. Dispersion of particles and trace gases nearby a city highway: Mobile laboratory measurements in

Finland1. Pirjola L, Paasonen P, Pfeiffer D, et al (2006) Dispersion of particles and trace gases nearby a city highway: Mobile laboratory measurements in Fin 40, 867–879. https://doi.org/10.1016/j.atmosenv.2005.10.018

Pirker, L., Gradišek, A., Višić, B., Remškar, M., 2020. Nanoparticle exposure due to pyrotechnics during a football match. Atmos. Environ. 233, 117567. https://doi.org/10.1016/j.atmosenv.2020.117567

Polash Mukerjee, Shambhavi Shukla, A.R., 2016. Through the thick air [WWW Document]. Down to earth. URL https://www.downtoearth.org.in/coverage/air/delhi-air-pollution-56180 (accessed 2.22.21).

Prakash, D., Payra, S., Verma, S., Soni, M., 2013. Aerosol particle behavior during Dust Storm and Diwali over an urban location in north western India. Nat. Hazards 69, 1767–1779. https://doi.org/10.1007/s11069-013-0780-1

Pratap, V., Saha, U., Kumar, A., Singh, A.K., 2021. Analysis of air pollution in the atmosphere due to firecrackers in the Diwali period over an urban Indian region. Adv. Sp. Res. 68, 3327–3341. https://doi.org/10.1016/j.asr.2021.06.031

Pushpawela, B., Jayaratne, R., Morawska, L., 2018. Differentiating between particle formation and growth events in an urban environment. Atmos. Chem. Phys. 18, 11171–11183. https://doi.org/10.5194/acp-18-11171-2018

Qi, X.M., Ding, A.J., Nie, W., Petäjä, T., Kerminen, V.-M., Herrmann, E., Xie, Y.N., Zheng, L.F., Manninen, H., Aalto, P., Sun, J.N., Xu, Z.N., Chi, X.G., Huang, X., Boy, M., Virkkula, A., Yang, X.-Q., Fu, C.B., Kulmala, M., 2015. Aerosol size distribution and new particle formation in the western Yangtze River Delta of China: 2 years of measurements at the SORPES station. Atmos. Chem. Phys. 15, 12445–

12464. https://doi.org/10.5194/acp-15-12445-2015

Rakowska, A., Wong, K.C., Townsend, T., Chan, K.L., Westerdahl, D., Ng, S., Močnik, G., Drinovec, L., Ning, Z., 2014. Impact of traffic volume and composition on the air quality and pedestrian exposure in urban street canyon. Atmos. Environ. 98, 260–270. https://doi.org/10.1016/j.atmosenv.2014.08.073

Ravindra, K., Mor, S., Kaushik, C.P., 2003. Short-term variation in air quality associated with firework events: A case study. J. Environ. Monit. 5, 260–264. https://doi.org/10.1039/b211943a

Reche, C., Querol, X., Alastuey, A., Viana, M., Pey, J., Moreno, T., Rodríguez, S., González, Y., Fernández-Camacho, R., De La Campa, A.M.S., De La Rosa, J., Dall'Osto, M., Prévôt, A.S.H., Hueglin, C., Harrison, R.M., Quincey, P., 2011. New considerations for PM, Black Carbon and particle number concentration for air quality monitoring across different European cities. Atmos. Chem. Phys. 11, 6207–6227. https://doi.org/10.5194/acp-11-6207-2011

Riesenfeld, E., Chalupa, D., Gibb, F.R., Oberdörster, G., Gelein, R., Morrow, P.E., Utell, M.J., Frampton, M.W., 2000. Ultrafine particle concentrations in a hospital. Inhal. Toxicol. 12, 83–94. https://doi.org/10.1080/08958378.2000.11463201

Rivas, I., Kumar, P., Hagen-Zanker, A., 2017. Exposure to air pollutants during commuting in London: Are there inequalities among different socio-economic groups? Environ. Int. 101, 143–157. https://doi.org/10.1016/j.envint.2017.01.019

Rohan Jayaratne, E., Pushpawela, B., Morawska, L., 2016. Temporal evolution of charged and neutral nanoparticle concentrations during atmospheric new particle formation events and its implications for ion-induced nucleation. Front. Environ. Sci. Eng. 10, 1–9. https://doi.org/10.1007/s11783-016-0862-x

Rohra, H., Tiwari, R., Khare, P., Taneja, A., 2018. Indoor-outdoor association of particulate matter and bounded elemental composition within coarse, quasi-accumulation and quasi-ultrafine ranges in residential areas of northern India. Sci. Total Environ. 631–632, 1383–1397. https://doi.org/10.1016/j.scitotenv.2018.03.095

Rönkkö, T., Kuuluvainen, H., Karjalainen, P., Keskinen, J., Hillamo, R., Niemi, J. V., Pirjola, L., Timonen, H.J., Saarikoski, S., Saukko, E., Järvinen, A., Silvennoinen, H., Rostedt, A., Olin, M., Yli-Ojanperä, J., Nousiainen, P., Kousa, A., Dal Maso, M., 2017. Traffic is a major source of atmospheric nanocluster aerosol. Proc. Natl. Acad. Sci. U. S. A. 114, 7549–7554. https://doi.org/10.1073/pnas.1700830114

Rönkkö, T., Pirjola, L., Ntziachristos, L., Heikkilä, J., Karjalainen, P., Hillamo, R., Keskinen, J., 2014. Vehicle engines produce exhaust nanoparticles even when not fueled. Environ. Sci. Technol. 48, 2043–2050. https://doi.org/10.1021/es405687m

Rönkkö, T., Timonen, H., 2019. Overview of Sources and Characteristics of Nanoparticles in Urban Traffic-Influenced Areas. J. Alzheimer's Dis. 72, 15–28. https://doi.org/10.3233/JAD-190170

Rönkkö, T., Virtanen, A., Kannosto, J., Keskinen, J., Lappi, M., Pirjola, L., 2007. Nucleation mode particles with a nonvolatile core in the exhaust of a heavy duty diesel vehicle. Environ. Sci. Technol. 41, 6384–6389. https://doi.org/10.1021/es0705339

Rönkkö, T., Virtanen, A., Vaaraslahti, K., Keskinen, J., Pirjola, L., Lappi, M., 2006. Effect of dilution conditions and driving parameters on nucleation mode particles in diesel exhaust: Laboratory and on-road study. Atmos. Environ. 40, 2893–2901. https://doi.org/10.1016/j.atmosenv.2006.01.002

Rückerl, R., Schneider, A., Breitner, S., Cyrys, J., Peters, A., 2011. Health effects of particulate air pollution: A review of epidemiological evidence. Inhal. Toxicol. https://doi.org/10.3109/08958378.2011.593587

Saffari, A., Daher, N., Shafer, M.M., Schauer, J.J., Sioutas, C., 2013. Seasonal and spatial variation of trace elements and metals in quasi-ultrafine (PM0.25) particles in the Los Angeles metropolitan area and characterization of their sources. Environ. Pollut. 181, 14–23. https://doi.org/10.1016/j.envpol.2013.06.001

Sahoo, P.K., Mangla, S., Pathak, A.K., Salãmao, G.N., Sarkar, D., 2020. Pre-to-post lockdown impact on air quality and the role of environmental factors in spreading the COVID-19 cases - a study from a worst-hit state of India. Int. J. Biometeorol. 1–18. https://doi.org/10.1007/s00484-020-02019-3

Salma, I., Németh, Z., 2019. Dynamic and timing properties of new aerosol particle formation and consecutive growth events. Atmos. Chem. Phys. 19, 5835–5852. https://doi.org/10.5194/acp-19-5835-2019

Salma, I., Németh, Z., Kerminen, V.M., Aalto, P., Nieminen, T., Weidinger, T., Molnár, Á., Imre, K., Kulmala, M., 2016. Regional effect on urban atmospheric nucleation. Atmos. Chem. Phys. 16, 8715–8728. https://doi.org/10.5194/acp-16-8715-2016

Sarangi, B., Aggarwal, S.G., Gupta, P.K., 2015. A simplified approach to calculate particle growth rate due to self-coagulation, scavenging and condensation using SMPS measurements during a particle growth event in New Delhi. Aerosol Air Qual. Res. 15, 166–179. https://doi.org/10.4209/aaqr.2013.12.0350

Sarangi, B., Aggarwal, S.G., Kunwar, B., Kumar, S., Kaur, R., Sinha, D., Tiwari, S., Kawamura, K., 2018. Nighttime particle growth observed during spring in New Delhi: Evidences for the aqueous phase oxidation of SO2. Atmos. Environ. 188, 82–

96. https://doi.org/10.1016/j.atmosenv.2018.06.018

Sarangi, B., Aggarwal, S.G., Sinha, D., Gupta, P.K., 2016. Aerosol effective density measurement using scanning mobility particle sizer and quartz crystal microbalance with the estimation of involved uncertainty. Atmos. Meas. Tech. 9, 859–875. https://doi.org/10.5194/amt-9-859-2016

Saraswat, A., Apte, J.S., Kandlikar, M., Brauer, M., Henderson, S.B., Marshall, J.D., 2013a. Spatiotemporal land use regression models of fine, ultrafine, and black carbon particulate matter in New Delhi, India. Environ. Sci. Technol. 47, 12903–12911. https://doi.org/10.1021/es401489h

Saraswat, A., Apte, J.S., Kandlikar, M., Brauer, M., Henderson, S.B., Marshall, J.D., 2013b. Spatiotemporal land use regression models of fine, ultrafine, and black carbon particulate matter in New Delhi, India. Environ. Sci. Technol. 47, 12903–12911. https://doi.org/10.1021/es401489h

Sarath Guttikunda, 2020. Data Analysis : How Has the Lockdown Changed the Pollution Over North India ? Wire, latest news.

Sarkar, S., Khillare, P.S., Jyethi, D.S., Hasan, A., Parween, M., 2010. Chemical speciation of respirable suspended particulate matter during a major firework festival in India. J. Hazard. Mater. 184, 321–330. https://doi.org/10.1016/j.jhazmat.2010.08.039

Sartini, C., Sajani, S.Z., Ricciardelli, I., Delgado-Saborit, J.M., Scotto, F., Trentini, A., Ferrari, S., Poluzzi, V., 2013. Ultrafine particle concentrations in the surroundings of an urban area: Comparing downwind to upwind conditions using Generalized Additive Models (GAMs). Environ. Sci. Process. Impacts 15. https://doi.org/10.1039/c3em00228d

Sati, A.P., Mohan, M., 2014. Analysis of air pollution during a severe smog episode of November 2012 and the Diwali Festival over Delhi, India. Int. J. Remote Sens. 35, 6940–6954. https://doi.org/10.1080/01431161.2014.960618

Schmid, O., Möller, W., Semmler-Behnke, M., A. Ferron, G., Karg, E., Lipka, J., Schulz, H., Kreyling, W.G., Stoeger, T., 2009. Dosimetry and toxicology of inhaled ultrafine particles. Biomarkers. https://doi.org/10.1080/13547500902965617

Schraufnagel, D.E., 2020. The health effects of ultrafine particles. Exp. Mol. Med. 52, 311–317. https://doi.org/10.1038/s12276-020-0403-3

Segalin, B., Fornaro, A., Kumar, P., Klemm, O., Andrade, M.F., Trezza, B.M., Busse, A., Filho, W.J., Gonçalves, F.L.T., 2020. Chemical composition of quasi-ultrafine particles and their sources in elderly residences of São Paulo megacity. Aerosol Air Qual. Res. 20, 1002–1015. https://doi.org/10.4209/aaqr.2019.09.0462

Seigneur, C., 2009. Current understanding of ultrafine participate matter emitted from mobile sources. J. Air Waste Manag. Assoc. https://doi.org/10.3155/1047-3289.59.1.3

Seong, H., Choi, S., Lee, K., 2014. Examination of nanoparticles from gasoline direct-injection (GDI) engines using transmission electron microscopy (TEM). Int. J. Automot. Technol. 15, 175–181. https://doi.org/10.1007/s12239-014-0019-5

Sgro, L.A., Sementa, P., Vaglieco, B.M., Rusciano, G., D'Anna, A., Minutolo, P., 2012. Investigating the origin of nuclei particles in GDI engine exhausts. Combust. Flame 159, 1687–1692. https://doi.org/10.1016/j.combustflame.2011.12.013

Sharma, H.K., Swami, M., Swami, B.L., 2012. Optimizing Performance of at-grade Intersection with Bus Rapid Transit Corridor and Heterogeneous Traffic. Int. J. Transp. Sci. Technol. 1, 131–145. https://doi.org/10.1260/2046-0430.1.2.131

Sharma, M., Dixit, O., 2015. Comprehensive Study on Air Pollution and Green House Gases (GHGs) in Delhi. Biochem. J. 465, 79–87.

Sharma, S., Malik, J., Suresh, R., Ghosh, P., 2016. Analysis of Odd-Even scheme phase-II.

Shen, L., Wang, H., Lü, S., Li, L., Yuan, J., Zhang, X., Tian, X., Tang, Q., 2016. Observation of aerosol size distribution and new particle formation at a coastal city in the Yangtze River Delta, China. Sci. Total Environ. 565, 1175–1184. https://doi.org/10.1016/j.scitotenv.2016.05.164

Shen, X.J., Sun, J.Y., Zhang, Y.M., Wehner, B., Nowak, A., Tuch, T., Zhang, X.C., Wang, T.T., Zhou, H.G., Zhang, X.L., Dong, F., Birmili, W., Wiedensohler, A., 2011. First long-term study of particle number size distributions and new particle formation events of regional aerosol in the North China Plain. Atmos. Chem. Phys. 11, 1565–1580. https://doi.org/10.5194/acp-11-1565-2011

Shen, Y., Wang, J., Gao, Y., Chan, C.K., Zhu, Y., Gao, H., Petäjä, T., Yao, X., 2020. Sources and formation of nucleation mode particles in remote tropical marine atmospheres over the South China Sea and the Northwest Pacific Ocean. Sci. Total Environ. 735, 139302. https://doi.org/10.1016/j.scitotenv.2020.139302

Shi, J.P., Harrison, R.M., Brear, F., 1999a. Particle size distribution from a modern heavy duty diesel engine, in: Science of the Total Environment. Elsevier Science Publishers B.V., pp. 305–317. https://doi.org/10.1016/S0048-9697(99)00214-4

Shi, J.P., Khan, A.A., Harrison, R.M., 1999b. Measurements of ultrafine particle concentration and size distribution in the urban atmosphere, in: Science of the Total Environment. pp. 51–64. https://doi.org/10.1016/S0048-9697(99)00189-8

Shi, J.P., Mark, D., Harrison, R.M., 2000. Characterization of particles from a current

technology heavy-duty diesel engine. Environ. Sci. Technol. 34, 748–755. https://doi.org/10.1021/es990530z

Shukla, S., Raman Anisha, 2016. The gas chamber called Delhi. The Pioneer.

Siingh, D., Gautam, A.S., Kamra, A.K., Komsaare, K., 2013. Nucleation events for the formation of charged aerosol particles at a tropical station - Preliminary results. Atmos. Res. 132–133, 239–252. https://doi.org/10.1016/j.atmosres.2013.05.024

Singh, A., Pant, P., Pope, F.D., 2019. Air quality during and after festivals: Aerosol concentrations, composition and health effects. Atmos. Res. https://doi.org/10.1016/j.atmosres.2019.05.012

Singh, D.P., Gadi, R., Mandal, T.K., 2011. Characterization of particulate-bound polycyclic aromatic hydrocarbons and trace metals composition of urban air in Delhi, India, in: Atmospheric Environment. pp. 7653–7663. https://doi.org/10.1016/j.atmosenv.2011.02.058

Singh, D.P., Gadi, R., Mandal, T.K., Dixit, C.K., Singh, K., Saud, T., Singh, N., Gupta, P.K., 2010. Study of temporal variation in ambient air quality during Diwali festival in India. Environ. Monit. Assess. 169, 1–13. https://doi.org/10.1007/s10661-009-1145-9

Singh, S., Nalwa, H.S., 2007. Nanotechnology and Health Safety – Toxicity and Risk Assessments of Nanostructured Materials on Human Health. J. Nanosci. Nanotechnol. 7, 3048–3070. https://doi.org/10.1166/jnn.2007.922

Snyder, M.G., Venkatram, A., Heist, D.K., Perry, S.G., Petersen, W.B., Isakov, V., 2013. RLINE: A line source dispersion model for near-surface releases. Atmos. Environ. 77, 748–756. https://doi.org/10.1016/j.atmosenv.2013.05.074

Solomon, P.A., 2012. An Overview of Ultrafine Particles in Ambient Air. Em Air Waste

Manag. Assoc. Mag. Environ. Manag. Waste Manag. Assoc. 18–27.

Sorribas, M., Adame, J.A., Olmo, F.J., Vilaplana, J.M., Gil-Ojeda, M., Alados-Arboledas, L., 2015. A long-term study of new particle formation in a coastal environment: Meteorology, gas phase and solar radiation implications. Sci. Total Environ. 511, 723–737. https://doi.org/10.1016/j.scitotenv.2014.12.011

Sportisse, B., 2007. A review of parameterizations for modelling dry deposition and scavenging of radionuclides. Atmos. Environ. https://doi.org/10.1016/j.atmosenv.2006.11.057

Srinivas, R., Panicker, A.S., Parkhi, N.S., Peshin, S.K., Beig, G., 2016. Sensitivity of online coupled model to extreme pollution event over a mega city Delhi. Atmos. Pollut. Res. 7, 25–30. https://doi.org/10.1016/j.apr.2015.07.001

Srishti, C., 2016. CSIR scientists lead the way for Green Diwali, develop eco-friendly firecrackers [WWW Document]. Mint. URL https://www.livemint.com/Science/2BaiCY0cE1WjhztFP1eDEL/CSIR-scientists-lead-the-way-for-Green-Diwali-develop-ecof.html (accessed 2.22.21).

Srivastava, A., Jain, V.K., 2008. Source apportionment of suspended particulate matters in a clean area of Delhi: A note. Transp. Res. Part D Transp. Environ. 13, 59–63. https://doi.org/10.1016/j.trd.2007.09.001

Stanier, C.O., Khlystov, A.Y., Pandis, S.N., 2004. Nucleation events during the Pittsburgh Air Quality Study: Description and relation to key meteorological, gas phase, and aerosol parameters 38, 253–264. https://doi.org/10.1080/02786820390229570

Stapleton, E.M., O'Shaughnessy, P.T., Locke, S.J., Altmaier, R.W., Hofmann, J.N., Beane Freeman, L.E., Thorne, P.S., Jones, R.R., Friesen, M.C., 2018. A task-based

analysis of black carbon exposure in Iowa farmers during harvest. J. Occup. Environ. Hyg. 15, 293–304. https://doi.org/10.1080/15459624.2017.1422870

Suni, T., Sogacheva, L., Lauros, J., Hakola, H., B̈ack, J., Kurtén, T., Cleugh, H., Van Gorsel, E., Briggs, P., Sevanto, S., Kulmala, M., 2009. Cold oceans enhance terrestrial new-particle formation in near-coastal forests. Atmos. Chem. Phys. 9, 8639–8650. https://doi.org/10.5194/acp-9-8639-2009

Tan, S.H., Roth, M., Velasco, E., 2017. Particle exposure and inhaled dose during commuting in Singapore. Atmos. Environ. 170, 245–258. https://doi.org/10.1016/j.atmosenv.2017.09.056

Tanda, S., Ličbinský, R., Hegrová, J., Goessler, W., 2019. Impact of New Year's Eve fireworks on the size resolved element distributions in airborne particles. Environ. Int. 128, 371–378. https://doi.org/10.1016/j.envint.2019.04.071

Terzano, C., Di Stefano, F., Conti, V., Graziani, E., Petroianni, A., 2010. Air pollution ultrafine particles: toxicity beyond the lung. Eur. Rev. Med. Pharmacol. Sci. 14, 809–21.

Thorley, A.J., Ruenraroengsak, P., Potter, T.E., Tetley, T.D., 2014. Critical Determinants of Uptake and Translocation of Nanoparticles by the Human Pulmonary Alveolar Epithelium. ACS Nano 8, 11778–11789. https://doi.org/10.1021/nn505399e

Tiwari, S., Bisht, D.S., Srivastava, A.K., Pipal, A.S., Taneja, A., Srivastava, M.K., Attri, S.D., 2014. Variability in atmospheric particulates and meteorological effects on their mass concentrations over Delhi, India. Atmos. Res. 145–146, 45–56. https://doi.org/10.1016/j.atmosres.2014.03.027

Tiwari, S., Bisht, D.S., Srivastava, A.K., Shivashankara, G.P., Kumar, R., 2013. Interannual and Intraseasonal Variability in Fine Mode Particles over Delhi:

Influence of Meteorology. Adv. Meteorol. 2013, 1–9. https://doi.org/10.1155/2013/740453

Tiwari, S., Srivastava, M.K., Bisht, D.S., 2008. Chemical Characteristics of Water Soluble Components of Fine Particulate Matter, PM 2.5 , at Delhi, India. J. Earth Sci. India I, 72–86.

Tiwari, Suresh, Hopke, P.K., Pipal, A.S., Srivastava, A.K., Bisht, D.S., Tiwari, Shani, Singh, A.K., Soni, V.K., Attri, S.D., 2015. Intra-urban variability of particulate matter (PM2.5 and PM10) and its relationship with optical properties of aerosols over Delhi, India 166, 223–232. https://doi.org/10.1016/j.atmosres.2015.07.007

TOI, 2020. Supreme Court allows use of green crackers for 2 hours | India News - Times of India. Time India.

TOI, 2016. Supreme Court bans sale of firecrackers in Delhi, NCR - Times of India [WWW Document]. Time India.

Torricelli, A.A.M., Novaes, P., Matsuda, M., Alves, M.R., Monteiro, M.L.R., 2011. Efeitos adversos na superfície ocular relacionados à poluição ambiental. Arq. Bras. Oftalmol. https://doi.org/10.1590/S0004-27492011000500016

Tsang, H., Kwok, R., Miguel, A.H., 2008. Pedestrian exposure to ultrafine particles in Hong Kong under heavy traffic conditions. Aerosol Air Qual. Res. 8, 19–27. https://doi.org/10.4209/aaqr.2007.09.0041

Tunved, P., Hansson, H.C., Kerminen, V.M., Ström, J., Dal Maso, M., Lihavainen, H., Viisanen, Y., Aalto, P.P., Komppula, M., Kulmala, M., 2006. High natural aerosol loading over boreal forests. Science (80-.). 312, 261–263. https://doi.org/10.1126/science.1123052

TV Venkateswaran, 2019. Eco-friendly crackers: How green is your Diwali? - The

Federal [WWW Document]. Fed. URL https://thefederal.com/the-eighth-column/eco-friendly-crackers-how-green-is-your-diwali/ (accessed 5.13.20).

Väkevä, M., Hämeri, K., Puhakka, T., Nilsson, E.D., Hohti, H., Mäkelä, J.M., 2000. Effects of meteorological processes on aerosol particle size distribution in an urban background area. J. Geophys. Res. Atmos. 105, 9807–9821. https://doi.org/10.1029/1999JD901143

Varghese, M., Leena, P.P., Murugavel, P., Bankar, S., Todekar, K., Chowdhuri, S., Safai, P.D., Malap, N., Konwar, M., Dixit, S., Rao, Y.J., Prabha, T. V., 2020. New particle formation observed from a rain shadow region of the Western Ghats, India. Toxicol. Environ. Chem. 1–29. https://doi.org/10.1080/02772248.2020.1789134

Vecchi, R., Bernardoni, V., Cricchio, D., D'Alessandro, A., Fermo, P., Lucarelli, F., Nava, S., Piazzalunga, A., Valli, G., 2008. The impact of fireworks on airborne particles. Atmos. Environ. 42, 1121–1132. https://doi.org/10.1016/j.atmosenv.2007.10.047

Vehkamaki, H., Kulmala, M., Lehtinen, K.E.J., Noppel, M., 2003. Nucleation of Water - Sulfuric Acid Vapours : Parameterisation for High 37, 3392–3398.

Venkataraman, C., Rao, G.U.M., 2001. Emission factors of carbon monoxide and size-resolved aerosols from biofuel combustion. Environ. Sci. Technol. 35, 2100–2107. https://doi.org/10.1021/es001603d

Versura, P., Profazio, V., Cellini, M., Torreggiani, A., Caramazza, R., 1999. Eye Discomfort and Air Pollution. Ophthalmologica 213, 103–109. https://doi.org/10.1159/000027401

Vincent, J.H., 2007. Aerosol sampling : science, standards, instrumentation and applications. John Wiley & Sons.

Vu, T. V., Delgado-Saborit, J.M., Harrison, R.M., 2015. Review: Particle number size distributions from seven major sources and implications for source apportionment studies. Atmos. Environ. 122, 114–132. https://doi.org/10.1016/j.atmosenv.2015.09.027

Wang, D., Guo, H., Cheung, K., Gan, F., 2014. Observation of nucleation mode particle burst and new particle formation events at an urban site in Hong Kong. Atmos. Environ. 99, 196–205. https://doi.org/10.1016/j.atmosenv.2014.09.074

Wang, H., Maher, B.A., Ahmed, I.A., Davison, B., 2019. Efficient removal of ultrafine particles from diesel exhaust by selected tree species: implications for roadside planting for improving the quality of urban air. Environ. Sci. Technol. https://doi.org/10.1021/acs.est.8b06629

Wang, J., Pikridas, M., Spielman, S.R., Pinterich, T., 2017. A fast integrated mobility spectrometer for rapid measurement of sub-micrometer aerosol size distribution, Part I: Design and model evaluation. J. Aerosol Sci. 108, 44–55. https://doi.org/10.1016/j.jaerosci.2017.02.012

Wang, S.C., Flagan, R.C., 1990. Scanning electrical mobility spectrometer. Aerosol Sci. Technol. 13, 230–240. https://doi.org/10.1080/02786829008959441

Wang, Z., Wu, Z., Yue, D., Shang, D., Guo, S., Sun, J., Ding, A., Wang, L., Jiang, J., Guo, H., Gao, J., Cheung, H.C., Morawska, L., Keywood, M., Hu, M., 2017. New particle formation in China: Current knowledge and further directions. Sci. Total Environ. 577, 258–266. https://doi.org/10.1016/j.scitotenv.2016.10.177

Wang, Z.B., Hu, M., Sun, J.Y., Wu, Z.J., Yue, D.L., Shen, X.J., Zhang, Y.M., Pei, X.Y., Cheng, Y.F., Wiedensohler, A., 2013a. Characteristics of regional new particle formation in urban and regional background environments in the North China Plain.

Atmos. Chem. Phys. 13, 12495–12506. https://doi.org/10.5194/acp-13-12495-2013

Wang, Z.B., Hu, M., Yue, D.L., He, L.Y., Huang, X.F., Yang, Q., Zheng, J., Zhang, R.Y., Zhang, Y.H., 2013b. New particle formation in the presence of a strong biomass burning episode at a downwind rural site in PRD, China. Tellus, Ser. B Chem. Phys. Meteorol. 65, 19965. https://doi.org/10.3402/tellusb.v65i0.19965

Wehner, B., Wiedensohler, A., Heintzenberg, J., 2000. Submicrometer aerosol size distributions and mass concentration of the Millennium fireworks 2000 in Leipzig, Germany. J. Aerosol Sci. 31, 1489–1493. https://doi.org/10.1016/S0021-8502(00)00039-2

Wehner, B., Wiedensohler, A., Tuch, T.M., Wu, Z.J., Hu, M., Slanina, J., Kiang, C.S., 2004. Variability of the aerosol number size distribution in Beijing, China: New particle formation, dust storms, and high continental background. Geophys. Res. Lett. 31, 1–4. https://doi.org/10.1029/2004GL021596

Wentzel, M., Gorzawski, H., Naumann, K.H., Saathoff, H., Weinbruch, S., 2003. Transmission electron microscopical and aerosol dynamical characterization of soot aerosols. J. Aerosol Sci. 34, 1347–1370. https://doi.org/10.1016/S0021-8502(03)00360-4

Westerdahl, D., Fruin, S., Sax, T., Fine, P.M., Sioutas, C., 2005. Mobile platform measurements of ultrafine particles and associated pollutant concentrations on freeways and residential streets in Los Angeles. Atmos. Environ. 39, 3597–3610. https://doi.org/10.1016/j.atmosenv.2005.02.034

Wiedensohler, A., 1988. An approximation of the bipolar charge distribution for particles in the submicron size range. J. Aerosol Sci. 19, 387–389. https://doi.org/10.1016/0021-8502(88)90278-9

Wood, S.N., 2008. Fast stable direct fitting and smoothness selection for generalized additive models. J. R. Stat. Soc. Ser. B Stat. Methodol. 70, 495–518. https://doi.org/10.1111/j.1467-9868.2007.00646.x

Wood, S.N., Li, Z., Shaddick, G., Augustin, N.H., 2017. Generalized Additive Models for Gigadata: Modeling the U.K. Black Smoke Network Daily Data. J. Am. Stat. Assoc. □□□□. https://doi.org/10.1080/01621459.2016.1195744

Wu, Z., Hu, M., Lin, P., Liu, S., Wehner, B., Wiedensohler, A., 2008. Particle number size distribution in the urban atmosphere of Beijing, China. Atmos. Environ. 42, 7967–7980. https://doi.org/10.1016/j.atmosenv.2008.06.022

Wu, Z., Hu, M., Liu, S., Wehner, B., Bauer, S., Ma ßLing, A., Wiedensohler, A., Petäjä, T., Dal Maso, M., Kulmala, M., 2007. New particle formation in Beijing, China: Statistical analysis of a 1-year data set. J. Geophys. Res. Atmos. 112, 1–10. https://doi.org/10.1029/2006JD007406

Xiao, S., Wang, M.Y., Yao, L., Kulmala, M., Zhou, B., Yang, X., Chen, J.M., Wang, D.F., Fu, Q.Y., Worsnop, D.R., Wang, L., 2015. Strong atmospheric new particle formation in winter in urban Shanghai, China. Atmos. Chem. Phys. 15, 1769–1781. https://doi.org/10.5194/acp-15-1769-2015

Xue, J., Xue, W., Sowlat, M.H., Sioutas, C., Lolinco, A., Hasson, A., Kleeman, M.J., 2019. Seasonal and Annual Source Appointment of Carbonaceous Ultrafine Particulate Matter (PM 0.1) in Polluted California Cities. Environ. Sci. Technol. 53, 39–49. https://doi.org/10.1021/acs.est.8b04404

Yadav, S.K., Kompalli, S.K., Gurjar, B.R., Mishra, R.K., 2021. Aerosol number concentrations and new particle formation events over a polluted megacity during the COVID-19 lockdown. Atmos. Environ. 118526.

https://doi.org/10.1016/j.atmosenv.2021.118526

Yadav, S.K., Kumar, M., Sharma, Y., Shukla, P., Singh, R.S., Banerjee, T., 2019. Temporal evolution of submicron particles during extreme fireworks. Environ. Monit. Assess. 191, 576. https://doi.org/10.1007/s10661-019-7735-2

Yadav, S.K., Kumar, M., Sharma, Y., Shukla, P., Singh, R.S., Banerjee, T., 2019. Temporal evolution of submicron particles during extreme fireworks. Environ. Monit. Assess. 191, 576. https://doi.org/10.1007/s10661-019-7735-2

Yadav, Shailendra Kumar, Mishra, R.K., Gurjar, B.R., 2019. Ultrafine Particles in Concern of Vehicular Exhaust—An Overview, in: Agarwal, A.K., Dhar, A., Sharma, N., Shukla, P.C. (Eds.), Engine Exhaust Particulates. Springer, Singapore, Singapore, pp. 7–38. https://doi.org/10.1007/978-981-13-3299-9_2

Yang, F., Kaul, D., Wong, K.C., Westerdahl, D., Sun, L., Ho, K. fai, Tian, L., Brimblecombe, P., Ning, Z., 2015. Heterogeneity of passenger exposure to air pollutants in public transport microenvironments. Atmos. Environ. 109, 42–51. https://doi.org/10.1016/j.atmosenv.2015.03.009

Yang, L., Gao, X., Wang, X., Nie, W., Wang, J., Gao, R., Xu, P., Shou, Y., Zhang, Q., Wang, W., 2014. Impacts of firecracker burning on aerosol chemical characteristics and human health risk levels during the chinese new year celebration in jinan, china. Sci. Total Environ. 476–477, 57–64. https://doi.org/10.1016/j.scitotenv.2013.12.110

Yao, L., Garmash, O., Bianchi, F., Zheng, J., Yan, C., Kontkanen, J., Junninen, H., Mazon, S.B., Ehn, M., Paasonen, P., Sipilä, M., Wang, M., Wang, X., Xiao, S., Chen, H., Lu, Y., Zhang, B., Wang, D., Fu, Q., Geng, F., Li, L., Wang, H., Qiao, L., Yang, X., Chen, J., Kerminen, V.M., Petäjä, T., Worsnop, D.R., Kulmala, M.,

Wang, L., 2018. Atmospheric new particle formation from sulfuric acid and amines in a Chinese megacity. Science (80-.). 361, 278–281. https://doi.org/10.1126/science.aao4839

Yao, L., Wang, M.Y., Wang, X.K., Liu, Y.J., Chen, H.F., Zheng, J., Nie, W., Ding, A.J., Geng, F.H., Wang, D.F., Chen, J.M., Worsnop, D.R., Wang, L., 2016. Detection of atmospheric gaseous amines and amides by a high-resolution time-of-flight chemical ionization mass spectrometer with protonated ethanol reagent ions. Atmos. Chem. Phys. 16, 14527–14543. https://doi.org/10.5194/acp-16-14527-2016

Yegambaram, M., Manivannan, B., Beach, T.G., Halden, R.U., 2015. Role of environmental contaminants in the etiology of Alzheimer's disease: a review. Curr. Alzheimer Res. 12, 116–46.

Young, L.H., Lee, S.H., Kanawade, V.P., Hsiao, T.C., Lee, Y.L., Hwang, B.F., Liou, Y.J., Hsu, H.T., Tsai, P.J., 2013. New particle growth and shrinkage observed in subtropical environments. Atmos. Chem. Phys. 13, 547–564. https://doi.org/10.5194/acp-13-547-2013

Yu, F., Luo, G., 2009. Simulation of particle size distribution with a global aerosol model: Contribution of nucleation to aerosol and CCN number concentrations. Atmos. Chem. Phys. 9, 7691–7710. https://doi.org/10.5194/acp-9-7691-2009

Yu, F., Luo, G., Ma, X., 2012. Regional and global modeling of aerosol optical properties with a size, composition, and mixing state resolved particle microphysics model. Atmos. Chem. Phys. 12, 5719–5736. https://doi.org/10.5194/acp-12-5719-2012

Yu, H., Ren, L., Kanawade, V.P., 2017. New Particle Formation and Growth Mechanisms in Highly Polluted Environments. Curr. Pollut. Reports 3, 245–253. https://doi.org/10.1007/s40726-017-0067-3

Yu, H., Zhou, L., Dai, L., Shen, W., Dai, W., Zheng, J., Ma, Y., Chen, M., 2016. Nucleation and growth of sub-3 nm particles in the polluted urban atmosphere of a megacity in China. Atmos. Chem. Phys. 16, 2641–2657. https://doi.org/10.5194/acp-16-2641-2016

Yue, D., Hu, M., Wu, Z., Wang, Z., Guo, S., Wehner, B., Nowak, A., Achtert, P., Wiedensohler, A., Jung, J., Kim, Y.J., Liu, S., 2009. Characteristics of aerosol size distributions and new particle formation in the summer in Beijing. J. Geophys. Res. Atmos. 114. https://doi.org/10.1029/2008JD010894

Yue, D.L., Hu, M., Wang, Z.B., Wen, M.T., Guo, S., Zhong, L.J., Wiedensohler, A., Zhang, Y.H., 2013. Comparison of particle number size distributions and new particle formation between the urban and rural sites in the PRD region, China. Atmos. Environ. 76, 181–188. https://doi.org/10.1016/j.atmosenv.2012.11.018

Yue, D.L., Hu, M., Zhang, R.Y., Wang, Z.B., Zheng, J., Wu, Z.J., Wiedensohler, A., He, L.Y., Huang, X.F., Zhu, T., 2010. The roles of sulfuric acid in new particle formation and growth in the mega-city of Beijing. Atmos. Chem. Phys. 10, 4953–4960. https://doi.org/10.5194/acp-10-4953-2010

Zhang, M., Wang, X., Chen, J., Cheng, T., Wang, T., Yang, X., Gong, Y., Geng, F., Chen, C., 2010. Physical characterization of aerosol particles during the Chinese New Year's firework events. Atmos. Environ. 44, 5191–5198. https://doi.org/10.1016/j.atmosenv.2010.08.048

Zhang, Q., Jia, S., Yang, L., Krishnan, P., Zhou, S., Shao, M., Wang, X., 2021. New particle formation (NPF) events in China urban clusters given by sever composite pollution background. Chemosphere 262, 127842. https://doi.org/10.1016/j.chemosphere.2020.127842

Zhang, R., Khalizov, A., Wang, L., Hu, M., Xu, W., 2012. Nucleation and growth of nanoparticles in the atmosphere. Chem. Rev. 112, 1957–2011.

Zhang, Y.M., Zhang, X.Y., Sun, J.Y., Lin, W.L., Gong, S.L., Shen, X.J., Yang, S., 2011. Characterization of new particle and secondary aerosol formation during summertime in Beijing, China. Tellus, Ser. B Chem. Phys. Meteorol. 63, 382–394. https://doi.org/10.1111/j.1600-0889.2011.00533.x

Zhao, D., Chen, H., Yu, E., Luo, T., 2019. PM 2.5 /PM 10 ratios in eight economic regions and their relationship with meteorology in China. Adv. Meteorol. 2019, 1–15. https://doi.org/10.1155/2019/5295726

Zhao, S., Yu, Y., Yin, D., He, J., 2017. Effective density of submicron aerosol particles in a typical Valley City, Western China. Aerosol Air Qual. Res. 17, 1–13. https://doi.org/10.4209/aaqr.2015.11.0641

Zhao, S., Yu, Y., Yin, D., Liu, N., He, J., 2014. Ambient particulate pollution during Chinese Spring Festival in urban Lanzhou, Northwestern China. Atmos. Pollut. Res. 5, 335–343. https://doi.org/10.5094/APR.2014.039

Zheng, J., Ma, Y., Chen, M., Zhang, Q., Wang, L., Khalizov, A.F., Yao, L., Wang, Z., Wang, X., Chen, L., 2015. Measurement of atmospheric amines and ammonia using the high resolution time-of-flight chemical ionization mass spectrometry. Atmos. Environ. 102, 249–259. https://doi.org/10.1016/j.atmosenv.2014.12.002

Zhu, B., Wang, H., Shen, L., Kang, H., Yu, X., 2013. Aerosol spectra and new particle formation observed in various seasons in Nanjing. Adv. Atmos. Sci. 30, 1632–1644. https://doi.org/10.1007/s00376-013-2202-4

Zhu, Y., Yan, C., Zhang, R., Wang, Z., Zheng, M., Gao, H., Gao, Y., Yao, X., 2017. Simultaneous measurements of new particle formation at 1s time resolution at a

street site and a rooftop site. Atmos. Chem. Phys. 17, 9469–9484. https://doi.org/10.5194/acp-17-9469-2017

Zimmerman, A., Petters, M.D., Meskhidze, N., 2020. Observations of new particle formation, modal growth rates, and direct emissions of sub-10 nm particles in an urban environment. Atmos. Environ. 242. https://doi.org/10.1016/j.atmosenv.2020.117835

Zuurbier, M., Hoek, G., Oldenwening, M., Lenters, V., Meliefste, K., van den Hazel, P., Brunekreef, B., 2010. Commuters' exposure to particulate matter air pollution is affected by mode of transport, fuel type, and route. Environ. Health Perspect. 118, 783–789. https://doi.org/10.1289/ehp.0901622

7 ANNEXURE

Annexure I

Annexure I: KW-Hypothesis test summary

KW-Hypothesis Test Summary				
	Null Hypothesis	Test	Sig.	Decision
1	The medians of Total PNC [#/CM^3] are the same across categories of Day.	Independent-Samples Median Test	.000	Reject the null hypothesis.
2	The distribution of Total PNC (10 nm to 1000 nm; #/CM^3) is the same across categories of Day.	Independent-Samples Kruskal-Wallis Test	.000	Reject the null hypothesis.
3	The medians of Nucleation mode (10 nm to 20 nm; #/CM^3) are the same across categories of Day.	Independent-Samples Median Test	.000	Reject the null hypothesis.
4	The distribution of Nucleation mode (10 nm to 20 nm; #/CM^3) is the same across categories of Day.	Independent-Samples Kruskal-Wallis Test	.000	Reject the null hypothesis.

5	The medians of Small Aitken mode (20 nm to 50 nm; #/CM^3) are the same across categories of Day.	Independent-Samples Median Test	.000	Reject the null hypothesis.
6	The distribution of Small Aitken mode (20 nm to 50 nm; #/CM^3) is the same across categories of Day.	Independent-Samples Kruskal-Wallis Test	.000	Reject the null hypothesis.
7	The medians of Large Aitken Mode (50 nm to 100 nm; #/cm^3) are the same across categories of Day.	Independent-Samples Median Test	.024	Reject the null hypothesis.
8	The distribution of Large Aitken Mode (50 nm to 100 nm; #/cm^3) is the same across categories of Day.	Independent-Samples Kruskal-Wallis Test	.001	Reject the null hypothesis.
9	The medians of Accumulation mode (100 nm to 1000 nm; #/CM^3) are the same across categories of Day.	Independent-Samples Median Test	.000	Reject the null hypothesis.

10	The distribution of Accumulation mode (100 nm to 1000 nm; #/CM^3) is the same across categories of Day.	Independent-Samples Kruskal-Wallis Test	.000	Reject the null hypothesis.
Asymptotic significances are displayed. The significance level is .05.				

Annexure II

Annexure-II: Kruskal-Wallis test for PMs and its PNSD

Location	Parameter	Sig.	Decision	Parameter	Sig.	Decision
Najafgarh	QuasiUFP	0.000	Rejected	TVC	0.000	Rejected
	Subfine	0.022	Rejected	C&T	0.029	Rejected
	Fine	0.000	Rejected	WS (m/s)	0.119	Retain
	Coarse	0.235	Retain	RH (%)	0.000	Rejected
	$PM_{0.5}$	0.000	Rejected	SR (W/mt^2)	0.038	Rejected
	PM_1	0.000	Rejected			
	$PM_{2.5}$	0.000	Rejected			
	PM_{10}	0.000	Rejected			
Pitampura	QuasiUFP	0.000	Rejected	TVC	0.000	Rejected
	Subfine	0.000	Rejected	C&T	0.000	Rejected
	Fine	0.000	Rejected	WS (m/s)	0.000	Rejected

	Coarse	0.000	Rejected	RH (%)	0.000	Rejected
	$PM_{0.5}$	0.000	Rejected	SR (W/mt^2)	0.229	Retain
	PM_1	0.000	Rejected			
	$PM_{2.5}$	0.000	Rejected			
	PM_{10}	0.000	Rejected			
Panchkuian	QuasiUFP	0.000	Rejected	TVC	0.000	Rejected
	Subfine	0.011	Rejected	C&T	0.000	Rejected
	Fine	0.000	Rejected	WS (m/s)	0.208	Retain
	Coarse	0.192	Retain	RH (%)	0.000	Rejected
	$PM_{0.5}$	0.000	Rejected	SR (W/mt^2)	0.070	Retain
	PM_1	0.000	Rejected			
	$PM_{2.5}$	0.000	Rejected			
	PM_{10}	0.000	Rejected			

Annexure III

Annexure-III: Kruskal -Wallis Test statistics of different size bins at three locations

LOCAT-ION	PNSD	N-E DAY	N-O DAY	E-O DAY	PMs	N-E DAY	N-O DAY	E-O DAY
	Sig. Level	p-value			Sig. Level	p-value		
NJF	Quasi UFP	0.021 Reject	0.000 Reject	0.267 Retain	$PM_{0.5}$	0.019 Reject	0.000 Reject	0.256 Retain
	Subfine	1.000 Retain	0.126 Retain	0.026 Reject	PM_1	0.107 Reject	0.000 Reject	0.322 Retain
	Fine	0.065 Retain	0.000 Reject	0.029 Reject	$PM_{2.5}$	0.108 Reject	0.000 Reject	0.261 Retain
	Coarse	…	…	…	PM_{10}	0.108 Reject	0.000 Reject	0.261 Retain

PTM	QuasiUFP	0.000 Reject	0.001 Reject	1.000 Retain	$PM_{0.5}$	0.000 Reject	0.001 Reject	1.000 Retain
	Subfine	0.000 Reject	0.001 Reject	1.000 Retain	PM_1	0.000 Reject	0.001 Reject	1.000 Retain
	Fine	1.000 Retain	0.000 Reject	0.009 Reject	$PM_{2.5}$	0.000 Reject	0.001 Reject	1.000 Retain
	Coarse	1.000 Retain	0.000 Reject	0.000 Reject	PM_{10}	0.000 Reject	0.001 Reject	1.000 Retain
PANC	QuasiUFP	0.027 Reject	0.000 Reject	0.058 Retain	$PM_{0.5}$	0.030 Reject	0.000 Reject	0.050 Retain
	Subfine	0.466 Retain	0.009 Reject	0.219 Retain	PM_1	0.031 Reject	0.000 Reject	0.041 Reject
	Fine	0.008 Reject	0.000 Reject	0.187 Retain	$PM_{2.5}$	0.031 Reject	0.000 Reject	0.041 Reject

	Coarse	…	…	…	PM_{10}	0.031 Reject	0.000 Reject	0.041 Reject

Annexure-IV: Kruskal -Wallis Test statistics of TVC and C&T count along with meteorological parameters at Three locations

LOCATION	PARAMETER	N- E DAY	N-O DAY	E-O DAY
	Sig. Level	p-value		
NJF	TVC	0.674 Retain	0.000 Reject	0.000 Reject
	C&T	0.108 Retain	0.032 Reject	1.000 Retain
	WS (m/s)	…	…	…
	RH (%)	0.073 Retain	0.000 Reject	0.004 Reject
	SR (W/mt^2)	0.755 Retain	0.032 Reject	0.466 Retain

PTM	TVC	0.000 Reject	0.000 Reject	0.027 Reject
	C&T	0.004 Reject	0.000 Reject	0.513 Retain
	WS (m/s)	0.000 Reject	0.000 Reject	0.770 Retain
	RH (%)	0.054 Retain	0.000 Reject	0.242 Retain
	SR (W/mt^2)	…	…	…
PANC	TVC	0.000 Reject	0.000 Reject	0.033 Retain
	C&T	0.004 Reject	0.000 Reject	0.205 Retain
	WS (m/s)	…	…	…

	RH (%)	0.063 Retain	0.000 Reject	0.332 Retain
	SR (W/mt^2)	…	…	…

Annexure-V: Summary of different size bin along with TVC and C&T count at Three locations (Normal Day)

Location	Parameter	Normal Day PNC (#/L)				Normal Day PNC (#/L)	Vehicle Count (per half hour)	
		Quasi UFP	Subfine	Fine	Coarse	PM_1	Vehicular count	C & T count
Najafgarh	Mean	$3.62x10^6$	$8.67x10^4$	$1.18x10^3$	$2.79x10^2$	$3.71x10^6$	$3.93x10^3$	$8.71x10^2$
	SD	$4.16x10^6$	$2.21x10^4$	$3.22x10^2$	$1.08x10^2$	$4.30x10^5$	$2.67x10^2$	$1.21x10^2$
	Min.	$3.06x10^6$	$5.70x10^4$	$8.99x10^2$	$1.77x10^2$	$3.12x10^6$	$3.52x10^2$	$7.54x10^2$
	Max.	$4.16x10^6$	$1.16x10^5$	$1.88x10^3$	$5.71x10^2$	$4.28x10^6$	$4.37x10^3$	$1.13x10^3$
Pitampura	Mean	$2.86x10^6$	$1.45x10^5$	$4.63x10^3$	$1.68x10^3$	$3.00x10^6$	$2.33x10^3$	$1.06x10^3$
	SD	$2.66x10^6$	$5.78x10^4$	$1.02x10^3$	$2.84x10^2$	$6.43x10^5$	$1.18x10^2$	$1.02x10^3$

	Min.	2.83x 10^6	5.37 x10^4	3.15 x10^3	1.17 x10^3	1.70x10^6	2.11x10^2	1.06x1 0^3
	Max.	2.80x 10^6	2.24 x10^5	6.08 x10^3	2.13 x10^3	3.86x10^6	2.55x10^3	1.07x1 0^3
Panch kuian	Mean	3.12x 10^6	6.17 x10^4	4.60 x10^3	1.49 x10^3	3.28x10^6	3.86x10^3	1.00x1 0^3
	SD	3.07x 10^6	1.16 x10^4	6.95 x10^3	2.88 x10^2	3.53x10^5	1.61x10^2	1.01x1 0^3
	Min.	3.10x 10^6	4.38 x10^4	3.45 x10^3	1.13 x10^3	2.57x10^6	3.56x10^2	1.01x1 0^3
	Max.	3.09x 10^6	8.11 x10^4	6.03 x10^3	1.99 x10^3	3.70x10^6	4.16x10^3	1.02x1 0^3

Annexure-VI: Summary of different size bin along with TVC and C&T count at Three locations (Odd Day)

Location	Parameter	Odd Day PNC (#/L)				Normal Day PNC (#/L)	Vehicle Count (per half hour)	
		Quasi UFP	Subfine	Fine	Coarse	PM_1	Vehicular count	C & T count
Najafgarh	Mean	$2.27x10^6$	$3.52x10^4$	$6.79x10^2$	$2.01x10^2$	$2.30x10^6$	$2.99x10^3$	$6.94x10^2$
	SD	$2.20x10^6$	$1.23x10^4$	$2.49x10^2$	$8.07x10^1$	$6.86x10^5$	$7.19x10^2$	$2.04x10^2$
	Min.	$2.24x10^6$	$1.72x10^4$	$3.50x10^2$	$6.09x10^1$	$1.37x10^6$	$4.10x10^2$	$9.06x10^1$
	Max.	$2.21x10^6$	$5.48x10^4$	$1.12x10^3$	$3.69x10^2$	$3.65x10^6$	$3.63x10^3$	$9.80x10^2$
Pitampura	Mean	$2.17x10^6$	$8.17x10^4$	$3.29x10^3$	$1.22x10^3$	$2.25x10^6$	$1.76x10^3$	$8.91x10^2$
	SD	$1.91x10^6$	$3.02x10^4$	$6.12x10^2$	$2.39x10^2$	$7.49x10^5$	$2.59x10^2$	$8.85x10^2$

	Min.	2.09x 10^6	4.76 x10^4	2.32 x10^3	8.81 x10^2	1.50x10^6	1.20x10^3	8.99x1 0^2
	Max.	2.02x 10^6	1.40 x10^4	4.31 x10^3	1.81 x10^3	4.18x10^6	2.13x10^3	9.10x1 0^2
Panch kuian	Mean	1.86x 10^6	4.02 x10^4	3.16 x10^3	1.37 x10^3	1.91x10^6	2.95x10^3	7.90x1 0^2
	SD	1.71x 10^6	1.78 x10^4	6.22 x10^2	3.69 x10^2	7.89x10^5	4.67x10^2	7.76x1 0^2
	Min.	1.81x 10^6	1.31 x10^4	2.05 x10^3	8.29 x10^2	6.41x10^5	1.55x10^3	8.04x1 0^2
	Max.	1.78x 10^6	7.46 x10^4	4.48 x10^3	2.28 x10^3	3.33x10^6	3.86x10^3	8.09x1 0^2

Annexure-VII: Summary of different size bin along with TVC and C&T count at Three locations (Even Day)

Location		Even PNC (#/L)				Even Day PNC (#/L)	Vehicle Count (per half hour)	
		Quasi UFP	Subfine	Fine	Coarse	PM_1	Vehicular count	C & T count
Najafgarh	Mean	$2.77x10^6$	$6.23x10^4$	$9.28x10^2$	$2.31x10^2$	$2.83x10^6$	$3.11x10^3$	$7.14x10^2$
	SD	$2.54x10^6$	$4.69x10^4$	$2.36x10^2$	$6.03x10^1$	$1.14x10^6$	$7.50x10^2$	$2.05x10^2$
	Min.	$2.70x10^6$	$1.03x10^4$	$6.88x10^2$	$1.35x10^2$	$9.35x10^5$	$8.40x10^2$	$2.42x10^2$
	Max.	$2.64x10^6$	$1.83x10^5$	$1.58x10^3$	$3.86x10^2$	$4.63x10^6$	$3.81x10^3$	$9.94x10^2$
Pitampura	Mean	$2.05x10^6$	$7.91x10^4$	$4.40x10^3$	$1.93x10^3$	$2.13x10^6$	$2.00x10^3$	$9.59x10^2$
	SD	$1.90x10^6$	$3.07x10^4$	$1.49x10^3$	$6.40x10^2$	$5.75x10^5$	$2.41x10^2$	$9.42x10^2$

	Min.	$2.03x10^6$	$4.42x10^4$	$2.49x10^3$	$1.09x10^3$	$1.45x10^6$	$1.29x10^3$	$9.72x10^2$
	Max.	$2.00x10^6$	$1.25x10^5$	$6.78x10^3$	$3.16x10^3$	$3.20x10^6$	$2.47x10^3$	$9.78x10^2$
Panchkuian	Mean	$2.43x10^6$	$7.84x10^4$	$3.67x10^3$	$1.35x10^3$	$2.54x10^6$	$3.31x10^3$	$8.55x10^2$
	SD	$2.22x10^6$	$7.41x10^4$	$9.89x10^2$	$4.13x10^2$	$9.09x10^5$	$1.45x10^2$	$8.27x10^2$
	Min.	$2.37x10^6$	$2.37x10^4$	$2.19x10^3$	$8.59x10^2$	$1.17x10^6$	$2.85x10^3$	$8.60x10^2$
	Max.	$2.32x10^6$	$2.82x10^5$	$6.63x10^3$	$2.83x10^3$	$4.13x10^6$	$3.57x10^3$	$8.61x10^2$

Annexure VIII

Sampling location and instrumental Setup


HORIBA
SO2 0.0242
HORIBA
CO